THE
PHYSICAL REVIEW

A journal of experimental and theoretical physics established by E. L. Nichols in 1893

SECOND SERIES, VOL. 72, NO. 12 DECEMBER 15, 1947

Proton-Proton Scattering at 14.5 Mev

ROBERT R. WILSON*
Harvard University, Cambridge, Massachusetts

AND

EDWARD J. LOFGREN,** J. REGINALD RICHARDSON,*** BYRON T. WRIGHT***
Radiation Laboratory, University of California, Berkeley, California

AND

ROBERT S. SHANKLAND
Case Institute of Technology, Cleveland, Ohio

(Received September 2, 1947)

The scattering of 14.5 Mev protons by protons has been studied by using a coincidence counting method. The 14.5 Mev protons were obtained from the 37-inch synchrocyclotron at Berkeley. The measurements of the differential scattering cross section are absolute and extend from 10° to 45°. The accuracy was not high, about ten percent, because the pulsed nature of the synchrocyclotron beam introduced a large background of accidental counts. At small angles the scattering is significantly larger than that predicted by S wave scattering only. This indicates the effect of P wave scattering such as that due to a repulsive potential well. The results are not inconsistent with those found at 8 and 10 Mev.

WHEN a deflected beam of 14.5 Mev protons was obtained from the 37-inch synchrocyclotron at Berkeley, it became desirable to study the scattering of protons from protons by means of the same experimental techniques which had previously been developed and used at Princeton, where 8 Mev protons were available. The results obtained at that energy[1] were most consistent with the scattering predicted by the S wave contribution only.[2] The accuracy was not great enough to exclude P wave scattering effects except for those predicted by the neutral meson theory. The same equipment was subsequently used at Berkeley with 10 Mev protons, and more precise data were obtained.[3] These results have been analyzed by Peierls and Preston,[4] and by Foldy.[4]

Peierls and Preston find from these data a mean range of the proton-proton force of 2.5 $\times 10^{-13}$ cm, and that the P scattering is compatible with a repulsive square well of this range and of 10 Mev in magnitude. However, Foldy has criticized this analysis and expressed disagreement with the above conclusions.

* Now at Cornell University, Ithaca, New York.
** Now at the University of Minnesota, Minneapolis, Minnesota.
*** Now at the University of California, Los Angeles, California.
[1] R. R. Wilson and E. C. Creutz, Phys. Rev. 71, 339 (1947).
[2] Breit, Thaxton, and Eisenbud, Phys. Rev. 55, 1018 (1939).
[3] R. R. Wilson, Phys. Rev. 71, 384 (1947).
[4] R. E. Peierls and M. A. Preston, Phys. Rev. 72, 250 (1947); L. L. Foldy, Phys. Rev. 72, 125 (1947).

At 14.5 Mev the P wave effects predicted by the various theories should be much more pronounced than at the lower energies and it was hoped that even rough measurements would be useful. The method used, essentially that previously employed, was a coincidence counting arrangement in which the narrow incident proton beam was scattered by a very thin nylon foil. When a proton is scattered from one of the hydrogen nuclei in the nylon foil, that hydrogen nucleus or proton will then recoil, traveling in a direction perpendicular to the direction of the scattered proton. Two proportional counters were mounted on a movable table, as shown in Fig. 1, such that if the scattered proton entered the *defining counter*, the associated recoil proton would surely enter the *monitoring counter* and then register a coincidence.[5] On the other hand, if the proton was scattered from another element in the foil, or had been scattered from the beam defining slit, no coincidence would be recorded since such a scattering process would not be accompanied by a recoil proton at 90°. The details of the equipment and method have been described in another article.[1] The second alignment procedure described in reference (1) was used in the present experiment. The electronic circuits were similar to those used at Princeton but were more elaborate. They were borrowed from the Los Alamos Laboratory for the experiment. The amplifiers were the Elmore model 500 with a time of rise of roughly 0.2 microseconds. The proportional counters were filled with a mixture consisting of ninety-five percent argon and five percent carbon dioxide at a total pressure of about 25 cm Hg. The bias voltages of the discriminators were set as low as was possible without getting too many accidentals. Higginbotham scaling circuits were used to record the number of pulses in each proportional counter as well as the number of coincidences. The proton beam current integrating system was changed somewhat from that used at Princeton and it will be described later in this article.

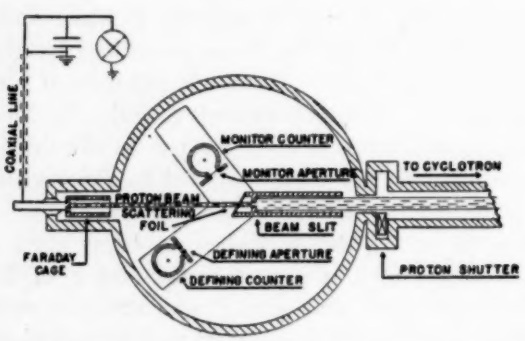

FIG. 1. Schematic drawing of the scattering chamber and integrating system.

The scattering foil, nylon $(C_{12}H_{22}N_2O_2)_x$ about 2×10^{-4} cm thick, was placed at the center of the scattering chamber and mounted so that the normal to the plane of the scattering foil made an angle of 30° with the direction of the incident proton beam which was 2.0 mm in diameter. (Fig. 1.) The scattered protons entered the "*defining proportional counter*" through a circular aperture of 2.47 mm diameter which was 7.8 cm from the center of the scattering foil. The aperture of the monitor counter, which was mounted so that it received the recoil protons at 90° with respect to the defining counter, had an oval aperture $\frac{3}{16}$ in. wide and $\frac{5}{16}$ in. high, and it was 3.7 cm distant from the scattering foil. Of course, the recoil and scattered protons could not be distinguished, but, for the purposes of this paper, those protons which entered the defining counter will be called scattered protons and those which entered the monitor counter will be called recoil protons.

The solid angle of the monitor counter was large to insure that the recoil protons associated with all protons entering the defining counter would enter the monitoring counter. However, for the smallest angles at which the scattering was studied, i.e., 10° and 12° with respect to the incident proton beam, the vertical aperture of the monitor counter was not large enough and thus, for geometrical reasons, in a small proportion of cases for protons which entered the defining counter the associated recoil protons could not enter the monitor counter. One can readily demonstrate that in the plane of scattering (the horizontal plane) the spreading of the recoil protons at the monitor counter due to the finite size of the scattering area and the defining aperture is less than 75 percent of the total width

[5] The monitor counter was actually adjusted at 89½° with respect to the defining counter to allow for a relativistic effect on the angle between scattered and recoil protons. Since the monitor counter subtended an angle of 7°, this adjustment was not essential.

of the monitor aperture and that it does not change rapidly with the angle. Hence, there was no loss due to the horizontal spreading at any angle. On the other hand, the vertical spreading of the recoil protons at small scattering angles was corrected as follows: The incident proton beam of circular cross section was separated into six narrow vertical sections of equal base length. Corresponding to each of these sections the vertical density distribution at the monitor aperture of recoil protons corresponding to scattered protons uniformly entering the circular defining aperture was numerically and geometrically calculated. The distributions from each of the narrow beam sections were then added together to give the final vertical recoil distribution at the monitor aperture. This is shown in Fig. 2. The effect of multiple scattering on the distribution was determined in the same way that is discussed at length in reference (1) and was found to be negligible. The vertical arrows in Fig. 2 indicate the positions of the top and bottom of the monitor counter. The fractional correction to be added to the observed coincidence rate is the ratio of the area outside the arrows to that included inside the arrows. At 10° this correction amounts to (13±1) percent. Similar numerical calculations showed the correction to be (8±1) percent at 12°, (3±1) percent at 14°, and less than 0.2 percent at 18°. Since the final results have statistical errors of about 10 percent, it was felt that the above degree of approximation for the correction was adequate.

The proton-proton coincidences in the proportional counters, together with the individual counting rates in each counter, were observed at each scattering angle θ during a series of ten minute runs of the cyclotron. During each ten minute run, the proton beam was maintained at as constant intensity as possible. In order to normalize each run, however, and reduce the measurements to an absolute basis, it was necessary to measure the integrated proton beam current during each ten minute observation. This was accomplished by permitting the primary proton beam, after it had passed entirely through the scattering chamber, to enter a Faraday cup collector. The Faraday chamber was connected to a standard mica condenser through a concentric solid core dialectric cable (8PGU) and the potential of this system relative to ground was measured by a quadrant electrometer. The capacitance of the entire system relative to ground was 0.101 microfarads. The electrical connections are shown in Fig. 1. It was determined that the coaxial cable did not contribute any leakage current due to the effects of the slow neutrons from the cyclotron. The condenser was a standard (Pye) instrument chosen because of its low leakage rate and small soakage charge. The system was checked for both leakage and soakage at frequent intervals and these effects were found to be negligible in comparison to the other uncertainties of measurement. A quadrant electrometer was connected heterostatically with the needle at 90 volts above ground. The deflections were measured by a lamp and scale arrangement; a typical deflection of the light spot during a ten minute run being about 7 cm on the scale at a meter from the electrometer mirror. The condenser was ungrounded at the beginning of each run and the observation consisted of recording the position of the light spot at the end of the ten minute interval, and then determining the zero position by again grounding the condenser system and reading the deflection immediately afterwards with the grounding switch again open to eliminate contact potential differences. As a control, the electrometer was observed during runs when the shutter of the scattering chamber was closed so that no protons could enter, and it was always found that the deflections were negligible. The integrating system was calibrated before each set of runs with an RCA instrument which applied a known voltage to

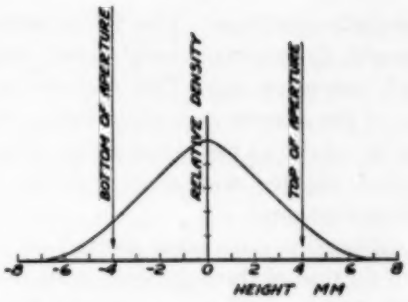

FIG. 2. The distribution of protons in the vertical direction along the aperture of the monitor counter. The protons striking outside the arrows would not enter both the defining and monitor counters, and hence would not cause coincidences.

the standard condenser. The RCA instrument in turn was calibrated several times against a standard potentiometer. The day-by-day calibrations of the system were remarkably uniform, because the graph of the electrometer deflections *vs.* applied voltage was strictly linear in the range of operations.

The calibration data were plotted on a graph giving deflection of the light spot against applied calibration voltage. The best straight line drawn through all the calibration points gives: 1 cm deflection = 0.01238 volts. This figure combined with the capacity of the integrating system yields: 1 cm deflection $=1.250\times10^{-9}$ coulombs collected, which is equivalent to $N_p=7.81\times10^{9}$ protons in the incident beam per cm deflection. The uncertainty in N_p is about 2 percent.

The beam from a synchrocyclotron comes in short bursts about 50 microseconds long and with a recurrence rate of about 600 per second. This produced a very high rate of counting during the pulse for any appreciable average counting rate and so the number of accidental coincidences was significant. The correction for the accidentals is complicated because the background counts in the proportional counters, many times the counts resulting from protons scattered by protons, were caused in part by protons and in part by neutrons. Unfortunately, the neutron pulse, which probably comes from protons striking the dees or deflector, was not of the same length as the deflected proton pulse.

If one assumes that the neutron pulse has a square shape and is of length δ and that the proton pulse has a similar shape but of length $f\delta$, then one can derive a correction formula in the usual way to get:

$$n_a=\frac{2\tau}{R\delta}\left[n_1n_2+\left(\frac{1}{f}-1\right)n_1^{p}n_2^{p}\right] \qquad (1)$$

where n_a is the number of accidentals per second, n_1 and n_2 the total counting rates in each channel, n_1^{p} and n_2^{p} the counting rates in each channel due to protons only, τ the resolving time of the coincidence system, and R the repetition rate. This formula is at least dimensionally correct and since in practice the lumped constant $2\tau/R\delta$, and f were determined under nearly the same conditions that data were taken, the formula can be expected to be a good approximation. The lumped constant $2\tau/R\delta$ was determined to be $(1.0\pm0.1)\times10^{-5}$ seconds^{-1} by observing the accidental rate when the proton beam was shuttered off just before entering the scattering chamber. The background counting rates in the proportional counters were then due altogether to the neutron bursts and the second term in Eq. (1) was zero. The fraction f was determined by misaligning the proportional counters such that the angle between them was sufficiently far from 90° so that no true coincidences should have occurred. Several ten minute runs were made during which n_a, n_1, and n_2 were recorded. After each of these runs, the proton beam was shuttered off and a two-minute run was made to determine the counting rate of the proportional counters due to neutrons only. Subtracting these rates from n_1 and n_2 gave n_1^{p} and n_2^{p} respectively. It was then possible to solve (1) for $(1/f-1)$. The average result of several runs was $(1/f-1)=3.0\pm0.4$ or $f=0.25\pm0.02$.

In a typical cyclotron run of ten minutes duration, the data taken consisted of the number of counts in each channel, i.e., n_1 and n_2, the total number of coincidences, and the electrometer deflection. A blank run of one or two minutes duration during which the shutter was placed in the proton beam was made immediately following most runs. From these data, it was possible to calculate n_1^{p} and n_2^{p} and, by using Eq. (1), the number of accidental counts could be determined and subtracted from the observed number of coincidences to give the true coincidences. Because of the pulsed nature of the beam, the average value of the corrections was rather high, in many cases being about twenty-five percent of the observed coincidences.

In order to assign an absolute value to the scattering cross section it was necessary to know the number of hydrogen nucleii in the nylon scattering foil per square centimeter normal to the beam. This was determined from interferometer measurements of the thickness and a knowledge of the density and composition of the nylon foil.[6]

The Jamin interferometer index was set on the center of a system of white light fringes and then

[6] The foil was obtained from the DuPont Company, Wilmington, Delaware.

the foil, still mounted on its holder, was placed in one of the light paths so that the light passed through the same area of foil and at the same angle as did the protons in the scattering experiment. The compensator shift necessary to bring the fringe system back to index was recorded as c. The fringes were not as sharp as previously because of the inhomogenity of the foil, but the position of the center could be estimated. The compensator was calibrated with sodium light, a shift c' corresponding to one sodium light fringe. In five trials, c was found to be 0.810 ± 1.6 percent and c' to be 0.364 ± 1.4 percent where the errors are r.m.s. deviations from the mean. The index of refraction, n, was determined by a comparison of samples of the same foil with calibrated oils using a geologist's polarizing microscope. These comparisons gave for n values of 1.545 ± 0.003 and 1.520 ± 0.003 for the two directions of polarization. An average of n equal to 1.533 ± 0.004 was used. The estimated probable error is based upon the intervals between the refractive indices of the liquids between which the nylon was bracketed. If λ is the average wave-length of sodium light the thickness of the foil in the direction of the proton beam is given by $t=c/c'\lambda/(n-1)=2.46\cdot10^{-4}$ ±2.3 percent cm.

The number of hydrogen nuclei per square centimeter, N_H, will be given by $N_H=tdh/m$, where d is the density of nylon, h is the fraction of hydrogen in the nylon by weight, and m is the mass of the hydrogen atom. The density was determined by comparing the weight in air and the weight in water (with a wetting agent) of 3 samples of the same material using a micro balance. Each of these trials gave 1.13 g/cm^3 with an uncertainty due to weighing of $\frac{1}{2}$ percent. There is an additional uncertainty of about $\frac{1}{2}$ percent due to water content of the foil. This estimate of the error due to water content is based upon the increase in weight of a vacuum dried sample exposed to humid air. The fraction of hydrogen in the nylon was determined by weighing the water of combustion of weighed samples, which were dried in a vacuum desiccator before combustion with dry oxygen.[7] Two trials gave 0.0986 and 0.0972 with an estimated probable error of ±1 percent. From the formula $(C_{12}H_{22}N_2O_2)_x$ one can compute $h=0.0980$. The DuPont Company reports $h=0.101$ from the weights of the reactants in the nylon polymer. All four of the above determinations were averaged with equal weight to give $h=0.099\pm1$ percent. These data give a value for N_H of $(1.64\pm2\frac{1}{2}$ percent$)\times10^{19}$ hydrogen atoms per square centimeter normal to the beam.

A check on this value of N_H was obtained by comparing the stopping power of the foil with the stopping power of air for 4.05 cm α's in a pulse analyser.[8] The foil was placed at the beginning of the range of the α's and oriented so they went through at the same angle as the protons. It was found that, because of the inhomogenity of the foil, the α's emerged in two groups with a loss of range of 0.22 and 0.30 cm. If the decrease of range, r, is taken as the average of these figures, the number of hydrogen atoms per square centimeter will be, $N_H=hrd_aW_n/mSW_a$, where d_a is the density of air, W_a is the average atomic weight of air, W_n is the molecular weight of nylon, and S is the relative stopping power of nylon. S was computed as 19.68 from the formula $(C_{12}H_{22}N_2O_2)_x$ by using atomic stopping powers tabulated by L. H. Gray.[9] From these numbers one gets $N=1.53\cdot10^{19}$, but the uncertainties in r are so large that this value is given only as a gross check of the value given by the former method.

The energy of the scattered proton varies with scattering angle and incident energy as $E_0\cos^2\theta$. This made it possible to determine the incident energy E_0 by observations of the falling off of the coincidence rate with decreasing angle θ with a 10 mil Al foil placed behind the aperture of the monitor counter. As θ was decreased, the energies of the recoil protons decreased as $E_0\sin^2\theta$ until the energy of the recoil protons was such that only half of them would penetrate the 10 mil Al foil and cause coincidences with the associated scattered protons. This thickness of the Al foil corresponded to the recoil protons' mean range and from this their energy could be determined from the range-energy relationship for protons in aluminum. The angle at which fifty percent of

[7] This was done by Charles Koch, Chemistry Department, University of California, Berkeley, California.

[8] These measurements were made by Albert Ghiorso, Radiation Laboratory, University of California, Berkeley, California.

[9] L. H. Gray, Proc. Camb. Phil. Soc., 40, 72 (1944).

the recoil protons penetrated the foil was determined from a curve of scattering yield plotted as a function of the scattering angle θ. In the region where the range of the recoil protons was close to the thickness of the Al foil, a typical straggling curve was observed. The curve began to drop at a scattering angle of about 42.2° (the intersection of the extrapolation of the linear part of the curve and the 100 percent yield plateau). It reached zero at about 38.2°, and passed the 50 percent point at 40.2°. The Al foil, which was accurately 9.99 mils in thickness, corresponds to the range of a 6.0 Mev proton[10] and dividing this energy by $\cos^2(90–40.2)$ gives 14.5 Mev for the energy of the protons in the cyclotron beam. Since the spread of the curve was close to that expected from straggling and geometry alone, the protons in the incident beam were probably uniform in energy to within a few percent. However, the only precautions that were taken to keep the proton beam monoenergetic were to keep the running conditions of the synchrocyclotron, particularly the deflector voltage and magnetic field, as constant as possible.

The proportional counters were filled with a mixture of argon gas containing five percent CO_2 at a pressure of about 25 cm Hg. The counters were pumped and refilled after every second cyclotron run. Thin nylon foils (2×10^{-4} cm) behind the counter apertures separated the counter volume from the high vacuum of the scattering chamber. The very low specific ionization of the high energy protons made it difficult to obtain good counting plateaus. To correct this difficulty, aluminum absorbers of the proper thickness were placed immediately behind the counter apertures to slow down the protons to an energy of a few Mev. Thus their paths in the counters were nearer the end of their range where the specific ionization was much larger and hence the proportional counter pulses were also much larger. Because the energy of the scattered protons changed so rapidly with angle, it was necessary to use three sets of foils to cover the range of angles under investigation. For angles near 45°, both scattered and recoil protons had an energy of about 7 Mev. Hence aluminum foils of 10 mils thickness were placed behind the apertures of each counter. For scattering angles from $\theta=10°$ to $\theta=18°$, the energy of the scattered proton varied from 14 to 13 Mev. A 43 mil Al foil was used behind the aperture of the defining counter for values of $\theta=10°$, 12° and 14°; and a 38 mil Al foil was used for the data taken at 18°. On the other hand, at these angles the energy of the recoil protons varied between 0.44 and 1.5 Mev and hence no foil except the thin nylon window was used behind the monitor or recoil counter aperture.

To insure that all the 0.44 Mev recoil protons associated with protons scattered at 10° were able to penetrate the nylon scatterer and the nylon counter window, those foils were made as thin as possible by repeated stretching. In addition, the scattering foil was placed at an oblique angle with respect to the incident proton beam so that as short a path as possible in the scatterer was presented to the recoil protons.

It was found that the stopping power of the scattering foil was equivalent to 0.3 cm of air, and since both this foil and the monitor counter window were made in the same way, the two foils together should have a stopping power of 0.6 cm of air and therefore should certainly pass protons of 0.37 Mev. Hence the 0.44 Mev recoil protons should have penetrated both foils easily. This was further checked by one run at $\theta=9°$ where more true coincidences were observed than at $\theta=10°$.

Many experimental troubles were experienced before reliable results were obtained. In part, the difficulties were caused by an underestimation of the accidental coincidences due to the pulsed nature of the synchrocyclotron beam; in part they were caused by an electronic difficulty that developed but which did not become apparent until it manifested itself by a short circuit that could be traced and repaired. A final difficulty was caused by the rapid variation of

TABLE I. Scattering cross sections of 14.5 Mev protons on protons.

$\theta_{c.m.}$	n	$\sigma_{c.m.}$	ϵ
20°	12	4.6×10^{-26} cm²	$\pm0.3\times10^{-26}$ cm²
24°	20	3.1	0.2
28°	7	3.6	0.4
36°	11	3.0	0.3
90°	34	3.34	0.2

[10] J. H. Smith, Phys. Rev. **71**, 32 (1947).

TABLE II. Scattering cross sections of 10 Mev protons[3] (for comparison).

Date	θ_{lab}	Coincidences per proton	Coinc. per proton/cosθ	Mean square error percent	$\sigma_{c.m.}$	$\theta_{c.m.}$
May 11 Foil *A*	45°	102.5	146	1.2	4.90*$\times 10^{-26}$	90°
	25°	129	142	1.4	4.77	50°
	20°	129.5	138	1.4	4.63	40°
	19°	130	137	1.3	4.60	38°
June 1 Foil *B*	45°	123.5	175	0.6	4.90*	90°
	22°	156	169	1.2	4.73	44°
June 16 Foil *C*	28°	53.7	60.8	1.8	4.72	56°
	26°	56.0	62.3	1.2	4.82**	52°
	18°	57.3	60.3	1.2	4.68	36°
	16°	58.1	60.5	1.5	4.70	32°
	14°	61.0***	63.0	2.0	4.88	28°
	12°	67.8****	69.5	3.0	5.39	24°

* The values of σ at 45° were adjusted to 4.90 for foils *A* and *B*.
** The values of σ for foil *C* were adjusted such that the average at 26° and 28° were equal to the value of σ at 25° for foil *A*.
*** The measured value of 60.5 was corrected by +0.8 percent for geometrical and multiple scattering loss.
**** The measured value of 60.5 was extrapolated to 66 using a number-bias curve; then a correction of 3 percent was added for the geometrical and multiple scattering loss.

pulse height with proton energy which is a function of scattering angle. The coincidence circuit resolving time τ originally used was 0.2 microsecond and the rise time of the linear amplifier was also of this order of magnitude. So long as the pulse heights in both counters were equal and large and low relative biases were used, no trouble was experienced in the coincidence circuit. However, when the pulse in one counter is very large and the other pulse is very small, then because of the rise time of the amplifier, the gate caused by the small pulse could have been delayed enough so as not to coincide with the gate caused by the larger pulse which would suffer no appreciable delay. As the scattering angle approached 10°, just such a condition occurred, since the pulses caused by the recoil protons became very large while the pulses caused by the scattered protons became very small. This condition was discovered by measuring scattering yield at a particular angle as a function of coincidence resolving time. At $\theta=45°$, where both proton pulses were the same height, the resolving time was varied from 0.1 μsec. to 0.4 μsec. without measurable effect. However, at $\theta=10°$ in changing from 0.2 μsec. to 0.4 μsec. a considerable increase in the scattering yield was noticed. At $\theta=12°$, 14°, and 18° the effect was intermediate. Hence, for small angles all data taken with the 0.2 μsec. resolving time were rejected. Since the rise time of the linear amplifiers was about 0.2 μsec., it was felt that the coincidence circuit resolving time of 0.4 μsec. was sufficiently large so that no counts were lost because of this effect of different pulse height. This fact was not established experimentally, as at 45°, because going to resolving times greater than 0.4 μsec. would have caused an excessively large accidental coincidence background and, furthermore, the equipment was not designed to produce larger resolving times.

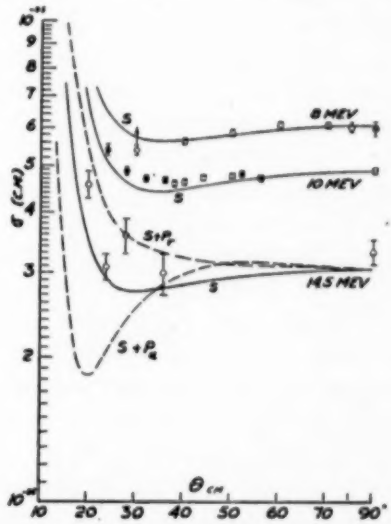

FIG. 3. The differential scattering cross section in the center of mass system as a function of the angle of scattering in the center of mass system. For comparison, the results obtained at 8 Mev[1] and 10 Mev[3] are also given. The measurements at 10 Mev are relative and have been adjusted arbitrarily at 90°. The measurements at 8 Mev are relative to the point at 90° which was determined absolutely. The solid curves represent the theoretically expected scattering on the basis of *S* wave scattering only.

Because of this fact and also the possibility that the foil window in the recoil proton counter was too thick to pass all the recoil protons at 10°, the scattering yield at 10° can be regarded as a lower limit. We feel, however, that neither of the above effects are appreciable in comparison to the final statistical probable error.

The results obtained[11] are given in Table I where θ is the scattering angle measured in the center of mass system (twice the angle actually measured), n is the number of ten minute runs at each angle, $\sigma_{c.m.}$ is the absolute scattering cross section per unit solid angle in the center of mass system, and ϵ is the experimental mean square error determined from the deviations of the values given by the ten minute runs from the mean. The values of σ are plotted in Fig. 3 as a function of θ. The curves were computed by L. L. Foldy on the assumption of a square well of depth 10.5 Mev and width e^2/mc^2 both for S wave scattering alone (solid curve), and for S plus P wave attractive (lower dashed curve) and repulsive (upper dashed curve). Also in Fig. 3, for comparison, are plotted the results obtained at 8 Mev[1] and 10 Mev.[3] The 10 Mev data are also given in Table II as they appear elsewhere[3] only in graphical form. A detailed theoretical analysis of the above experimental work will be included in a forthcoming paper by L. L. Foldy in this journal.

It is a pleasure to express our appreciation to Professor E. O. Lawrence for making the facilities of the Radiation Laboratory available to us.

[11] The values of σ given in Table I are slightly different for small angles than those given by us in a preliminary report, Phys. Rev. 71, 560 (1947) because there the wrong diameter of the defining counter aperture was used in calculating the geometrical loss correction. The correction was calculated correctly for the 10 Mev data.[3]

On the Interaction Between Neutrons and Electrons*

E. FERMI AND L. MARSHALL
Argonne National Laboratory and Institute for Nuclear Studies, University of Chicago, Chicago, Illinois
(Received September 2, 1947)

The possible existence of a potential interaction between neutron and electron has been investigated by examining the asymmetry of thermal neutron scattering from xenon. It has been found that the scattering in the center-of-gravity system shows exceedingly little asymmetry. By assuming an interaction of a range equal to the classical electron radius, the depth of the potential well has been found to be 300 ± 5000 ev. This result is compared with estimates based on the mesotron theory according to which the depth should be 12000 ev. It is concluded that the interaction is not larger than that expected from the mesotron theory; that, however, no definite contradiction of the mesotron theory can be drawn at present, partly because of the possibility that the experimental error may have been underestimated, and partly because of the indefiniteness of the theories which makes the theoretical estimate uncertain.

INTRODUCTION

THE purpose of this paper is to investigate an interaction between neutrons and electrons due to the possible existence of a short range potential between the two particles. If such a short range force should exist, one would expect some evidence of it in the scattering of neutrons by atoms. The scattering of neutrons by an atom is mostly due to an interaction of the neutrons with the nucleus. In addition, there is a somewhat smaller interaction of neutrons and the electron system which has been observed by Bloch and his co-workers in their work on polarization of neutrons. This interaction is due to the magnetic field produced by the electronic currents within the atom acting on the magnetic moment of the neutron and will be referred to as magnetic interaction. Except for negligible higher order perturbations that will be discussed later, the magnetic interaction should not exist for atoms in which the electrons are bound in closed shells. In the present work, noble gases have been used in order to eliminate perturbations due to this magnetic interaction.

Besides the magnetic interaction, one might expect also the existence of a spin independent potential energy between neutron and electron. Such an interaction could be expected, for example, according to the current mesotron theories of nuclear forces. According to these theories, proton and neutron are basically two states of the same particle, the nucleon. A neutron can transform into a proton according to the reaction:

$$N = P + \bar{\mu}. \qquad (1)$$

(N = neutron, P = proton, $\bar{\mu}$ = negative mesotron)

Actually, a neutron will spend a fraction of its time as neutron proper (left-hand side of Eq. (1)) and a fraction of its time in a state that can be described as a proton with a negative mesotron nearby, (right-hand side of Eq. (1)). The system oscillates with extremely high frequency between these two forms and the fraction of the time spent in either of them is different depending on the specific form of mesotron theory.

According to the estimate given in Section 4, the neutron may spend 20 percent of the time as proton and negative mesotron and 80 percent of the time as neutron proper.

If these views are correct, in the immediate vicinity of a neutron one would expect an electric field of a strength equal to that produced by a charge $0.2e$, e being the proton charge. Of course, this field would extend only to a very small distance, because it would be screened by the negative charge of the mesotron, which is present whenever the nucleon is in the proton form. Indeed, the range of this electric force would be of the order of magnitude of the distances of the negative mesotron from the nucleon, that is about 10^{-13} cm. This force should be attractive and could be represented as a potential hole of

* Footnote added in proof: Havens, Rabi and Rainwater (Phys. Rev. 72, 634 (1947)) have published results similar to the present ones obtained by a somewhat different method. Their results are in essential agreement with those of the present work.

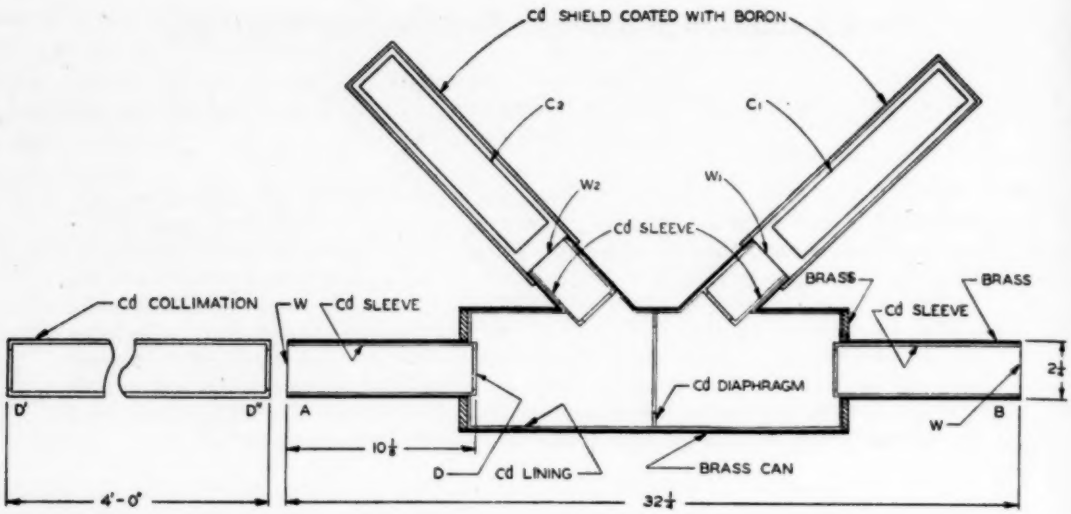

FIG. 1. Diagram of apparatus.

extremely small diameter. In the present paper, an attempt to detect an interaction of this type between neutrons and electrons is described.

If the scattering of neutrons were due only to nuclear interaction, one would expect the scattering to be spherically symmetrical in the center-of-gravity system whenever the wave-length of the neutron is large compared with nuclear dimensions. This last condition is very amply fulfilled for thermal neutrons which have a wave-length of the order of 2×10^{-8} cm, about 20,000 times larger than the nuclear dimensions. One would expect, therefore, that thermal neutrons should be scattered by nuclei in spherically symmetrical waves in the center-of-gravity system.

Deviations from the spherical symmetry can be due to several causes. The scattering atoms may be paramagnetic, in which case there is the magnetic interaction already discussed. A second reason for possible asymmetries in the scattering is interference of the waves scattered by different atoms. Such interference will be expected, both in solid and liquid elements and in gases with more than one atom in the molecule. Finally, asymmetric scattering could be due to a short range potential interaction whose investigation is the main object of this paper.

In order to eliminate the first two types of asymmetry, the experiments to be described were performed on xenon at pressures of the order of one atmosphere. An attempt was made to detect deviations from the spherical symmetry in the scattering of slow neutrons by this element.

If a short range potential interaction between neutron and electron should actually exist, one would expect the scattered waves to result from the interference of a spherically symmetrical wave scattered by the nucleus and a non-symmetrical wave scattered by the electrons. This last wave is expected to be non-symmetrical because the electrons are spread through a region of dimensions of the order of 10^{-8} cm, comparable to the wave-length of the neutrons. The interference of these two waves should make the intensity of the scattered beam a function of the scattering angle, as will be discussed in detail in Section 3.

SECTION 1. EXPERIMENTAL PROCEDURE

The apparatus used for the experiment is shown in Fig. 1. It consists of a tank of the dimensions and shape indicated in the figure, lined with cadmium as indicated, except for the four windows A, B, W_1, W_2. A beam of thermal neutrons from the thermal column of the heavy water pile at the Argonne National Laboratory was allowed to pass along the axis of this tank. The beam was collimated by the cadmium diaphragms D, D'', D' $1\frac{1}{2}$ inches in diameter. The tank was filled with xenon at the pressure of about one atmosphere and the neutrons scattered by the gas were recorded by the 2 BF_3-counters

C_1 and C_2. The counter C_1 records the neutrons scattered at an angle of about 45° with the direction of the primary beam and the counter C_2 records neutrons scattered at an angle of 135°. In order to correct unavoidable differences in sensitivity and geometry between the two counters, all the apparatus can be turned around, so that the neutrons enter through window B instead of entering through window A. Cadmium screens could be inserted in front of the windows W_1 and W_2. In all measurements Cd differences were taken.

Each run of the experiment consisted of four measurements, each of which was a cadmium difference. Two of them were taken with the apparatus in the position indicated in the figure (position A) and two with the apparatus turned around (position B). With the apparatus in position A, one takes first the number of counts in C_1 and C_2 with xenon inside the tank. The counts so observed must be corrected for a background. This is obtained by taking a second series of counts while the xenon is frozen out of the tank into a liquid air trap, not shown in the figure. Let n_{1a} and n_{2a} be the net number of counts per minute in the two counters. The same two measurements are performed successively with the whole tank in position B. Let n_{1b} and n_{2b} be the net number of counts observed in the counters C_1 and C_2 on this second measurement. The expression

$$\rho=[(n_{1a}/n_{2a})(n_{2b}/n_{1b})]^{\frac{1}{2}} \qquad (2)$$

gives the ratio of the scattering in the two directions at 45° and 135° corrected for the possible differences in sensitivity of the two counters.

The numbers from a typical run are given in Table I.

Two series of measurements were made, with two different pairs of counters. In each series, ten complete measurements like the one given above were taken. The consistency of the two series may be seen in Table II.

The result is

$$\rho=1.0235\pm0.0085. \qquad (3)$$

The errors indicated are mean square errors obtained by a statistical study of the consistency of the various runs. They are only slightly larger than the statistical errors calculated from the actual number of counts.

SECTION 2. CORRECTIONS

Some corrections must be applied to the results (3) in order to arrive at the true ratio of the intensities scattered in the center-of-gravity system for scattering angles 45° and 135°.

Although xenon is rather heavy, one cannot altogether neglect the fact that the center of gravity of the neutron-atom system does not coincide with the center of the atom. In computing the correction due to this effect one must also take into account the fact that the scattering atoms are in thermal agitation at room temperature. There is, in addition, a geometrical correction. Although the beam going through the tank is rather well collimated, it still diverges a little while going through the tank. This introduces an asymmetry which is not eliminated by switching the tank from position A to position B and must be, therefore, corrected by calculation. Here is a brief outline of the methods used for calculating these corrections.

TABLE I. Data of a typical run.

Position	Counter	Cd	Xe	c/min	c/min cadmium difference	Net
A	C_1	no	yes	720		
					434	
		yes	yes	286		
						$448=n_{1a}$
		no	no	276		
					−14	
		yes	no	290		
A	C_2	no	yes	690		
					429	
		yes	yes	261		
						$421=n_{2a}$
		no	no	262		
					8	
		yes	no	254		
B	C_1	no	yes	726		
					414	
		yes	yes	312		
						$406=n_{1b}$
		no	no	311		
					8	
		yes	no	303		
B	C_2	no	yes	635		
					400	
		yes	yes	235		
						$392=n_{2b}$
		no	no	227		
					8	
		yes	no	219		

TABLE II. Comparison of data from two pairs of counters.

	$\frac{n_{1a}}{n_{2a}}$	$\frac{n_{2b}}{n_{1b}}$
First pair of counters	1.064	0.916
	1.064	0.975
	0.986	1.030
	1.017	0.920
	1.035	0.966
	1.104	1.019
	1.110	0.919
	1.155	1.019
	1.127	0.964
	—	0.955
Average	1.074±0.018	0.968±0.014
	$\rho=\left(\frac{n_{1a}n_{2b}}{n_{2a}n_{1b}}\right)^{\frac{1}{2}}=1.020\pm0.012$	
Second pair of counters	0.943	1.031
	1.000	1.091
	0.892	1.047
	1.059	1.074
	0.884	1.116
	1.035	1.109
	1.020	1.028
	0.932	1.044
	0.971	1.100
	1.005	1.183
	—	1.093
Average	0.974±0.019	1.083±0.014
	$\rho=\left(\frac{n_{1a}n_{2b}}{n_{2a}n_{1b}}\right)^{\frac{1}{2}}=1.027\pm0.012$	

Combined result: $\rho=1.0235\pm0.0085$.

a. Doppler Effect Correction

We consider an infinitely collimated beam of monochromatic neutrons being scattered by a gas, whose atoms move with a Maxwell distribution of velocity. The scattered neutrons are observed in a direction forming an angle θ with the direction of the primary beam and are observed with a counter covering a small solid angle $\Delta\omega$ Two alternative assumptions are made as to the sensitivity of this counter: (1) the counter is a "thin" detector, in which case the sensitivity follows the $1/v$-law; (2) the counter is a "thick" detector, in which case the sensitivity is independent of the velocity of the neutron. If one assumes that the scattering of the neutrons is spherically symmetrical in the center-of-gravity system, one can calculate in a straightforward way the dependence upon θ of the number of counts recorded. One finds that the angular dependence is represented by the following factors:

For assumption 1,

$$1+\frac{\cos\theta}{A}\left(1+\frac{KT}{MV^2}\right), \tag{4}$$

and for assumption 2,

$$1+\frac{1}{A}\left(2\cos\theta-1+\frac{KT}{MV^2}\right). \tag{5}$$

A is the atomic weight of the scattering atoms, M and V are mass and velocity of the neutrons. In both formulae, terms of the order of $1/A^2$ have been neglected.

In the actual case, the neutrons used were not monochromatic, but had approximately a Maxwellian distribution corresponding to room temperature. The correction factors (4) and (5) must, therefore, be averaged for such a distribution. The correction factors so averaged are for assumption 1,

$$1+(2\cos\theta/A), \tag{6}$$

and for assumption 2,

$$1+(2\cos\theta-\tfrac{1}{2})/A. \tag{7}$$

In the actual cases, θ has the two values 45° and 135°, and we are interested in the ratio of the correction factors for these two values. Within our approximation, this ratio is the same for assumptions (1) and (2) and equal in both cases to:

$$1+\frac{2\sqrt{2}}{A}=1.022 \quad \text{for} \quad \text{Xe}(A=130). \tag{8}$$

b. Other Geometrical Corrections

The experimental results must also be corrected for another reason. The beam entering the tank is collimated by an opening of 1.5 in. diameter at D and an opening of equal diameter at D', the distance between the two being 178 cm. The beam that passes through these two diaphragms is slightly spread and is, therefore, surrounded by a penumbra which increases with the distance from D. Consequently the two counters C_1 and C_2 see a beam of slightly different shape. As already pointed out, this difference between the two counters is not corrected by inversion of the tank.

In order to correct for this effect, the following procedure was adopted. An auxiliary experiment

was carried out in order to determine the sensitivity of the counters to thermal neutrons originating at different places. A counter was surrounded with cadmium, shaped as in Fig. 2, and was mounted on the tool holder of a lathe so that it was possible to move it parallel to itself into any desired position. A small source of thermal neutrons was obtained by exposing a small copper plate weighing about one gram to a beam of thermal neutrons. The neutrons scattered by this copper plate were recorded for a number of positions of the counter. In all cases the average of the readings obtained with the counter at two positions symmetrical with respect to a plane perpendicular to the neutron beam and passing through the copper scatter was taken. This procedure corrects for the asymmetries of the source. In this way, the sensitivity of the counter surrounded by its cadmium shield was mapped as a function of the relative position of the source of scattered neutrons with respect to the counter.

The geometric corrections were calculated by dividing the volume of the beam seen by either of the counters C_1 or C_2 in about 200 parts. For each such section, the intensity of the radiation scattered into each counter was computed using the previously described calibration of the counter sensitivity and all the results were added. In this calculation, the Doppler correction and the correction due to the absorption of the beam were included. This rather lengthy calculation gave the following result.

If the scattering were symmetrical in the center-of-gravity system, the front counter C_1 would record a slightly larger number of counts than the back counter C_2. The ratio of the number of counts would be $\rho=1.024$ in the case of Xe. It should be noticed that this number is quite close to the corresponding number (8) obtained by applying only the Doppler correction and assuming that otherwise the geometry is ideally well collimated. This indicates that the error due to lack of collimation is a minor one. The calculated values of ρ should be compared with the observed value (3). The difference can be attributed to a deviation of the scattering from the spherical symmetry in the center-of-gravity system.

The observed relative difference between forward and backward scattering, with all corrections, is therefore

$$-0.0005\pm0.0085. \tag{9}$$

SECTION 3. CALCULATION OF AN UPPER LIMIT FOR THE ELECTRON-NEUTRON INTERACTION

Both the sign and magnitude of the interaction between neutrons and electrons can be calculated from the ratio of the scattering intensities for the scattering angles 45° and 135°.

A short-range interaction between the neutron and other particles such as the nucleus or the electrons can always be represented in the Hamiltonian by terms proportional to the δ-function of the vector leading from the other particle to the neutron. Accordingly, the interaction of the neutron with the nucleus shall be represented by:

$$a\delta(\vec{r}), \tag{10}$$

and the interaction with each electron by terms of the form,

$$b\delta(\vec{r}-\vec{r}_e), \tag{11}$$

where $\vec{r}$ is the radius vector from the nucleus to the neutron, and $\vec{r}_e$ is the radius vector from the nucleus to one of the electrons. The constants a and b give a measure of the interactions of the neutron with the nucleus and with one electron. They have the dimensions of energy times volume. Indeed, when the interaction is weak, as is

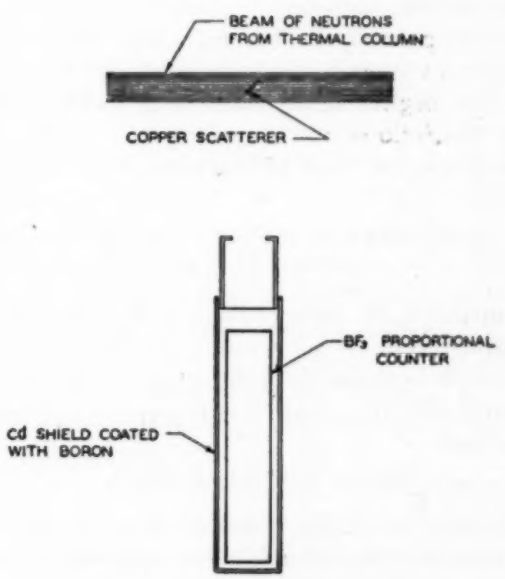

FIG. 2. Arrangement used to make geometrical corrections.

the case for the neutron-electron interaction, the coefficient b is simply equal to the volume integral of the potential energy between the two particles. If the potential energy between electron and neutron is a function $U(r)$ of the distance r between the two particles, then

$$b=4\pi\int_0^\infty U(r)r^2dr. \tag{12}$$

We can now apply the Born approximation in order to find out the scattering in the various directions due to the interactions (10) and (11). A straightforward calculation, based on the Born approximation gives the following differential cross section for scattering within the element of solid angle $d\omega$:

$$d\sigma=\frac{M^2d\omega}{4\pi^2\hbar^4}(a+bZ\mathfrak{F}(\theta))^2. \tag{13}$$

$\mathfrak{F}(\theta)$ represents the form factor of the electron distribution. A simple expression for the form factor has been given by Bethe.[1] By means of his results, the form factors at 45° and 135° can be calculated for Xe ($Z=54$). One finds

$$\mathfrak{F}(45°)=0.776,$$
$$\mathfrak{F}(135°)=0.515.$$

The difference of the form factor for the two scattering angles is responsible for the asymmetry in the scattering.

In the parenthesis of formula (13), the second term is very small compared with the first and one can neglect terms containing b^2. It follows that the ratio of the intensity scattered in two directions at 45° and 135° is given by:

$$1+2Z[\mathfrak{F}(45°)-\mathfrak{F}(135°)]\frac{b}{a}=1+28.2\frac{b}{a}. \tag{14}$$

Comparison of these values with the experimental result (9) allows one to determine the ratio b/a between the interaction constants for neutron-electron and neutron-xenon nucleus. One finds

$$b/a=-0.00002\pm0.00030. \tag{15}$$

In order to obtain b, we calculate the nuclear interaction constant a from the scattering cross section.

The scattering cross section of xenon was determined by comparison of the scattered intensity (average of the net counts in the two counters C_1 and C_2) when the tank was filled with xenon or nitrogen. The scattering cross section of the molecule N_2 was assumed to be 20×10^{-24}. It was found in this way that the scattering cross section of xenon is 4.4×10^{-24}. Disregarding the very small correction due to the electron interaction term b, it follows from (13) that the scattering cross section is given by

$$M^2a^2/\pi\hbar^4. \tag{16}$$

From this formula one finds

$$a=2.46\times10^{-42}\ \text{ergs}\times\text{cm}^3 \quad \text{for Xe.} \tag{17}$$

The sign of a is almost certainly positive. This choice is justified by the fact that nuclear interaction constants have been found to be positive for almost all nuclei.[2]

From (15) and (17) the value of b can be calculated. One finds

$$b=(-5\pm74)\times10^{-47}\ \text{ergs}\times\text{cm}^3. \tag{18}$$

As previously stated, the experimental error is a mean square error computed from the coherence of the various sets of measurements and it is only slightly in excess of the statistical error. In spite of that, one cannot guarantee that the actual value of b will lie within the limits as indicated in formula (18). It should be noted that the interaction constant b is found to be of the order of 10,000 times smaller than the constant of the interaction between a neutron and a proton or even smaller.

If the constant b should ultimately turn out to be negative it would mean that the potential between neutron and electron is negative (attractive force).

According to (12), b is the volume integral of the potential hole. Experiments of the type here discussed do not allow an independent determination of the depth and volume of the potential hole. If one assumes arbitrarily, that the potential hole has a volume equal to the classical volume of the electron,

$$V_{el}=(4\pi/3)(e^2/mc^2)^3=0.94\times10^{-37}\ \text{cm}^3, \tag{19}$$

one finds from (18) the depth of the attractive

[1] H. A. Bethe, Ann. d. Physik **5**, 385 (1930).

[2] E. Fermi and L. Marshall, Phys. Rev. **71**, 666 (1947).

potential to be

$$\overline{U(r)} = b/V_{el} = (-6 \pm 79) \times 10^{-10} \text{ ergs} = -300 \pm 5000 \text{ ev.} \quad (20)$$

Before concluding this section, the effect of two possible perturbations should be discussed. It has been stated in the introduction that for atoms in which the electrons are bound in closed shells, no magnetic interaction between the neutron-electron system is to be expected. While this is certainly true in first approximation, one might, in reality, expect a small perturbation of this type to appear in second approximation, through the interaction of the magnetic moment of the neutron with currents in virtual excited states of the noble gas electron system. A closer discussion shows, however, that the contribution of the second order effect is quite negligible. By applying the conventional methods of quantum mechanics, one can readily estimate the interaction constant corresponding to this perturbation. This constant is found to be of the order of magnitude

$$(e\hbar/2Mc)^2 e^2 \lambda\!\!\!^{-2}/mc^2 R^3 \approx 10^{-48} \text{ ergs} \times \text{cm}^3. \quad (21)$$

In this formula $e\hbar/(2Mc)$ is the nuclear magneton, $\lambda\!\!\!^{-}$ is its wave length divided by 2π, R is the average radius of the electronic orbit.

It is seen that the correction (21) is entirely negligible compared with the value (18) of b.

There is a second possible interaction between neutron and atom that could lead to an asymmetric scattering. When the neutron passes by the atom and penetrates the electronic system, it is exposed to an electric field due to the unscreened part of the nuclear charge. Since the neutron is moving, this electric field in the frame of reference of the neutron gives rise to an apparent magnetic field. This last interacts with the magnetic moment of the neutron, giving rise to a mutual energy, which might be capable of contributing a scattering asymmetry. A closer discussion shows that the error introduced by neglecting this effect is negligible. The main reason is that scattering due to the interaction just mentioned is always connected with a change in the spin direction of the neutron. There can be, therefore, no strengthening of this effect by interference with the large nuclear scattering, since in the latter case, change of the spin direction of the neutron on scattering is always coupled with a change in the spin state of the nucleus.

SECTION 4. COMPARISON WITH THE MESOTRON THEORY

The results (18) or (20) should be compared with the expectations of the mesotron theory.

From the qualitative discussion already given in the introduction it is clear that, according to the mesotron theory, a short-range attractive potential between neutron and electron should be expected. On the other hand, because of the indefiniteness of the mesotron theories, it is not feasible to predict in a precise way the strength of the interaction to be expected. Indeed, most mesotron theories require elimination of divergences by cutting off the field at a distance from the nucleon of the order of 10^{-13} cm, which is just the expected range of the electric field surrounding the neutron.

A second point that should be mentioned in this connection is the influence on the neutron-electron interaction of the size of the electron. If we take the classical picture of the electron as a small sphere throughout whose volume negative electricity is spread, and we assume also, in a purely classical way, that the neutron is surrounded by a short range electric field, one would expect that the range of the interaction is of the order of magnitude of the largest of the two lengths, radius of the electron and range of the electric field surrounding the neutron. If the radius of the electron is larger than the range of the electric field, the interaction will extend, therefore, to a distance of the order of the electron radius. In this sense, the size of the electron influences the expected potential hole in that if the radius of the electron is taken larger, the potential hole becomes shallower and wider. Actually, one can determine on this classical model that the interaction constant, namely, the volume integral over the potential hole, is not influenced by the size of the electron. We can, therefore, in these estimates, regard the electron as a point-charge.

One possible approach to a semi-quantitative estimate of the interaction to be expected, according to the mesotron theory, is the following.

According to the most simple forms of mesotron theory, the wave function describing the

mesotrons in the vicinity of the nucleus is of the form

$$(e^{-\mu cr/\hbar})/r, \tag{22}$$

where μ is the mesotron mass. To this wave function there corresponds a density distribution of the mesotrons proportional to the square of (22); namely, to

$$\frac{\exp[-2\mu cr/\hbar]}{r^2}. \tag{23}$$

One can then calculate in an elementary way the electric field E at a distance r from the center of the neutron,

$$E=\frac{ze}{r^2}\exp[-2\mu cr/\hbar], \tag{24}$$

where z is the fraction of the time that the neutron spends in the state represented by the right-hand side of Eq. (1) (proton and negative mesotron).

From (24) one can immediately calculate the potential energy for an electron in the electric field surrounding the neutron. One finds

$$U=-e\int_r^\infty Edr$$

$$=-ze^2\int_r^\infty (dr/r^2)\exp[-2\mu cr/\hbar]. \tag{25}$$

From (25) and (12) we obtain finally the interaction constant

$$b=-(\pi/3)(ze^2\hbar/\mu^2c^2)^2. \tag{26}$$

A simple procedure for estimating the value of z is given here. One of the objectives of the mesotron theory is to explain the neutron magnetic moment as the magnetic moment of the virtual mesotron field surrounding the neutron. If such an interpretation is correct and if we assume further that each mesotron bears a magnetic moment equal to $e\hbar/2\mu c$, we are led to the estimate that the average number of mesotrons near a neutron is 0.2. Therefore, in calculating the numerical value of (26), we shall use $z=0.2$. Assuming a mesotron mass 200 times larger than the electron mass, we find from (26)

$$b=-1.8\times10^{-45}. \tag{27}$$

If we spread the interaction over the potential hole having the volume (19) we find that the depth of the potential hole is 12,000 ev.

SECTION 5. CONCLUSIONS

The comparison of the last result with the experimentally found depth of -300 ± 5000 ev indicates an experimental value appreciably less than the theoretical estimate. This does not necessarily mean that this experiment decisively contradicts the mesotron theory. On one hand, the experimental error may be somewhat larger than has been indicated. On the other hand, the theory outlined is obviously exceedingly crude. It may very well be that some mesotron theory eventually will lead to a lower estimate of the depth of the well. It would seem that the experimental result is sufficiently conclusive to exclude the so-called strong coupling theories according to which $z=0.5$ and the depth is therefore about 30,000 ev which appears to be well outside of our experimental error.

A final conclusion one might draw from these experiments is that no interaction of an order of magnitude larger than that predicted by the mesotron theory exists between neutron and electron.

Our thanks are due to Dr. A. Wattenberg for help in this experiment.

Scattering of Slow Neutrons by Ortho- and Parahydrogen*

R. B. SUTTON,[a] T. HALL,[b] E. E. ANDERSON,[c] H. S. BRIDGE,[d] J. W. DEWIRE,[e] L. S. LAVATELLI,[f] E. A. LONG,[g] T. SNYDER,[h] R. W. WILLIAMS[i]
University of California, Los Alamos Scientific Laboratory, Santa Fe, New Mexico

Measurements have been made of the scattering cross sections of ortho- and parahydrogen for neutrons of energies in the range 10°K to 30°K. Using the Schwinger-Teller theory the results have been correlated with the scattering cross section of free protons for slow neutrons and with the range of a square-well $n-p$ potential. The measured cross sections show the energy dependence expected from the theory; they imply a free proton cross section of 19.7 barns and a force range of 1.5×10^{-13} cm, the first value agreeing within experimental error with the accepted figure, but the second falling significantly below the result 2.8×10^{-13} cm obtained by Breit, Thaxton and Eisenbud for the $p-p$ force. The singlet state of the deuteron is again shown to be virtual, and the possibility of a neutron spin of $\frac{3}{2}$ is eliminated since the data in this case would imply a free proton cross section of only 7 barns.

1. INTRODUCTION

THE values of the total scattering cross sections of ortho- and para-hydrogen give information about the range of the neutron-proton force, the dependence of this force on the relative orientation of the spins of the neutron and proton, and the binding energy of the singlet state of the deuteron; also the scattering cross section for neutrons by free protons can be obtained.[1]

The scattering cross section of slow neutrons by free protons can be written as the sum of two terms

$$\sigma=\tfrac{3}{4}\sigma_1+\tfrac{1}{4}\sigma_0,$$

where $\sigma_1=4\pi a_1^2$ and $\sigma_0=4\pi a_0^2$. The scattering cross section for the case of parallel spins is σ_1 and for the case of anti-parallel spins is σ_0. The scattering amplitudes, a_1 and a_0, are given by

$$a_1=k^{-1}\sin\delta_{0,1},\quad a_0=k^{-1}\sin\delta_{0,0},$$
$$k=(\tfrac{1}{2}ME_1)^{\frac{1}{2}}/\hbar,$$
E_1 = neutron energy (laboratory system),
M = neutron mass.

The δ's are the phase shifts of the scattered neutron wave with respect to the incident wave, and depend on the form of the neutron-proton interaction. With the assumption of a square-well form of the potential function representing the neutron-proton interaction, each phase shift can be expressed in terms of the width, a (assumed the same for the singlet and triplet interaction) and the depth of the well, or in terms of a and the binding energy of the deuteron state in question. Thus a determination of a_1 will yield a value of a since the binding energy of the deuteron in the triplet state is known. The relative signs of a_1 and a_0 indicate whether the singlet state of the deuteron is real or virtual. The value of a_0 and of a will give the binding energy in the singlet state. As is shown in reference 1, when scattering occurs from hydrogen molecules the cross section per molecule is a combination of a_1 and a_0 which differs depending on whether the scattering occurs from ortho- or parahydrogen. Thus a knowledge of the ortho- and parahydrogen cross sections can be used to obtain a_1 and a_0.

Early experiments by Halpern, Estermann, Simpson and Stern[2] and by Brickwedde, Dun-

* This paper is based on work performed under Contract No. W-7405-Eng-36 with the Manhattan Project at the Los Alamos Scientific Laboratory of the University of California.

[a] Now at Carnegie Institute of Technology, Pittsburgh, Pennsylvania.
[b] Now at University of Chicago, Chicago, Illinois.
[c] Now at Milwaukee-Downer College, Milwaukee, Wisconsin.
[d] Now at Massachusetts Institute of Technology, Cambridge, Massachusetts.
[e] Now at Cornell University, Ithaca, New York.
[f] Now at Harvard University, Cambridge, Massachusetts.
[g] Now at University of Chicago, Chicago, Illinois.
[h] Now at General Electric Research Laboratories, Schenectady, New York.
[i] Now at Massachusetts Institute of Technology, Cambridge, Massachusetts.

[1] J. Schwinger and E. Teller, Phys. Rev. 52, 286 (1937).

[2] J. Halpern, I. Estermann, O. C. Simpson, and O. Stern, Phys. Rev. 52, 142 (1937).

ning, Hoge, and Manley[3] on the scattering of slow neutrons by various ortho-para-concentrations of liquid hydrogen showed the ortho-hydrogen cross section to be several times larger than the para-hydrogen cross section. From these results it was shown that the neutron-proton force was spin dependent and that the singlet state of the deuteron was virtual. However, the neutron energies used were high enough to cause para- to ortho-hydrogen conversion so that the elastic para-cross section could not be determined. Further, the liquid used for the scattering material may have introduced effects due to intermolecular forces. Therefore the experiment was repeated by Alvarez and Pitzer[4] using the time-of-flight technique to obtain very slow monochromatic neutrons, and using a 40 cm path of hydrogen gas as a scattering material. The ortho- and para-hydrogen cross sections were obtained for 20°K neutrons by measurement of the transmission through gas of normal ortho-para-concentration (75 percent, 25 percent) and through 99.8 percent pure parahydrogen; the gas in each case was kept at 20.4°K. Results of this experiment gave $\sigma_o' = 100 \pm 3 \times 10^{-24}$ cm^2 and $\sigma_p' = 5.2 \pm 0.6 \times 10^{-24}$ cm^2 per molecule (where the primes refer to values not corrected for Doppler effect, and the subscripts o and p refer to ortho- and para-hydrogen respectively). Thus the results and conclusions from the previous experiments were verified. However, an analysis of these data by Schwinger[5] gave a value of a for a rectangular-well of either zero or 8×10^{-13} cm, and a free proton scattering cross section of 16.6×10^{-24} cm^2. Both of these results were in disagreement with existing values. The measured neutron-proton scattering cross section is about 20×10^{-24} cm^2; the proton-proton force range which might have been expected here is 2.8×10^{-13} cm. Because of these discrepancies it was decided to reinvestigate the problem.

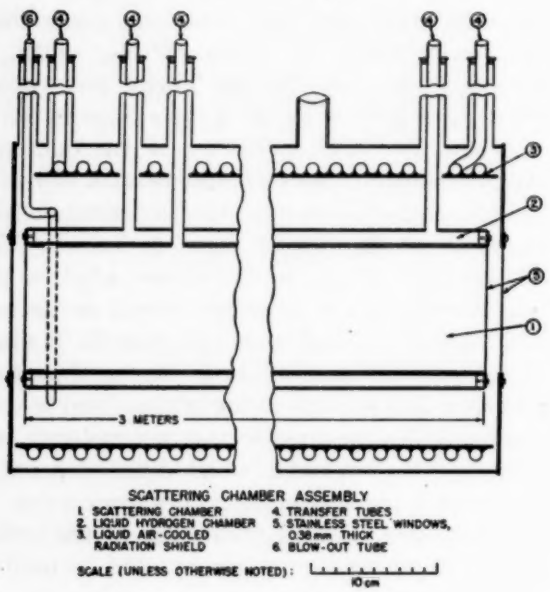

FIG. 1.

2. EXPERIMENTAL METHOD AND APPARATUS

The experimental method used was that of measuring the transmission of neutrons through samples of ortho- and para-hydrogen gas at about 20°K.

The following considerations affect the choice of scatterer and of neutron energy. In order to avoid effects which might arise due to intermolecular forces in the scattering material, it is preferable to have the hydrogen in the gaseous state. The energy of the neutrons with respect to the hydrogen molecule must be below 0.023 ev (260°K) to avoid inducing para- to ortho-transitions, the cross section for this process being many times the para-elastic cross section. As a result, the scatterer used was hydrogen gas in a tube at the temperature of liquid hydrogen boiling at a pressure of about 60 cm of mercury. The range of neutron energies used was from 0.0008 ev (~10°K) to 0.0025 ev (~30°K).

The scattering chamber assembly is shown in Fig. 1. A central brass cylinder, 4 in. diameter, 3 meters long, was sealed at the ends with 0.015 in. thick stainless steel windows and was surrounded by a concentric brass cylinder of the same length and 5 in. diameter. The central cylinder contained the scattering gas, and the shell between the two cylinders was filled with the refrigerant liquid hydrogen. This assembly was in turn mounted inside a radiation shield, consisting of a brass tube of 7½ in. diameter, wrapped with ½ in. copper tubing, through which liquid air was circulated. The outside vacuum

[3] F. G. Brickwedde, John R. Dunning, Harold J. Hoge, and John H. Manley, Phys. Rev. **54**, 266 (1938).
[4] Luis W. Alvarez and Kenneth S. Pitzer, Phys. Rev. **58**, 1003 (1940).
[5] J. Schwinger, Phys. Rev. **58**, 1004 (1940).

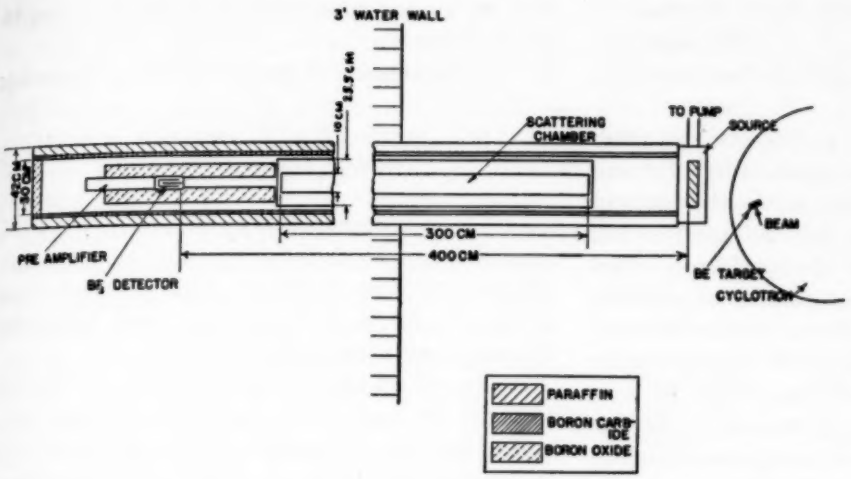

FIG. 2. Experimental arrangement. (In the legend for Fig. 2, shading lines for paraffin should be rotated through 90°. The shading in the figure should continue to the right-hand side of the diagram.)

case, through which the transfer and lead-in tubes passed, was a brass cylinder of 10 in. diameter. The inner containers were supported by the transfer tubes, as shown, and by appropriately placed micarta spacers. The design was very similar to that used by Alvarez and Pitzer,[4] but gave a much longer path length.

The thermal insulation was remarkably good. Despite the large size of the assembly, it was possible with fifty liters of liquid hydrogen to cool the scattering chamber to liquid hydrogen temperatures and to maintain very steady thermal conditions for a period of 15 to 20 hours.

Neutrons of high energy were produced by bombarding a beryllium target with deuterons in the 42-inch Los Alamos cyclotron. These neutrons were slowed down in paraffin placed as near to the target as possible (see Fig. 2). In order to increase the number of subthermal neutrons the paraffin source was cooled to liquid air temperature. This increased the yield of these neutrons by about a factor of four over the yield from the paraffin at room temperature; it also shifted the maximum of the number-velocity distribution from 3300 meters per second to 2000 meters per second.[5a] The paraffin moderator was 5 cm thick and was supported below a liquid air chamber; copper cooling vanes attached to the chamber passed through and around the paraffin. The assembly was mounted in a vacuum chamber. This thickness of paraffin has been found to give maximum slow neutron intensity and have only about 100 μsec. neutron half-life when at room temperature. It was assumed that the lifetime could be only lower when the paraffin was at liquid air temperature.

As shown in Fig. 2, the paraffin source was at one end of a collimator, inside of which the scattering chamber and detector were placed. The purpose of the collimator was to make certain that the only neutrons reaching the detector came from the source and went through the scatterer. The collimator was constructed of a layer of B_4C (1.3 g per cm^2) surrounded by 5 cm of paraffin. To prevent neutrons which were scattered in the liquid hydrogen surrounding the scattering chamber from reaching the detector, the scattering chamber was lined with 0.030-inch cadmium sheet. Further collimation was provided by a cadmium diaphragm between the source and scattering tube; the opening in the diaphragm was slightly smaller than the windows in the scattering tube. The detector was surrounded by a B_2O_3 collimator of $3\frac{1}{2}$ in. wall thickness. To demonstrate the adequacy of the shielding, the exit window of the scattering tube was covered with cadmium. No neutrons in the 10°K to 30°K region were observed.

The time of flight of the neutrons was measured by a modulation method, similar to that described by Baker and Bacher,[6] by Bacher,

[5a] The characteristics of liquid hydrogen as a moderator were also investigated. By the use of this the neutron intensity in the 20°K region was increased by about a factor of ten over the intensity from room temperature paraffin. The maximum of the number-velocity curve occurred at about 1540 meters per second.

[6] C. P. Baker and R. F. Bacher, Phys. Rev. **59**, 332 (1941).

Baker and McDaniel,[7] and by B. D. McDaniel.[8] The modulation equipment and BF_3 detector were constructed at Cornell University and are described in reference 8.

The beam modulation required for the time-of-flight measurement was obtained by applying the voltage to the cyclotron arc in the form of square pulses. Even when this voltage was off, ions were accelerated in the cyclotron. This resulted in a neutron background of uniform intensity around the modulation cycle. Although this intensity was not serious for measurements on room temperature neutrons, where the neutron intensity was high, it was necessary to remove this background in the present experiment since the intensity of 20°K neutrons was quite low. This was accomplished by also modulating the cyclotron dee-voltage so that acceleration could take place only during a 300 μsec. time interval which began at the time the arc was turned on.

In an experiment such as this one there is possibility of error arising from the counting of scattered neutrons. The amount of the effect will depend on the geometry of the experiment. Two types of such error were considered. One may be due to neutrons which scatter elastically through a very small angle and hence reach the detector at their proper time. Another may be due to neutrons initially of energy too high to arrive at the detector at a time such that they would be counted, but which are slowed down by an inelastic collision to such a velocity that they may arrive at a time when pulses are being recorded. Calculation showed that the first type of effect gives a ratio of elastically scattered to transmitted intensity of about 10^{-3} for the geometry used, and the second type gives a ratio of about 10^{-6}.

The transmission of the scattering gas for any one of the time-of-flight (energy) intervals was obtained by the following method. The number of counts C_A occurring in the given energy interval and the total number of counts T_A over the whole cycle (i.e., for all energies) were each recorded for a number of runs with the scattering gas in the chamber. Similar readings, C_B and T_B, were taken for runs with no scattering gas in the chamber.

The transmission of the gas was then given by

$$\frac{C_A}{T_A} \div \frac{C_B}{T_B} \times N,$$

where N is a normalization factor equal to the ratio of T_A to T_B each for the same neutron flux incident on the scatterer. This method thus eliminates effects of changes in sensitivity of the BF_3 counting system during a run.

C (for each of the twelve channels) and T were recorded for each of several runs of about one-half to one hour duration with the scattering gas in. The number of counts from a stable neutron monitor (fission detector) was also recorded for each run. The gas was pumped out and several blank runs were taken. If the sensitivity of the BF_3 system was stable, N could be obtained from the total counts and the monitor counts. In order to eliminate effects of possible changes in sensitivity in the counting system N was also obtained by measuring the ratio of total counts to monitor counts for several two-minute intervals, and measuring the sensitivity of the BF_3 system between each interval with an $\alpha-Be$ source. This was done with the scatterer in and with the scatterer out. If we call the ratio

$$\frac{\text{(Total counts/Monitor counts)}}{\text{Total counts per sec.}}$$

(the counts in the numerator being due to the beam, those in the denominator due to the $\alpha-Be$ source) A for scatterer in and B for scatterer out, then N is given by A/B.

The transmission is related to cross section in the following way:

$$T=e^{-nl\sigma_t} \tag{1}$$

where n = number of hydrogen molecules per cc, l is the length of the scattering path and σ_t is given by

$$\sigma_t=f_o\sigma_o+f_p\sigma_p+\sigma_c, \tag{2}$$

f_o is the fraction of hydrogen molecules in the ortho-state, f_p the fraction in the para-state, σ_o and σ_p are the scattering cross sections of ortho- and para-hydrogen respectively, and σ_c is the capture cross section per molecule. Thus in order to determine σ_o and σ_p it is necessary to

[7] R. B. Bacher, C. D. Baker, and B. D. McDaniel, Phys. Rev. 69, 443 (1946).
[8] B. D. McDaniel, Phys. Rev. 70, 832 (1947).

know f_o and f_p, for two different concentrations of scattering gas, and σ_e. σ_e at the neutron energies used was obtained by extrapolation of the measured value for 0.025 ev, assuming σ_e varied inversely with neutron velocity. The value used for 0.025 ev neutrons was 0.62×10^{-24} cm^2 per molecule.[9]

One scattering sample was 99.9 percent parahydrogen. To obtain this sample, liquid hydrogen was condensed over activated charcoal for a period of about 48 hours. Measurements of the thermal conductivity of the gas evaporated from this liquid were made at intervals of time, by the method described in Farkas and Farkas.[10] When the conductivity showed no further change with time it was assumed that equilibrium had been reached. At this point $f_p=0.999$ and $f_o=0.001$. Samples of gas were taken when the parahydrogen had been introduced into the scattering chamber, and also when the scattering runs were completed. These samples showed the same conductivity as a sample taken from the converter. Thus it was concluded that the concentration had remained unchanged during the experiment.

For the second concentration normal hydrogen gas was used. The equilibrium concentration at room temperature in this case is $f_o=0.75$ and $f_p=0.25$. It was apparent that when the gas was kept in the scattering chamber at liquid hydrogen temperatures, conversion from ortho- to parahydrogen took place. The rate of conversion was such that over a period of about six hours f_o went from 0.75 to 0.45. Several runs, each of about one-half hour duration, were taken with each filling of scattering gas. N as a function of time was obtained by measuring the ratio A (defined above) at several times while each filling was in the scattering chamber. The value of N used for each run was that corresponding to the time half-way through the run in question.

The rate of conversion from ortho- to parahydrogen could be obtained in two ways. First, samples of gas were taken from the scattering chamber at the conclusion of the series of runs and f_o is measured. (The concentration at the

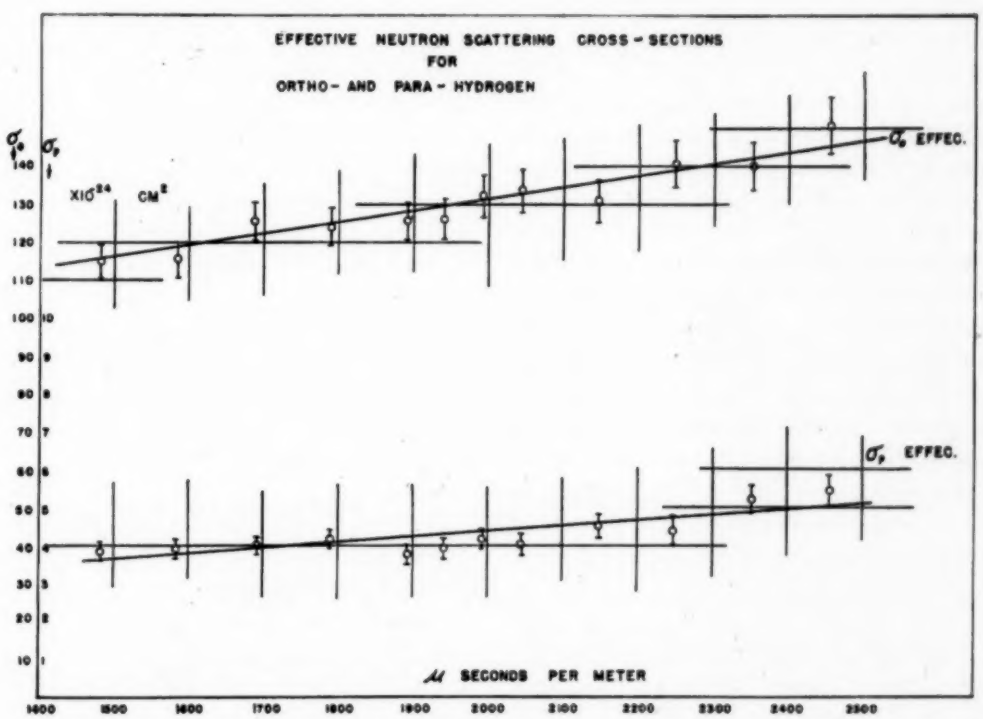

FIG. 3.

[9] This value was obtained from work done on the Manhattan Project.
[10] A. Farkas and L. Farkas, *Orthohydrogen, Parahydrogen and Heavy Hydrogen* (Cambridge University Press, 1935).

time of filling the scattering tube was $f_o=0.75$.) Since conversion is expected to occur at an exponential rate,[10] f_o at any time could be found. A second method for determining f_o *vs.* time was possible by making use of the variation of the transmission with time. The experimental results indicated that $\log\sigma_t$ *vs.* time was a straight line (actually the sum of the values of $\log\sigma_t$ for each of the twelve time-of-flight regions was plotted). This is to be expected since σ_p is so much smaller than σ_o. Since Eq. (2) can be written as

$$d(\log f_o)/dt = (1+(\sigma_p+\sigma_c)/(\sigma_o-\sigma_p)f_o)d(\log\sigma_t)/dt \quad (3)$$

the slope of $\log f_o$ *vs.* time could be obtained. (Since the term on the right-hand side of the equation contains f_o and since $\log f_o$ *vs.* time should be a straight line, it is not accurately true that $\log\sigma_t$ *vs.* time should be a straight line. However, the term $(\sigma_p+\sigma_c)/(\sigma_o-\sigma_p)f_o$ has a value only about 0.09, so that changes in f_o such as occurred from the first to the last run in a series made on one gas filling can change the value of the term in the brackets by only about 5 percent. This leads to a maximum error of 2 percent in f_o obtained from the curve of f_o *vs.* time in this manner.)

Unfortunately the two determinations did not agree; in fact the values of f_o, corresponding to seven hours in the scattering chamber, given by the two methods differed by as much as 20 percent.

The values used for f_o were obtained from the transmission data. This method was assumed to give more nearly correct results since not only did this method give the expected time variation of f_o (whereas only the end points could be obtained by the conductivity method) but also f_o was essentially determined from the entire sample of gas, whereas the thermal measurements were made on a small sample taken from the chamber. These samples could lead to error if, for example, the ortho-para-concentration was not uniform in the scattering chamber.

In the case of the para-measurement the results given were obtained in five runs on one filling of para-hydrogen, and in two runs with no gas in the chamber. With gas in, the lowest number of counts in one channel was 1000, the highest 14,000. With gas out, these were 800 and 10,800 respectively. The pressure of gas used was about 55 cm Hg. The transmission measured varied from 0.58 to 0.45 over the energy region used. The cross section is shown in Fig. 3. The errors shown are made up of the probable errors obtained from the number of counts and the errors in A and B, obtained from the mean square deviations in the separate values (2.9 percent). The value of σ plotted have not been corrected for Doppler effect due to the thermal motion of the H_2 molecules.

In the ortho-measurement, two fillings of the scattering chamber were used. On one filling three runs were taken, the lowest and highest number of counts recorded being 640 and 10,000 respectively. On the other filling five runs were taken, the corresponding counts being 880 and 13,000. Six runs were taken with no gas in the chamber. The lowest and highest number of counts were 2000 and 25,000 respectively. Gas pressures of about 7 cm Hg were used; the transmissions were about 0.40. The cross sections obtained from the two sets of runs differed by only 2 percent. Figure 3 shows the average of both sets. The errors shown consist of the probable errors from the number of counts, the errors in A and B (1.5 percent), and an estimated error of 2 percent in f_o.

TABLE I. Theoretical dependence of effective cross section on energy.

$\sigma'_{\text{ortho}}=(2k'_{1,1}+k'_{1,0})(a_1-a_0)^2+k'_{1,1}(3a_1+a_0)^2$;
$\sigma'_{\text{para}}=k'_{0,0}(3a_1+a_0)^2$.

Neutron energy, ev	$k'_{1,1}$	$k'_{0,0}$	$k'_{1,0}$	$2k'_{1,1}+k'_{1,0}$
0.0008673	7.702	7.696	2.158	17.563
0.001250	6.953	6.946	1.853	15.760
0.001463	6.685	6.675	1.741	15.112
0.001723	6.435	6.423	1.637	14.506
0.001830	6.351	6.338	1.601	14.302
0.002386	6.012	6.000	1.460	13.484

3. INTERPRETATION OF RESULTS

The theory of slow neutron scattering in ortho- and para-hydrogen is given in reference (1), where it is shown that

$$\sigma_{000;\,000}=k_{0,0}(3a_1+a_0)^2,$$
$$\sigma_{000;\,101}=k_{1,0}(a_1-a_0)^2, \quad (4)$$
$$\sigma_{101;\,101}=k_{1,1}[(3a_1+a_0)^2+2(a_1-a_0)^2],$$

where $\sigma_{J'v's';Jvs}$ is the cross section for the

TABLE II. Values of free proton cross section σ_f and force range a implied by observed values σ'_{ortho} and σ'_{para}.

Neutron energy, ev	Obs. σ'_{ortho}, barns	Obs. σ'_{para}, barns	$(3a_1+a_0)^2$ barns	$(a_1-a_0)^2$ barns	$-a_1$, 10^{-12} cm	a_0, 10^{-12} cm	σ_f, barns	a, 10^{-12} cm
0.0008673	145	4.98	0.647	7.97	0.505	2.32	19.3	1.33
0.001250	133	4.40	0.634	8.10	0.510	2.33	19.6	1.43
0.001463	128	4.19	0.628	8.19	0.518	2.34	19.8	1.58
0.001723	124	3.97	0.618	8.20	0.520	2.34	19.8	1.61
0.001830	122	3.90	0.615	8.25	0.522	2.35	19.9	1.65
0.002386	116	3.58	0.597	8.26	0.526	2.35	19.9	1.72

process in which the H_2 molecule goes from rotational level J to J', vibrational level v to v' and spin state s to s'; the $k_{v',v}$ are functions of the neutron energy given explicitly in reference (1), Eqs. (38) and (40), and a_1 and a_0 are the amplitudes of the triplet and singlet, scattered waves, respectively.

However, because of the thermal motion of the H_2 molecules, one measures not the actual cross section at the energy of the neutron beam, but an average of the cross section weighted over an energy range; i.e., for a beam of neutrons of velocity v the measured cross section σ' is

$$\sigma'(v)=\frac{1}{v}\int_{\underline{u}}|v-\underline{u}|\sigma(|\underline{v}-\underline{u}|)N(\underline{u})d\underline{u}, \quad (5)$$

where $N(u)$ is the distribution of the molecular velocity u. Hamermesh and Schwinger[11] have obtained expressions for the quantities σ' by expanding the functions $k_{v',v}$ as power series in the neutron energy E_1, substituting the early terms of the series into (5) and integrating exactly. They thus obtain a new set of functions $k'_{v',v}$ which, replacing the $k_{v',v}$ in (4) will give the *effective* cross section $\sigma'_{J'v's';Jvs}$. The coefficients $k'_{v',v}$ have been calculated for the energies of this experiment using the Schwinger-Hamermesh expressions; the values are listed in Table I. The temperature of the H_2 gas was taken to be 19.5°K and the average separation $\bar{r}$ of the protons in the H_2 molecule to be 0.765×10^{-8} cm.[12] We are grateful to Drs. Hamermesh and Schwinger, who provided us with the expressions described in reference (11) and in addition recalculated the coefficients at neutron energy 20°K, and to Mr. Benjamin Sussholz who carried out an independent evaluation of the quantities $k'_{0,0}$, using expressions of a different form, thus insuring the results of a rather involved calculation.

In this experiment, the H_2 gas, at the low temperature of 20°K, is all initially at the zero vibrational level and zero or first rotational level, the zero rotational level occurring only with the para spin state and the first rotational level only with the ortho spin state. In addition, the neutrons to be counted are all too slow to produce the rotational or vibrational level changes 0→1 or the rotational change 1→2. For these reasons the only possible collision processes are those of Eq. (4). Accordingly for these measurements

$$\begin{aligned}\sigma'_{para}&=\sigma'_{000;\,000}=k'_{0,0}(3a_1+a_0)^2,\\ \sigma'_{ortho}&=\sigma'_{000;\,101}+\sigma'_{101;\,101} \quad (6)\\ &=(2k'_{1,1}+k'_{1,0})(a_1-a_0)^2+k'_{1,1}(3a_1+a_0)^2.\end{aligned}$$

Substitution of the experimental results into (6) yields values of $(a_1-a_0)^2$ and $(3a_1+a_0)^2$. These imply a value for the free proton cross

TABLE III. Values of σ'_{ortho} and σ'_{para} implied by $\sigma_f=20.8$ barns and $a=2.8\times10^{-12}$ cm.*

Neutron energy, ev	Implied σ'_{para} barns	Implied σ'_{ortho} barns
0.0008673	2.86	155
0.001250	2.58	139
0.001463	2.48	134
0.001723	2.39	128
0.001830	2.36	127
0.002386	2.23	119

* Implied values are: $-a_1=0.584\times10^{-12}$ cm; $a_0=2.36_3\times10^{-12}$ cm; $(a_1-a_0)^2=8.679$ barns; $(3a_1+a_0)^2=0.372$ barns; $\sigma'_{ortho}=8.679\times(2k'_{1,1}+k'_{1,0})+0.372k'_{1,1}$; $\sigma'_{para}=0.372k'_{0,0}$.

[11] M. Hamermesh and J. Schwinger, Phys. Rev. **55**, 679 (1939).

[12] The exact procedure for calculating the $k'_{v',v}$ is to substitute average values for r, r^2, etc. as they occur in the theoretical formula; formulae obtained in this way are given in a forthcoming paper by Hamermesh and Schwinger in Phys. Rev. In the present paper, r has been replaced by $\bar{r}$ wherever it occurs, with a consequent error of about ⅓ percent in the $k'_{v',v}$.

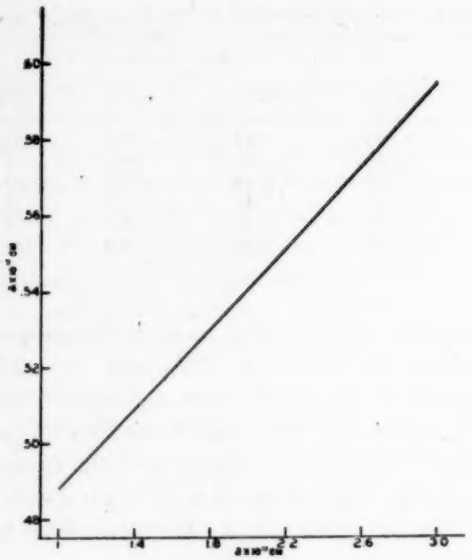

FIG. 4. Theoretical dependence of amplitude a_1 on range a.

section σ_f since

$$\begin{aligned}\sigma_f&=\tfrac{3}{4}\sigma_1+\tfrac{1}{4}\sigma_0\\&=\tfrac{3}{4}(4\pi a_1^2)+\tfrac{1}{4}(4\pi a_0^2)\\&=\frac{\pi}{4}[(3a_1+a_0)^2+3(a_1-a_0)^2].\end{aligned}\tag{7}$$

In order to obtain an implied value for the force range, we also get from Eqs. (6) values for a_1 and a_0 themselves, and then use the theoretical relation between a_1 and a as given by Breit and Kittel.[13] Of the four sets of solutions to Eqs. (6), the two with positive a_1 are ruled out because the triplet state, being real, must have a negative a_1,[14] and a third solution is ruled out because the implied value of the force range is much too large (8 or 9×10^{-13} cm). The remaining solution may be substituted into the theoretical relation, which, for slow neutrons (of energy much less than the deuteron binding energy), is simply[13]

$$\begin{aligned}\alpha^2a_1^2=1+\alpha a+0.3447\alpha^2a^2\\+0.0246\alpha^3a^3-0.0117\alpha^4a^4+\cdots\end{aligned}\tag{8}$$

where $\alpha=(M|E_0|/\hbar^2)^{\frac{1}{2}}=2.29\times10^{12}$ cm^{-1}, M = neutron mass, and E_0 = binding energy (triplet state). The relation (8) between amplitude and force range is shown in Fig. 4.

Given any two of the values σ'_{ortho}, σ'_{para}, σ_f and a, one may infer the remaining two by use of Eqs. (6), (7), and (8). Thus in Table II the data of this experiment are used to predict σ_f and a. σ_f compares well with the directly measured cross section 21×10^{-24} cm^2.[15] ** a appears to differ from the value found for the p-p force range which was found to have a most probable value 2.8×10^{-13} cm, and to fall definitely within the interval 2.8×10^{-13} cm ±25 percent.[16]

One may prefer to consider the correlation in the opposite manner; in Table III and Figs. 5 and 6 the accepted numbers $\sigma_f=20.8$ barns and $a=2.8\times10^{-13}$ cm are used to predict σ'_{ortho} and σ'_{para}; the same is done in Table IV and Figs. 5 and 6 for the values $\sigma_f=19.7$ barns and $a=1.54\times10^{-13}$ cm, which provide the best fit for our data. Tables II–IV and Figs. 5 and 6 together give fully the relations between theory and experiment for these two pairs of quantities.

4. DISCUSSION

The implied value of the free proton cross section agrees within experimental error with direct measurements. However, the implied force range cannot be brought into coincidence with the p-p measurements.

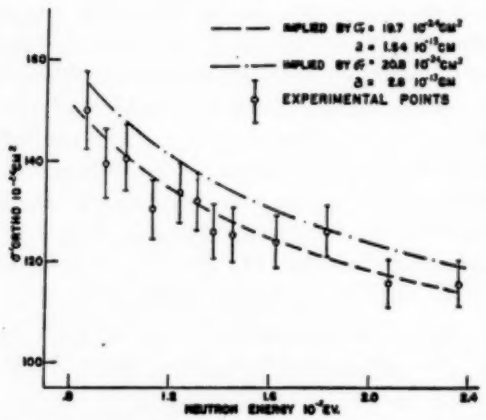

FIG. 5. Effective orthohydrogen cross section.

[13] Breit and Kittel, Phys. Rev. 56, 744 (1939).
[14] E. Fermi, Ricerca Scient. VIII–II, 13 (1936).
[15] Henry B. Hanstein, Phys. Rev. 59, 489 (1941).
** This value is in good agreement with that of 20.8 $\times10^{-24}$ cm^2 which was based on measurements by members of the Manhattan Project.
[16] Breit, Thaxton, and Eisenbud, Phys. Rev. 55, 1018 (1939).

Because of the smallness of $(3a_1+a_0)^2$ as compared to $(a_1-a_0)^2$, σ'_{ortho} and σ_f are dependent almost entirely on each other alone (see Eqs. (6) and (7)). Hence it is the ortho-measurement which gains added reliability from the check obtained with the well-established value σ_f, and any significant error in the implied range must be due to the observed σ'_{para}. A comparison of the σ'_{para} columns in Tables II, III, and IV shows that the observed σ'_{para} would have to be about 60 percent too large if the deviation from the p-p range were caused in this way. One systematic error which could produce this discrepancy would be the contamination of the para-gas with ortho-. A contamination of about one to two percent would be sufficient to account for this. If a determination with a second para sample had been made, this possibility would perhaps have been reduced. If the hydrogen capture cross section does not vary inversely with neutron velocity over such a wide range of velocities, then the para-hydrogen cross section can be considerably different from the values given, since at the energies used the capture and scattering cross sections are of comparable magnitude.

The errors described in the experimental section add to about ±5 percent for both para- and ortho-. Since the energy dependence of the cross sections is in good agreement with theory, we may obtain the limits of the implied range by giving a spread of ±5 percent (which will be about three times the probable error) to the average values of $(a_1-a_0)^2$ and $(3a_1+a_0)^2$ listed in Table II. This permits a maximum square-well range of 1.99×10^{-13} cm and a minimum of 1.12×10^{-13} cm.

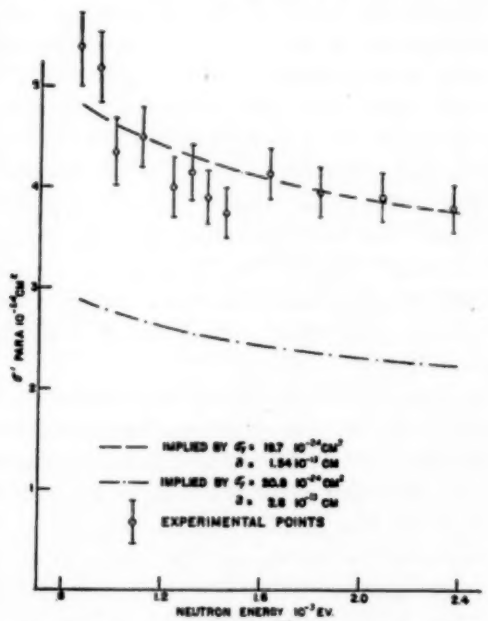

FIG. 6. Effective parahydrogen cross section.

TABLE IV. Values of σ'_{ortho} and σ'_{para} implied by $\sigma_f=19.7$ barns and $a=1.54\times10^{-13}$ cm.*

Neutron energy, ev	Implied σ'_{ortho} barns	Implied σ'_{para} barns
0.0008673	148	4.82
0.001250	133	4.35
0.001463	127	4.18
0.001723	122	4.02
0.001830	121	3.97
0.002386	114	3.76

* Implied values are: $-a_1=0.516\times10^{-13}$ cm; $a_0=2.33_9\times10^{-13}$ cm; $(a_1-a_0)^2=8.151$ barns; $(3a_1+a_0)^2=0.626$ barns; $\sigma'_{\text{ortho}}=8.151\times(2k'_{1,1}+k'_{1,0})+0.626k'_{1,1}$; $\sigma'_{\text{para}}=0.626k'_{0,0}$.

The results indicate that the neutron spin must be $\frac{1}{2}$ rather than $\frac{3}{2}$. The scattering theory was generalized to arbitrary neutron spin by Schwinger;[17] for neutron spin $\frac{3}{2}$ his formulae reduce to

$$\sigma'_{\text{para}}=\tfrac{1}{4}k'_{0,0}(5a_2+3a_1)^2$$

and

$$\sigma'_{\text{ortho}}=\tfrac{1}{4}k'_{1,1}[(5a_2+3a_1)^2+10(a_2-a_1)^2]+20k'_{1,0}(a_2-a_1)^2 \quad (9)$$

while

$$\sigma_f=\frac{\pi}{16}[(5a_2+3a_1)^2+15(a_2-a_1)^2] \quad (10)$$

where a_2 and a_1 are the amplitudes of the hypothetical quintuplet and triplet scattered waves respectively. Our results for 20°K neutrons, substituted into (8), imply a free proton scattering cross section of only 7 barns, so that a neutron spin of $\frac{3}{2}$ is incompatible with these data.[18]

5. CONCLUSION

The observed values of the ortho- and parahydrogen scattering cross sections generally confirm the Schwinger-Teller theory; they are consistent with a free proton cross section of about

[17] J. Schwinger, Phys. Rev. **52**, 1250 (1937).

[18] Similar measurements in reference (5) indicated that the neutron spin is $\frac{1}{2}$; however at that time σ_1 was believed to be 14 barns, which affected the treatment of the correlation.

21 barns, and for an assumed square-well n-p interaction they imply a force range of 1.54×10^{-13} cm, experimental error allowing this value to lie between 1.12 and 1.99×10^{-13} cm.

6. ADDITIONAL ACKNOWLEDGMENTS

We are very grateful to Professor Edward Teller for guidance in problems of the scattering theory, and to Professor Robert Wilson, Mr. Anton Grubman, and Mr. Frederic de Hoffman for cooperation in the course of the experiment and in its evaluation.

This paper is based on work performed under Contract No. W-7405-eng-36 with the Manhattan Project at the Los Alamos Scientific Laboratory of the University of California.

PHYSICAL REVIEW VOLUME 72, NUMBER 12 DECEMBER 15, 1947

Search for Positron-Electron Branching in Certain Beta Emitting Isotopes

W. C. BARBER
Department of Physics, University of California, Berkeley, California

(Received August 13, 1947)

The β-rays emitted by the isotopes Ga^{70}, As^{76}, Br^{80}, Br^{82}, Rb^{86}, Rh^{104}, Ag^{108}, In^{116}, Sb^{122}, Sb^{124}, I^{128}, Re^{186}, and Au^{198} have been examined for positrons by the "trochoidal" method of Thibaud. Br^{80} is the only one of the above isotopes which was found to emit positrons as well as electrons. In studying Rb, a new activity of about 40-day half-life was found.

1. INTRODUCTION

WHEN a radioactive isotope of charge Z is isobaric with stable isotopes of charge $Z-1$ and $Z+1$ there exists the possibility of decay by positron emission or orbital electron capture as well as by electron emission. There are many isotopes in this situation, yet only a few of them are known to emit both positrons and electrons. The present experiments were undertaken with the idea that a sensitive detection method might show this branching in cases where it had hitherto been undetected. The trochoid provides an efficient means of making a complete separation of positrons and electrons, hence it was selected for the experiments.

2. EXPERIMENTAL APPARATUS

The trochoid was first used by Thibaud[1] to verify the existence of positrons and to study some of their properties. The instrument as used in the present experiments is simply a brass vacuum chamber shaped like a 270-degree section of a doughnut. A source is placed at one end of the chamber, and a Geiger-Müller counter is mounted at the other. The chamber fits between the poles of a circular-pole electromagnet in such a way that electrons from the source describe trochoidal paths around to the detector. When the magnet current is reversed only positrons can reach the detector. A diagram of the apparatus with a possible electron trajectory is shown in Fig. 1.

To make the source readily changeable a vacuum tight "well" with a 0.001-in. copper window was mounted in the source position. Absorption of the β-rays was studied by putting aluminum absorbers in the well between the source and the window. In experiments where it was desirable to have a minimum of absorbing material between source and detector the well was not used, and the source was mounted directly inside the vacuum chamber.

The counter had a 0.001 inch aluminum window which was waxed onto a cylindrical brass shell. The brass shell had three slots on one side through which the β-particles entered. Plateaus of about 100 volts were obtained when the counter was filled with 3 cm of argon and 2 cm of alcohol.

The apparatus was tested by measuring the relative number of positrons and electrons emitted by Cu^{64}. It was found, as is well known,[2] that the observed ratio of electrons to positrons depends on the source thickness and on the counter-window thickness. With a source 0.0002 in. thick and a 0.001-in. aluminum counter

[1] J. Thibaud, Phys. Rev. **45**, 781 (1934).

[2] K. Sinma and F. Yamasaki, Scientific Papers of the Institute of Physical and Chemical Research, Tokyo, **35**, 16 (1938).

TABLE I. Data on nuclei examined for positron emission.

Isotope	Half life	Upper limit for ratio of positrons to electrons	Window thickness source and counter mg/cm² aluminum equivalent
Ga^{70}	20 min.	0.005	30
As^{76}	27 hrs.	0.0003	14
Br^{80}	18 min.	0.03*	30
Br^{82}	34 hrs.	0.004	30
Rb^{86}	19.5 days	0.003	13
Rh^{104}	4.2 min.	0.001	30
Ag^{108}	2.3 min.	0.005	7
In^{116}	54 min.	0.001	24
Sb^{122}	2.8 days	0.001	30
Sb^{124}	60 days	0.005	13
I^{128}	26 min.	0.002	30
Re^{186}	90 hrs.	0.001	7
Au^{198}	2.7 days	0.001	7

* Observed ratio.

window the ratio was 1.6 which is in agreement with the results of Sinma and Yamasaki.[2]

Also it was found that the counting rate observed with a given sample increases slightly as the magnetic field is increased. For example, measurements on the electrons from Rb^{86} (E_0 =1.6 Mev) showed that the counting rate increased 6 percent when the magnetic field was increased from 9000 to 9500 gauss at the center of the magnet. This effect probably arises from the better focussing of the β-particles by the higher fields, and thus with a constant magnetic field the counting efficiency of the apparatus depends slightly on the energy of the β-rays being examined. In the present experiments the results are rough, and any errors introduced by this effect are negligible.

Because many of the isotopes emit γ-rays, which cannot be completely shielded from the counter, finding a method of determining the background counting rate is somewhat of a problem. In these measurements the background was found in one of two ways. When the sample was placed inside the vacuum chamber, the background count was made with the magnetic field equal to zero. In this case a correction of about 20 percent was required because the counter was less efficient with the field on. When the sample was placed in the source well, the background was taken by leaving the magnetic field unchanged and putting an aluminum absorber of 700 to 1000 mg/cm² in front of the source.

Energy measurements of the β-rays were made in the trochoid by the method of absorption in aluminum. In order to be certain that the usual relation between range and upper energy limit is valid for absorption measurements made in the strong magnetic field of the trochoid, absorption curves were taken on the electrons from P^{32} (E_0=1.72 Mev) and Br^{82} (E_0=0.47 Mev). The Feather relation with the constants given by Bleuler and Zünti[3]

$$R\ (\mathrm{g/cm^2}) = 0.571 E_0\ (\mathrm{Mev}) - 0.161 \qquad (1)$$

yielded the known upper energy limits within experimental error.

All of the isotopes studied were produced by (n,γ) reactions, using the neutrons produced by the 60-inch cyclotron in Berkeley. The neutrons were slowed by surrounding the sample with paraffin, but the amount of paraffin was not sufficient to eliminate the $(n,2n)$ reaction.

In the study of bromine, sources of high specific activity were obtained by the method of Szilard and Chalmers.[4]

3. EXPERIMENTAL RESULTS

Table I lists the isotopes which were studied. Each of these is known to be an electron emitter. The only one which was found also to emit positrons is Br^{80}. When the magnetic field was

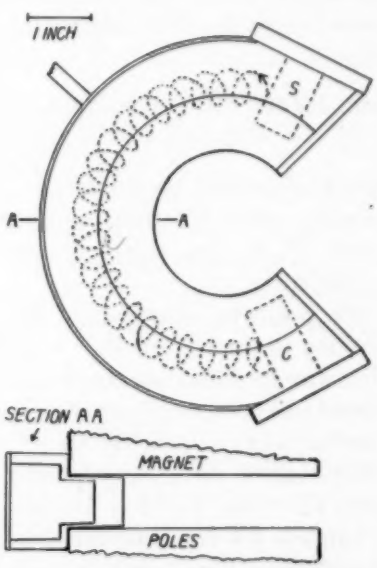

FIG. 1. Drawing of the trochoid. The positions of the source and counter are shown in dashed lines at S and C. An electron trajectory is shown as a dashed curve from the source to counter.

[3] E. Bleuler and W. Zünti, Helvetica Physica Acta 19, 375 (1946).
[4] L. Szilard and T. A. Chalmers, Nature 134, 462 (1934).

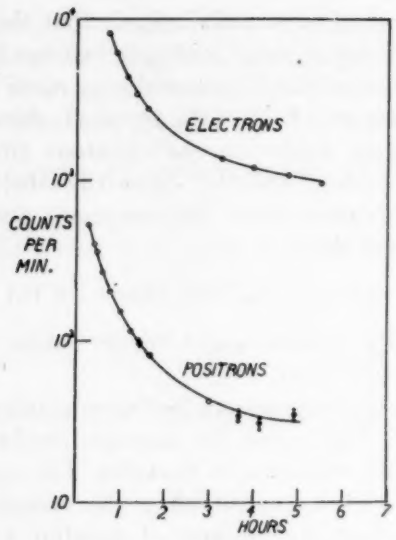

FIG. 2. Decay curves of the electrons and positrons emitted by Br^{80}. The ratio of electrons to positrons is equal to 35.

set for positrons, each of the other isotopes gave a counting rate which was not significantly different from the background counting rate. An estimate of the number of positrons which could have been detected is also given in Table I. This ratio has been calculated by assuming that positrons would have been detected if they had been present in greater numbers than four times the standard error in the background counting rate. Thus

$$\text{upper limit for the ratio of positrons to electrons} = (4/N_e)(N_b/T)^{\frac{1}{2}}, \quad (2)$$

where N_b = background counting rate; N_e = electron counting rate; T = time of counting the background. T is also equal to the time of counting positrons.

That the positrons emitted by the bromine sample belong to the isotope Br^{80} is shown in an interesting way by following the decay curves of the electrons and positrons from the same sample. The observed decay curves are shown in Fig. 2. The explanation of the curves follows from the well-known fact[5] that Br^{80} has an upper isomeric state of half-life 4.4 hours which always decays to the lower state. The lower state decays with half-life 18 minutes to Kr^{80} or Se^{80}. Bombardment of Br with slow neutrons produces both states, hence the decay curve shows first an 18-minute period which goes over into the 4.4-hour period as soon as all the original lower state nuclei are gone. The positron decay curve has the same form as the electron decay curve, and the ratio of electrons to positrons is independent of time and has the value 35.

The absorption of Br^{80} positrons in aluminum is plotted in Fig. 3. The background, caused chiefly by the γ-rays from Br^{82}, did not permit the absorption measurement to be made down to 10^{-3} of the initial intensity. Comparison, by the method of Feather,[6] of this absorption curve with the curve taken using P^{32} yields $E_0 = 0.73$ Mev. (The error in this result could be as much as 0.1 Mev.) According to Eq. (1) this corresponds to a range of 0.26 g/cm² which is about what one would estimate from the shape of the curve.

The elements arsenic and rubidium showed slight positron activities after bombardment with neutrons from the cyclotron. However, careful study showed that these positrons followed decay curves different from those of the isotope under study.

In the case of arsenic the positron activity amounted to only 0.05 percent of the electron activity and the decay curve indicated that these positrons could be attributed to As^{74}, formed by an $(n,2n)$ reaction. This result is in

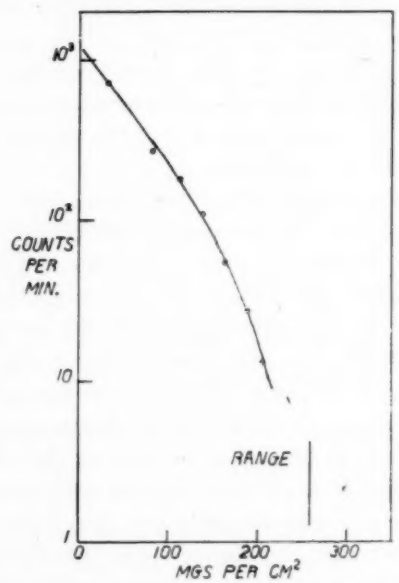

FIG. 3. Absorption of the Br^{80} positrons in aluminum. The data were corrected for decay of the sample and the background was subtracted before the curve was plotted. The range is estimated as 0.26 g/cm².

[5] E. Segrè, R. S. Halford, and G. T. Seaborg, Phys. Rev. **55**, 321 (1939).

[6] N. Feather, Proc. Camb. Phil. Soc. **34**, 599 (1938).

disagreement with a report by Harteck, Knauer, and Schaeffer[7] that approximately 2 percent of the As^{76} atoms decay by positron emission.

The neutron bombarded rubidium showed a positron activity of about one percent of the electron activity, with the positron activity having a somewhat longer half-life. This new positron activity was measured again in a strong sample of rubidium which was produced by bombarding strontium with 18-Mev deuterons from the 60-inch Berkeley cyclotron. The rubidium was chemically separated from the other reaction products, and the half-life of the positron activity was measured roughly as 40 days. These two methods of production suggest that the activity is due to Rb^{84}, which could decay to Kr^{84} by positron emission, from the reactions

$$Rb^{85}(n,2n)\rightarrow Rb^{84}, \quad Sr^{86}(d,\alpha)\rightarrow Rb^{84}.$$

Study of this activity is being continued.

4. DISCUSSION

It is interesting that all of the isotopes which were studied prefer to decay by electron emission. This result can be explained by the fact that all the radioactivities were produced by (n, γ) reactions on stable isotopes. In the present study only those radioactive isotopes which have stable isobars with Z smaller or larger by one were investigated. This type of radioactivity only occurs in elements of odd Z; these have only one or two stable isotopes. Thus capture of a neutron usually yields a radioactive isotope which is on the excess neutron side of the stability curve.

As a check on this hypothesis, a survey of the isotope chart was made for all known radioactive isotopes which have stable isobars on each side. Forty such isotopes whose assignment was considered reliable were found. Twenty-one occur in elements with one stable isotope and nineteen in elements with two stable isotopes.

When there is only one stable isotope, those cases which have more neutrons than the stable one include ten electron emitting isotopes and three isotopes which show branching decay. Those cases which have fewer neutrons than the stable one include four which emit positrons or capture orbital electrons, one which emits electrons, and three with branching decay.

The elements with two stable isotopes show even more rigid behavior. When the radioactive isotope has more neutrons than the heavier stable isotope, it is always an electron emitter (four cases). When the radioactive isotope has fewer neutrons than the lighter stable isotope, it is always a positron emitter (four cases). When the radioactive isotope lies between the two stable ones, it is sometimes an electron emitter (seven cases) and sometimes shows branching decay (four cases).

These statistics clearly indicate that the radioactive isotope usually decays toward the isobar which is nearer the stability curve.

It is possible also to estimate the energy difference of two of these isobars as follows. Measurements with the trochoid indicate that except for Br^{80}, the isotopes measured have a ratio of electrons to positrons which is approximately 500 or greater. From the Fermi theory of beta decay it is possible to calculate what difference in energy will produce a ratio of approximately 500 electrons to one positron. If the positron and electron transitions are equally allowed, and if the maximum total energy, W_0, of the electron spectrum is twice that of the positron spectrum, then the ratio of electrons to positrons will be approximately 500. (W_0 is equal to the maximum kinetic energy of the β-particle plus its rest energy.) (In the case of Br^{80} the electron decay must be one degree more forbidden than the positron decay because in this case the ratio of the total energies is just two.)

Thus the fact that no positrons are observed usually means that the total energy of the transition from the isotope of charge Z to the isobar $Z+1$ is at least twice as great as the total energy of the transition to the isobar $Z-1$.

ACKNOWLEDGMENTS

The author wishes to express his appreciation to Dr. R. Leininger for help with the chemistry problems involved in the work, to Professor A. C. Helmholz for supplying the strong rubidium sample, and in particular to Professor E. Segrè who suggested the problem and furnished valuable advice for carrying it out. The cooperation of Dr. J. G. Hamilton and the members of the crew of the 60-inch Berkeley cyclotron is gratefully acknowledged.

[7] P. Harteck, F. Knauer, and W. Schaeffer, Zeits. f. Physik **109**, 153 (1938); *ibid.* **113**, 287 (1939).

New Barium and Cesium Isotopes: 12.0d Ba^{131}, 10.2d Cs^{131}, and Long-Lived Ba^{133}*

SEYMOUR KATCOFF**
Argonne National Laboratory, University of Chicago, Chicago, Illinois

(Received August 11, 1947)

A new Ba-Cs chain of probable mass assignment of 131 has been formed by neutron activation of barium. The Ba^{131} isotope decays predominately by orbital electron capture with a half-life of 12.0 days, emitting gamma-radiations of about 0.26 Mev, 0.5 Mev, and roughly 1.2 Mev (the latter in low intensity). Detected also were 31-kev x-rays and 0.42-Mev and 0.24-Mev conversion electrons. The Cs^{131} decays exclusively by K-electron capture with a half-life of 10.2 days, emitting no detected gamma-rays. The Ba^{133} has a minimum half-life of 20 years and is very probably the lower state to which the 37.8 hour Ba^{133} decays. The former decays by K-capture and emits 31-kev x-rays, 0.36-Mev gamma-rays, 0.34-Mev conversion electrons, and possibly 4.3-kev x-rays.

I. INTRODUCTION

THE stable Ba and Cs isotopes and their percent abundances are as given in Table I. Neutron bombardment of barium is known to give 85m Ba^{139} and 37.8h Ba^{133}. It appeared probable that if Ba^{131} has a half-life of the order of several days that it might be detected in some barium carbonate which had received an intense irradiation at the center of the Clinton pile. (This is the same $BaCO_3$ sample that was used to determine the neutron-absorption cross section[1] of 85m Ba^{139}.) A considerable amount of activity actually was found when a radio-chemical analysis for Ba was performed 21 days after the end of the bombardment. Some of this purified Ba was then allowed to stand four days, and a radiochemical analysis for Cs was made. Some activity was found, and this was assigned to a radioactive Cs daughter of the new Ba isotope. The long-lived Ba^{133} was discovered after the Ba^{131} had decayed to a negligible activity.

12.0d Ba^{131}

In order to prove definitely that the first activity was really that of an isotope of Ba, some fractional precipitation experiments were performed. Three aliquots of the irradiated $BaCO_3$ were taken and labeled Ba *b*, Ba *c*, and Ba *d*. Then Ba *b* was scavenged six times with $La(OH)_3$ precipitations and twice with $Fe(OH)_3$ precipitations. It was then precipitated two times as $BaCl_2$ and once as $BaCrO_4$. Sample Ba *c* was treated likewise except that two $Ba(NO_3)_2$ and one more $BaCrO_4$ precipitations were added. Sample Ba *d* was first subjected to seven $La(OH)_3$ and two $Fe(OH)_3$ precipitations. It was precipitated three times as $Ba(NO_3)_2$, once as $BaCrO_4$, and four times as $BaCl_2$. Then it was subjected to slow fractional precipitation as $BaCO_3$. It was brought down in four batches and labeled Ba d_1, Ba d_2, Ba d_3, and Ba d_4. Each of these was then reprecipitated as $BaCrO_4$. The results are given in Table II.

The specific activity was essentially the same for all six samples when measured through 213-mg Al/cm² or through 1.8-g Pb/cm². The deviations from constant specific activity for the measurements made without added absorber can be completely accounted for by the differences in self-absorption of the very weak radiations corresponding to the differences in the weights of the samples. Therefore, it is established that this is an active isotope of Ba.

Its half-life was determined by following the decay of a sample covered with 1.8-g/cm² of lead. This amount of lead absorbs completely the radiations of the Cs daughter of this Ba isotope. The

TABLE I. Stable isotopes of Ba and Cs.

Ba^{130}	Ba^{132}	Cs^{133}	Ba^{134}	Ba^{135}	Ba^{136}	Ba^{137}	Ba^{138}
0.101	0.097	100	2.42	6.59	7.81	11.32	71.66

* This work was originally reported in Manhattan Project Reports CC-3148 (June 1, 1945) and CC-3456 (March 11, 1946); see also Plutonium Project Record IX B, 12.1.1 and IX B, 12.2 (1946).

** Now at Los Alamos Scientific Laboratory, Los Alamos, New Mexico.

[1] S. Katcoff, Manhattan Project Report CC-2908 (April 7, 1945); Plutonium Project Record IX B, 7.59.4 (1946).

half-life was found to be 12.0 days for a decay time of nine half-lives. Absorption measurements in lead and in aluminum were made on freshly purified Ba samples. The lead-absorption curves (Figs. 1 and 2) show a 0.5-Mev γ-ray, a small amount of a harder γ-ray (roughly 1.2 Mev), and one or more softer γ-rays (roughly 0.26 Mev and below). The aluminum-absorption curves (Fig. 3) indicate 31.5-kev x-rays, 0.42-Mev conversion electrons, and 0.24-Mev conversion electrons. The latter two energies correspond fairly well with the 0.5-Mev γ-rays and 0.26-Mev γ-rays, respectively. From these measurements (especially from the large proportion of 31.5-kev x-rays) it seems that most of the disintegrations take place by K-electron capture. Some positron emission might also occur, especially since 0.5-Mev γ-rays are observed, part of which might be annihilation radiation.

10.2d Cs^{131}

The Cs daughter of this Ba decayed exponentially with a half-life of 10.2 days for a period of eight half-lives. A few periodic extractions were made of the Cs from the Ba. These indicated a 12-day half-life for the Ba and definitely established the fact that the 10.2d Cs is a daughter of this 12.0d Ba. The absorption of the Cs radiations in aluminum is shown in Fig. 4. This indicates only a 31.0-kev x-ray and some extremely soft radiation. Absorption in copper shows only a 30.8 kev x-ray. A lead absorber 1.8 g/cm² thick reduced the count of a Cs sample, which gave 30,000 c/m without absorber, to zero. Therefore, no γ-rays are emitted by this isotope, unless their energy is less than a few kev.[2] The very soft

TABLE II. Results of precipitations.

Sample No.	Weight of sample	Activity per milligram through no added absorber	through 213-mg Al/cm²	through 1.8-g Pb/cm²
Ba *b*	14.3 mg	545 c/m	160 c/m	215 c/m
Ba *c*	21.7	491	159	220
Ba d_1	14.1	556	162	212
Ba d_2	14.7	536	161	211
Ba d_3	8.4	602	161	224
Ba d_4	22.6	485	157	215

[2] In a recent note, Phys. Rev. **71**, 382 (1947), Fu-Chun Yu, Donald Gideon, and J. D. Kurbatov reported the emission of highly converted 0.145-Mev gamma-rays by Cs^{131}. These were not observed in the experiments reported here. The other data given in their note are in general agreement with the data given here.

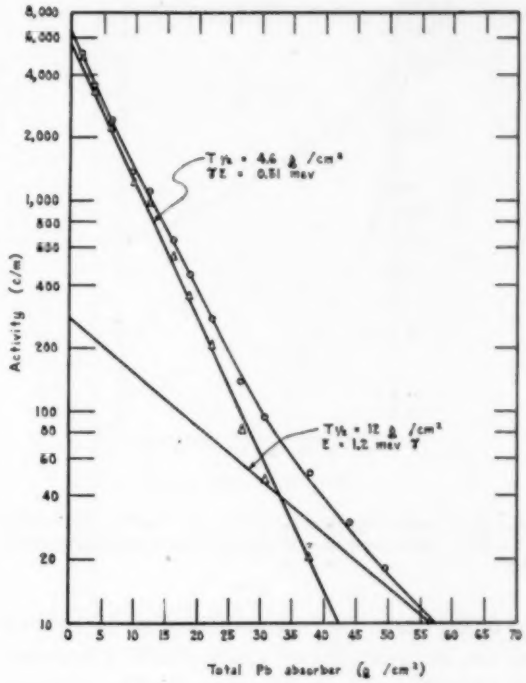

FIG. 1. Lead-absorption curve of Ba^{131}.

radiation shown by the first part of the absorption curve in aluminum is probably the L x-radiation. The other x-rays are very likely the K x-rays of Xe (29.6 kev) which follow the capture of the K electrons by this Cs isotope. The only isotope previously known which decays purely by orbital electron capture and does not emit γ-rays is 600d V^{49}.

II. MASS ASSIGNMENT TO CHAIN: 12.0d Ba→10.2d Cs

Mass numbers 129 and 131 are the only two possibilities which permit an active Ba isotope to be formed by neutron bombardment of ordinary barium and to have an active Cs daughter.[3] Mass number 129 can be eliminated by considering the neutron cross section of normal barium for the formation of this 12.0d Ba. This was found

[3] One other possibility is that the 10.2d Cs is an isomer of stable Cs^{133} which decays to the ground state by emission of 31-Kev γ-rays. This was made very improbable by the critical absorption measurements of B. Finkle, which indicated that the 10.2d Cs does decay to Xe. See B. Finkle, Phys. Rev. **72**, 1260 (1947).

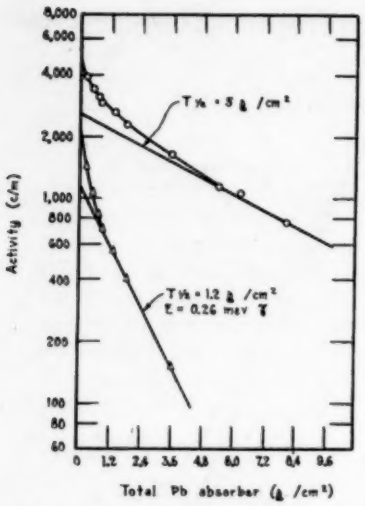

FIG. 2. Lead-absorption curve of Ba^{131}. Δ0.5-Mev and 1.2-Mev components subtracted from original points (cricles).

to be 0.006 barn. Ba^{129} would have to be formed by an $(n, 2n)$ reaction on stable Ba^{130}, whose isotopic abundance is 0.10 percent. The isotopic cross section would then be six barns. Such a high cross section for an $(n, 2n)$ reaction in a neutron flux, which is mostly near thermal, is extremely improbable. Therefore, it is fairly certain that the correct mass number of these isotopes is 131, and that Ba^{131} is formed from Ba^{130} by an (n, γ) process. The calculation of the cross section is based on the assumption that the decay of the 12.0d Ba takes place almost entirely by K-capture and that the γ-rays are internally converted to only a small extent. That is, one K x-ray was assumed for every disintegration. The counting efficiency of these x-rays was taken to be one percent (private communication from D. W. Engelkemeier).

III. LONG-LIVED Ba^{133}

Nine months after the neutron irradiation of the barium some residual activity was still present in a sample which had been extensively purified subsequent to the bombardment. After these nine months the sample was dismounted and purified further by making one $BaCO_3$ precipitation, two $BaCl_2$ precipitations, two $Fe(OH)_3$ scavenging precipitations, and one $BaCrO_4$ precipitation. The specific activity, as observed through 139 mg/cm² of aluminum absorber, was unchanged to within a possible experimental error of 10 percent. The observed activity must therefore be that of a long-lived isotope of barium.

The supernatant solution which remained from the $BaCO_3$ precipitation of this sample was radiochemically analyzed for cesium. Eight months had been allowed for a possible Cs daughter to grow in. Two hours after separation from the barium the cesium extract had an activity, though no added absorber, of about 2 c/m. Under similar conditions the parent barium sample had an activity of 2000 c/m; through 213 mg/cm² of aluminum absorber this activity was 360 c/m. Thus it seems that this long-lived Ba isotope has no active Cs daughter unless the latter is very short-lived, very long-lived, or has very soft radiations.

Over a period of 20 months the decay of this Ba activity could not be detected to within a possible error of 5–6 percent. This sets a lower limit of 20 years on the half-life. The radiations were investigated by means of absorption measurements. A lead-absorption curve (Fig. 5) indicates the presence of a 0.36-Mev gamma-ray. Aluminum-absorption curves (Fig. 6) show 0.34-

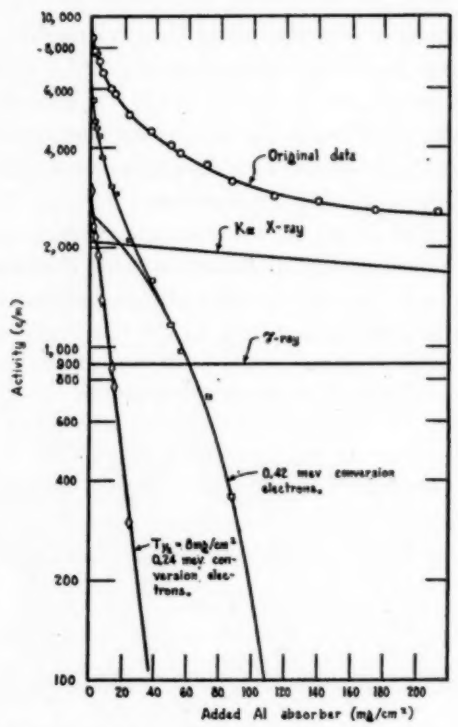

FIG. 3. Aluminum-absorption curves of Ba^{131}.

Mev conversion electrons, a 32-kev x-ray, and possibly a 4.6-kev x-ray. Critical absorption measurements were made with Sn, Sb, Te, and iodine absorbers in order to establish the origin of the harder x-rays. The absorbers were made by using solutions or suspensions of the elements in question in a fixed quantity of 6N HCl. These were placed in disk-shaped cells whose diameter was 7 cm and whose height was 2 cm. The bottom of each cell was made of mica. About 14 absorbers were used for each of the four elements. The x-rays showed half-thicknesses of 31 mg/cm² and 30 mg/cm² with Sn and Sb absorbers, respectively, whereas they showed half-thicknesses of 69 mg/cm² and 70 mg/cm² with Te and iodine absorbers, respectively. This clearly identifies the radiation as the K x-rays of Cs, the energy of which is 30.7 kev. Very few, if any, positrons are emitted because no 0.5-Mev annihilation γ-rays are observed. Therefore this long-lived Ba must decay by means of orbital electron capture. The soft 4.6-kev x-ray indicated by the aluminum-absorption curve (Fig. 6) is probably the L x-radiation of Cs, the energy of which is 4.3 kev.

The mass assignment can be made by a consideration of the cross section which was found for the formation of this isotope. By assuming that one 30.7-kev x-ray was formed for each dis-

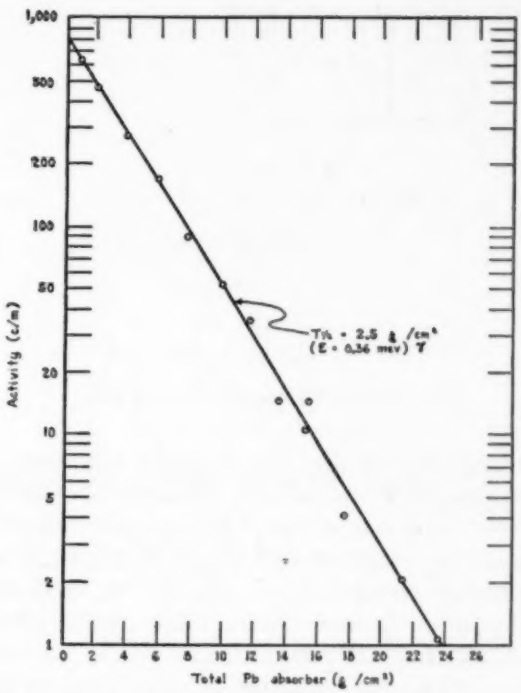

FIG. 5. Lead-absorption curve of >20y Ba^{133}.

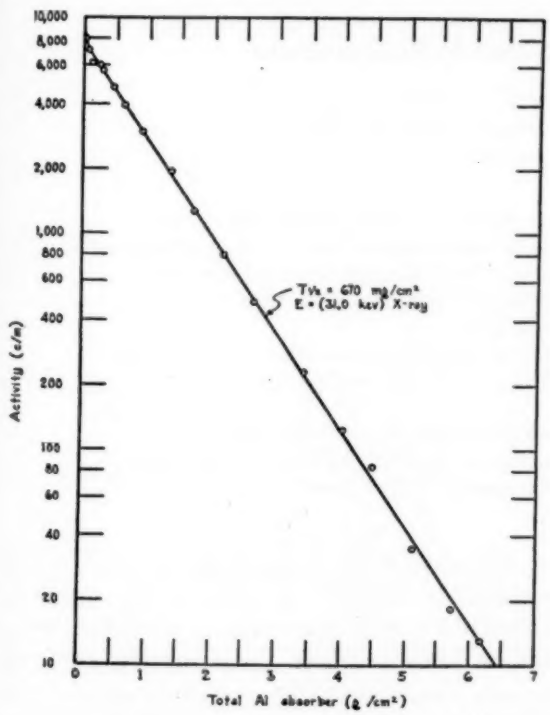

FIG. 4. Aluminum-absorption curve of Cs^{131}.

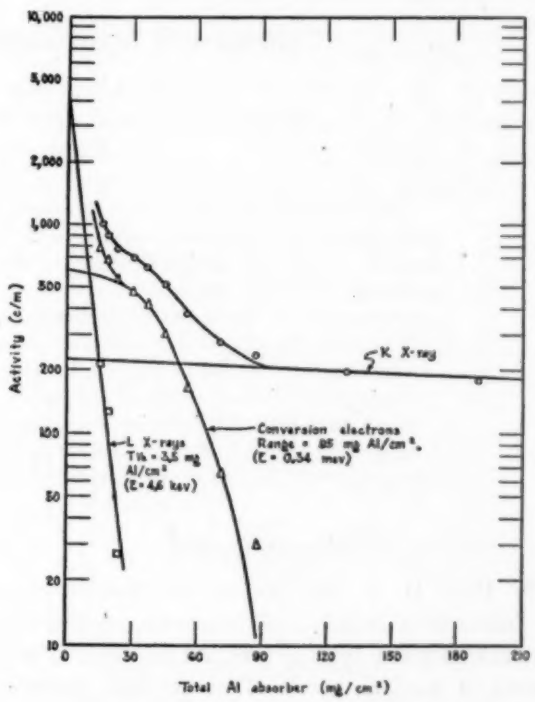

FIG. 6. Aluminum-absorption curve of >20y Ba^{133}.

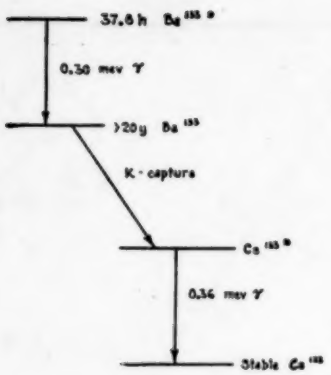

FIG. 7. Probable decay scheme of Ba^{133}.

integration and that the counting efficiency of these x-rays is one percent, this cross section for normal barium is at least 0.006 barn (corresponding to the minimum half-life of 20 years). If assignment is made to mass 129, then it could only have been formed from stable Ba^{130}, whose abundance is 0.10 percent, by an $(n, 2n)$ reaction. This would mean that the isotopic cross section for this process is at least 6 barns, which is extremely improbable since most of the pile neutrons are of low energy. Furthermore, Ba^{129} would decay to an active Cs^{129}, and no such activity could be detected. Assignment of the long-lived Ba to mass 131 is ruled out by the fact that it does not decay to the 10.2d Cs^{131}. The only possible remaining assignment is to mass 133. In this case the isotope could be formed from stable Ba^{132}, whose abundance is also 0.10 percent, by an (n, γ) reaction. The isotopic cross section for this process is then a minimum of about 6 barns. Thus an assignment to mass 133 is fairly certain. The 37.8h Ba which is also assigned to mass 133 is known to decay by isomeric transition. The lower state can now be identified as this >20y Ba^{133}. The decay scheme is probably as shown in Fig. 7.

This paper is based on work performed at the Metallurgical Laboratory of the University of Chicago under Contract W-7401-eng-37 for the Manhattan Project, and the information contained therein will appear in Division IV of the Manhattan Project Technical Series. Counting of the long-lived Ba^{133} is continuing at Los Alamos.

PHYSICAL REVIEW VOLUME 72, NUMBER 12 DECEMBER 15, 1947

Coincidence Measurements. Part I. Beta Spectra

M. L. WIEDENBECK AND K. Y. CHU
Department of Physics, University of Michigan, Ann Arbor, Michigan

(Received August 25, 1947)

The necessary and sufficient conditions for a simple β spectrum (not accompanied by internally converted γ radiation) are discussed. It is generally considered that the $\beta-\gamma$ coincidence rate per recorded β particle decreases with an increase of absorber thickness for a complex β spectrum. Although this is the most common condition, it is possible for the ratio to remain constant or even rise as the β absorber thickness is increased.

The ratio, $N_{\beta\gamma}/N_{\beta}$, is also calculated for simple spectra followed by non-delayed conversion electrons as well as for conversion in metastable levels of lifetime long compared with the resolving time of the coincidence circuit.

Data have been obtained for several nuclei including antimony^{124} (60 days), cesium^{134} (1.7 years), europium^{154} (5–8 years), gold^{198} (2.7 days), hafnium^{181} (55 days), iridium^{192,194} (60 days), mercury^{203,205} (51.5 days), osmium^{193} (17 days), and potassium^{42} (12.4 hours).

1. INTRODUCTION

IN Part II of this set of articles we shall indicate a simple and accurate method for determining the total absolute conversion coefficients of nuclear levels. This method demands little knowledge of the γ radiation involved in the transition if the β spectrum is simple but a considerable amount of information must be available if the β spectrum is complex. Since little is known about the structure of most complex β emitters we have limited our investigation to nuclei which have simple β spectra.

It was therefore thought advisable to consider first the nature of the β radiation of several nuclei to which this method seems applicable.

Two methods have commonly been used to determine whether a β spectrum is simple or complex. The first can be obtained from the energy distribution of the ejected β particles as obtained with a β spectrograph. The symmetry of this distribution as well as the linearity of the Fermi plot are then used as the criteria of a single β transition. This method is somewhat difficult and cannot be used for energies below $\sim$0.2 or 0.3 Mev due to the distortion of the β distribution by scattering and window absorption. The spectrograph method also becomes difficult for short-lived materials.

The second method involves the study of the number of $\beta-\gamma$ coincidences per observed β particle as a function of the β absorber thickness. This is a simple procedure which can be carried out with nuclei which emit low energy β radiation. It can also be applied to short lived nuclei (possibly to lifetimes as short as several seconds). Such coincidence measurements were carried out by Langer, Mitchell, and McDaniel[1] as early as 1939. Since then a considerable amount of work has been carried out by the Indiana group on the level structure of nuclei by these methods.

We shall attempt to examine the coincidence conditions for simple and complex spectra which do not involve internal conversion, as well as simple spectra followed by converted γ radiation.

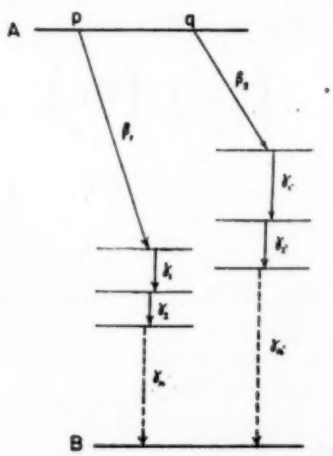

FIG. 1. Decay of nucleus A to nucleus B by complex β-spectra. p is the fraction of nuclei which emit β rays of energy β_1. $q=1-p$.

[1] L. M. Langer, A. C. G. Mitchell, and P. W. McDaniel, Phys. Rev. 56, 422 (1939).

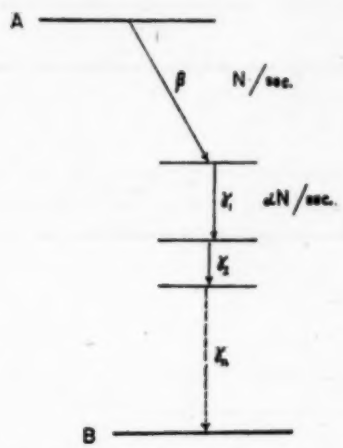

FIG. 2. Simple β decay followed by a series of γ rays. γ' is internally converted. The conversion coefficient is α.

2. THEORY

Let us assume that nucleus A decays by β emission to nucleus B as indicated in Fig. 1. The fraction of nuclei which emit β particles of maximum energy β_1 is given by "p," those decaying with the maximum energy β_2 is "q." A series of γ rays follows each β disintegration. These are designated $\gamma_1, \gamma_2 \cdots \gamma_n$ for the former case and $\gamma_{1'}, \gamma_{2'} \cdots \gamma_{n'}$ for the latter case.

An arrangement is now set up with the source of radiation fixed rigidly to a γ ray counter. The source also faces a β counter. Absorbers can be placed between the source and the β counter.

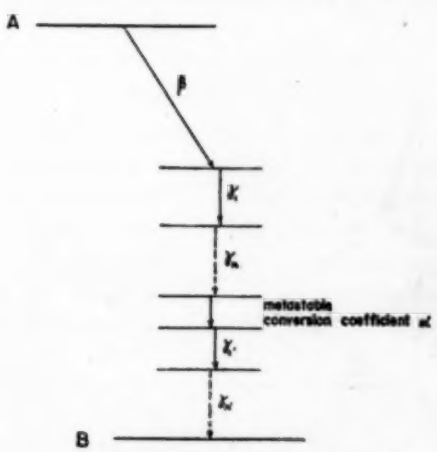

FIG. 3. Simple β spectrum followed by γ rays. One γ ray is internally converted and delayed.

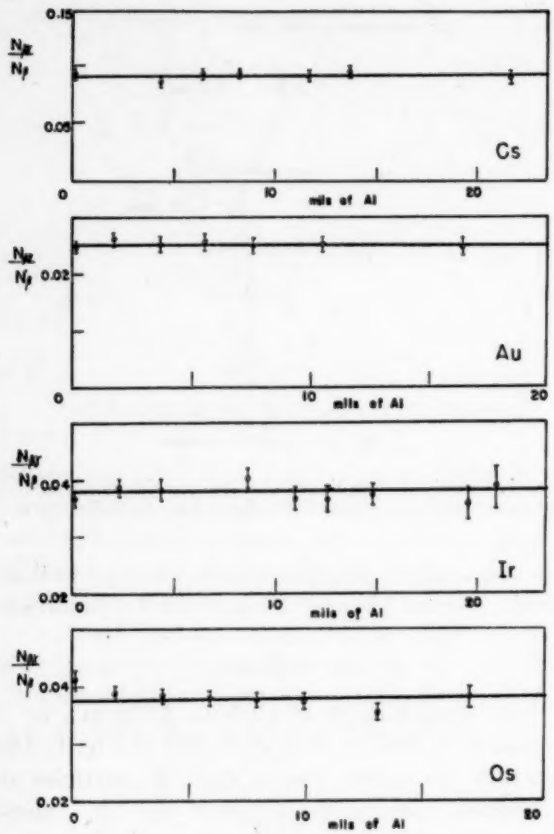

FIG. 4. $\beta-\gamma$ coincidence rate per observed β particle as a function of absorber thickness. These four nuclei appear to have simple β spectra.

The fraction of β_1 and β_2 particles transmitted by the absorber is given by F_1 and F_2, respectively. In addition, it is assumed that the efficiency of the γ counter is small so that the number of γ rays recorded is directly proportional to the number passing through the counter. (In practice the efficiency is ~ 1 percent or less.)

Further, the fraction of the sphere subtended by the β and γ counters is σ_β and σ_γ, respectively. Their respective efficiencies being ϵ_β and ϵ_{γ_n}. (The efficiency of the γ counter depends upon the energy of the γ radiation.)

The ratio

$$R_1 = N_{\beta\gamma}/N_\beta$$

$$= \left[pF_1\left(\sum_1^n \epsilon_n\right) + qF_2\left(\sum_{1'}^{n'} \epsilon_{n'}\right)\right]\sigma_\gamma \Big/ [pF_1 + qF_2].$$

It is clear that for a simple spectrum, i.e., p or $q=0$, without internal conversion, $R_1 =$ constant, since the ratio is independent of F.

Complex Spectra

For the complex spectrum in Fig. 1 we must consider several cases. First, if

$$\left(\sum_{1'}^{n'} \epsilon_{n'}\right) > \left(\sum_1^n \epsilon_n\right)$$

the ratio, R_1, will decrease until F_2 becomes 0. Thereafter it will remain constant at a value,

$$R_1 = \left(\sum_1^n \epsilon_n\right)\sigma_\gamma.$$

The point at which the curve reaches a constant value gives the energy of β_2, the lower energy β ray. This is by far the most common case.

On the other hand, if

$$\left(\sum_{1'}^{n'} \epsilon_{n'}\right) < \left(\sum_1^n \epsilon_n\right),$$

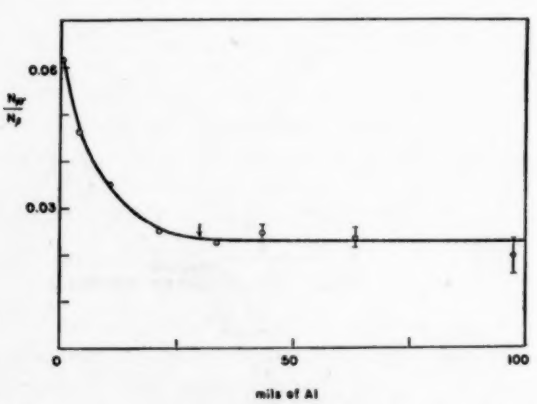

FIG. 5. Coincidence rate for Sb^{124} showing a complex β spectrum.

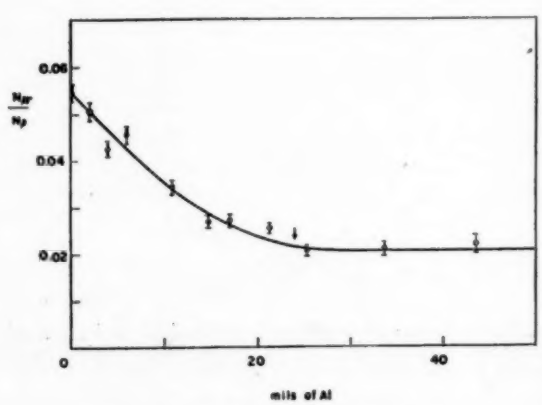

FIG. 6. Complex β spectrum of Eu^{154}.

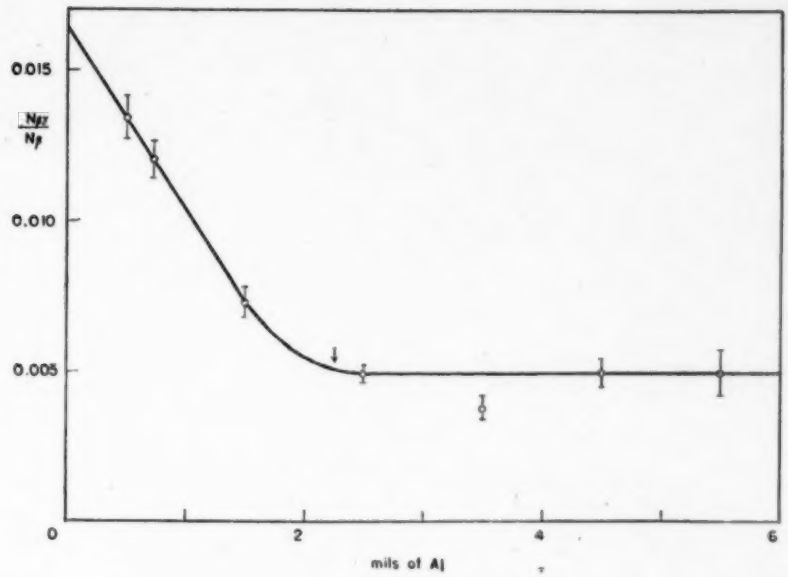

FIG. 7. Coincidence rate curve for $Hg^{203,205}$.

the ratio R_1 will rise with an increase in absorber thickness becoming

$$R_1=\left(\sum_1^n \epsilon_n\right)\sigma_\gamma$$

at the point where no β_2 are transmitted through the absorber.

The third case to consider occurs if

$$\left(\sum_{1'}^{n'} \epsilon_{n'}\right)=\left(\sum_1^n \epsilon_n\right).$$

This would give rise to R_1=constant and as such would appear to be a simple spectrum. Therefore, if no internal conversion exists, the constancy of R_1 is a necessary condition for a simple β spectrum but not a sufficient condition.

Effect of Internal Conversion

For a simple β spectrum followed by a series of γ rays, one of which is internally converted (but not delayed) with a conversion coefficient α (Fig. 2), we have a similar relationship. F_1 is again the fraction of the β radiation transmitted through the absorber and F_2 the corresponding fraction of the conversion electrons.

$$R_2=N_{\beta\gamma}/N_\beta=\left\{F_1\left[(1-\alpha)\epsilon_1+\sum_2^n \epsilon_n\right]+F_2\alpha\sum_2^n \epsilon_n\right\}\sigma_\gamma-\tfrac{1}{2}\alpha F_1F_2\sigma_\beta\epsilon_\beta\sigma_\gamma\left(\sum_2^n \epsilon_n\right)\Big/[F_1+\alpha F_2]-\alpha F_1F_2\sigma_\beta\epsilon_\beta/2.$$

The last term in the numerator as well as in the denominator arises from the possibility that both the β particle and the conversion electron enter the β counter which, however, records only one particle. In practice $\sigma_\beta\epsilon_\beta/2$ may be $\sim$0.05 or less and as such these terms can be neglected. Thus R_2 would appear similar to R_1 (a complex spectrum) except for the cases (a) $\alpha\sim1$, (b) $\alpha\ll1$ or (c) if $n\gg1$. In the above-mentioned cases $R_2\simeq$constant. Several converted lines each having a conversion coefficient much less than unity would also appear as a true simple spectrum.

Metastable States

In Fig. 3 we have indicated a simple β spectrum followed by a series of γ rays, one of which has a lifetime greater than the resolving time of the coincidence circuit. The conversion coefficient is α, F_1 is the fraction of the β rays transmitted through the absorber and F_2 the corresponding fraction of the conversion electron.

Then

$$R_3=N_{\beta\gamma}/N_\beta=\left[F_1\left(\sum_1^n \epsilon_n\right)+\alpha F_2\left(\sum_{1'}^{n'} \epsilon_{n'}\right)\right]\sigma_\gamma\Big/F_1+\alpha F_2$$

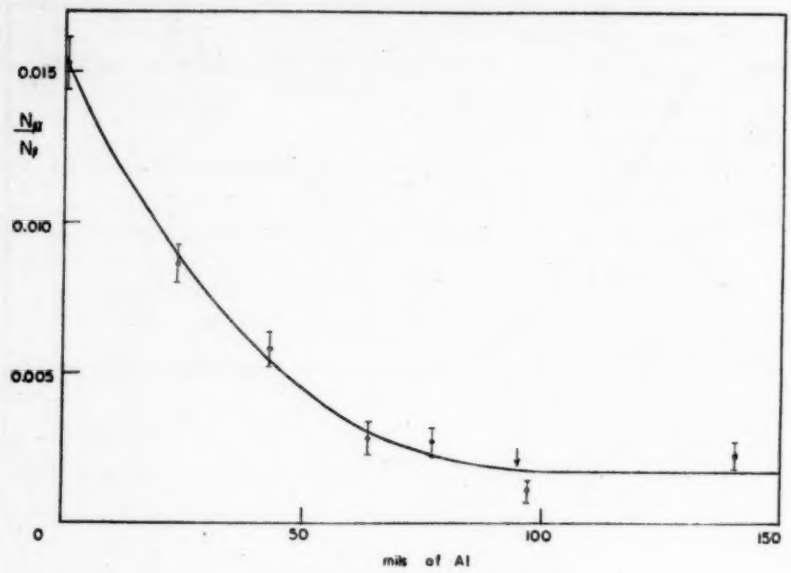

FIG. 8. $\beta-\gamma$ coincidences of K^{42}. The end point of the lower energy component of β radiation is not sharp but appears to be $\sim$1.5 Mev.

similar to the case of a complex β spectrum. Again the shape of the curve is determined by the values of

$$\left(\sum_{1}^{n}\epsilon_n\right) \quad \text{and} \quad \left(\sum_{1'}^{n'}\epsilon_{n'}\right).$$

One considerable difference exists, however, most generally for a complex β spectrum: the sum,

$$\left(\sum_{1'}^{n'}\epsilon_{n'}\right),$$

for the set of γ rays associated with the lower energy β particle is greater than the corresponding sum for the higher energy particle, thus causing a decrease in R_1 with an increase in absorber thickness. For delayed radiation, on the other hand, the converted electrons should be expected to be of low energy and may be followed by few γ rays. As such it may often be found that R_3 will rise as the absorber thickness is increased.

We see, therefore, that a simple β spectrum gives rise to a value $N_{\beta\gamma}/N_\beta$=constant, while a complex spectrum may give rise to any shape of curve. This method can then be used to identify many of the complex spectra and to indicate which are possibly simple. Whenever possible it is desirable to have additional proof of the simplicity from the spectrograph method.

3. EXPERIMENTAL

The nature of the β spectra has been investigated for a group of nuclei having relatively long half-lives. Many of these were produced by slow neutron bombardment at Oak Ridge, while some were produced by deuteron bombardment.

For the coincidence measurements, self-quenching argon-ether counters of brass construction were used. The radiation was admitted through an end window of $\frac{1}{2}$ to 1 mil Cellophane. When it was desired to count only γ radiation, a small plug could be fitted into the window frame. The background of these counters without shielding was normally $\sim$30/100 seconds.

Each counter was attached to a fast scaling unit so that the individual counting rate was at all times available. Sharp pulses (rise time $\sim$0.1 microsecond) from a pulse former before the scaler were fed to a coincidence circuit. The resolving time of this circuit could be varied between $\sim$0.25 to 2.5 microseconds. Since the variation in the time of the initiation of a discharge in counters may be $\sim$0.3$\rightarrow$0.4 microsecond, the resolving time ordinarily used was $\sim$0.6 microsecond.

Simple Spectra

Of the group of nuclei studied, cesium[134], gold[198], iridium[192,194], and osmium[193] appear to be simple, i.e., the ratio $N_{\beta\gamma}/N_\beta$=constant. These curves are shown in Fig. 4. Samples of

these four elements were obtained from Oak Ridge. Some samples of gold were also produced by deuteron bombardment with the Michigan cyclotron.

The upper limit of the β spectrum of Cs^{134} has been found by Kalbfell and Cooley[2] to be 0.9 Mev. Using Feather's rule, we obtain a value of 0.8 Mev for the upper limit.

The $\beta-\gamma$ coincidence rate of gold[198] has been studied by Clark[3] who found that the coincidence rate did not decrease with an increase in absorber thickness. More recently Siegbahn[4] has made a study of the shape of the β spectrum and has found that it is simple. As is seen in Fig. 4, we find that the $\beta-\gamma$ rate is not dependent upon absorber thickness. The upper limit of the spectrum from the absorption end point of 0.332 g/cm^2 is 0.91 Mev.

Both the iridium[192, 194] (60 days) and osmium[193] (17 days) $\beta-\gamma$ rates appear to be independent of the absorber thickness within the limit of error. However, it may be of significance that the first few points of the osmium curve fall slightly higher than the following points. This seems to be a real effect and may possibly be attributable to internal conversion.

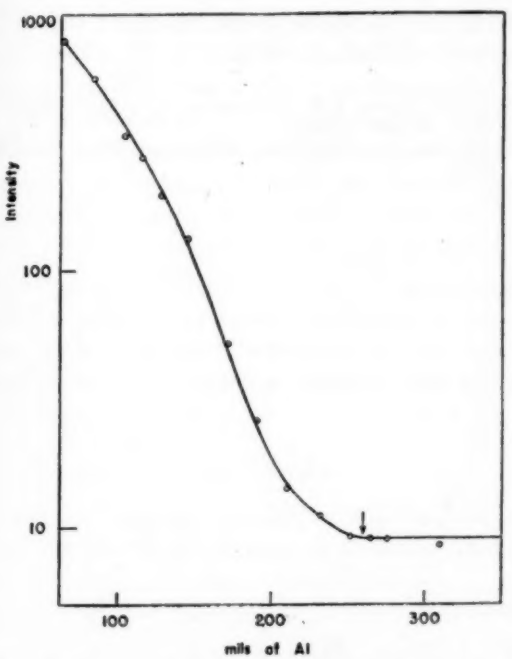

FIG. 9. β absorption curve for K^{42}. The end point for the high energy component is 3.57 Mev according to Feather's rule.

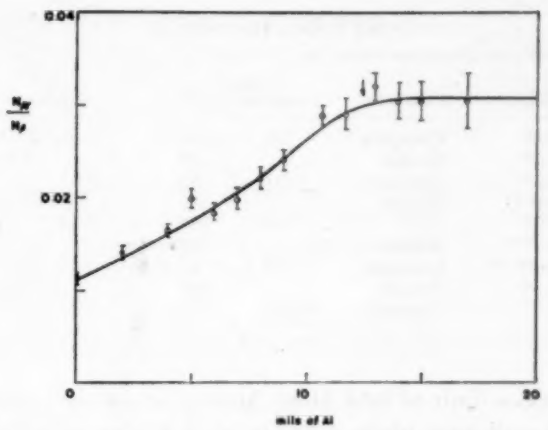

FIG. 10. $N_{\beta\gamma}/N_\beta$ as a function of absorber thickness for Hf^{181}. The rise may be due to the presence of the metastable state of half-life 22 microseconds.

Absorption measurements give an upper limit of 0.68 Mev for the spectrum of iridium.

Complex Spectra

A beta spectrograph study of Sb^{124} (60 days) has been carried out by Hales and Jordan.[5] This work indicated that the β spectrum is complex with end points at 0.78 and 2.48 Mev. Previously Mitchell, Langer, and McDaniel[6] had found that the $\beta-\gamma$ coincidence rate was independent of the β energy and the end point which they obtained by absorption was given as 1.53 Mev.

Our coincidence curve is shown in Fig. 5. The $\beta-\gamma$ rate per β particle clearly decreases by a factor of 2.5 in the initial portion. From this curve a value of 0.67 Mev is obtained for the low energy component of the β spectrum. An absorption curve of the β radiation gives an upper limit of the high energy β radiation at 2.45 Mev. These values are in good agreement with the data of Hales and Jordan.

Coincidence measurements have also been made with europium[154] (5–8 years). The curve, shown in Fig. 6, indicates the complexity of the β spectrum. The low energy spectrum has an

[2] D. C. Kalbfell and R. A. Cooley, Phys. Rev. **58**, 91 (1940).
[3] A. F. Clark, Phys. Rev. **61**, 242 (1942).
[4] K. Siegbahn, Proc. Roy. Soc. **187**, 527 (1947).
[5] E. B. Hales and E. B. Jordan, Phys. Rev. **64**, 202 (1943).
[6] A. C. G. Mitchell, L. M. Langer, and P. W. McDaniel, Phys. Rev. **57**, 1107 (1940).

TABLE I. Beta ray energies.

Isotope	β spectrum	End point mg/cm² of Al		Energies	
Sb^{124}	Complex	204	1160	0.67	2.45
Cs^{134}	Simple		269		0.80
Eu^{154}	Complex	177	388	0.62	1.0
Au^{198}	Simple		332		0.91
Hf^{181}	?	98	184	0.34	0.64
$Ir^{192,194}$	Simple		208		0.68
$Hg^{203,205}$	Complex	15.3	77.5	0.11	0.44
Os^{193}	Simple		184		0.64
K^{42}	Complex	~660	1770	~1.52	3.57

upper limit of 0.62 Mev. Absorption of the total β radiation gives a value of 1.0 Mev for the higher energy β radiation.

The corresponding curve is shown for $Hg^{203,205}$ (51.5 days) in Fig. 7. The low energy β radiation corresponds to an energy of 0.11 Mev, while the total absorption curve gives a value of 0.44 Mev for the high energy component.

Potassium[42] (12.4 hours) prepared by deuteron bombardment also shows a complex spectrum (Fig. 8). It was very difficult to obtain the end point of the low energy spectrum, but an estimate of 1.5 Mev can be given. The high energy radiation was found to be completely absorbed by 1.77 g/cm² of aluminum, i.e., $E_{max}=3.6$ Mev (Fig. 9). This seems to be in agreement with the cloud-chamber work of Kurie, Richardson, and Paxton.[7] It appears that the higher energy β transition is not followed by γ radiation.

Hafnium

The decay of hafnium[181] (55 days) has been shown by De Benedetti and McGowan[8] to involve a metastable state of lifetime 22 microseconds. This is long compared to the resolving time (~0.5 microsecond) of the coincidence circuit used. It is interesting to note that the curve, Fig. 10, rises as the β absorber thickness is increased. A constant value is obtained when the thickness is ~12 to 13 mils of aluminum. It is not known whether or not the β spectrum itself is simple. From the data it would seem that the spectrum may really be simple, the rise being brought about by the delayed conversion electrons of lower energy.

4. SUMMARY OF RESULTS

In Table I, we have tabulated the β energies which we have found for these nine nuclei. All β energies except the low energy component of Hf and Hg are calculated from Feather's rule, i.e., $M(g/cm^2)=0.54E_{max}-0.16$.

[7] F. N. D. Kurie, J. R. Richardson, and H. C. Paxton, Phys. Rev. **49**, 368 (1936).
[8] S. De Benedetti and F. K. McGowan, Phys. Rev. **70**, 569 (1946).

Coincidence Measurements. Part II. Internal Conversion

M. L. WIEDENBECK AND K. Y. CHU
Department of Physics, University of Michigan, Ann Arbor, Michigan

(Received August 25, 1947)

It has been found that for a nucleus which has a simple β spectrum followed by internally converted γ radiation, the total absolute conversion coefficient can be obtained simply from single counting and coincidence rates. The method is independent of source strength, solid angle of counters, and counting efficiencies. The procedure could also be applied to processes involving complex β decay if the branching ratio were known.

The shape of the $\beta_{-e}-$ per observed β particle (i.e. $N_{\beta e}-/N_\beta$) curve is dependent upon the relative energies of the β particle and the conversion electrons as well as upon the conversion coefficient α.

The conversion coefficients have been obtained for gold[198], cesium[134], and iridium[193,194].

1. INTRODUCTION

INTERNAL conversion coefficients have been most commonly obtained from a beta spectrograph study of the radiation emitted by a radioactive source. If a γ ray is partially internally converted the monoenergetic conversion electrons appear as a peak superimposed on the smooth continuous β ray background. The conversion coefficient is then found by comparing the area under the excess peak with the total area under the continuous β curve. Clearly this method is difficult and generally does not lend itself to a high degree of accuracy. As an example, we may note the case of the 0.4-Mev line of gold[198]. Richardson[1] obtained a value of $\alpha=10$ percent, Plesset[2] 4 percent, and Siegbahn[3] ~ 1 percent. In addition, the spectrograph method cannot be easily applied to short-lived materials or to those which require the accurate measurement of energies below a few hundred kilovolts.

2. THEORY

Let us consider the decay scheme indicated in Fig. 1. N is the number of disintegrations per second, γ_1 is converted with a conversion coefficient α, $\gamma_2 \cdots \gamma_n$ represent non-converted γ rays, $\epsilon_1 \cdots \epsilon_n$ are the respective efficiencies of the γ counter for the γ radiation, ϵ_β is the efficiency of the β counter, σ with the appropriate subscript is the fraction of the sphere subtended by the counter. It is assumed that the efficiency of the γ counter is $\ll 1$ (actually ~ 0.01).

Coincidences are then measured between the β rays and conversion electrons. The source is fixed to counter (2). This coincidence rate is:

$$N_{\beta e^-}=2\alpha N\sigma_{\beta_1}\epsilon_\beta\sigma_{\beta_2}\epsilon_\beta$$

(if $\alpha\sigma_\beta$ is small). The counting rate of counter (1) is:

$$N_{\beta_1}=(1+\alpha)N\sigma_{\beta_1}\epsilon_\beta.$$

We next consider the $\beta-\gamma$ coincidence rate by placing an aluminum plug in front of the window of counter (1). Counter (2) is left unchanged.

$$N_{\beta\gamma}=(1+\alpha)N\sigma_{\beta_2}\epsilon_\beta\sigma_\gamma\left[\frac{(1-\alpha)}{(1+\alpha)}\epsilon_1+\sum_2^n\epsilon_n\right]$$

and the γ counting rate is

$$N_\gamma=N\sigma_\gamma\left[(1-\alpha)\epsilon_1+\sum_2^n\epsilon_n\right].$$

The ratio is then found

$$R=N_{\beta e^-}/N_\beta/N_{\beta\gamma}/N_\gamma\leqq 2\alpha/(1+\alpha)^2.$$

In the more exact case when α and σ_β may become large, a correction must be made in the β counting rate, N_β, and in the $\beta-\gamma$ rate, $N_{\beta\gamma}$, for the probability that both the β particle and the conversion electron will simultaneously pass through the same counter and be counted as a single particle. Considering this, the ratio becomes

$$R\leqq 2\alpha/[1+\alpha-(\alpha/2)\sigma_{\beta_2}\epsilon_{\beta_2}]^2.$$

[1] J. Richardson, Phys. Rev. **55**, 609 (1939).
[2] E. H. Plesset, Phys. Rev. **62**, 181 (1942).
[3] K. Siegbahn, Proc. Roy. Soc. **189**, 527 (1947).

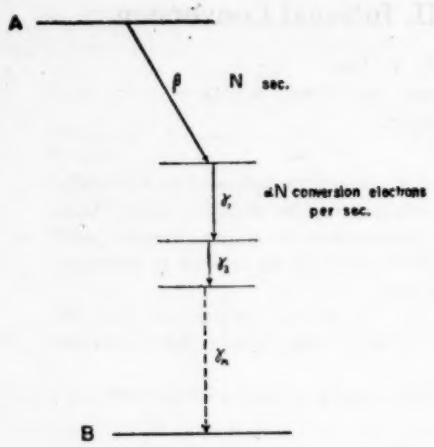

FIG. 1. Decay of nucleus A to nucleus B by the emission of a simple β spectrum. A series of γ rays, $\gamma_1 \cdots \gamma_n$ follow the β decay. γ_1 is internally converted with a conversion coefficient α.

In practice $\sigma_{\beta_2} \sim 0.1$, $\epsilon_{\beta_2} \sim 1$, so that if this correction were neglected the error introduced for $\alpha = 0.1$ would be ~ 0.5 percent. For $\alpha = 1$ the error would be ~ 2.5 percent.

A similar equation can be found for a cascade level scheme in which several γ lines are partially converted. For example, if γ_1 is converted with a coefficient α_1 and γ_2 with a coefficient α_2, then

$$R = N_{\beta e^-}/N_\beta / N_{\beta\gamma}/N_\gamma$$
$$= 2[\alpha_1 + \alpha_2 + \alpha_1\alpha_2]/[1+\alpha_1+\alpha_2]^2.$$

The total conversion coefficient $\alpha = \alpha_1 + \alpha_2$. If $\alpha_1\alpha_2$ is small $R \simeq 2\alpha/(1+\alpha)^2$. Even if α_1 and α_2 were as large as 0.1 the error introduced would be ~ 5 percent. Thus, in cases where R is small the total absolute conversion coefficient can be obtained. If R is large so that $\alpha_1\alpha_2$ could not be ignored, it would be necessary to know the relative values of α_1 and α_2.

All the previous calculations are for nuclei which have a simple β spectrum. Similar equations can be obtained for complex spectra, however, to obtain α it is necessary to know the branching ratio. We have, therefore, limited our experimental work to nuclei which apparently have simple β spectra.*

* Note added in proof: It is assumed throughout that both the conversion electrons and gamma rays are emitted without a preferred direction with respect to the beta particle.

Shape of $N_{\beta e^-}/N_\beta$ Curves as a Function of Absorber Thickness

The previous equations for α have been developed on the assumption that the γ rays and conversion electrons are not partially absorbed. In practice each must pass through a small thickness of material to enter the counter. It is, therefore, necessary to obtain the ratio $N_{\beta e^-}/N_\beta$ as a function of absorber thickness and extrapolate to zero absorber thickness. Such extrapolation ordinarily would introduce little error if counters with thin windows were used.

We again consider the decay indicated in Fig. 1. An absorber will be placed between the source and counter (1). Let F_1 and F_2 be the fraction of β particles and conversion electrons, respectively, which are transmitted by the absorber. Then

$$N_{\beta e^-} = (F_1 + F_2)\alpha N \sigma_{\beta_1}\sigma_{\beta_2}\epsilon_\beta^2,$$

and

$$N_{\beta 1} = (F_1 + \alpha F_2) N \sigma_{\beta_1}\epsilon_\beta,$$

$$N_{\beta e^-}/N_\beta = (F_1 + F_2)\alpha\sigma_{\beta_2}\epsilon_\beta/(F_1 + \alpha F_2).$$

Initially (with 0 absorber), F_1 and $F_2 = 1$.

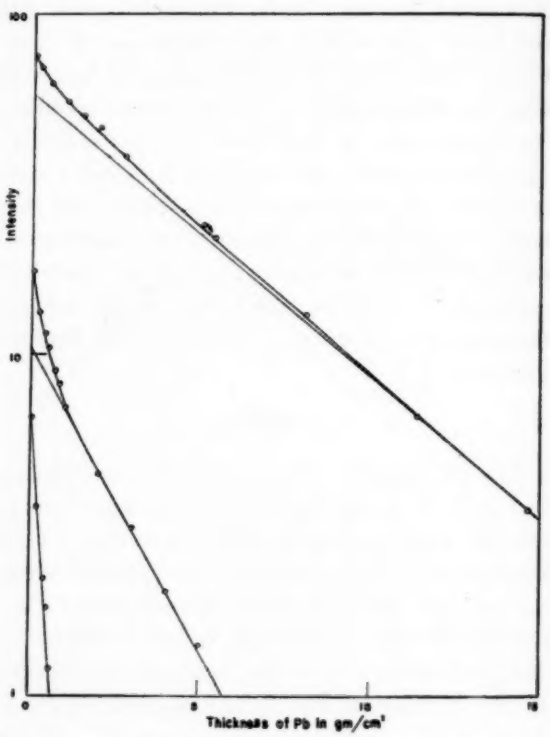

FIG. 2. Absorption curve of the γ rays of Au^{198}. Only the first portion is shown. This clearly is complex and can be broken into three components.

The initial and final values of the curve can be calculated. These are shown in Table I. That is, if F_1 is always equal to F_2, $N_{\beta e^-}/N_\beta$ as a function of absorber thickness will be a constant. If $F_1 > F_2$ (a) for small α the final value of this ratio will be $\approx \frac{1}{2}$ the initial value; (b) for large α the ratio again approaches a constant value. For $F_1 < F_2$ (i.e., essentially if the β energy is less than the e^- energy) the ratio will rise as the thickness is increased. This rise for small α will be $\sim 1/2\alpha$. Similar conditions exist if more than one γ ray is converted. The α then becomes the total conversion coefficient.

3. EXPERIMENTAL

In practice we have used the metal type self-quenching counters with an end window of $\frac{1}{2}$ mil Cellophane. A small brass disk was fitted into the end of counter (2). The sample was placed in a $\frac{1}{8}$-inch hole drilled through the center of the disk. This was found to be necessary to eliminate spurious coincidences resulting from the scattering of electrons from one counter to the other. In order to determine the conversion coefficient of a given nucleus it was found convenient to determine the ratio $N_{\beta e^-}/N_\beta$ as a function of absorber thickness. In all cases it was necessary to correct the β_{-e}- coincidences for $\beta-\gamma$ and $\gamma-\gamma$ coincidences. For most nuclei studied this was a very small correction in the region of interest. The value of $N_{\beta e^-}/N_\beta$ extrapolated to zero absorber thickness was then used in calculating α. We have investigated the effect of various absorbers, namely Cellophane and aluminum, on the extrapolated value and have found no difference.

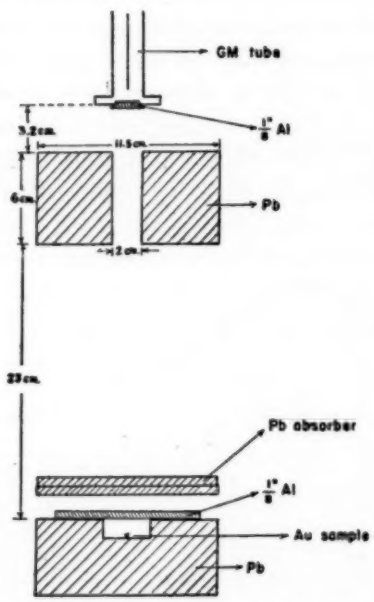

FIG. 3. The geometric arrangement used in obtaining the absorption curve for the γ radiation of Au^{198}. The source strength was ~50 millicuries.

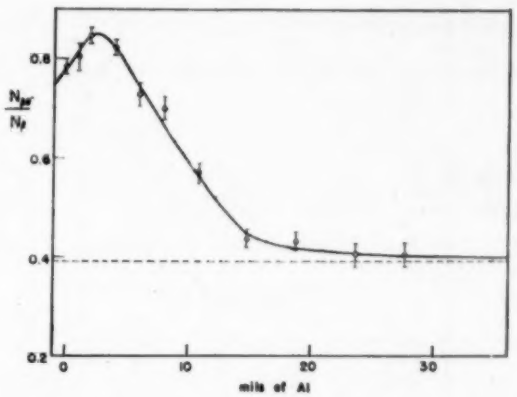

FIG. 4. The β conversion electron coincidence rate per observed β particle as a function of absorber thickness for Au^{198}. The extrapolated value is used to calculate α. The dotted line is the limit which the curve should approach if the e^- energy is less than the upper limit of the β energy.

Gold^{198}

Gold^{198} decays with a period of 2.7 days by the emission of a single β ray of energy 0.92 Mev. Siegbahn[3] has studied the γ radiation by observing the secondary electrons ejected from various radiators. He has found only one γ line of energy 0.401 Mev. However, Richardson,[1] from a cloud-chamber study, has observed three lines, namely, 70, 280, and 440 kev. Sizoo and Eijkman[4] have reported lines at 73, 250, and 410 kev and one of 2.5 Mev. Clark[5] in 1942 has reported $\gamma-\gamma$ coincidences from gold. It has been suggested by Siegbahn that these discrepancies may be due to other activities induced by deuterons on gold and that Au^{198} really emits only a simple β spectrum followed by a single γ ray.

It is mentioned by Siegbahn[3] that Norling[6] could not obtain any $\gamma-\gamma$ coincidence effects. This apparently is due to the extremely low efficiency of his lead counters for the lower energy

[4] G. J. Sizoo and C. Eijkman, Physica **6**, 332 (1939).
[5] A. Clark, Phys. Rev. **61**, 242 (1942).
[6] F. Norling, Ark. Mat. Astr. Fys. **A**, 27 (1941).

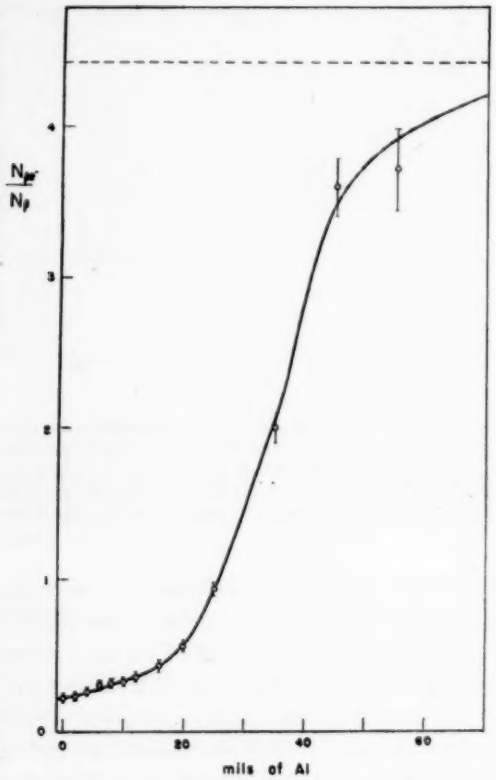

FIG. 5. Coincidence curve for Cs^{134}. The rise indicates that the ϵ^- energy exceeds the maximum β energy. The calculated limit is indicated by the dotted line.

γ radiation, since in making an absorption measurement of the γ radiation he points out: "The curve reveals the peculiar fact that the weak component is not counted at all, . . . On the other hand the soft component could be observed with a brass tube of 1 mm wall. . . . It ought to be possible to observe $\gamma-\gamma$ coincidences by the use of such counting tubes of brass, but the intensities of the available sources were too small for this purpose."

We have obtained γ ray absorption curves of strong ($\sim$50 millicuries) gold samples produced by slow neutron bombardment at Oak Ridge. As Siegbahn suggests, this sort of sample should be most free from other activities. Our absorption curve is found to be complex in the low energy region and can be broken into two components of energies $\sim$300 and 70 kev (Fig. 2) in addition to the 0.4-Mev line. The geometric arrangement is indicated in Fig. 3.

It is not possible to estimate the relative intensities, since apparently the efficiencies of the counters vary over a wide range in this energy region. This is clear from the fact that different types of counters give considerably different relative values, yet all the curves show the complexity.

We have also looked for and found $\gamma-\gamma$ coincidences both from the sources prepared by slow neutron capture and by deuteron bombardment on the Michigan cyclotron. It would therefore seem that the gold β radiation is followed by two γ rays emitted in cascade.

It has previously been mentioned that the 0.4-Mev line following the disintegration of gold is partially converted. From the β spectral distribution as obtained with a cloud chamber, Richardson[1] has found a value of $\sim$10 percent while Plesset,[2] from a β spectrograph study (using the photographic method) gives 4 percent and Siegbahn[3] $\sim$1 percent.

Using the coincidence method described above we have obtained the "$\beta_{-\epsilon^-}$ per observed β" curve indicated in Fig. 4. From the extrapolated rate and the $\beta-\gamma$ per observed γ rate we obtain a value $\alpha=4.70$ percent. It may be noted that the curve in Fig. 4 decreases with an increase in absorber thickness and seems to approach the theoretical value indicated by the dotted line.

The peculiar maximum in the $N_{\beta\epsilon^-}/N_\beta$ curve is apparently a real effect and presumably is due to the difference in absorption of the continuous β spectrum and the monoenergetic conversion electrons. In fact, a slope of zero should occur when $F_1/F_2=(dF_1/dx)/(dF_2/dx)$. Also the value of the absorber thickness at which the ratio is equal to the ratio at zero thickness should occur

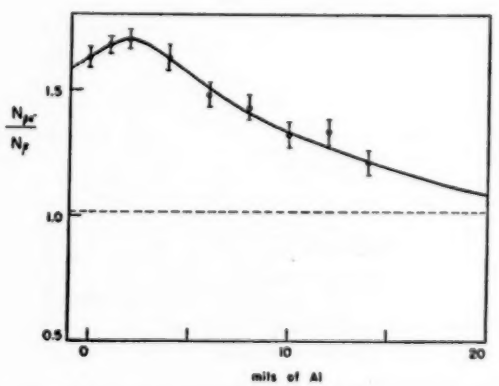

FIG. 6. Iridium coincidence curve. The ϵ^- energy is less than the β energy.

TABLE I. Calculated initial and final values of $N_{\beta e^-}/N_\beta$.

	Initial value	Final value
$F_1=F_2$	$(2\alpha/1+\alpha)\sigma_{\beta_2}\epsilon_\beta$	$(2\alpha/1+\alpha)\sigma_{\beta_2}\epsilon_\beta$
$F_1>F_2$	$(2\alpha/1+\alpha)\sigma_{\beta_2}\epsilon_\beta$	$\alpha\sigma_{\beta_2}\epsilon_\beta$
$F_1<F_2$	$(2\alpha/1+\alpha)\sigma_{\beta_2}\epsilon_\beta$	$\sigma_{\beta_2}\epsilon_\beta$

when $F_1=F_2$. That is, the absorption curves would cross at this point. It would be of interest to check these points by comparing the absorption of 0.4-Mev monoenergetic electrons (from a Van de Graaff machine) with the total absorption curve of gold.

Cesium[134]

In a similar manner, measurements were carried out on a sample of Cs^{134} produced by slow neutron bombardment in the Oak Ridge pile. It might be noted that the specific activities of most such samples are very large so that only an extremely small amount need be used as a counting source. The $N_{\beta e^-}/N_\beta$ curve as a function of absorber thickness is shown in Fig. 5. This curve clearly rises as should be expected if at least one of the converted lines has an energy greater than the upper energy limit of the continuous β spectrum. The total absolute conversion coefficient as calculated from the ratio $(N_{\beta e^-}/N_\beta)/(N_{\beta\gamma}/N_\gamma)$ is 2.51 percent. From this we see that the curve should rise to a value ~ 23 times the initial value. This final value is indicated by the dotted line in Fig. 5.

Relatively little is known concerning the γ radiation of Cs^{134}, however, once the relative conversion coefficients are found (if more than one line is converted), the absolute values of each can be obtained by using our absolute value for the total conversion coefficient.

TABLE II. Experimentally determined conversion coefficients.

Isotope	γ Energy	$\frac{N_{\beta e^-}}{N_\beta}$	$\frac{N_{\beta\gamma}}{N_\gamma}$	α
Au^{198}	0.401	0.0116	0.136	0.0470 ± 0.0024
Cs^{134}		0.00344	0.0719	0.0251 ± 0.0015
$Ir^{192,194}$		0.0247	0.0714	$0.286\ \pm0.014$

Iridium[192, 194]

Strong samples of iridium[192, 194] (60 days) were obtained by slow neutron bombardment. No special difficulties were encountered in obtaining the total conversion coefficient. The value obtained for α is 28.6 percent. The $N_{\beta e^-}/N_\beta$ curve is shown in Fig. 6. It clearly drops and seems to approach the predicted value (dotted line). The fact that it drops indicates that none of the conversion electrons have energies greater than the maximum energy of the β particles.

4. DISCUSSION

It would seem that by the coincidence methods herein described much data could be quickly and easily obtained concerning internally converted γ radiation. Unfortunately, we are at present limited to γ rays which follow a simple β spectrum. The same methods could be applied to disintegrations involving complex β spectra if the branching ratio were known. We have not as yet attempted to apply these procedures to disintegrations involving positron emission. Difficulties would probably arise from the annihilation radiation if the experimental procedure were not changed somewhat.

5. SUMMARY OF EXPERIMENTAL RESULTS

The experimental data on gold, cesium, and iridium are indicated in Table II.

A Photographic Apparatus for Angular-Distribution Measurements

SYLVAN RUBIN
W. K. Kellogg Radiation Laboratory, California Institute of Technology, Pasadena, California
(Received September 12, 1947)

A scattering camera was designed and constructed to measure the angular distribution of heavy charged particles emitted from nuclear reactions by means of the tracks which they produce in a photographic emulsion. It uses a single 2-in×4-in. plate to detect particles emitted in the angular range of 25° to 160° to the direction of the incident beam of bombarding particles. The camera has been used to investigate the angular distribution of the alpha-particles from the reaction $Li^7(p, \alpha)\alpha$, the long-range alpha-particles from $F^{19}(p, \alpha)O^{16}$, and the resonance scattering of protons in $Be^9(p, \gamma)B^{10}$. These reactions have been investigated over bombarding proton energies covering the range of interest in each reaction. This apparatus has been found to be effective for detailed measurements of angular distributions, with very high resolution of energy and of angle, even for reactions with very low yield, using thin solid targets. Fogging of the plates by soft x-rays from the target has been reduced by suitable target supports. Some results and conclusions concerning the above reactions are reported.

I. INTRODUCTION

THE determination of the angular distribution in the yield of nuclear reactions provides information on the characteristics of the quantum states involved in the reactions. The assignment of appropriate quantum numbers to various excitation levels in light nuclei is facilitated by a knowledge of the angular distribution in reactions involving those levels. The theory of the calculation of the angular distribution of resonance reactions is treated in several papers.[1–4]

Most of the experimental work on angular distributions between 1933 and 1940 was done with thick targets,[5–13] so that not much is known from these experiments of the variation of angular distribution with energy, except for Neuert's work.[14] Since 1940 several precision experiments have been done, giving detailed measurements of the angular distributions in a few light element reactions.

The reaction $H^2(d, p)H^3$ has been investigated up to 400 kev,[15,16] and the angular distribution is given by the function: $1+A\cos^2\theta$, where A increases smoothly to a value of 1.5 at 400 kev.

$H^2(d, n)He^3$ has been done from 500 kev to 1.8 Mev,[17] and the angular distribution is again given by $1+A\cos^2\theta$, with the curve for A *vs.* energy fitting smoothly to that for the protons from $H^2(d, p)H^3$, going to about 3.3 at 1.8 Mev.

$Li^7(p, \alpha)\alpha$ has been investigated up to 1.4 Mev.[18–20] It also fits the distribution function, $1+A\cos^2\theta$, at all energies; however A reaches a maximum of 2.1 at about 800 kev, and then slowly decreases.

$F^{19}(p, \alpha)O^{16}$ has been studied by several investigators,[21,22] and has been shown to have very complex distributions which change rapidly with energy. Results on this reaction are still very incomplete, because of the low yield of the long-

[1] E. Gerjuoy, Phys. Rev. **58**, 503 (1940).
[2] C. L. Critchfield and E. Teller, Phys. Rev. **60**, 10 (1941).
[3] E. Eisner, Phys. Rev. **65**, 85 (1944).
[4] G. Breit and B. T. Darling, Phys. Rev. **71**, 402 (1947).
[5] F. Kirchner, Physik. Zeits. **34**, 777 (1933).
[6] J. Giarratana and C. G. Brennecke, Phys. Rev. **49**, 35 (1936).
[7] A. E. Kempton, B. C. Browne, and R. Maasdorp, Proc. Roy. Soc. **157**, 386 (1936).
[8] H. Neuert, Physik. Zeits. **38**, 122 (1937).
[9] H. Neuert, Physik. Zeits. **38**, 618 (1937).
[10] H. Neuert, Zeits. f. tech. Physik **19**, 576 (1938).
[11] R. O. Haxby, J. S. Allen, and J. H. Williams, Phys. Rev. **53**, A921 (1938).
[12] A. Ellett and R. D. Huntoon, Phys. Rev. **54**, A87 (1938).
[13] R. O. Haxby, J. S. Allen, and J. H. Williams, Phys. Rev. **55**, 140 (1939).
[14] H. Neuert, Ann. d. Physik **36**, 437 (1939).
[15] R. D. Huntoon, A. Ellett, D. S. Bayley, and J. A. Van Allen, Phys. Rev. **58**, 97 (1940).
[16] H. P. Manning, R. D. Huntoon, F. E. Myers, and V. J. Young, Phys. Rev. **61**, 371 (1942).
[17] W. E. Bennett, C. E. Mandeville, and H. T. Richards, Phys. Rev. **69**, 418 (1946).
[18] V. J. Young, A. Ellett, and G. J. Plain, Phys. Rev. **58**, 498 (1940).
[19] C. D. Swartz, H. H. Rossi, B. Jennings, and D. R. Inglis, Phys. Rev. **65**, 80 (1944).
[20] S. Rubin, W. A. Fowler, and C. C. Lauritsen, Phys. Rev. **71**, 212 (1947).
[21] W. B. McLean, A. Ellett, and J. A. Jacobs, Phys. Rev. **58**, 500 (1940).
[22] H. H. Rossi and C. D. Swartz, Phys. Rev. **65**, 83 (1944).

range alphas, and the consequent difficulty of obtaining detailed data.

This paper describes a photographic technique for measurement of the angular distributions of some nuclear reactions. It has been used up to the present on the $Li^7(p, \alpha)\alpha$, and $F^{19}(p, \alpha)O^{16}$ reactions; and on the scattering of protons from beryllium.

II. APPARATUS

This "scattering camera" is partly based on the design published by Chadwick, May, Pickavance, and Powell,[23] which was a single-plate scattering camera for use in measuring the angular distribution of scattering of high energy particles from a cyclotron on a gas target. Its chief feature was the use of a single plate, so as to take advantage of the property of an emulsion of not only integrating the yield of heavy ionizing particles, but of defining their position of impact with the emulsion, and therefore their direction of travel from a sufficiently small source. This feature greatly increases the efficiency of a photographic plate over ionization chambers for a given angular resolution. Because both the solid angle subtended by the target at the chamber aperture, and that subtended by the chamber aperture at the target must be small, the yield will be inversely proportional to the square of the angular resolution for ionization chambers, or counters; whereas it is inversely proportional to the first power of the resolution for photographic plates used in this way, since there is no restriction on the solid angle subtended by the plate at the target.

The camera which has been constructed uses a single plate in a manner similar to that described by Chadwick, *et al.* However, to obtain still greater efficiency in detection it was decided to design it to use solid targets for either disintegration or scattering experiments, rather than the "tubular" gas target, in which energy loss in the consecutive axial elements contributing to the yield at each corresponding angle is accumulative. In a thin solid target there is only one element supplying particles at all angles and thus much less energy loss for a given yield, or conversely, more yield for a given energy resolution and angular resolution (Fig. 1).

For ease of construction the camera is a shallow cylindrical tank, about 6 in. in diameter and $1\frac{1}{2}$ in. deep, made of $\frac{1}{8}$-in. wall brass pump liner, with $\frac{3}{8}$-in. thick brass covers in which rubber gaskets are recessed. Six bolts, spaced uniformly around the exterior, clamp the two covers together to make the tank vacuum tight. The axis of the target-mounting assembly and collimating tube is 1 in. off-center, as indicated in the drawing, in order to allow sufficient space at one side for the plateholder. Two brass blocks, after being brazed to the exterior of the cylinder, were coaxially bored on a milling machine, and close-fitting circular flanges were soldered into these blocks so as to maintain accurate alignment. A reamed hole through each of these blocks for two of the six cover-clamping bolts positively aligns the covers with respect to this axis. The camera is mounted on the end of the beam analyzer of the electrostatic accelerator by means of the front flange, which also holds a tubular Lucite window and the tube containing the beam-defining aperture and shielding-baffle aperture. On the rear flange is mounted the target assembly and shield tube. The joints between all external components were sealed with rubber gaskets.

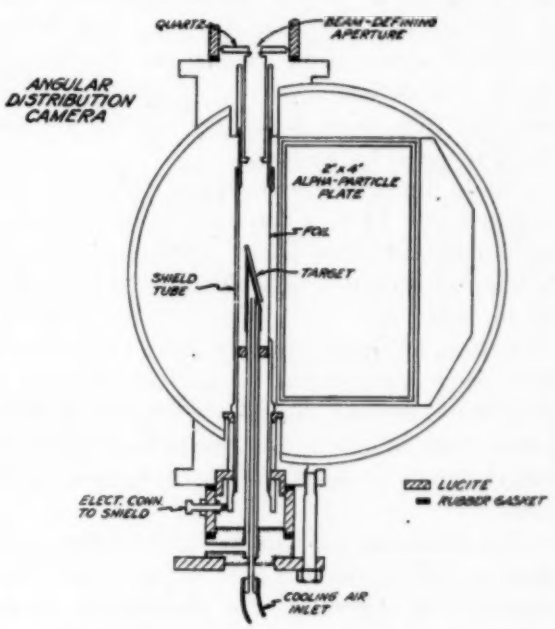

FIG. 1. Schematic drawing of scattering camera. One of several modifications.

[23] J. Chadwick, A. N. May, T. G. Pickavance, and C. F. Powell, Proc. Roy. Soc. **183**, 1 (1944).

The target is located at the central plane of the camera, on the off-center axis of the flanges. The various targets used have been mounted obliquely at 20°–25° to the incident beam, on a tubular thimble which slips on the end of a target-support tube. This tube is soldered to a brass disk which is separated from the rear flange by Lucite insulators to make possible measurements of the ion current to the target. For the work in which thin foil targets were used, the target mounting was modified to include a quartz window cemented in the rear disk, so that the ion beam, after penetrating the foil target, could be observed by the fluorescence it produced on the window. This was extremely useful in accurately aligning the beam in the camera. The target support tube is coaxial with a $\frac{1}{2}$-in. diameter shield tube which completely encloses it, and which is also insulated, so as to be part of a Faraday cage arrangement in which a negative potential of 90 volts on the shield relative to the target prevents loss of electrons from the target under ion bombardment. Into the front flange is screwed the aperture tube, with an insulated tip where it joins the shield tube mounted on the rear flange. The aperture tube carries a quartz disk with a small hole in its center for locating the ion beam, the beam defining aperture just below the quartz, and about $2\frac{1}{2}$ in. farther down a larger aperture to prevent ions scattered by the edges of the defining aperture from striking the electrostatic shield. The defining aperture is usually a $\frac{3}{32}$-in. circular, thin-edged hole, but can be stopped down to $\frac{1}{32}$ in. by an insert.

Cut in the wall of the shield tube is a rectangular slot, $1\frac{3}{4}$ in.$\times\frac{1}{4}$ in., in which is mounted an aluminum window frame. The frame is shaped to support a curved thin aluminum-foil window $\frac{3}{16}$ in. wide and $\frac{7}{8}$ in. long, of $\frac{5}{8}$-in. radius of curvature, in a position $\frac{5}{16}$ in. from the center of the target. Various foil thicknesses are used to stop the scattered particles from the incident beam, but to allow the reaction products of longer range to penetrate to the photographic plate.

The aluminum-foil window used for the earlier data on $Li^7(p, \alpha)\alpha$ was a straight, rather than curved, foil. However, the shortening of the tracks in the backward direction caused by the decrease of energy in the laboratory system, combined with the increased absorption of the straight foil at large angles from the normal, gave such short tracks at large backward angles that it was difficult to measure track density in this region. Use of a curved window after the first 4 plates was a considerable improvement, although there was not sufficient space available to make its radius equal to its distance from the target. Also, by using a set of removable aluminum window frames the window thickness could be changed more conveniently.

The photographic plates which have been used are 2-in.$\times$4-in. Eastman fine-grain alpha-particle plates with an emulsion about 20–25 microns thick. The plates were obtained about 2 dozen at a time, and successive batches were progressively better, giving closer grain spacing and clearer tracks. In the last emulsions used the mean-grain spacing is less than 1μ. All plates were on 0.043-in. glass, so as to be suitable for dark-field illumination with standard slide-illuminating condensers. One plate is used for each run, being mounted emulsion-side up in a plate holder fastened to one cover of the camera such that the long edge of the plate is parallel to the incident beam, which is 15 mm above the plane of the emulsion. Particles from the target, after penetrating the aluminum-foil window, thus strike the emulsion at a small angle to its plane along a circular arc on the emulsion at a constant distance of 50 mm from the target. From any point along this arc, between 25° and 155° to the direction of the incident beam, the entire effective target is visible through the aluminum window. The plate holder is closed by a light-tight hinged shutter which is operated from outside the camera with a lever mounted in a rubber diaphragm.

The most recent emulsions, which produce the best tracks, have such a low proportion of gelatine that there is frequent peeling of parts of the emulsion when the plate is put in a vacuum. This occurs along the edges of the plates, and sometimes quite a large piece of emulsion curls up or breaks off. To prevent these loose edges from projecting into the path of the particles to be detected a clip was made of 0.006-in. shim steel, to fit snugly on the front edge of the plate. The clip extends almost to the arc along which observations are to be made, and ensures that the

path to that arc from the target does not become obstructed by loose emulsion. Occasionally the peeling caused the loss of some data at the smallest or largest usable angles, in which cases the run was repeated.*

III. TARGETS

In preliminary tests, with various types of lithium and fluorine targets under proton bombardment, considerable trouble was encountered with fogging of plates, even after the target had been completely enclosed to prevent escape of any scattered protons. It was soon found that this was caused by soft x-rays from the target, as it could be eliminated by using only light elements in compounds with lithium or fluorine, and for the backing of thin targets. Thin targets of LiOH on steel or on aluminum gave excessive x-rays but were satisfactory on a beryllium backing. A thick CaF_2 target gave considerably more fog than a thick BeF_2 target. This variation in the action of various target-backing materials corresponds to the rapid increase in x-ray yield with atomic number.[24]

A run made with 700-kev protons bombarding a clean, thick, beryllium-metal target showed no significant yield of particles through an aluminum window of 3.93-mg/cm^2 surface density, so that beryllium provides a satisfactory backing for thin targets for proton bombardment, and was used for all the work described in this paper. This result is in agreement with the known ranges of the heavy particles from the disintegration of beryllium by protons.

The preliminary work on $F^{19}(p, \alpha)O^{16}$ was done with a thin BeF_2 target made by placing a drop of HF diluted with alcohol on the surface of a beryllium plate for a few seconds, then washing the excess off with alcohol. However, because of the very low cross section for long-range alphas, even this target gave excessive x-ray fogging. Although tracks were visible in it, they were difficult to count. Some targets were then made by mounting 0.5-micron thick beryllium foils on an oblique target thimble, with no backing behind the foil. The foils were coated with BeF_2 by holding a small drop of HF close to the foil for a short time. These made excellent thin targets, although fragile, requiring frequent replacement. Very satisfactory plates were obtained with no visible fog and easily observed tracks, in spite of the very low yield per proton.

IV. ASSOCIATED APPARATUS

The camera is mounted on the end of the ion-beam analyzer of the electrostatic generator which can, under present operating conditions, go to a voltage of 1.4 Mv. For the $Li^7(p, \alpha)\alpha$ experiments and the preliminary work on $F^{19}(p, \alpha)O^{16}$, a simple magnetic analyzer was used; for later work a combination electrostatic and magnetic analyzer was available. These analyzers, combined with an automatic electronic voltage-regulator operated by pick-up electrodes at the end of the analyzer, hold the voltage to within less than 1-kev variation, and hold the ion beam very steady in position.

The ion energy is determined by the output of a rotating sector generating voltmeter mounted in the top of the generator tank. This is calibrated with the narrow gamma-ray resonances of $F^{19}(p; \alpha, \gamma)O^{16}$ and $Be^9(p, \gamma)B^{10}$. In addition, since the advent of the electrostatic analyzer the analyzer deflection voltage has been found to be very convenient for ion-energy determination, and is also calibrated in terms of these γ-ray resonances.

The target assembly, electrically insulated by Lucite bushings, is connected to a low leakage 1 μf condenser, the voltage of which is measured by a quartz-fiber electrometer to give the integrated ion charge to the target. A galvanometer from the condenser to ground gives continuous readings of the instantaneous ion current.

V. MEASUREMENTS

The plates are measured on a microscope fitted with a mechanical stage driven by a micrometer screw and a paraboloidal dark-field illuminating condenser. Most of the observations are made with 8-power or 40-power objectives, depending on the track density, and a 25-power hyperplane eyepiece fitted with a counting reticle, dividing the circular field of view into about 16 squares (cut off a little at the corners).

* Note added in proof: The latest shipment of plates does not peel.

[24] M. S. Livingston, F. Genevese, and E. J. Konopinski, Phys. Rev. **51**, 835 (1937).

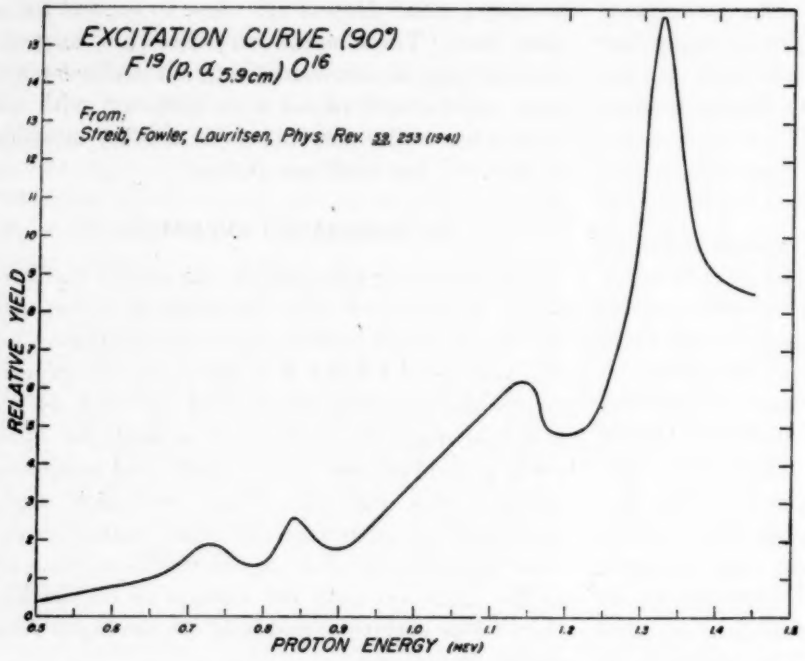

FIG. 2. Excitation curve for emission of long-range alpha-particles from proton bombardment of fluorine.

Before the plate can be measured it is necessary to lay out a coordinate system. The plate is examined under the microscope at several positions and adjusted each time so that the average direction of the tracks is parallel with the horizontal reticle lines, and a line is scribed on the plate through that point, also parallel with the reticle. This can be done to an accuracy of about 1° when the tracks are of reasonable length. The plate is then clamped on a coordinate-layout block which has lines scribed at 5° intervals radiating from a punch mark. The plate is adjusted so that the convergence point (actually a small area) of the lines previously scribed on the plate is centered on the punch mark, and the long edge is normal to the 90° line. This convergence point is about ½ in. off the plate, and the adjustment is made by checking with a straightedge. Two arcs are scribed on the emulsion, at 45.7- and 49.7-mm radius about the punch mark, with a sharp pair of dividers. Since the center of the target is 15 mm above the plane of the emulsion, the center of this 4-mm wide arc is at 50 mm from the target. Radial lines are drawn on the emulsion directly above the standard lines on the layout block. The plate is then ready for counting tracks.

It is clamped on the microscope stage, adjusted so that a radial line is parallel to the micrometer motion of the stage and passes through the center of the field of view. Starting near one edge of the 4-mm wide arc, all tracks are counted within a rectangular swath of a little less than 4 mm in length and some convenient width, depending on the track density. Various combinations of 8x and 40x objective, and 1-, 2-, or 4-squares width are used. The ratios of these widths, in actual distance, are known to about 3 percent by direct calibration measurements on a glass-reticle scale which had previously been measured on a comparator microscope. These calibration measurements were made with all available combinations of eyepieces and objectives.

The solid angle from the target is determined from the swath dimensions and the angle of incidence of the particles on the emulsion. For most counting, when the track density is most convenient, the 8x objective is used, and a swath 1 sq. wide (0.213 mm) and 0.140 in. long is counted. This, after correcting for the oblique incidence, is a solid angle from the target of 9.2×10^{-5} steradian, or 7.3×10^{-6} of a sphere. It is not difficult to count up to 1500 tracks in this area with this magnification, or several times more, using higher magnification. However, it is more convenient to use the lower magnification, thus setting an upper limit of about 2×10^{8} emitted particles (assuming isotropic distribution) for

each run. Even with thin targets this is usually obtained with a few hundred microcoulombs of bombarding particles.

After the counting is done at a sufficient number of different angles on the plate, depending on the detail and accuracy desired, the data is then corrected.

VI. CORRECTIONS

Three corrections are required for this method of obtaining angular distributions. First the angles measured in the plane of the plate must be converted to angles in a plane including the incident beam and the point where the tracks are observed. Since all measurements are made on an arc at 50 mm from the target, and the distance between the target and the plane of the plate is constant, this correction was computed only once and tabulated in the form of the cotangent of the corrected angle in terms of the observed angle. The formula used for this correction is

$$\sin\theta=\frac{\left(\sin^2\varphi+\left(\frac{h}{r}\right)^2\right)^{\frac{1}{2}}}{\left(1+\left(\frac{h}{r}\right)^2\right)^{\frac{1}{2}}},$$

where θ is the angle with respect to the incident beam, φ is the angle in the plane of the plate (observed), h is the normal distance from the target to the plate, and r is the radius from the target to the point of measurement.

The other two corrections are for conversion of the data in laboratory coordinates to center-of-mass coordinates, involving correcting both the angular coordinate and the yield per unit solid angle.

The correction to the angular coordinate is given by the exact expression:

$$\operatorname{ctn}\theta=\operatorname{ctn}\theta_c+\alpha\csc\theta_c,$$

where θ is the angle in laboratory coordinates, θ_c is the angle in C.M. coordinates, and

$$\alpha=\left[\frac{M_1M_2E_1}{MM_3Q+M_0M_3E_1}\right]^{\frac{1}{2}},$$

where M_0 is the mass of the stationary target nucleus, M_1 is the mass of the incident nucleus, M_2 is the mass of the observed nucleus, M_3 is the mass of the residual nucleus, $M=M_0+M_1=M_2+M_3$, E_1 is the energy of the incident nucleus, in laboratory coordinates, and Q is the reaction energy.

A convenient approximation, which is sufficiently accurate for this work, is

$$\operatorname{ctn}\theta_c=\operatorname{ctn}\theta-\alpha\csc\theta.$$

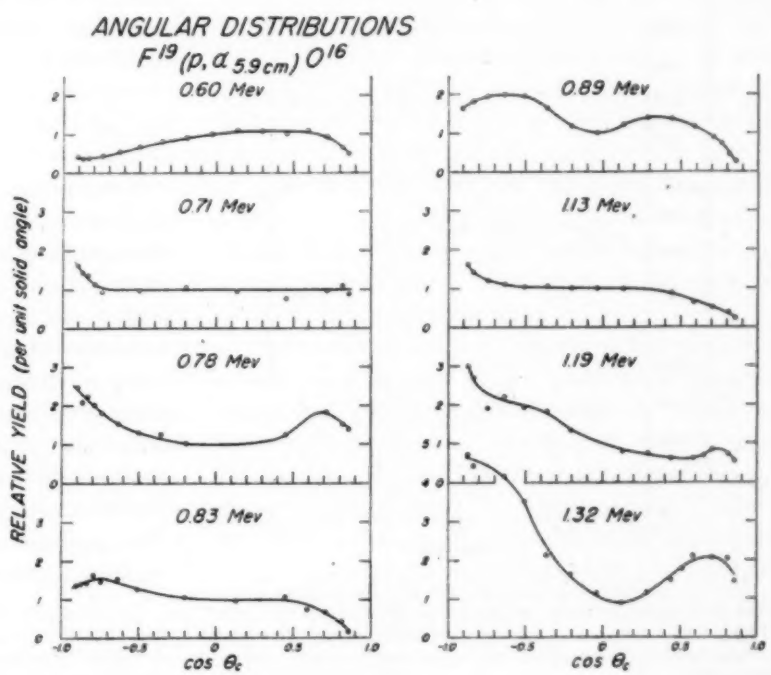

FIG. 3. Preliminary angular-distribution curves of long-range alphas from protons on fluorine. Yield coordinate normalized to unity at 90°.

Since the solid angles in which counts are made are very small in angular extent, the differential expression for the ratio of the solid angle in the C.M. system to that in the laboratory system is sufficiently accurate. It is

$$\frac{d\Omega_c}{d\Omega}=\frac{\sin\theta_c}{\sin\theta}\cdot\frac{d\theta_c}{d\theta}=\frac{(1+2\alpha\cos\theta_c+\alpha^2)^{\frac{1}{2}}}{1+\alpha\cos\theta_c}\simeq 1+2\alpha\cos\theta_c.$$

If N is the number of tracks in equal solid angles in the laboratory system and N_c the number in equal solid angles in the C.M. system, then

$$N_c=N\left(\frac{d\Omega}{d\Omega_c}\right)\simeq N(1-2\alpha\cos\theta_c).$$

The use of the first approximation to the correction is sufficiently accurate, since the maximum value of α in any of this work was 0.11 for proton scattering on Be^9. In this case the error in neglecting higher terms is about 2 percent at extreme angles. This is small compared to the statistical uncertainty in the number of tracks at each angle.

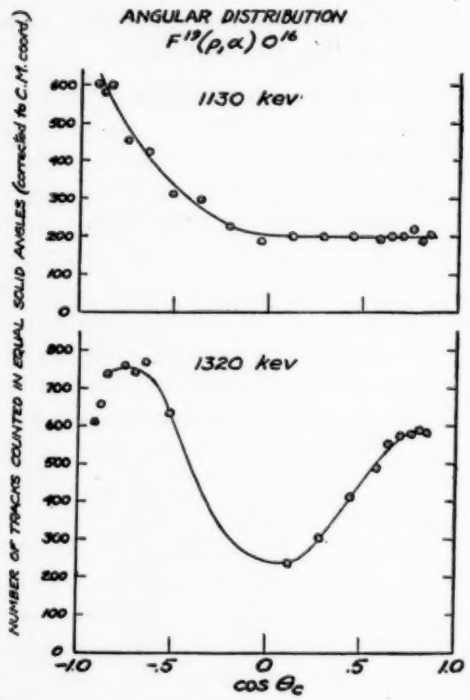

FIG. 4. Angular distribution curves of long-range alphas. Relative bombardment adjusted to give same 90° yield. The yield coordinate is approximately equal to actual tracks counted, so that statistical uncertainty can be estimated.

VII. RESULTS

I. $Li^7(p, \alpha)\alpha$ reaction

The results of the work on the angular distribution of the alpha-particles emitted in this reaction over a range of proton energies of 400 to 1400 kev have been previously published.[20]

II. $F^{19}(p, \alpha)O^{16}$ reaction

Another problem investigated was the reaction $F^{19}(p, \alpha)O^{16}$, leading to the emission of 5.9-cm alphas and O^{16} in its ground state. Because of the resonance character of this reaction in the energy range of 600- to 1400-kev proton energy, it was desired to investigate the angular distribution of the alphas at the various resonances, shown in Fig. 2.[25] For this purpose it was necessary to use a sufficiently thin target to obtain adequate resolution. This reaction proved to be considerably more difficult to work with than the $Li^7(p, \alpha)\alpha$ reaction, because of the low yield. It was necessary to make considerably heavier bombardments to obtain a sufficient yield of the alpha-particles, and, as a result, the plates became somewhat fogged by the x-rays from the thick beryllium-target backing. However, a preliminary set of curves was obtained, although the fogging of the plates limited the extent and accuracy of the track counting. They show a considerable variation of the character of the angular distribution from one resonance to another, as is shown in Fig. 3, but the accuracy is insufficient for analysis of the angular distributions into cosine powers.

Some plates were obtained later, using a different type of target. A thin foil of beryllium metal about 0.5μ thick, prepared by evaporation,[26] was mounted on the target support and coated with a thin film of BeF_2 by holding it in HF vapor for a short time. This target produced negligible x-ray intensity, so that the plates were free from x-ray fog. The track counting was much easier and more reliable, and more tracks were counted than on the earlier plates. However, these plates were not satisfactory because of a faulty window. The problem of separating the alphas and the scattered protons, especially above 1 Mev where

[25] J. F. Streib, W. A. Fowler, and C. C. Lauritsen, Phys. Rev. 59, 253 (1941).

[26] The beryllium foils were made by Dr. H. Bradner, Radiation Laboratory, Berkeley, California.

the alphas do not have very much more range than the protons, also contributed to the difficulty of working with this reaction, since the residual range of the alphas was very short after penetrating the foil which stopped the protons.

After a new window was prepared two plates, at 1140 kev and at 1330 kev, were obtained. These angular distributions are shown in Fig. 4. It will be noted that they essentially agree with the preliminary distributions in indicating a very complex variation of yield with angle.

The asymmetric character of these angular distributions indicates that interference effects in the wave function of the emitted alphas are being produced by adjacent or overlapping levels in the compound Ne^{20} nucleus, as odd powers of $\cos\theta$ in the angular distribution function can arise only from interference terms in the wave function. Also, the shapes of the distributions at small angles to the beam, where the effect of high powers of $\cos\theta$ will be significant, are such that terms of higher power than $\cos^2\theta$ appear to be needed to fit the data. If terms up to $\cos^3\theta$ or $\cos^4\theta$ are needed, this indicates an appreciable effect from *d*-wave incident protons.

At low energy the shift toward higher yield in the forward direction, instead of backward, as observed at higher energies, tends to agree with McLean, Ellett, and Jacobs'[21] result at 400 kev.

The angular distributions at 1140 and 1330 kev are satisfactorily fitted by the expressions—

$$1140 \text{ kev: } 1-\tfrac{1}{3}\cos\theta+\cos^2\theta-\cos^3\theta;$$
$$1330 \text{ kev: } 1-\cos\theta+6\cos^2\theta+\cos^3\theta-5\cos^4\theta.$$

The even powers of $\cos\theta$ at the prominent resonance at 1330 kev may be compared with the theoretical angular distribution from an assumed $^2P_{\frac{1}{2}}$ (even parity) ground state of F^{19}, reacting with *d*-wave protons to produce a compound level of $J=2$, which can decay to He^4 and the ground state of O^{16}. This is $\cos^2\theta-\cos^4\theta$, which is in fair agreement with the observed distribution at this resonance, if it be assumed that the constant term represents background caused by adjacent levels, and the odd powers of $\cos\theta$ are due to interference between the resonance and the background wave functions.[27]

[27] The fitting of the cosine power functions, and the calculation of the theoretical angular distributions were done by Professor R. F. Christy in the course of analyzing the data presented in this paper.

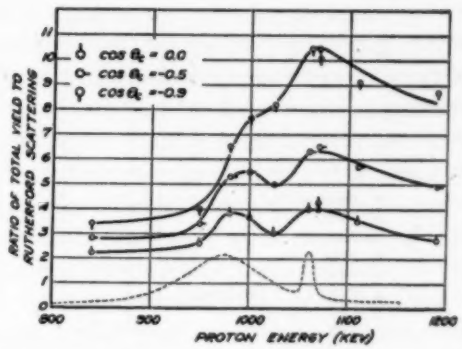

FIG. 5. Excitation curves of resonance scattering of protons from beryllium. Dotted curve is γ-ray yield from beryllium target of the same thickness.

The weaker resonance at 1140 kev shows a larger interference effect, so that an estimate of the character of this level is less clear.

Some penetration factors recently calculated by R. F. Christy show that the apparent yield from *d*-wave protons in this reaction is not unreasonable.

III. $Be^9(p, p)$ scattering

It was thought that an investigation of the angular distribution of the protons scattered from Be^9 at the γ-ray resonance energies in the reaction $Be^9(p, \gamma)B^{10}$ would give some information on the reason for the difference in the character of the two prominent γ-ray resonances at 972 and 1060 kev, shown in the dotted curve of Fig. 5.[28] The 972-kev resonance is a broad one and the 1060-kev resonance is very narrow, suggesting that the broad one may be due to *s*- or *p*-wave protons, and the narrow resonance to higher orbital momentum. A difference in orbital momentum might be expected to show up in the angular distribution of the resonance-scattered protons at the two energies.

The chief difficulty in observing the resonance scattering is that it is combined with Coulomb scattering, and these cannot easily be considered separately because of interference effects, especially at the angles where they are of equal magnitude. Furthermore, the reaction $Be^9(p, d)Be^8$ gives deuterons of approximately the same range as the elastically scattered protons, and the reaction $Be^9(p, \alpha)Li^6$ yields alphas of about half their

[28] C. C. Lauritsen, T. Lauritsen, and W. A. Fowler, Phys. Rev. 71, A279 (1947).

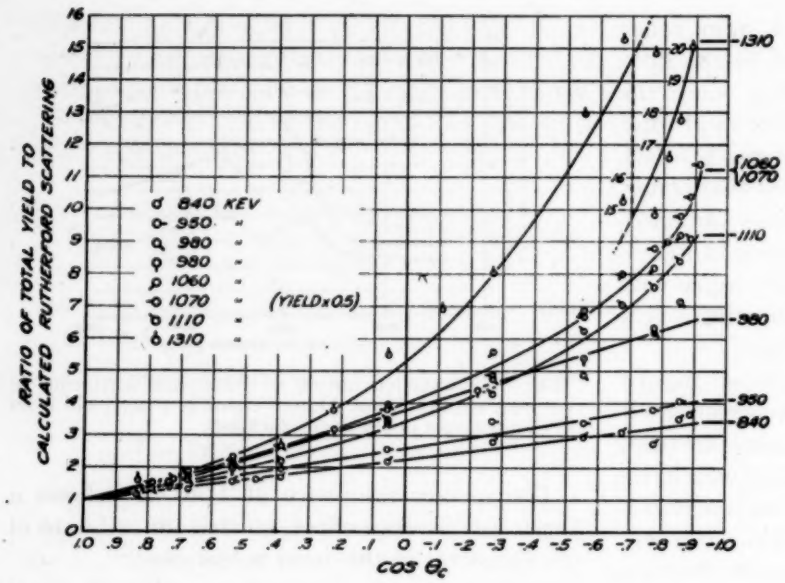

FIG. 6. Ratio of total yield of emitted particles to Rutherford scattering for various energies of protons bombarding beryllium.

range. All the emitted particles were included in the counting, since the deuteron tracks could not, in any case, be distinguished from the proton tracks, and the alpha-tracks were not easily recognizable. The very short ranges of all the particles meant that there were only about 10 grains per proton track, so that statistical fluctuations would make it difficult to distinguish them from the shorter, but more heavily ionizing, alpha-tracks.

A beryllium foil, 0.23 microns thick, was used for the scattering target. It was mounted on a 0.001-in. thick copper-foil washer, with a $\frac{5}{32}$-in. diameter aperture, set at 110° to the beam. The supporting thimble was cut out on one side below the target-supporting washer, so that particles observed at angles smaller than 110° came from the back of the target, and those observed at larger angles came from the front. No stopping window was used, as the particle ranges were already so short that it would have been useless to try to stop the alphas, as the remaining proton range would then be so short as to make the observations impossible.

Since the cross section for scattering is very large, an adequate yield of tracks is obtained, even from a very thin target, with a very small bombarding charge. To reduce the target current and improve the geometry a defining aperture of $\frac{1}{32}$-in. diameter was used, with a protective baffle of $\frac{1}{16}$-in. diameter, so that it was impossible for the beam to strike the copper-support foil. A smaller condenser (0.1 μf) was used in the current-integrating circuit. After some preliminary runs to determine the optimum bombarding charge, it was found that 1.20 microcoulombs of protons on the 0.23-micron foil was convenient.

Because of the shortness of the tracks a high magnification was more satisfactory for seeing them easily, using a 40-power objective and the 25-power eyepiece with the counting reticle. At this magnification it was possible to count track densities as high as 20,000 tracks per sq. mm before they became too numerous to easily distinguish individual tracks. The exposure of the plates was adjusted to make the track density approximately 20,000 per sq. mm at 25°, so that the much smaller yield at large angles would be sufficient to obtain good statistics. The results given below are based on measurements of 10 plates,[29] taken at various energies in the neighborhood of the γ-ray resonances.

The Rutherford scattering of protons on Be^9 per unit solid angle is given by

$$n(\theta)=1.04\frac{n_0N}{\beta}\left(\frac{10r_0}{9E}\right)^2,$$

where n_0 is the number of incident protons, N is the number of Be atoms/cm², $\beta=(1-\cos\theta)^2$

[29] Three of these plates were measured by G. S. Kenny, who is carrying out further development of this method.

$=4\sin^4(\theta/2)$, $r_0=2.82\times10^{-13}$ cm, and $E=$proton energy in Mev, which holds in the center-of-mass coordinate system. The tracks were counted in various areas, depending on the track density, then multiplied by an appropriate factor so that they would all correspond to a "standard" area of 0.140-in. length by 4-squares width (0.176 mm) in the counting reticle. Calculating this solid angle and putting it in the scattering formula, along with the beryllium-foil data, the following working formula is obtained:

$$N_R=\frac{184.}{\beta E^2},$$

where N_R is the number of tracks in the "standard" counting area.

The correction of the observed angles and yield to C.M. coordinates was made on the assumption that the observed particles were elastically scattered protons, for which $\alpha=\frac{1}{9}$ (independently of E_p, since $Q=0$).

The resulting yield data was treated in several ways to see what analysis would be most suitable. The ratio of the observed yield to the calculated Rutherford scattering was plotted against $\cos\theta_c$ for each plate. This is shown in Fig. 6. These curves show that the deviation from Rutherford scattering becomes very marked at large angles, especially at the higher energies used.

The data is also plotted as total yield minus Rutherford scattering in Fig. 7. Since the ratio to Rutherford scattering is large at large angles, the total yield at the large angles becomes more nearly equal to the additional yield as interference effects become small, if it is assumed that the additional yield is due to resonance scattering of protons. The two wave functions will give interference terms which will be strong where the two primary intensities are of equal magnitude, but the total yield will be not much different from the larger, when one is much stronger than the other. For this reason the yield at large angles minus Rutherford scattering ought to be a reasonable estimate of the additional effect caused either by resonance scattering or by another reaction. The fact that these curves rise sharply at small angles indicates the probability that the increase is due to interference terms between resonance yield of protons and the Rutherford scattering, as the yield of alphas or deuterons would not show any interference effect.

Figure 5 gives excitation curves of the resonance scattering at various angles. The points are taken from the smoothed curves of Fig. 6. They show two maxima which appear to correspond to the two γ-ray-emitting levels, although considerably broadened. Figure 5 also shows the γ-ray yield from a beryllium foil of the same thickness. The very considerable broadening of the reso-

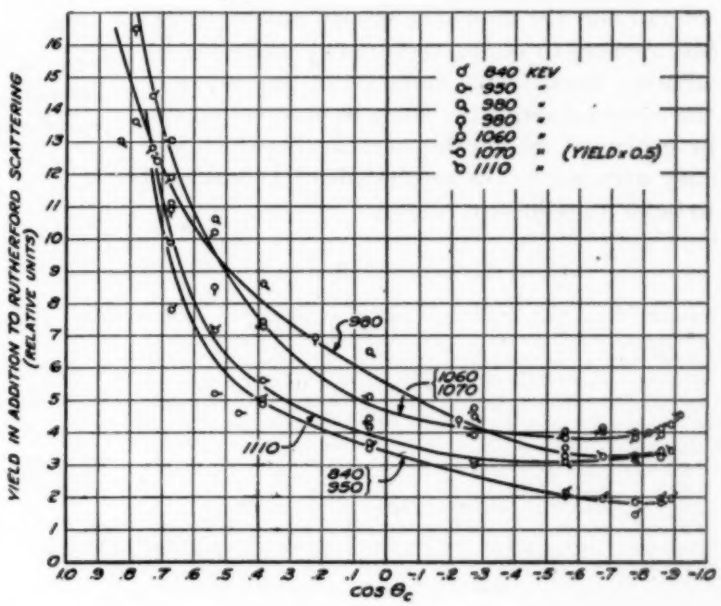

FIG. 7. Total yield after subtracting Rutherford scattering at various proton energies.

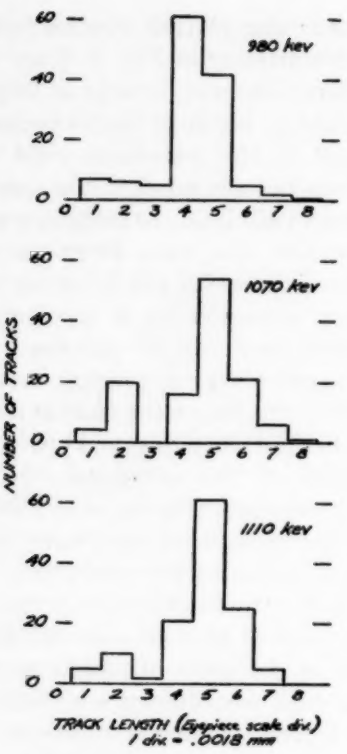

FIG. 8. Range distribution curves. Maximum is at correct range in emulsion for scattered protons; group at ~2 div. range is approximately range of alphas from $Be^9(p, \alpha)Li^6$. Deuterons from $Be^9(p, d)Be^8$ are not distinguishable from protons.

nances for scattering, especially at the low energy side, cannot be accounted for solely by interference with Rutherford scattering, which would tend to shift the resonance toward higher energy, but appears to require additional scattering by adjacent levels. Some variation of the energy of the maximum with the angle of observation can be explained by interference effects, which will vary with angle. The results must be considered to be of a preliminary nature.

It is difficult to correlate the width of the broad γ-ray resonance with the large ratio of total yield to Rutherford scattering observed at large angles, since the width of 100 kev seems to require s-wave protons for γ-ray production, yet for s-wave protons, using Bethe's formula for the ratio of total yield to Rutherford scattering,[30] the maximum scattering ratio at 180° is about 7. If we assume that the deuteron yield is of the same order of magnitude as the alpha-yield which may be about 20 percent of the total, as shown in Fig. 8, then in the backward direction they would make up about half the total yield. In that case the ratio of the remaining yield, which would be the resonance-scattered protons, to the Rutherford scattering would be brought down to about 6, but the theoretical ratio would be somewhat reduced from 7 by the increased total width, so that this is not a satisfactory explanation. Another possibility is that we are dealing with more than one resonance in the emission of heavy particles, or that there is a strong background in addition to the resonance, which could change the critical quantities sufficiently to account for this effect with resonance scattering of s-wave protons. It may also be that the broad γ-ray resonance is due to p-wave protons, and that it is the large width which needs to be explained.

The author is grateful to Professors C. C. Lauritsen, T. Lauritsen, R. F. Christy, and W. A. Fowler for their aid and advice in this work.

This work was carried out under contract of the laboratory with the Office of Naval Research, and under a fellowship grant to the author from the National Research Council.

[30] H. A. Bethe, Rev. Mod. Phys. 9, 176 (1937), formula 625.

Relation of Frequency of Occurrence of Small Cosmic-Ray Bursts to Areas of Sunspots and Other Variables*

JAMES W. BROXON
Department of Physics, University of Colorado, Boulder, Colorado
(Received August 13, 1947)

This paper deals with the frequency of occurrence of small cosmic-ray bursts represented by 2.9 to 3.6 millions of pairs of ions in a heavily shielded chamber of 13.3 liters effective volume containing air at 160 atmospheres. An earlier investigation by Chree's method of superposed epochs had indicated 27-day recurrences in fluctuations of the frequency, somewhat comparable to the 28-day recurrences found in the cosmic-ray intensity as represented by the daily average ionization current in the same chamber corrected for bursts and for variations in atmospheric pressure. Here the analysis is continued to investigate the possibility of a dependence of the small-burst frequency upon terrestrial magnetic character and sunspot area comparable to that found for the C-R intensity, as well as the relation between the latter and the burst frequency. While some positive correlation between the burst frequency and the corrected ionization current is indicated, the relation does not appear to be intimate. Pulses in the burst frequency representing deviations of more than seven percent from the mean are found associated with the primary pulses in sunspot area, particularly the negative pulse, and roughly in phase opposition. No clear-cut relation to the magnetic character is indicated. A large negative barometric coefficient is found for the burst frequency, at least for the early months of the year, amounting to about −3 or −4 percent per mm Hg. An explanation of the observations is suggested in terms of the production of the small bursts and the (corrected) ionization in the shielded chamber through the agency of different types of radiation.

IN a recent paper,[1] the author reported a preliminary investigation of the frequency of occurrence of certain small cosmic-ray bursts occurring in a shielded, high pressure chamber at Boulder (lat. 40°N; long. 105°16′W; alt. 5440 ft.) by Chree's "superposed-epoch" method of analysis. The analysis was carried out for the limited range of day numbers from −45 to +45. Irregular pulses were found both preceding and subsequent to both positive and negative primary pulses. Both subsequent and preceding difference curves and the combination difference curve displayed pulses with peaks at about 27 days preceding and subsequent to the primary pulses. These secondary pulses amounted to about 3 or 4 percent of the average frequency of approximately 37 small bursts per day (corrected for grounding time) and about 10 percent of the primary pulses.

As explained in the earlier paper,[1] the investigation was limited to bursts producing deflections between 1.0 and 1.25 mm on the photographic record, representing 2.9 to 3.6 millions of pairs of ions in the chamber. The effective volume of the chamber was 13.3 liters, and it contained air at a pressure of about 160 atmospheres. The thick-walled steel chamber was surrounded by 5 inches of lead, and was further shielded by the stone walls of the building in whose basement it was located. Since the ionization chamber[2] was formed by excavating a spherical cavity from a solid steel cylinder, the shielding provided by the chamber walls varied from a little over 7 cm of steel for vertical rays through a maximum of

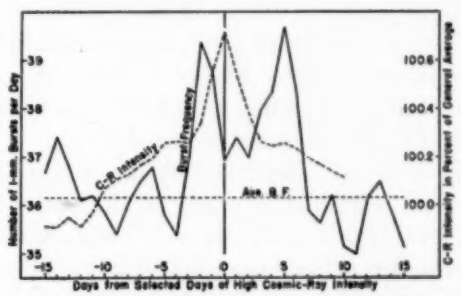

FIG. 1. Primary positive pulse in the cosmic-ray intensity as measured by the corrected ionization current, together with corresponding pulse in frequency of 1-mm bursts. Zero days are the five in each month of greatest cosmic-ray intensity as indicated by the average current. In this and subsequent diagrams, the number of 1-mm bursts designated is the number observed in 24 hours without correction for the grounding period of 2 minutes in each hour.

* A preliminary report of this work was given at the meeting of the American Physical Society at Montreal, Canada, June 19, 1947.

[1] J. W. Broxon, Phys. Rev. **70**, 494 (1946).

[2] J. W. Broxon, Phys. Rev. **37**, 1320 (1931). Figure 3, p. 1323, shows a longitudinal section of the chamber. The collecting electrode and the plug holding the cones have been modified, but the dimensions of the chamber are correctly designated here.

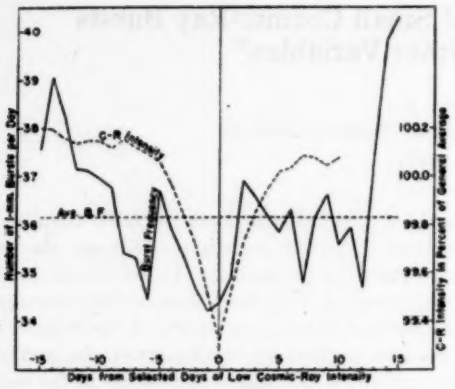

FIG. 2. Primary negative pulse in cosmic-ray intensity, together with corresponding pulse in frequency of 1-mm bursts.

over 14 cm at a zenith angle of about 42°, to a minimum of about 4 cm for horizontal rays. The somewhat non-uniform shielding afforded by the chamber walls and surrounding lead can perhaps be regarded as roughly equivalent to a lead shield of about 18-cm thickness. The chamber was further shielded by the building. Its location was in the basement near the foot of one of the outer stone walls whose thickness was 2.5 ft. at the bottom and which extended some 70 ft. above the chamber. It is difficult to estimate the shielding afforded by the building with its towers and numerous buttresses as well as concrete beams and floors and interior stone walls. Dr. Whaley has estimated that it was roughly equivalent in absorbing power to 39 cm of lead. With the exception of a very small solid angle subtended by a portion of a nearby sunken window, it would appear that the shielding afforded by the building would probably amount to some 15 cm of lead for any direction, and certainly much more than 40 cm for certain directions. In the present investigation, the same data were employed as in the preceding paper;[1] the number of small bursts per day during the period of observation (June, 1938, to November, 1939, inclusive) was not corrected for the two-minute grounding period each hour, and the nearest integral number was employed when corrections were applied because of lack of data for some of the 24 hours of the day. Also, no corrections were applied for variations of atmospheric pressure or other variables.

The indications of recurrence of variations in the frequency of occurrence of the small bursts are reminiscent of the recurrences of variations of the daily average ionization current in the same chamber during the same period of observation. Secondary pulses in the latter, after correction for bursts and for variations of barometric pressure, were found by the author[3] to occur at approximately 28-day intervals, and to extend at least as far as four such intervals before and after the corresponding primary pulses. Because the primary pulses in the daily average ionization current were also found[4] to have associated with them very definite inverse pulses in the terrestrial magnetic character and also in the total sunspot area, it was thought that there might likewise be found some such relation for the frequency of occurrence of the small bursts

First it was decided to investigate further the relation between the frequency of the small bursts and the (corrected) average ionization current. As mentioned formerly,[1] no clear relation was displayed among the four groups of 90 zero days each, which were selected as the 5 days in each of the 18 months during which the average ionization current was greatest or least or the small-burst frequency was greatest or least. As stated, "17 zero days selected for their large number of 1-mm bursts were identical with days selected on the basis of large average cosmic-ray ionization current, and 22 zero days selected for their small number of 1-mm bursts were identical with those selected for their small average current. On the other hand, 9 zero days selected for their large number of 1-mm bursts were identical with those selected on the basis of small average current, and 13 zero days selected for their small number of 1-mm bursts were identical with those selected for their large average current."

To test the relation further, the zero days selected on the basis of large or small average (corrected) C-R ionization current were employed for the burst-frequency data, just as was done in investigating the relation between the average C-R ionization current and either magnetic character or sunspot areas in earlier work.[4] Figure 1 shows the curve obtained for the frequency of the small bursts by Chree's method for the 18-month interval, with zero days selected on the basis of high average C-R ionization current,

[3] J. W. Broxon, Phys. Rev. 59, 773 (1941).
[4] J. W. Broxon, Phys. Rev. 62, 508 (1942).

from day number −15 to +15. As in all the diagrams, the ordinates indicate the number of bursts per 24-hour day, not corrected for the 2-minute grounding period each hour. The dotted curve represents the corresponding average C-R ionization current for the same zero days, expressed in percent of its over-all mean. This is the same dotted curve designated in Figs. 1 and 6 of reference 4 as representing the primary pulse in the cosmic-ray intensity, and extends only to $n=10$ for positive day numbers. While the frequency of the small bursts is seen to be above average in the neighborhood of the zero days selected on the basis of their large average ionization currents, there are peaks on either side of the zero, and the shape of the curve does not correspond at all well to the form of the curve representing the C-R intensity or average ionization current. A striking feature of the burst-frequency curve is the magnitude of the departures from

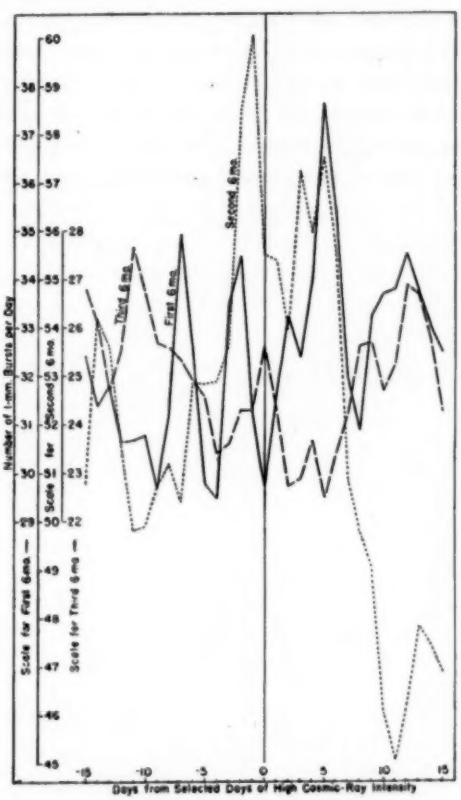

FIG. 3. These curves represent variations of frequency of 1-mm bursts in the neighborhood of the primary positive pulses in C-R intensity for each of the three successive six-month intervals of the period of investigation. The corresponding pulses in C-R intensity are not shown; their peaks would fall on day number zero, of course, as in Fig. 1.

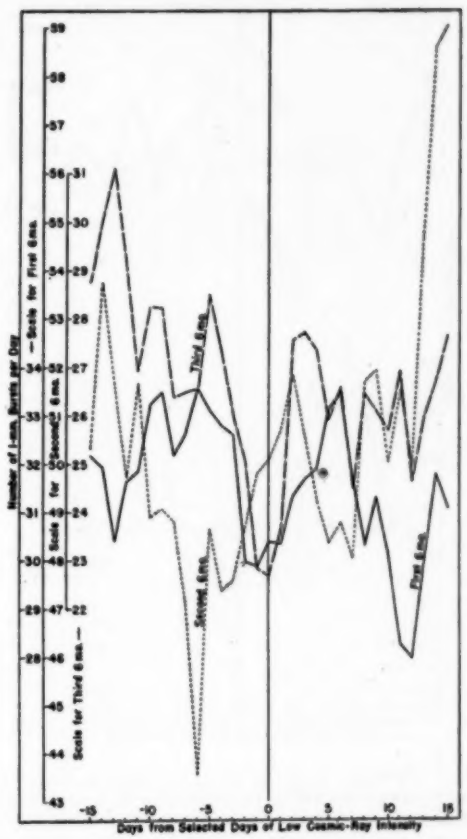

FIG. 4. These curves represent variations of frequency of 1-mm bursts in the neighborhood of the primary negative pulses in C-R intensity (not shown) for the successive 6-month intervals.

the average which extend to some 9 percent in comparison with the primary positive peak in the C-R intensity which departs less than 0.7 percent from the average.

Figure 2 shows the curve obtained for the frequency of the small bursts with zero days selected on the basis of small C-R intensity (or average ionization current) for the 18-month interval. The dotted curve here represents the primary negative pulse in the C-R intensity, and is identical with the dotted curve of Figs. 2 and 7 of reference 4. Here there is a considerable dip in the burst-frequency curve in the immediate neighborhood of the selected days of low C-R intensity, but the curve fluctuates about the average a little further from the zero days, and there are other dips nearly as low. The high values a couple of weeks before and after the zero day number are rather striking. Altogether, there

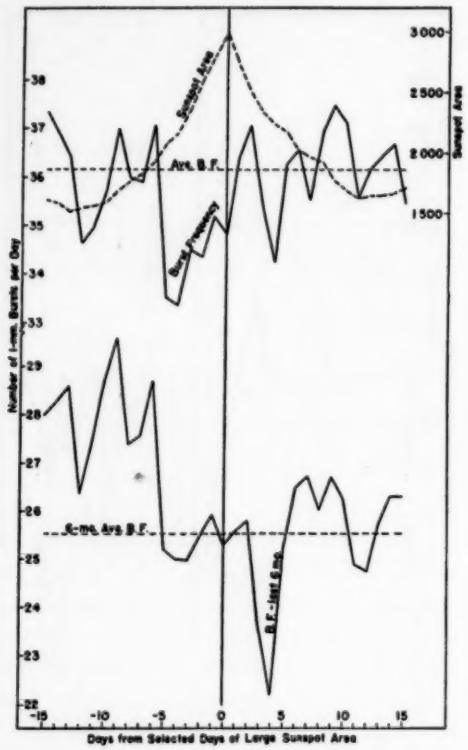

FIG. 5. Primary positive pulse in sunspot area, together with corresponding pulse in frequency of 1-mm bursts for the 18 months, are shown by upper curves. The lower curve represents the variation of burst frequency with respect to zero days of large sunspot area selected only from the last 6 months.

does not seem to be a very close correspondence between the two curves.

Because of the irregularities of the burst-frequency curves associated with the positive and negative primary pulses in the C-R intensity for the 18-month interval, and because it was observed that the frequency of occurrence of the small bursts was considerably greater during the winter and spring months than during the summer and fall months, it was decided to form corresponding separate diagrams for zero days restricted to 6-month intervals. These are shown in Figs. 3 and 4. The curves for the first 6 months and for the third 6 months were obtained with zero days selected from the months June–November, inclusive, of 1938 and 1939, respectively, while those for the second 6 months were obtained with zero days selected from the intervening months, December–May. The dependence of the frequency of occurrence of the small bursts upon the season is roughly shown by the scales employed for the individual curves of these diagrams. For Fig. 3 the zero days are those selected on the basis of high C-R intensity (or average ionization current), while for Fig. 4 the zero days are those of low C-R intensity.

To the writer it appears that about all that is provided by Figs. 3 and 4 is further confirmation of the indications of Figs. 1 and 2 that there is not a very intimate relation between the frequency of occurrence of the small bursts and the intensity of the hard component of the cosmic radiation as represented by the average ionization current. It should be borne in mind, of course, that appreciably more random fluctuations should be expected for a 6-month than for an 18-month interval, because of the smaller number of data involved. Rather more of a direct relation appears in the curves for the winter and spring months than in those for the summer and fall months which seem to represent quite random fluctuations. Because of the much larger number of bursts during the second 6-month interval, this interval has a very considerable influence in determining the shapes of the curves of Figs. 1 and 2 for the 18-month interval.

To investigate the relation between burst frequency and sunspot area, zero days were chosen

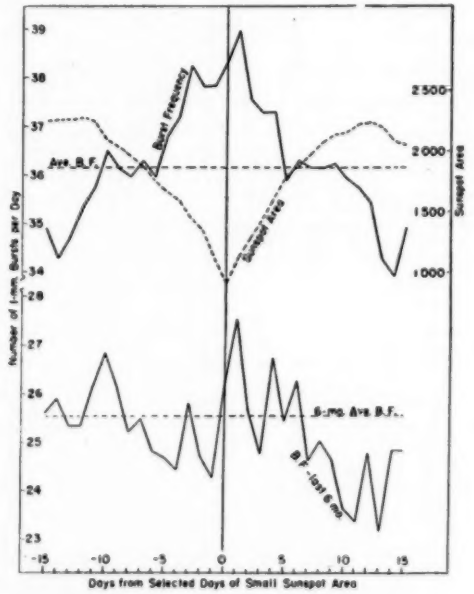

FIG. 6. Primary negative pulse in sunspot area, together with corresponding pulse in frequency of 1-mm bursts for the 18 months, are shown by upper curves. The lower curve shows variations of burst frequency with zero days of small sunspot area selected only from the last 6 months.

on the basis of sunspot area. This differed from the procedure in reference 4 for establishing the relation between C-R intensity and either sunspot area or magnetic character, for there the zero days were selected on the basis of C-R intensity. For Fig. 5 the zero days were the five of greatest sunspot area in each month. The sunspot data are the same as employed in reference 4. The sunspot-area values used represent the sum of the areas of all visible sunspots, corrected for foreshortening, in terms of one-millionth of the sun's visible hemisphere as unit. The upper burst-frequency curve was obtained with zero days for all eighteen months, as was the dotted curve representing the primary positive pulse in sunspot area. While the average total sunspot area during the 18 months, 1889.3 units, is not designated in Figs. 5 and 6, this is not very much greater than the value corresponding to the horizontal line representing the average burst frequency. Although the burst-frequency curve is quite irregular and represents quite random fluctuations about the average over most of the range (−15 to +15) of day numbers investigated, there is a rather especially deep and broad dip in the curve extending nearly 8 percent below the average, with its lowest point at 4 days before the zero days of large sunspot area. Unfortunately, we have no mathematical criteria to assist in deciding when such a deviation is "significant." The author is inclined toward the view that the curve does provide some indication of an inverse relation between variations in burst frequency and sunspot area. Because of the much lower frequency of occurrence of the bursts during the summer and fall months, a separate curve with zero days from only the last 6 months has been included in this and some subsequent diagrams. In Fig. 5 the burst-frequency curve for the last 6 months also shows a decided dip, narrower than in the 18-month curve and with its tip at $n=+4$, with quite high values in the region $n=-15$ to -6.

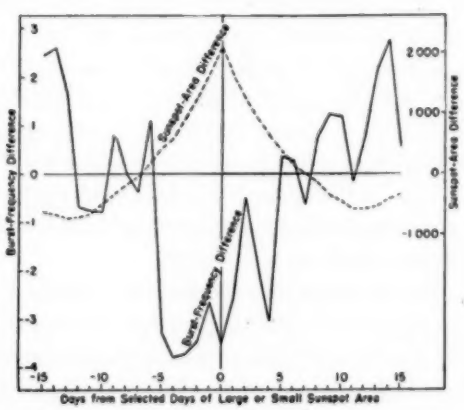

FIG. 7. Primary "difference" pulse in sunspot area, together with corresponding difference pulse for burst frequency for the 18 months. These curves were obtained by subtracting ordinates of the upper curves of Fig. 6 from the corresponding ordinates of Fig. 5.

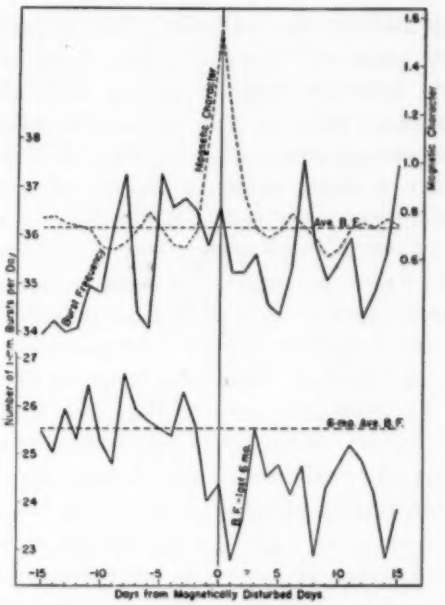

FIG. 8. Primary positive pulse in magnetic character, together with corresponding fluctuations in frequency of 1-mm bursts for the 18 months, shown by upper curves. Lower curve represents variation of burst frequency relative to magnetically disturbed days selected only from the last 6 months.

The curves of Fig. 6 were constructed by a procedure precisely analogous to that followed in the case of Fig. 5, except that here the zero days were the five of least total sunspot area in each month. The burst-frequency curve for the 18 months here shows a very definite pulse in phase opposition to the negative primary pulse in sunspot area. It is above the average for an interval of some 10 days, and well centered relative to the zero days of least sunspot area, with its highest peak (representing a deviation a little less than 8 percent from the average) at day number 1. The burst frequency is also definitely below average two weeks before and after the zero days. This seems to constitute the best indication of an interrelation between burst fre-

quency and another variable which is provided by this analysis. This indication of an inverse relation between burst frequency and sunspot area appears quite as clear-cut as that provided by the comparable curves of Figs. 6 and 7 of reference 4 which show an inverse relation between sunspot area and C-R intensity as measured by the average ion current. The curve for the last 6 months, however, cannot be considered to provide further substantiation; it scarcely indicates any relation between the variables.

Figure 7 shows "difference" curves obtained from the 18-month curves of Figs. 5 and 6 in the usual manner, ordinates being obtained by subtracting the ordinates in Fig. 6 from the corresponding ordinates in Fig. 5. The burst-frequency difference curve of Fig. 7 also displays a definite pulse in burst frequency in approximate phase opposition to the primary pulse in the sunspot-area difference curve.

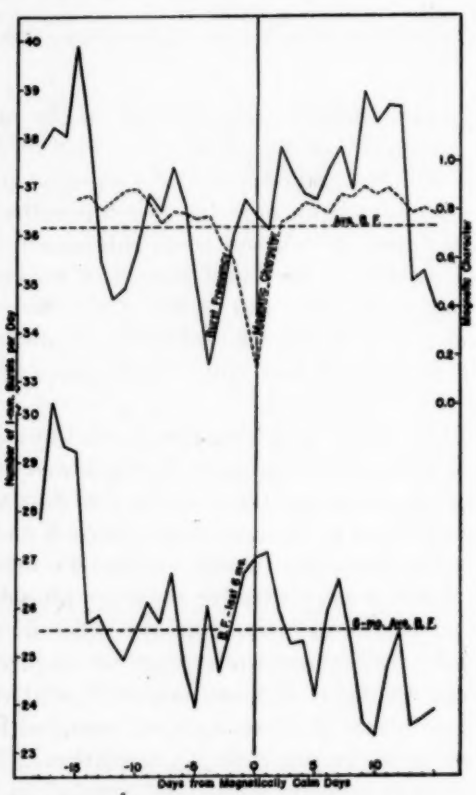

FIG. 9. Primary negative pulse in magnetic character, together with corresponding fluctuations in frequency of 1-mm bursts for the 18 months, are shown by upper curves. Lower curve represents variation of burst frequency relative to magnetically calm days selected only from the last 6 months.

Figures 8, 9, and 10 represent the results of an investigation of a possible relation of the burst frequency to magnetic character, carried out step by step in accordance with the procedure employed in obtaining Figs. 5, 6, and 7, respectively. In this case, the world-wide magnetic character numbers employed in reference 4 were used in place of sunspot areas, and the zero days were the five magnetically disturbed or calm days in each month selected by van Dijk. The actual character numbers are designated on the scales of ordinates. While the average magnetic character number for the 18 months is not designated in Figs. 8 and 9, its value, 0.753, is not far above that corresponding to the line representing average burst frequency.

The upper burst-frequency curve of Fig. 8, obtained with zero days for the entire 18 months, displays quite large and apparently random fluctuations with no evidence of a relation to the primary positive pulse in the magnetic character, at least within 15 days preceding or following the magnetically disturbed days. The lower curve of Fig. 8, obtained with zero days from only the last 6 months, might conceivably be considered to provide a weak indication of an inverse relation in view of the dip at day number 1. Since the dips at day numbers 8 and 14 are quite comparable to this, however, such an indication must be regarded as quite unconvincing.

In the upper, 18-month, burst-frequency curve of Fig. 9, some evidence of a direct relation between burst frequency and magnetic character seems to be provided by the sharp dip centered at 4 days preceding the magnetically calm days and descending 7 percent below the average. The curve is quite irregular, however, and the dips at day numbers -12 and $+15$ make the indication less convincing. The curve for the last 6 months appears to indicate only random fluctuations. It might be considered to afford the barest hint of an inverse relation.

The burst-frequency "difference" curve of Fig. 10, obtained from the 18-month curves of Figs. 8 and 9, appears to provide some indication of a direct relation between the burst frequency and magnetic character, but the indication is weakened by the irregularity of the curve, particularly the dip at day numbers -6 and -7, and the high value at $+15$. Such indication as exists seems to

be due almost entirely to the burst-frequency curve of Fig. 9, associated with magnetically calm days.

In summarizing the results of this analysis, it may be remarked that while it indicates that the frequency of occurrence of the 1-mm bursts is likely to be above or below average when the cosmic-ray intensity (as measured by the corrected average ionization current) is particularly high or low, respectively, the forms of the burst-frequency curves associated with the primary pulses in C-R intensity indicate that there is not a very intimate relation between these variables.

Good evidence is found for an inverse relation between the burst frequency and sunspot area. This is more clear-cut in the case of sunspot minima than in the case of sunspot maxima. This inverse relation appears to be generally comparable to that found earlier to exist between C-R intensity and sunspot area, though the curves obtained here are somewhat less regular than those of the earlier paper, and do not show any indication of the phase lag found there. There is one very striking difference in the magnitudes involved. The pulses in small-burst frequency associated with primary pulses in sunspot area extend to nearly 8 percent deviation from the average, while the primary pulses in the mean corrected ionization current represent[4] only 0.5 to 0.7 percent deviation.

There is very little evidence of a relation between the frequency of the small bursts and terrestrial magnetic character. Lack of correlation with magnetic character can scarcely be regarded as conclusive evidence of a lack of dependence upon the terrestrial magnetic field, of course, in view of the extraordinary definition of magnetic "character." It is rather striking, however, that the earlier work indicated a very clear-cut inverse relation between the C-R intensity and magnetic character. Such relation as is indicated in the present instance appears to be rather of opposite character.

Because of the heavy shielding employed, it is apparent that both the average ionization current and the bursts observed in the chamber must have been caused by penetrating radiations. If both were caused by the same radiation, then one might suppose that both should display corresponding variations in relation to variations in magnetic character as well as in sunspot areas, and also that their variations should display a much closer mutual relationship than is apparent in Figs. 1 and 2, just as they both display recurrences of variations at the comparable intervals of 27 or 28 days,[1, 3] variations amounting to about 0.2 percent in the current and 3 or 4 percent in the burst frequency. It occurs to one that the situation might be explicable by virtue of the fact that the daily average ionization currents were corrected for variations in barometric pressure (as well as for bursts), while no such correction was applied in the case of the burst frequencies. If the burst frequency does depend to a considerable extent upon barometric pressure (it will be shown later that it does), then it is perhaps remarkable that without correction there are still inverse pulses in the burst frequency related to the primary pulses in the sunspot area as shown in Figs. 5, 6, and 7. At present it appears likely that the ionization current (after correction for bursts) and the small bursts may be due in considerable part to two different types of penetrating radiation. If, for instance, the average ionization current in the chamber were brought about largely through the agency of mesotrons and if the small bursts were, to a considerable extent,

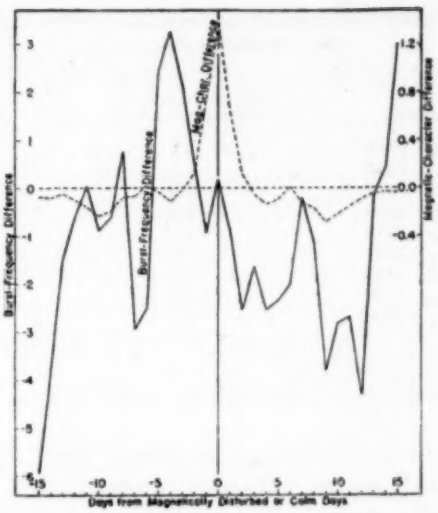

FIG. 10. Primary "difference" pulse in magnetic character, together with corresponding differences in burst frequency for the 18 months: These curves were obtained by subtracting ordinates of the upper curves of Fig. 9 from the corresponding ordinates of Fig. 8.

TABLE I. Correlation between burst frequency and barometric pressure.

Month	Bar. coeff. of B. F. in percent per mm Hg	Corr. coeff.
Aug. 1938	2.4	0.18
Nov. 1938	−1.1	0.30
Jan. 1939	−4.0	0.73*
Feb. 1939	−2.4	0.57
Mar. 1939	−3.5	0.60
Apr. 1939	−1.6	0.23
Apr. 1939	−3.3	0.48**
June 1939	−2.7	0.28
Aug. 1939	−2.1	0.18

* Last day omitted.
** Correlation of B. F. with Bar. Press. for *preceding* day.

the result of the action of neutrons,[5] then, if these are produced by different processes and their respective intensities do not bear precisely similar relations to other variables or for any reason do not display closely similar fluctuations in time, the relations displayed in this investigation and those leading up to it might be capable of explanation on this basis.

The small-burst frequencies were employed in this investigation without any correction for possible barometric or other effects, because the uncorrected frequencies had displayed[1] the 27-day recurrences. Because the analysis provided indications that the small bursts and the ionization after correction for bursts may be produced through the agency of two different types of radiations, while permitting the supposition that some of the results might be explicable in terms of a barometric effect on the burst frequency, it was decided to carry out a preliminary investigation of such an effect. Consequently, a least-squares' analysis of the relation between the number of 1-mm bursts per day and the average barometric pressure for the day was carried out for 8 of the 18 months. The particular months investigated were selected partly because of distribution in season, and partly because of the range of variation of barometric pressure during the month. The results are collected in Table I.

The second column in Table I gives the barometric coefficient for the frequency of the small bursts in percent of the average for the month (designated in the first column) per mm Hg variation in the barometric pressure. The third column gives the correlation coefficient. Data for the last day of January were omitted because the correlation coefficient was thereby nearly doubled. For April, values obtained by associating the number of 1-mm bursts for each day with the mean barometric pressure for the preceding day are also included.

Table I shows that for 7 of the 8 months investigated, large negative barometric coefficients, of the order of 1 to 4 percent decrease in burst frequency per mm Hg increase in barometric pressure, were indicated. The single positive coefficient obtained was for August, 1938. For this, as for August, 1939, the correlation coefficient was so small as to render the correlation quite meaningless. It is quite common to consider that a correlation is not really significant or reliable unless the correlation coefficient is three times as great as its mean error. On this basis, only January, February, and March, of the months investigated, display reliable correlations. The data for April also satisfy this criterion for reliability if the number of bursts for each day is associated with the mean barometric pressure for the *preceding* day rather than for the day on which the bursts occurred. This might conceivably be due to a lag in the representation of some higher atmospheric conditions by barometric pressure at the earth's surface at this season of the year. Because casual observation of the data did not indicate that such an improved correlation would result from a corresponding treatment of data for the other months, this was not attempted. The extreme lack of significance of the coefficients obtained for the two August months is made apparent by the fact that, for both of these, the mean error in the correlation coefficient was about equal to the correlation coefficient itself. In fact, if data for August 29 are omitted from August, 1938, the barometric coefficient for that month is reduced from 2.4 to 1.1, and the correlation coefficient from 0.18 to 0.09. For November and June the correlation coefficients are about twice their mean errors.

It will be noted that the most reliable barometric coefficients of burst frequency all have large negative values. These are all for months with higher than average burst frequency, less than average barometric pressure, fairly large

[5] C. F. v. Weizsäcker, in Part 7 of *Cosmic Radiation* (Edited by W. Heisenberg; translation by T. H. Johnson; Dover Publications, New York, 1946), ascribes cosmic-ray bursts under thick shields to mesons of spin zero.

range of variation of barometric pressure, and certainly in the case of January and February, low temperature. The August months had higher average barometric pressures than the average for the year, higher temperatures, and considerably lower than average small-burst frequency.

To obtain a single value somewhat representative of the "significant" barometric coefficients, an average has been obtained by weighting the values for January, February, and March, and the second (delayed) value for April according to their respective correlation coefficients. This procedure yields -3.4 percent per mm Hg. This is definitely of a higher order of magnitude than the barometric coefficient for the corrected ionization current in the same shielded chamber. The mean value of the latter for the 18 months was -0.145 percent per mm Hg.

It is seen that the barometric coefficients, as well as the Chree analysis, indicate that the small bursts and the corrected ionization current in the heavily shielded chamber are produced through the agency of different types of radiation. The observed dependence of the burst frequency upon barometric pressure, at least during a certain season, makes it seem desirable to repeat the Chree analysis after applying barometric corrections to the burst frequency. Their very different barometric coefficients, however, make it seem very unlikely that such a procedure would indicate any better correlation between burst frequency and ionization current in the shielded chamber. The very large barometric coefficient for the burst frequency indicates a much greater likelihood of a correlation between the frequency of the small bursts and a soft component[6] of the cosmic radiation. Such a soft component, to account for the bursts, must produce a radiation capable of penetrating the thick shield and actuating the bursts while contributing little to the average ionization. It should be borne in mind that with air in the chamber at 160 atmospheres, it would not be possible to collect efficiently the ions of a burst if these ions were finally produced by the action of any short-range particles producing high ion density.

The large barometric coefficient found for the small bursts in this investigation corresponds strikingly to the much earlier observations of Steinke, Gastell, and Nie.[7] Employing a large chamber (500 liters) containing CO_2 at rather low pressure (2 kg CO_2; hence, about 2 atmospheres) shielded by 10 cm of lead, they observed a barometric coefficient of about -5 percent per mm Hg. For the ionization current they found a barometric coefficient of only 0.2 percent per mm Hg. Both these coefficients correspond closely to the values obtained here. They did not observe a barometric effect for large bursts, but only for small ones ($1-7\times10^6$ E. Q., occurring at the rate of one in two hours or oftener). Moreover, the effect decreased with increased shielding, being no longer observable with 30 cm of iron. They attributed the latter situation to an increased number of bursts being caused by secondary radiation from the shield and consequently not susceptible to variations resulting from changes in barometric pressure. They considered the very large barometric coefficient for the small bursts obtained with the 10-cm lead shield to indicate their association with an extremely soft component of the cosmic radiation.

Montgomery and Montgomery[8] also observed a negative barometric coefficient for cosmic-ray bursts. Employing a 50-liter Dowmetal chamber containing nitrogen at 14.5 atmospheres and shielded by about 4 cm of lead on top, and measuring bursts greater than 1.6×10^6 ions, they obtained an estimated barometric coefficient of -0.5 percent per mm Hg at sea level, and about -7 at 4300 meters (where the burst frequency was 90 to 150 per hour), though variation with altitude there indicated a coefficient less than half as great.

In summarizing the evidence for the supposition that the small bursts and the (corrected) ionization in the shielded chamber are produced through the agency of different types of radiation, we have first the lack of close correlation between variations of these as indicated by Figs.

[6] W. Kolhörster, Physik. Zeits. **40**, 107 (1939), found 27-day fluctuations in cosmic-ray intensity out of phase with sunspot relative numbers, etc. He used a dual telescope arrangement measuring the vertical intensity. While there does not appear to be a definite statement regarding shielding, it seems likely that very little shielding was employed.

[7] E. G. Steinke, A. Gastell, and H. Nie, Naturwiss. **21**, 898 (1933).

[8] C. G. Montgomery and D. D. Montgomery, Phys. Rev. **47**, 429 (1935).

1, 2, 3, and 4. Also, while both burst frequency and corrected ionization current display recurrences of variations at intervals of 27 or 28 days, primary pulses in the former (expressed in percent) are about 60 times as great as in the latter, and secondary pulses are about 20 times as great. Also, while both display variations in general phase opposition to those in sunspot area, the pulses in burst frequency (expressed in percent) in this instance are some 11 to 16 times as great as the primary pulses in the ionization current. The corrected ionization current displays a clear-cut relation to magnetic character not displayed by the raw burst-frequency data; it remains to be seen whether correction for barometric variations would bring out a closer relation between burst frequency and magnetic disturbances. Finally, while the barometric coefficient for the frequency of the small bursts is of the same sign as that for the corrected ionization current, it is some 20 times as great, at least for the season when the dependence upon barometric pressure is clearly evident. The indication here provided that the bursts are associated with a soft component calls to mind the fact that Korff[9] found the rate of production of neutrons to be associated with the soft component.

The writer wishes to acknowledge helpful comments by Dr. W. F. G. Swann and the continued cooperation of Dr. V. A. Long and Dr. R. M. Whaley.

[9] S. A. Korff, Phys. Rev. 59, 949 (1941).

PHYSICAL REVIEW VOLUME 72, NUMBER 12 DECEMBER 15, 1947

Gamma-Rays from the Alpha-Particle Bombardment of Na, Mg, Al, Si, P, S

ERNEST POLLARD AND D. E. ALBURGER
Sloane Physics Laboratory, Yale University, New Haven, Connecticut*

(Received September 12, 1947)

Na, Mg, Al, Si, P, S targets have been bombarded by 7.2-Mev helium ions. The emission of gamma-radiation has been observed. Lead absorption coefficients were obtained in all cases. The values lie close to the minimum of the lead absorption curve. In the case of Al, absorption in copper has been measured and, in addition, absorption of Compton recoil electrons by aluminum has been measured by a coincidence method. The results show that a gamma-ray of energy 3.5±0.3 Mev is present. This agrees with a transition from the Q_2 to Q_0 state observed in the $Al^{27}(\alpha p)Si^{30}$ reaction. Unequivocal energy assignments cannot be made for the remaining reactions. However, lead absorption experiments indicate the following probable values: *S*, 1.6±0.3 Mev; Mg, 3.2±0.6 Mev; Na, 2.3±0.3 Mev. The values for elements Si and P cannot be assigned until it is clear whether the absorption is above or below the minimum. Lead absorption coefficients are given. Since the gamma-ray energies are generally higher than the difference between energy levels obtained from other information, it is likely that in these cases direct transitions are preferred to cascade.

1. INTRODUCTION

IN the region between sodium and chlorine there has been a considerable amount of experimental work on the nuclear energy levels as revealed by the formation of groups of particles in transmutations[1] or of inelastically scattered protons.[2] Relatively little recent work has been done on the direct observation of radiation due to transitions between levels of excitation produced in the bombardment process. Savel,[3] bombarding with polonium alpha-particles, has observed the presence of gamma-radiation from fluorine, sodium, magnesium, and aluminum, and measured the absorption coefficients in lead. Speh[4] has shown that the energy of the radiation from fluorine bombarded by polonium alpha-

* Assisted by the Office of Naval Research under Contract N6ori-44.

[1] For example, C. J. Brasefield and E. Pollard, Phys. Rev. 50, 296, 890 (1936); A. N. May and R. Vaidyanathan, Proc. Roy. Soc. A155, 519 (1936); O. Haxel, Zeits. f. Physik 90, 373 (1934), and Zeits. f. Tech. Physik 11, 410 (1935), H. L. Schultz, W. L. Davidson, Jr., and L. H. Ott, Phys. Rev. 58, 1043 (1940).

[2] R. H. Dicke and J. Marshall, Phys. Rev. 63, 86 (1943).

[3] P. Savel, Ann. de physique 4, 88 (1935).

[4] K. D. Speh, Phys. Rev. 50, 689 (1936).

TABLE I.

Process	Q values (Mev)
$Na^{22}(\alpha p)Mg^{25}$	1.9; −0.4; −2.1; −3.1
$Mg^{24,25,26}(\alpha p)Al^{27,28,29}$	−1.2; −2.0; −2.9
$Al^{27}(\alpha p)Si^{30}$	2.22; −0.06; −1.44; −2.49
$Si^{28,29,30}(\alpha p)P^{31,32,33}$	−2.4; −3.2; −4.0
$P^{31}(\alpha p)S^{34}$	0.0; −1.2; −2.6; −4.6
$S^{32}(\alpha p)Cl^{35}$	−2.35; −2.85; −3.6
$Al^{27}(pp)Al^{27}$	0; −0.82; −1.90; −2.53; −3.28
$Mg^{24,25,26}(pp)Mg^{24,25,26}$	0; −1.23; −2.58; −3.59

particles has two components, the harder of which is excited only by alpha-particles above 4-Mev energy. The excitation function for gamma-radiation from sodium has been studied by Kovács.[5]

As a result of the observation of proton groups emitted under alpha-particle bombardment, the nuclear energy change (Q) values, given in Table I, have been observed. No study has been made of neutron energies in this region. Some additional information about the general character of levels is available from inelastic scattering and from (dp) reactions.

The present work was carried out with a doubly ionized helium beam of 7.2-Mev energy produced by a cyclotron. Radiation from the six elements Na, Mg, Al, Si, P, S was readily detected and absorption coefficients measured.

2. EXPERIMENTAL METHOD

The bombarding and detecting arrangements can be seen from Fig. 1. The beam is brought out approximately 20 inches from the cyclotron vacuum chamber into a bombardment chamber,

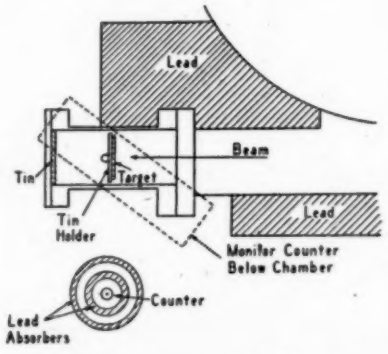

FIG. 1. Experimental arrangement for absorption measurements on gamma-radiation from targets under cyclotron bombardment.

[5] M. Kovács, Phys. Rev. 70, 895 (1946).

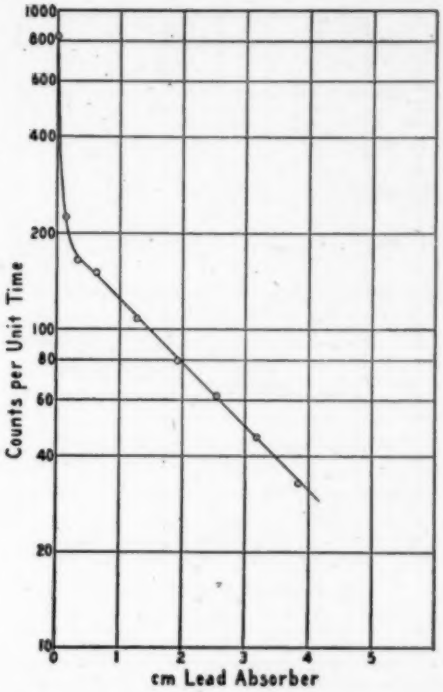

FIG. 2. Absorption of gamma-radiation from thorium-active deposit.

as indicated. Lead shields reduce the "wild" radiation from the dees and walls of the cyclotron. The background counting rate with a pure tin target, which is not transmuted by alpha-particles of 7.2 Mev energy, was found to be $\frac{1}{10}$ to $\frac{1}{3}$ that due to radiation from the six elements bombarded. The targets were thick enough to absorb completely the alpha-particles. These consisted of sheets of the metal itself in the case of aluminum or magnesium, sodium metal fastened on to a tin backing sheet with polystyrene cement, silicon powder fused into a slab and glued to a tin plate with polystyrene cement, red phosphorus stuck by adhesion to a tin plate, and sulfur powder mixed with gold dust (to permit conduction of the beam current) and fused on to a tin plate.

The counter used for absorption was a Herbach-Rademan type GLC-11. The counts were referred to a standard absorption by a monitor proportional counter set to count gamma-rays. The procedure was to count simultaneously on the monitor and the absorption counter, until a fixed number of monitor counts was recorded. In this way errors in beam integration were

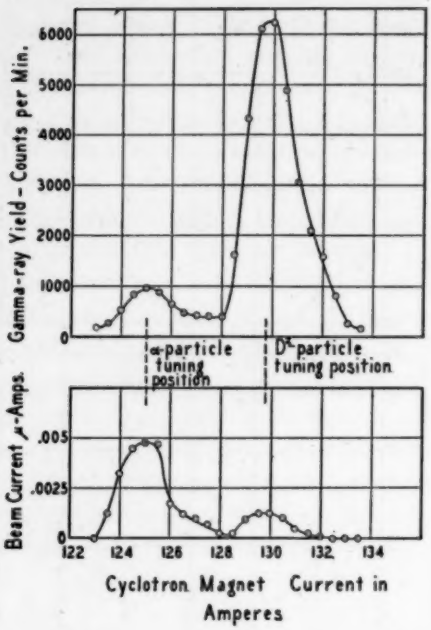

FIG. 3. Cyclotron beam current and gamma-ray yield from an Al target as a function of cyclotron magnet current.

eliminated. The data were very reproducible, the absorptions on each run being repeated several times with fluctuations of the order of those expected from a Poisson distribution. In each case a background absorption curve with a tin target was taken and deducted. The absorbers were cylindrical, with lead shields placed over the top and bottom to absorb scattered radiation. The distance from target to counter was five inches. In order to check the way in which the geometry affected the absorption coefficient, runs were taken with thorium active deposit and Na^{24}. The thorium active deposit results are shown in Fig. 2. The absorption coefficients correspond to soft components plus a single hard component of energy 2.62 Mev. The straight line gives a coefficient in agreement with the theoretical value for this energy. An additional run was taken with annihilation radiation which gave the absorption coefficient 1.73 per cm corresponding to 0.49 Mev, which again checks the validity of the method.

A second method of energy study was used in the case of aluminum. Two beta-ray counters, with thin windows, were placed facing each other on a line with the cyclotron target. A lead radiator ($\frac{1}{8}$-inch thickness) was located in the nearer counter to provide recoil electrons from the incident gamma-radiation. Aluminum sheet absorbers were then placed between the two thin windows, and the number of coincidence counts recorded for a standard number registered by the nearer counter. By determining at what absorption the coincidences fall to background, the energy of the gamma-ray is calculated by use of the absorption formula for an electron of energy E Mev: Range (g/cm^2 Al) $=0.571E-0.161$ and adding a correction (up to 0.25 Mev) for the energy retained by the gamma-quantum in a Compton recoil.

The cyclotron differs from a radioactive source in that deuterons and molecular hydrogen may be present. The coincidence experiments with an aluminum target were performed several days after change from deuterium to helium. It was found possible to separate the He^{++} beam from the H_2^+ and D^+ by adjustment of the magnetic field. To be certain that H_2^+ or D^+ contamination was not responsible for the results, an Al target was bombarded and counts observed with variation of the cyclotron magnetic field. The results

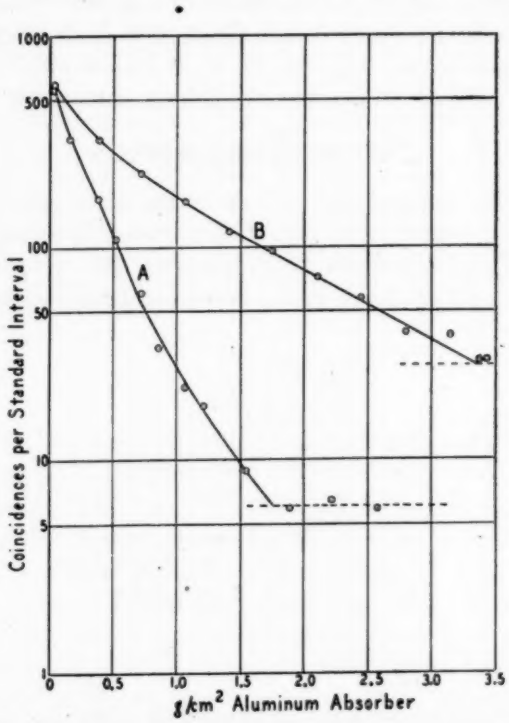

FIG. 4. Coincidence counting of recoil electrons produced by gamma-rays from an aluminum target. *A*, cyclotron tuned to He^{++} maximum; *B*, cyclotron tuned to D^+ maximum.

are shown in Fig. 3. It can be seen that the yield due to D^+ and H_2^+ drops to zero before the He^{++} yield is at a maximum. As a further proof, absorption curves for the secondary electrons were plotted by the coincidence method at the He^{++} maximum value and at the D^+ value, as shown in Fig. 4. In the He^{++} case, curve *A*, the end point corresponds to 3.5 Mev while in the D^+ case, curve *B*, it is 6.8 Mev. Finally, a curve was taken with the cyclotron tuned on the low field side of the He^{++} resonance which agreed exactly with the curve taken at the peak. Had any D^+ contamination been present its effect would have been greatly reduced by this procedure. The fact that no change occurred argues against the presence of D^+. We therefore consider that deuterium or molecular hydrogen contamination of the beam is insufficient to affect our results.

3. EXPERIMENTAL RESULTS

The element aluminum was most carefully studied. Special attention was paid to this element because it has been worked on carefully by various types of natural-source bombardment and has recently been investigated in this laboratory by Benson.[6] The results of lead absorption measurements are shown in Fig. 5. The absorption was carried out to 4 cm with cylindrical absorbers and out to 8 cm with additional flat, lead plates. The majority of the radiation is in a single component with an absorption coefficient $\tau = 0.436 \pm 0.015$. There is a slight indication of a lower energy group which might be associated with the 2.5-minute position activity of P^{30}.

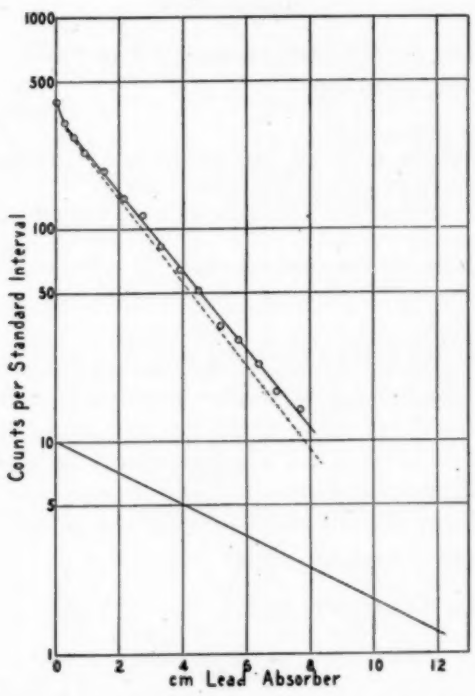

FIG. 5. Absorption of gamma-radiation from Al under alpha-particle bombardment showing the maximum possible neutron yield correction.

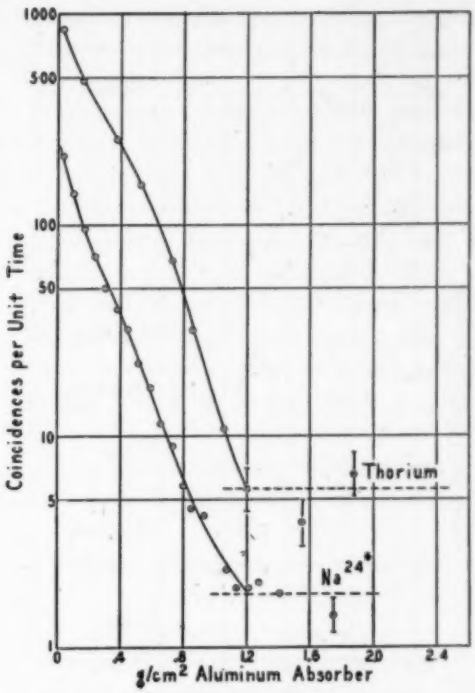

FIG. 6. Coincidence counting of recoil electrons produced by gamma-rays from thorium-active deposit and Na^{24}.

The absorption coefficient is quite low and there exists the possibility that neutrons are present in the radiation, adding a component of low absorption coefficient. By carrying the absorption out to 8 cm, it was hoped that a slight curvature might show the presence of such a neutron component. Using a neutron absorption coefficient of 0.17 cm^{-1}, it is possible to estimate the *maximum possible* correction which could be applied. The dotted line shows the slope contained by deducting a neutron yield of 1/40 the gamma-count. A higher neutron yield gives a convex absorption curve which is without meaning. The "corrected" value is $\tau = 0.455\ cm^{-1}$.

[6] B. B. Benson (in course of publication).

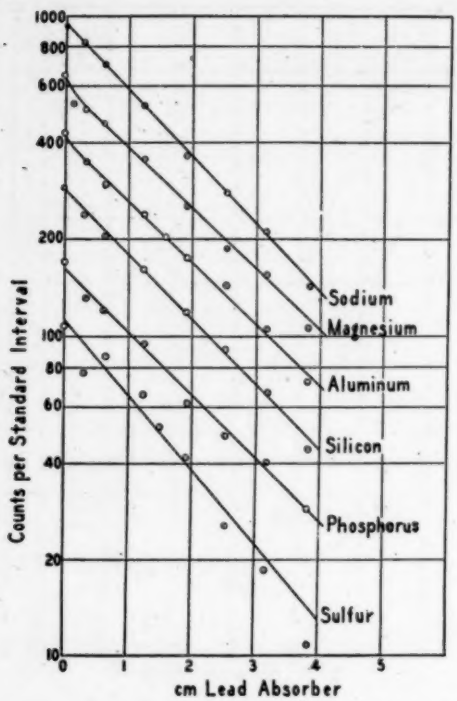

FIG. 7. Absorption of gamma-radiation from Na, Mg, Al, Si, P, and S under alpha-particle bombardment.

To determine to which side of the lead absorption minimum this coefficient corresponds, the absorption in copper was measured. The value obtained corresponds to a single absorption coefficient $\tau=0.28$ cm^{-1}, which fits a gamma-ray energy of close to the minimum absorption value of 5 Mev for copper. The limits of error are quite high but the measurement proves that the gamma-ray energy is on the high side of the lead absorption minimum. The best value of the maximum gamma-ray energy present was obtained from the coincidence counting of Compton recoil electrons. The absorption of these in aluminum is shown in curve A of Fig. 4. The end point occurs at 1.72 g/cm^2 which gives a maximum energy of 3.5 ± 0.3 Mev. This in good agreement with the uncorrected lead absorption data which give an absorption coefficient of 0.444 ± 0.017 or an energy between 2.7 and 3.7 Mev.

In order to justify the method of coincidence counting, runs were taken with thorium-active deposit and Na^{24} sources. The end points obtained are 2.62 Mev and 2.65 Mev, which agree satisfactorily with 2.62 Mev and 2.76 Mev, respectively. The curves are shown in Fig. 6. In the case of sodium it is known that two components of energy 1.38 Mev and 2.76 Mev are present in equal abundance. While there is some difference between the sodium curve and the single-component thorium curve, it is slight. It is therefore felt that nothing can be said about the presence of components of lower than maximum energy unless the yield is at least three times higher than the maximum energy component. The results for aluminum can be summarized as follows: At least 30 percent of the total radiation is of energy 3.5 ± 0.3 Mev. There is evidence of a weak component of much lower energy, probably less than 0.5 Mev.

The elements Na, Mg, Si, P, S were studied by lead gamma-ray absorption only with results including aluminum as shown in Fig. 7. It can be seen that with the possible exception of magnesium and aluminum, the radiation is predominantly of one absorption coefficient. The values, together with possible energies, are given in Table II which includes estimates of the yield based on a yield of 10 from aluminum. Total counts recorded at zero absorption are also given.

4. DISCUSSION

Alpha-particle bombardment can cause the following processes:

1. Simple capture.
2. Inelastic scattering, i.e., capture and re-emission of the alpha-particle with reduced energy.
3. Transmutation with emission of a neutron. (α,n) reaction.
4. Transmutation with emission of a proton. (α,p) reaction.

TABLE II. Absorption coefficients and yield of gamma-rays produced by alpha-particle bombardment.

Element	μ-cm^{-1}	Gamma-ray energies (Mev)	Rel. yield	Total counts at zero abs.
Sodium	0.485 ± 0.017	2.3 ± 0.3 (probable) or 5.2 ± 0.5	9.0	12,600
Magnesium	0.448 ± 0.017 >14	3.2 ± 0.6	7.3 0.7	12,400
Aluminum	0.444 ± 0.017 >14	3.6 ± 0.5	10.0 0.5	8,830
Silicon	0.478 ± 0.016	2.4 ± 0.3 (probable) or 4.9 ± 0.5	1.4	5,300
Phosphorus	0.460 ± 0.027	2.7 ± 0.3 or 4.2 ± 0.5 (probable)	2.7	4,340
Sulfur	0.555 ± 0.080	1.6 ± 0.3	1.2	5,040

In principle the radiation observed can be due to any or all of these processes. The relative probabilities can now be discussed.

Simple Capture. If it is assumed that the capture process yields one gamma-quantum only, then the general trend of mass values indicates that passage to a nucleus four mass units greater requires release of 10 Mev or so. This is greater than the observed energies. It is, of course, possible that two or more gamma-quanta are emitted, in which case the reasoning above is invalid.

Inelastic Scattering. This is a process which has been observed in the bombardment of Li by alpha-particles and for a variety of nuclei under proton bombardment. It would appear to be unlikely that a considerable yield of inelastically scattered alpha-particles could emerge through the potential barrier with energies reduced by 3–4 Mev, as required for Mg, Al, and P. This process, therefore, seems improbable.

(α,n) *Process.* For the case of the elements Na^{23}, Al^{27}, and P^{31}, which have a single isotope, there is less energy available for the (α,n) reaction than the (α,p) reaction both because the mass of the neutron is rather greater and because radioactive nuclei, which are in general more massive, are formed. This relative lack of available energy could therefore be expected to discriminate against this process, since the high energy of the observed gamma-rays points to a high probability of excitation to about 4 Mev. For the other three elements, this reasoning is not so valid.

(α,p) *Process.* The existence of excited states produced in the (α,p) process is well known. The Q values given in Table I show that the target elements Na^{23}, Al^{27}, and P^{31} give rise to product nuclei in states of excitation between 4 and 5 Mev above ground. There would appear to be a strong likelihood that for these three elements the gamma-radiation should agree with differences between levels already found by proton group observation. In the case of Mg and Si, there are present three isotopes each. Moreover, the observations made on proton groups in the (α,p) reactions do not indicate very high degrees of excitation. Therefore, one can assume that (α,n) reactions may well be responsible in these cases. Sulfur is very nearly a single isotope. The greatest degree of excitation from S^{32} would be expected from the (α,p) process which is, therefore, most likely to be responsible for the gamma-rays observed.

With these general points in mind we can suggest the following assignments, tentatively.

Sodium: The 2.3-Mev radiation probably corresponds to the first excited state of Mg^{26}. This agrees with the published Q-values as given in Table I.

Magnesium: No assignment can be given. The radiation is definitely of higher energy than expected from any other evidence.

Aluminum: The radiation is associated with the second excited state of Si^{30}. The energy from proton groups is 3.66 Mev while from this work it is 3.5 Mev.

Silicon: No assignment. The energy measured here is higher than expected from Q values for (α,p) reactions.

Phosphorus: Either the second or third excited state of S^{34}.

Sulfur: Second excited state of Cl^{35}.

While these assignments are not complete, one fact nevertheless appears. The gamma-ray yield is predominantly from states of high excitation. This checks with the observation that proton groups have higher population for higher excitation. The fact that the energy of the radiation runs about double the spacing between energy levels observed in other ways, is evidence that direct transitions are favored in a considerable number of cases. This seems to be certain in the case of the radiation from aluminum and probable in every other case but sodium.

Ionization Processes in a Long Discharge Tube with Application to Lightning Mechanism

F. H. MITCHELL* AND L. B. SNODDY
Rouss Physical Laboratory, University of Virginia, Charlottesville, Virginia

(Received August 26, 1947)

Properties of the progressive breakdown, occurring when an impulsive potential is applied to an electrode in one end of a discharge tube 14 cm in diameter and 12 meters long, have been investigated, principally by means of a high speed cathode-ray oscillograph. Potentials from 25 kv to 115 kv and pressures from 0.006 to 8.0 mm Hg were used, with dry air and hydrogen in the tube. Conditions in the discharge, when comparatively large over-voltages are impressed, have been discussed by several investigators, particularly with respect to impulses of positive polarity and in tubes of smaller diameter. These observations now have been extended to include the negative polarity. In addition, a low speed, low potential process has been obtained and its properties analyzed.

A possible application of the lightning theory to such discharges is given. The low speed impulse resembles the hypothetical lightning pilot streamer as to speed and current, and the speed is of the order of magnitude of the drift speed of electrons in the tip field, as assumed for the pilot streamer. The high speed processes are more similar to the lightning dart leaders. It is pointed out that conditions in the tube are such that propagation in this case may be controlled more by the presence of photo-electrons ahead of the tip than by a preliminary ionizing leader.

THE progressive character of the breakdown in long discharge tubes upon the application of impulsive potentials to an electrode in one end of the tube was first discussed by J. J. Thomson.[1] More recent investigations by Beams[2] and by Snoddy, Beams, and Dietrich[3] with the rotating mirror and with the high speed cathode-ray oscillograph have shown the similarity between such ionization processes and the general features of the lightning discharge. Impulses in tubes have been found to travel from the high potential end and, if the far end contains a grounded electrode, a return discharge of greater intensity and higher speed progresses back to the input electrode.

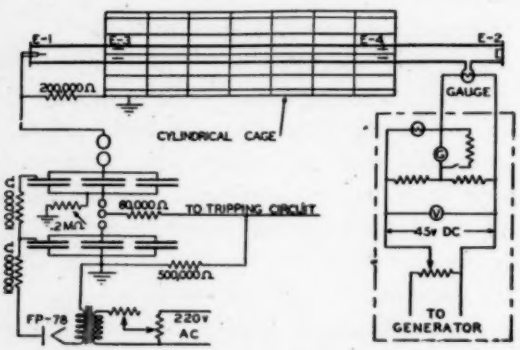

FIG. 1. Diagram of discharge tube with Marx circuit, cylindrical shielding cage, vacuum gauge circuit, and electrodes. Distance from *E*-3 to *E*-4 is 642 cm. Resistance values are approximate.

Similar processes have been found by Schonland and others[4] in the lightning discharge, and by Allibone and Meek[5] in long sparks in the laboratory. The lightning stroke is ordinarily initiated by a downward moving "leader," followed by an upward moving "return" stage of much greater intensity. The cloud end of the discharge is usually of negative polarity with respect to ground. Leaders for strokes over the same channel after the first discharge has occurred are generally continuous processes, called "dart" leaders, in contrast to the initial leader, which moves downward in a series of steps and is known as the "stepped" leader. The speeds of these leaders are fairly uniform for various strokes, averaging 1×10^{10} cm/sec for return strokes, 1×10^{9} cm/sec for stepped leaders, and 2×10^{7} cm/sec for the average speed of the stepped leader computed from the total time of its travel.

* Now at the University of Alabama, University, Ala.

[1] J. J. Thomson, *Recent Researches* (Clarendon Press, Oxford, 1893).

[2] J. W. Beams, Phys. Rev. **36**, 997 (1930).

[3] L. B. Snoddy, J. R. Dietrich, and J. W. Beams, Phys. Rev. **50**, 469 (1936); L. B. Snoddy, J. R. Dietrich and J. W. Beams, Phys. Rev. **52**, 739 (1937); J. R. Dietrich, "Progressive Breakdown in Long Discharge Tubes," dissertation, University of Virginia (1939), unpublished.

[4] B. F. J. Schonland and H. Collens, Nature **132**, 407 (1933); B. F. J. Schonland and H. Collens, Proc. Roy. Soc. **A143**, 654 (1934); **A152**, 595 (1935); B. F. J. Schonland, Proc. Roy. Soc. **A164**, 132 (1938); Phil. Mag. **23**, 503, (1937); K. B. McEachron and W. A. McMorris, G. E. Rev. **39**, 487 (1936); K. B. McEachron, J. Frank. Inst. **227**, 149 (1939); E. J. Workman, J. W. Beams, and L. B. Snoddy, Physics **7**, 375 (1936).

[5] T. E. Allibone and J. M. Meek, Proc. Roy. Soc. **A166**, 97 (1938); **A169**, 246 (1938).

It has been supposed that there may be a constantly moving preliminary "pilot" streamer preceding the stepped leader and furnishing a preionized path for the other stages.

The ionizing process in a long discharge tube offers certain advantages in the study of the mechanism of leader propagation. The channel is definitely fixed, and the time intervals are long enough for satisfactory measurements with the oscillograph. Furthermore, the return stage with its high luminosity and large current can be eliminated by insulating the far end of the tube from the ground. In the present work, observations in a 14-cm diameter tube have been extended in order to determine the applicability of the theory of lightning mechanism to discharges of this type.

APPARATUS

Most of the apparatus has been previously described.[3] The tube consisted of 15 sections of glass tubing each 80 cm long, 14 cm in internal diameter, and 5 mm thick, making a total length of 12 meters. The ends of the sections were ground flat and joined together with picein wax. Four brass electrodes were placed in the tube as in Fig. 1. Between E-3 and E-4 there was a grounded electrostatic shield (cylindrical cage, Fig. 1), and near E-2 were the drying traps of phosphorus pentoxide, the pumping system, a Pirani vacuum gauge, and an insulating column which could be evacuated sufficiently to prevent the discharge at E-2 from reaching the ground. Impulsive potentials were supplied by a Marx potential doubling circuit. The high speed cold cathode oscillograph of the single sweep Dufour type had a maximum sweep speed of 2×10^8 mm/sec with a cathode potential of 70 kv. Various auxiliary circuits were used to synchronize the oscillograph with the impulse in the tube.

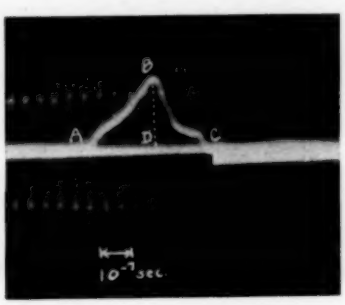

FIG. 2. Oscillogram for computing speed in air at 0.034 mm Hg pressure with −85 kv applied potential. Frequency of timing wave is 19.0 megacycles per sec.

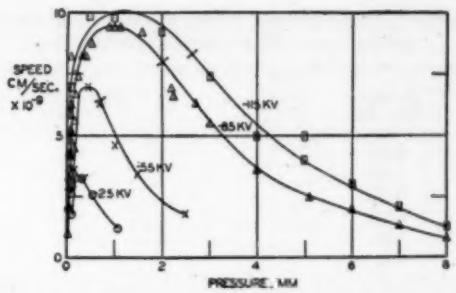

FIG. 3. Speed-pressure curves for high potential discharge in air. Negative applied potential.

HIGH POTENTIAL MEASUREMENTS

The term "high potential discharge" is used here to indicate the discharges in the tube which are propagated throughout its length without marked variation in speed, current, or luminosity. On the other hand, it is possible that the character of the impulse may change rapidly as it travels. In this case the speed, current, and luminosity vary greatly during the process of propagation. The latter condition gives rise to what are called "low potential discharges." In general, a high potential discharge results from large over-voltages at low pressures, and a low potential discharge from smaller potentials at higher pressures.

The speed of the ionizing process was computed from oscillograms such as Fig. 2. Electrodes $E3$ and $E4$ (Fig. 1) were connected through a potential divider unit to the vertical deflection plates of the oscillograph, while the sweep potential was applied to the horizontal plates. The sequence in this oscillogram was as follows: as the impulse progressed from E-1, it raised the tube potential. At A (Fig. 2) the potential of $E3$ began to rise, the potential difference between $E3$ and $E4$ continuing to increase to the point B and then decreasing. At B the discharge has reached $E4$. At C the potentials of $E3$ and $E4$ were approximately equal. The horizontal distance AD and the corresponding time interval on the timing wave shown in the background allowed computation of the average speed in this section of the tube, which was about 6 meters long. The distance to the ends of the tube was large enough

TABLE I. Input current in dry air as a function of pressure at −85 kv applied potential.

Pressure mm Hg	Max. current amperes
0.05	81
0.15	95
0.32	96
0.65	96
1.6	88
4.0	56

to reduce the effect of the electrode $E1$ as well as to avoid the effect of the reflected wave from $E2$.

The potential dividers were made symmetrical by making adjustments until an impulse applied simultaneously to both leads on the high potential side produced no oscillograph deflection. Leads to the oscillograph were kept symmetrically placed and about the same length. The effect of the charging current to the electrodes and oscillograph deflection system on the speed of the discharge was investigated by means of oscillograms of the potential across a resistance in series with one condenser bank of the Marx circuit. All connections to $E3$ and $E4$ were removed. From these, the time required for the discharge to travel the whole length of the tube was obtainable. There were no significant variations in speeds found by the two methods, indicating that the effect of the electrodes was comparatively small, also that the average speed between $E3$ and $E4$ was not greatly different from the average over the whole tube.

Figure 3 shows the speed-pressure curves for four negative applied potentials with dried air in the tube. The speeds were roughly 50 percent higher than for the positive potential as measured by Dietrich.[3] Under the same conditions, the speed was 20 percent to 50 percent higher in hydrogen than in air.

The current supplied to the tube by the input circuit was computed by Ohm's law from oscillograms of the potential drop across a 25-ohm resistance between one bank of condensers of the Marx circuit and ground. The maximum current varied from 50 to 100 amperes. At the lower speeds, it was approximately the value required to charge a conductor the size of the tube at the center of the shielding cage up to the applied potential in the required time. At the higher speeds the current was still increasing when the discharge reached the far end of the tube; its maximum was limited by the tube length in this case, rather than by the rate of charging. In Table I are given the values of current at several pressures.

At the lower pressures, the maximum potential at any given point in the tube was very nearly equal to the applied potential. As the pressure was increased, the potential sometimes remained at an intermediate value for a short time, then rose steadily to its maximum. This is illustrated in Fig. 4 and it was especially noticeable that speed and current were comparatively small. The magnitude of the initial rise was generally less with increasing pressure, and was always less at $E4$ than at $E3$ for the same conditions. When this situation existed, the potential drop along the tube was such that the maximum potential was not attained until further energy from the input circuit was fed into the ionized stem extending back to $E1$.

THE LUMINOUS COLUMN

Visual and photographic observations have previously shown[3] that, at low pressure and with positive applied potential, there occurs a marked contraction of the luminous column toward the tube axis. No such contraction has been found for the negative polarity at any pressure, as the column appeared to fill the tube uniformly.

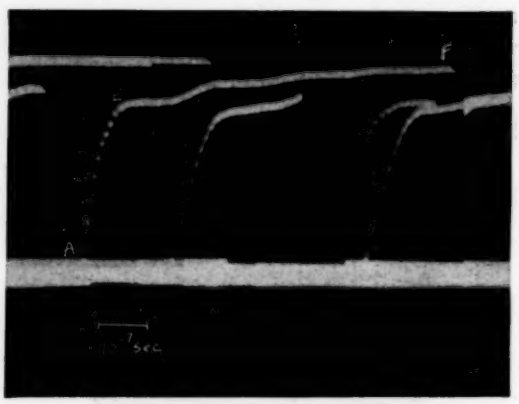

FIG. 4. Several oscillograms of potential from E-4 to ground. The maximum of the initial rise is at E and the final maximum at F. Hydrogen at 2.5 mm Hg pressure, −85 kv applied potential.

LOW POTENTIAL MEASUREMENTS

With a constant input potential the pressure in the tube was increased until the character of the impulse changed appreciably during its progress along the tube. Such a condition is characteristic of the above defined low potential discharge. To investigate this kind of discharge, the pressure was raised until there was a marked reduction in luminosity with distance. The speed in 50-cm lengths of the tube at various distances was measured in the same manner as before. Copper foil strips two inches wide wrapped on the outside of the glass were used as electrodes. For these readings, the oscillograph was used at full sensitivity (24 volts/mm). Figure 5 shows average speeds in various sections at 8 mm Hg for both positive and negative polarity. For the negative potential, oscillograms could not be obtained past $E4$, where the speed was 2.5×10^{8} cm/sec. The positive discharge continued past this point and was still measurable at 1×10^{8} cm/sec. The average speed between $E3$ and $E4$ from Fig. 5 is about half the speed for the corresponding conditions from Fig. 3 for negative polarity. The discrepancy may be attributed to the effect of the current taken to charge the electrodes and their circuits, which was a greater factor here than in the preceding measurements, since the speed from $E3$ to $E4$ would probably be less affected than that measured over a shorter section. Any effect at an electrode which reduces the speed makes it desirable to have the distance between electrodes as large as possible. We assume the actual change of speed is less than the apparent change caused by the oscillograph deflection circuit charging current. It is probable that the curves of Fig. 5 should be considered as showing the general characteristics of speed variation with distance and polarity rather than absolute values.

Another method of obtaining a low potential discharge consisted of placing a grounding spark gap at $E3$ to reduce the potential after the discharge had started in the tube. A damping resistance (minimum 250 ohms) was placed in series with the input circuit to prevent oscillations between $E1$ and $E3$, also to control the rate of energy supply. Values of speed in the section past the end of the visible luminosity are given in Fig. 6, and the corresponding maximum potentials in Fig. 7. Variation of applied potential and the spacing of the gap at $E3$ produced no noticeable effect except a displacement of the low potential discharge along the tube length. As would be expected, increase of the series resistance caused a slow decrease in the rate of charging of the tube. Oscillograms were obtainable for input series resistances up to 7×10^{4} ohms at 85 kv. At pressures below 0.1 mm Hg the delay in breakdown at $E3$ allowed the high potential impulse to travel the length of the tube. On the other hand, above 0.6 mm Hg the low potential section was crowded into a distance too short for oscillographic measurement.

All the oscillograms of the low potential discharge were taken with positive applied potential. No negative readings in the tip could be obtained under any of the conditions available in the experiments. In the negative case, as the distance of the foil electrodes from $E1$ was increased beyond $E3$ to the end of the high potential region of the discharge, there was a transition in the course of a few centimeters to a potential too low for the oscillograph to record.

The time rate of increase of potential, together with the speed, allowed the computation of approximate values of the ratio of field strength to pressure in the tip of the low potential discharge. This time rate could be obtained since the oscillograph was capable of recording a faster rise than was present in the low potential discharges. The ratio X/p in volts/cm/mm Hg is

TABLE II. Distance d in meters ahead of the stem in which ionization by collision can occur, from Eq. (3).

Volts	d $p=10$ mm Hg	d $p=1.0$ mm	d $p=0.1$ mm
1×10^{6}	1	3	10
1×10^{5}	0.3	1	3
5×10^{4}	0.2	0.7	2
1×10^{4}	—	0.3	1

TABLE III. Comparison of calculated and observed speed.

Applied potential volts	Pressure mm Hg	Speed cm/sec calculated	Speed cm/sec observed
1×10^{5}	1.0	*1×10^{10}	1×10^{10}
	2.5	5×10^{9}	8×10^{9}
	4.0	3×10^{9}	4×10^{9}
	8.0	1×10^{9}	1×10^{9}
5×10^{4}	1.0	7×10^{9}	5×10^{9}
	2.5	4×10^{9}	2×10^{9}

* Adjusted by fixing n_0.

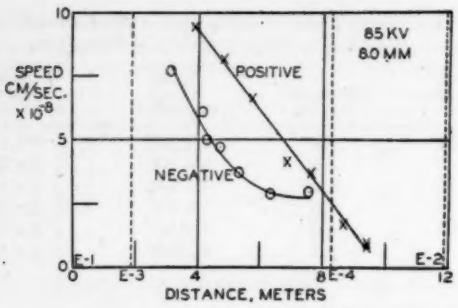

FIG. 5. Speed-distance curves of low potential discharge in air at 8.0 mm pressure and with 85 kv applied potential. Position of fixed electrodes is indicated by vertical dotted lines.

plotted against speed at the three pressures from 0.20 to 0.50 mm Hg in Fig. 8, from which it may be seen that the speed generally increased with X/p. The lowest speed recorded was 1.7×10^7 cm/sec at an X/p near 20.

DISCUSSION

The theory of the mechanism of leader propagation has yielded satisfactory explanation of the observed speeds and currents in the lightning leaders. They are thought to progress by electron motion in the high field near their tips. The region in which ionization by collision occurs extends some distance ahead of the highly ionized stem, and the presence of a comparatively few free electrons in this region is fundamental to the theory.[6] The drift velocity of electrons in a field is approximately[7]

$$S=(2EeL/\pi m)^{\frac{1}{2}}, \qquad (1)$$

where S is the speed, E the field strength, L the electron mean free path, e and m the charge and mass of the electron respectively. For the minimum breakdown field at the cloud level, this equation yields a speed of 3.7×10^7 cm/sec, which is lowered somewhat by several corrections. The value of X/p taken is about 40.

From such treatments it has been shown by Schonland[4] that the pilot streamer speed is of the order of magnitude of the drift velocity in the breakdown field. The stepped leader, on the other hand, makes use of electrons left from a preceding streamer and it travels much faster. On the assumption that the advance is caused by the filling of the region ahead of the tip, in which ionization by collision can occur, by avalanches starting from the original free electrons, it is found that the speed of propagation is given by

$$S=N^{\frac{1}{2}}\bar{v}d, \qquad (2)$$

where d is the distance in which the ionization can take place, $\bar{v}$ is the mean drift velocity, and N is the original concentration per cubic cm. Therefore, S depends on the number of electrons

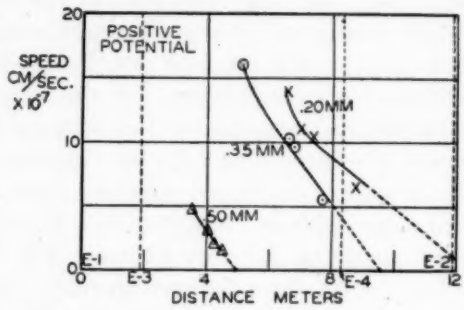

FIG. 6. Speed-distance curves of low potential discharge in air with E-3 grounded.

left from the previous discharge, and on the field at the tip, which determines $\bar{v}$ and d. For conditions supposed by Schonland to be reasonable in the lightning leader, N is about 1000, d about 6 cm, and the tip radius about 1 cm. In this manner the high velocities are explained without the assumption of excessively high fields.

The stepped leader is explained by Meek[8] as arising from recombination in the leader channel, resulting in decreasing conductivity and increasing fields at the cloud end of the steps. A new step is initiated when this field again reaches the breakdown value; for a pilot streamer current of about one ampere, the computed time between steps is fairly near the observed 50 microseconds.

The low potential leaders in the tube were obtained both by raising p and by lowering X. The ratio X/p was found to determine the speed and the possibility of propagation. The minimum X/p, substituted in Eq. (1), gives speeds near the measured minimum of 1.7×10^7 cm/sec. That is, the low potential discharges progressed

[6] A. M. Cravath and L. B. Loeb, Physics 6, 125 (1935); L. B. Loeb, Rev. Mod. Phys. 8, 267 (1936); L. B. Loeb, *Fundamental Processes of Electrical Discharges in Gases* (Wiley and Sons, 1939); G. Simpson, Proc. Roy. Soc. A111, 56 (1926).

[7] H. Jehle, Zeits. f. Phys. 82, 785 (1933).

[8] J. M. Meek, Phys. Rev. 55, 972 (1939).

until X/p reached 20, the minimum required for Townsend ionization,[9] and the speed at this point was approximately the pilot streamer speed. One ampere was about the minimum current in the tube, since the streamer would barely propagate at 85 kv with 7×10^4 ohms in series; the pilot streamer current is generally considered to be of this magnitude. In the tube a marked difference in conditions at the tip of the negative and the positive leaders was indicated. The rate of increase of potential on the oscillograms was greater for negative polarity, and it is consequently probable that the negative wave front was considerably steeper. It may be that the predominance of negative leaders in the lightning discharge is partly due to this effect. The existence of this low speed positive discharge points to the possibility that local positive irregularities in field distribution arising in a cloud may be somewhat smoothed out by a low energy discharge, while a negative distribution may build up until the discharge which finally occurs initiates a lightning leader.

The high potential impulse appears more analogous to the continuous lightning leaders in that the speed indicates a propagation in an ionized channel. It seems likely, however, that the free electrons are in this case photoelectrons, because of the brightly illuminated stem, an effect which might be considerably more important because of ultraviolet reflections at the glass walls. By assuming the same general mechanism of advance that Schonland has given for the lightning leader, Eq. (2) may be modified to apply to the case in which the photoelectric effect is important, the difference being that N can no longer be considered constant, because of absorption of the ionizing radiation by the air in the tube. Under the same assumptions for which Eq. (2) was derived by Schonland,[4] it is found that the field strength at the tip is, at least approximately, $X=V/2r$ volts/cm, where V is the applied potential and r the tube radius. Then the distance d in which a breakdown can occur (that is, when $X/p>40$) is given approximately by

$$d=(rV/80p)^{\frac{1}{2}}. \tag{3}$$

Table II shows values of d for the 14 cm diameter tube at various pressures and applied potentials.

At a distance l the number of photoelectrons is given by $n=n_0\exp(-alp/760)$, where n_0 is the concentration just ahead of the tip and a is the absorption coefficient whose value is 10 cm^{-1}, according to Cravath.[10] A minimum speed of propagation may be found by assuming as before that the entire region d must be filled with conducting filaments starting at the original photoelectrons; then the minimum speed is controlled by the time required for the region of d farthest from the stem to be so covered. Equation (2) becomes

$$S=n_0^{\frac{1}{2}}3\times10^7 d\exp[-10dp/2280]. \tag{4}$$

Substituting the value of d from Eq. (3), we obtain

$$S=3\times10^7 n_0^{\frac{1}{2}}(rV/80p)^{\frac{1}{4}}\times\exp[-(prV)^{\frac{1}{2}}/228(80)^{\frac{1}{4}}]. \tag{5}$$

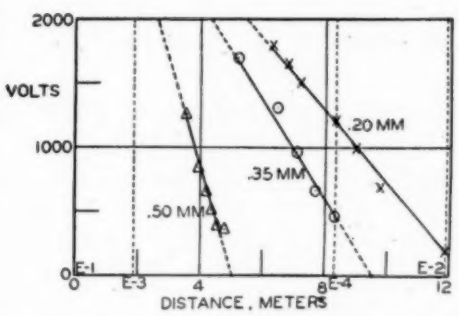

FIG. 7. Maximum positive potential above ground as function of distance with E-3 grounded and conditions same as for Fig. 6.

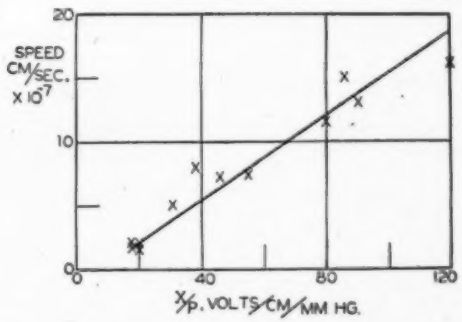

FIG. 8. Speed of low potential discharge in air as function of X/p for pressures of 0.20 mm to 0.50 mm Hg and for positive potential. Lowest speed 1.7×10^7 cm/sec at X/p about 20.

[9] F. H. Sanders, Phys. Rev. **41**, 667 (1932).

[10] A. M. Cravath, Phys. Rev. **47**, 254 (1935).

By assuming n_0 constant over the range of pressures of the experiments, and substituting the experimental values of S, r, p, and V for one set of conditions, one finds that $n_0 \cong 10^2$ ions per cubic cm, and Eq. (5) becomes

$$S = 1.5 \times 10^8 (rV/80p)^{\frac{1}{2}} \times \exp[-(prV)^{\frac{1}{2}}/228(80)^{\frac{1}{2}}]. \quad (6)$$

This equation cannot be expected to hold at low pressure, since loss by diffusion to the walls has not been taken into account. The agreement at the higher pressures is shown in Table III, in which the observed values are taken from Fig. 3.

The value of n_0 is of the order of one-tenth the magnitude assigned to the corresponding N in the lightning leader, so that the pre-ionization in the two cases may not be greatly different in its effect on the speed. However, a direct comparison of the speeds in the tube with those of the lightning leader is open to criticism. While the values of X/p are approximately the same in both cases, the low pressures prevailing in the tube cause a marked difference in the discharge characteristics. Diffusion to the walls becomes important, and recombination is practically negligible. The latter point might be expected to rule out the existence of a stepped leader such as that discussed by Meek, in which the stepping is a result of lowered conductivity in the column due to recombination. However, oscillograms showed that at certain pressures and potentials there was a lowering of conductivity in the tube, and thereby a limitation of the energy fed into the discharge until a fresh breakdown occurred. This effect, shown in Fig. 4, seems somewhat analogous to the stepped leader mechanism of Meek, except that in this case the loss of conductivity might be better attributed to diffusion to the tube walls than to recombination. The disappearance of the stepped leader in long sparks in air at low pressures has been noted by Allibone and Meek.[1]

The higher speed in hydrogen may be due partly to the greater drift speed resulting from the longer free path compared with air at the same conditions.

We wish to express our appreciation to Professor J. W. Beams for his continued interest and assistance in this work.

Internally Converted Radiation from Europium, Hafnium, and Osmium

J. M. CORK, R. G. SHREFFLER, AND C. M. FOWLER
Department of Physics, University of Michigan, Ann Arbor, Michigan

(Received September 5, 1947)

By use of semicircular focusing, magnetic spectrometers, together with absorption methods, the gamma-radiations emitted by europium 154, hafnium 181, and osmium 193 are evaluated. These energies are as follows: for europium (154)—122.4, 342.8, 407.8, and 1230 kev; for hafnium (181)—132.5, 345.5, 478.7, and 600 kev (by absorption); and for osmium (193)—129.1 kev. Two cases are shown where photoelectrons and conversion electrons from the same gamma-ray are of comparable intensity. The ability of the radioactive method in chemical analysis to show traces of impurities is demonstrated.

WITH the apparatus described in previous reports,[1] data have been obtained on the radioactivity of the following isotopes—europium 154, hafnium 181, and osmium 193. The samples studied were obtained through the Atomic Energy Commission by irradiation in the Oak Ridge pile.

EUROPIUM 154

Previous studies[2] had shown the existence of a radioactive isotope of europium of half-life about 6 years, whose beta-spectrum had an upper limit of 0.9 Mev. On exposing a supposedly very pure sample of europium to the neutron activity of the pile, a very intense radioactivity was induced by the (n, γ) reaction. Subsequent observations showed the probable presence of an impurity of the related element, neodymium. The active sample was studied by observing the absorption of its radiation in lead, copper, and aluminum with a string electrometer and ionization chamber, and photographically in the magnetic spectrometers.

A typical photogram of the beta-spectrum is shown in Fig. 1. The three horizontal strips represent different exposure times with the same magnetic field. Several lines due to internal conversion are apparent. If the internal conversion follows after the emission of a beta-particle from the excited europium, whose atomic number is 63, then the *K-L-M* differences present should be those of the next heavier element, namely, gadolinium. A collection of all measurable lines expressed in terms of energy is presented in Table I, and shown graphically in Fig. 2. The interpretation of each line is presented in column 2, and the final gamma-energies in the last column.

Two observations of special interest can be made in addition to that relating to the gamma-lines for this element. It is apparent that the gamma line of energy 0.122 Mev is satisfied both by a *K-L-M* combination characteristic of gadolinium (64), and europium (63). It must then be that in this case the ejection of photoelectrons in the parent europium by the uncon-

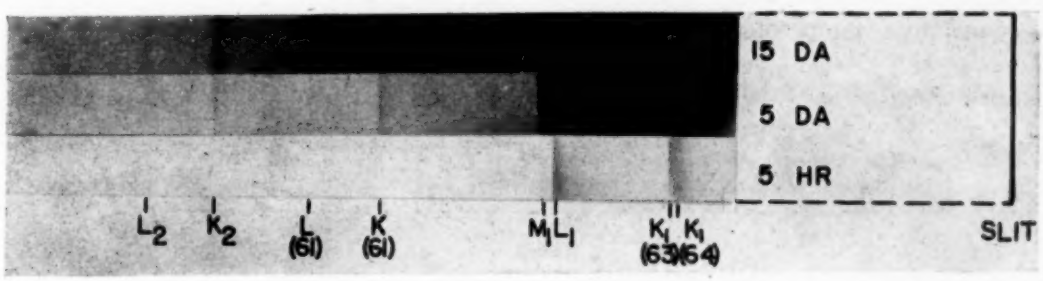

FIG. 1. The conversion spectrum of europium 154, for exposure times of 5 hours, 5 days, and 15 days.

[1] J. M. Cork, Phys. Rev. 72, 581 (1947).
[2] K. Fajans and A. Voigt, Phys. Rev. 60, 533 (1941).

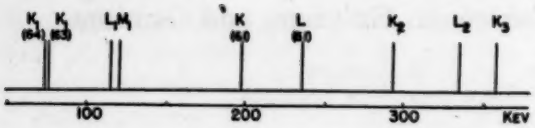

FIG. 2. The energy distribution of the complete europium 154 spectrum.

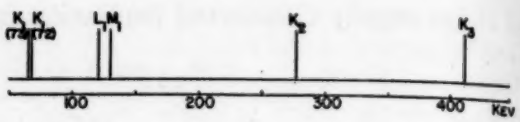

FIG. 4. The energy distribution of conversion lines for hafnium 181.

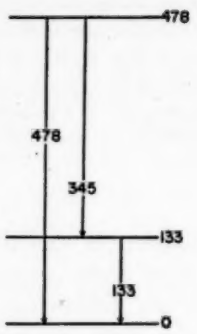

FIG. 5. Energy levels in tantalum 181 after the emission of a beta-particle from hafnium 181.

verted gamma-radiation happens to be of the same order of magnitude as the production of electrons by internal conversion in the relatively few decaying gadolinium nuclei.

It can also be observed that one group of lines have energy separations characteristic of the *K-L-M* differences for the element of atomic number 61. They satisfy a gamma-energy of 244 kev. This indicates that neodymium (60) might have been present as an impurity in the europium. However, no long half-lived activities have previously been reported in neodymium, and over the few months of the present observation the intensity of these lines has not diminished by any large amount. From the remaining lines, it can be concluded that in europium there are three strong gamma-rays of energy, 122.4, 342.8, and 407.8 kev. Absorption measurements in copper, iron, and lead indicate the presence of a higher energy gamma-ray at 1.23 Mev.

The upper limit of the beta-spectrum was observed by its absorption in aluminum (0.132 cm), and in the magnetic spectrometer to be about 0.93 Mev. A more complete study of the form of the beta-distribution is being made. No simple scheme is apparent that would reduce the number of levels required to satisfy the observed gamma-energies.

HAFNIUM

When hafnium is subjected to neutron radiation a radioactive isotope of mass 181 can be produced by the (n, γ) reaction. An activity of half-life 55 days had been reported by Hevesy,[3] but the radiation emitted was not recorded. A sample of pure hafnium oxide was strongly activated by irradiation in the pile. When placed in the magnetic spectrometer many conversion lines were obtained.

Table II shows collectively the energies of the observed lines together with their interpretation and the consequent energies of the gamma-rays. It is again evident that for the gamma-ray of energy 132.5 kev the photoelectrons are about equal in number to the conversion electrons so that two *K*-lines are present, one being for hafnium, and the other for tantalum. These are shown in the low energy photogram reproduced in Fig. 3. A summary of all observed lines with their corresponding energies is shown in Fig. 4. Evidence for the existence of an additional

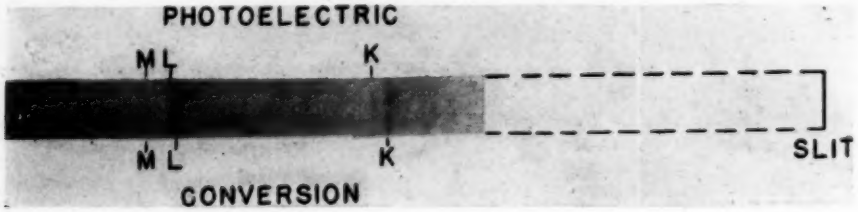

FIG. 3. Low energy portion of the beta-spectrum of hafnium 181, showing both photoelectric and internal conversion electrons.

[3] G. Hevesy and G. Levi, Nature 137, 185 (1936).

FIG. 6. Photogram showing the presence of iridium in the osmium specimen.

TABLE I. Beta-spectrum of europium.

Observed energy	Identification	Gamma-energy
71.8 kev	$K_1(64)$	122.1 kev
73.8	$K_1(63)$	122.4
114.4	L_1	122.8
120.0	M_1	121.9
197.0	$K(61)$	244.4
235.7	$L(61)$	243.6
292.4	K_2	342.7
334.5	L_2	342.9
357.5	K_3	407.8

TABLE II. Beta-spectrum of hafnium.

Observed energy	Identification	Gamma-energy
65.1 kev	$K_1(73)$	132.5 kev
67.0	$K_1(72)$	132.4
120.6	L_1	132.3
129.9	M_1	132.6
276.8	K_2	344.2
411.3	K_3	478.7

gamma-ray at an energy of about 0.60 Mev is obtained from measurements of the absorption in copper and aluminum.

The three observed gamma-rays offer the relationship that the sum of two of them is very close in value to that of the third, so that the level scheme of Fig. 5 appears valid, and must in part represent the possible levels in excited tantalum 181.

OSMIUM

A radioactive isotope of osmium of half-life 17 days had been reported.[4] This was produced by neutron bombardment and assigned to mass 193 being derived from the abundant natural isotope of mass 192 by the (n, γ) reaction. Powdered, metallic osmium was irradiated in the pile and as a result yielded a strong radioactivity.

When placed in the spectrometer, many lines were recorded in the spectrum photographically. The pattern of certain of the lines obtained seemed very familiar, and on analysis it was found to agree with the recorded[1] values for iridium. Certain additional strong lines were present.

In Fig. 6 the lines obtained with osmium are shown directly above the corresponding strong lines for iridium. Since the osmium was supposed to be chemically pure, it became of interest to know to what extent the iridium was present in order to evaluate this radioactive method as a tool for chemical analysis in certain cases. Dr. R. A. Wolfe made a rather exhaustive spectroscopic analysis of the osmium, and concluded that there was much less than one percent of iridium present. In spite of this small quantity, it is apparent that the lines are quite strong. Thus, impurities with extraordinary large capture cross sections may be revealed by the radioactive method when present in very minute quantities.

The strong lines attributed to osmium form an *L-M* combination characteristic of iridium as expected after beta-emission. They have energies of 126.2 and 115.6 kev, which yield a single gamma-ray of 129.1 kev.

This investigation was made possible by the support of the Office of Naval Research.

[4] G. T. Seaborg and G. Friedlander, Phys. Rev. 59, 400 (1941).

PHYSICAL REVIEW VOLUME 72, NUMBER 12 DECEMBER 15, 1947

Imprisonment of Resonance Radiation in Gases

T. HOLSTEIN
Research Laboratories, Westinghouse Electric Corporation, East Pittsburgh, Pennsylvania
(Received September 8, 1947)

It is known that resonance quanta are highly absorbable by normal atoms of the emitting gas; hence, under suitable conditions of gas density the eventual escape of these quanta from a gas-filled enclosure may require a large number of repeated absorptions and emissions. This "radiative" transport of excitation is determined essentially by the probability, $T(\rho)$, that a quantum traverses a layer of gas of thickness, ρ, without being absorbed; the dependence of $T(\rho)$ on the frequency distribution of the resonance line is investigated, and explicit expressions are derived for the cases of Doppler and dispersion broadening. The general transport problem is formulated in terms of a Boltzmann-type integro-differential equation involving $T(\rho)$; the variational method of obtaining steady-state solutions of this equation is discussed. The theory is then applied to the evaluation of the rate of decay of excitation in an infinite slab; the results are compared with Zemansky's measurements of the decay of radiation from an enclosure of mercury vapor. Finally, the application of the theory to a number of problems concerning excited atoms is discussed briefly.

I. INTRODUCTION

THE term "resonance" is applied to radiation emitted by an atom in an optical transition from an excited state to the ground state. Examples of such radiation are the sodium doublet (5890, 5896A) and the mercury lines 2537A and 1849A. In contrast to other components of atomic spectra which are emitted in transitions between excited states, the resonance lines are highly absorbable by the gas in its normal state. For instance, in mercury at 1 mm the 2537A line is appreciably absorbed in a distance of the order of 0.001 cm. Other resonance lines are similarly absorbed by small layers of gas.

Under such conditions, it is clear that when a resonance quantum is emitted by an individual atom, it is by no means assured an unimpeded transit to the walls of the enclosure. On the contrary, after traversing a short distance, it is most probably absorbed by another atom, thereby raising the latter to the state originally excited. The result of this process of emission and reabsorption is merely the transfer of excitation energy from atom to atom; the eventual escape of the radiation to the boundary of the enclosure may require a large number of such transfers. In such cases we speak of the radiation as being "imprisoned."

The first theoretical treatment of this phenomenon was given by K. T. Compton.[1] Regarding the transfer of excitation as a type of Brownian motion, Compton obtained, in effect, a diffusion-type equation for the density of excited atoms, n:

$$\partial n/\partial t = D\nabla^2 n, \tag{1.1}$$

with D given in terms of the mean free path of the quantum, λ, and the lifetime of the individual atom, τ, by the relation

$$D = \lambda^2/3\tau. \tag{1.2}$$

In order to compare (1.1) with the conventional kinetic theory expression

$$D = \lambda\bar{v}/3, \tag{1.3}$$

we must take into account an important difference between the motions of resonance quanta and material particles. Namely, in the latter case, the time of collision is always small compared to the mean time *between* collisions, whereas, in the case of quanta, even if one assures λ to be of the order of the dimensions of the enclosure ~ 1 cm, the time between collisions is much smaller than the time of collision, which for quanta is the lifetime of the excited state, $\tau \sim 10^{-8}$ sec. Denoting by τ' the mean time between collisions, we have the general relation

$$\bar{v} = \lambda/(\tau+\tau'). \tag{1.4}$$

For the case of material particles

$$\bar{v} = \lambda/\tau', \tag{1.5}$$

[1] K. T. Compton, Phys. Rev. **20**, 283 (1922).

whereas, for quanta

$$\bar{v}=\lambda/\tau. \tag{1.6}$$

Inserting (1.6) into (1.3), we obtain (1.2).

It should be emphasized that the essential feature of the treatment is the assumption of a definite mean free path, λ, for the motion of resonance quanta. This means that the probability of a quantum penetrating a distance ρ in the gas before being absorbed is given by an exponential law, $e^{-\rho/\lambda}$, which, in turn, is true only if the absorption coefficient of the gas varies little over the frequency spectrum of the resonance quantum. Because of the highly selective character of the absorption, however, we expect precisely the opposite; namely, the absorption coefficient varies appreciably over the frequency spectrum of the radiation. Thus, the value of λ to be inserted into (1.2) is uncertain; in fact, as the analysis given below will demonstrate, it is impossible to define a mean free path for the motion of resonance quanta.

The problem was next attacked by Milne,[2] who also assumed the existence of a mean free path. His results were not much different from Compton's.

A noteworthy advance was achieved by Kenty[3] who took the frequency spectrum of the line into account. Assuming a Doppler line to be emitted by each volume element of the gas, he attempted to calculate an average diffusion coefficient essentially by averaging (1.2) over the spectrum of the emitted radiation, but arrived at the surprising result that for an enclosure of infinite size this average was infinite, i.e., one could not define a diffusion coefficient for an infinite region. In treating the finite case Kenty still assumed that the decay was capable of description by a diffusion equation of the type (1.1) and confined himself to calculating an effective coefficient, D. Since, as will be shown below, the phenomenon cannot be formulated in terms of a diffusion equation, D could only be calculated to an order of magnitude. The results, nevertheless, are in fair agreement with those of the more exact theory, to be presented below, and with experimental results[4] over a limited range of pressure.

[2] E. A. Milne, J. Lond. Math. Soc. **1**, 1 (1926).
[3] C. Kenty, Phys. Rev. **42**, 823 (1932).
[4] M. W. Zemansky, Phys. Rev. **42**, 843 (1932).

II. TRANSMISSION OF RESONANCE RADIATION

The essential feature of the treatment presented in this report is the determination of the probability, $T(\rho)$, of the radiation traversing a distance ρ. Once $T(\rho)$ is known, we can readily set up equations describing the transfer of excitation between different volume elements of the enclosure. The basis of Compton's treatment, for example, is the assumption of a uniform absorption coefficient, $1/\lambda$, so that in his case

$$T(\rho)=e^{-\rho/\lambda}. \tag{2.1}$$

Since, however, the absorption coefficient of the medium, $k(\nu)$, is actually a sensitive function of the frequency in the spectral domain of the resonance radiation, we must average the monochromatic transmission factor:

$$T(\rho,\nu)=e^{-k(\nu)\rho}$$

over the frequency spectrum $P(\nu)$ of the radiation emitted from a given volume element, i.e.,

$$T(\rho)=\int P(\nu)e^{-k(\nu)\rho}d\nu. \tag{2.3}$$

Equation (2.3) is a crucial formula in our treatment; we therefore discuss it in some detail.

The absorption coefficient $k(\nu)$ is a characteristic of the gas in its normal state. The frequency variation of $k(\nu)$ is dealt with extensively in standard texts.[5] The different forms which it can assume are as follows:

(1) Natural absorption. This type of absorption is characteristic of isolated atoms at rest. The coefficient is given by the "dispersion" formula

$$k(\nu)=\frac{C}{1+[4\pi(\nu-\nu_0)/\gamma]^2}, \tag{2.4}$$

where ν is the impressed frequency, ν_0 the frequency at which $k(\gamma)$ is a maximum, and γ the reciprocal of the lifetime of the excited state, i.e., the probability per unit time that an excited atom radiates. C is a constant characterized by the density of normal atoms, N, the wave-length of radiation $\lambda_0=c/\nu_0$, and γ; it may be determined

[5] A. C. G. Mitchell and M. W. Zemansky, *Resonance Radiation and Excited Atoms* (The Macmillan Company, New York, 1934), to be referred to hereafter as MZ.

from a very general expression derivable from thermodynamic principles (cf. MZ pages 95–96, formula (28)).

$$\int k(\nu)d\nu=\frac{\lambda_0^2}{8\pi}\frac{g_2}{g_1}\frac{N}{\tau}, \tag{2.5}$$

where g_1 and g_2 are the statistical weights of the normal and excited atomic energy levels, and $\tau=1/\gamma$. One readily obtains for C the value

$$C=\frac{\lambda_0^2 N}{2\pi}\frac{g_2}{g_1}. \tag{2.6}$$

In the great majority of cases, natural absorption is unimportant because of the frequency broadening of the absorption line arising from the motion and mutual interaction of the atoms; these effects are described immediately below.

(2) Doppler-broadened absorption. This absorption prevails when the Doppler shift, because of the motion of the atoms, is large compared to the natural width. Each atom may be considered as capable of absorbing a single frequency for a given velocity of the atom and direction of propagation of the incident quantum. This frequency, ν, is given by the well-known relation

$$\nu=\nu_0[1+(v/c)\cos\psi], \tag{2.7}$$

where ψ is the angle between the directions of motion of the absorbing atom and the quantum. Since the velocity distribution of the atoms is Maxwellian, one can readily obtain the absorption coefficient. This turns out to be (cf. MZ, formulas (32), (34), and (35)):

$$k(\nu)=k_0\exp[-(\nu-\nu_0/\nu_0)^2(c/v_0)^2], \tag{2.8}$$

where

$$v_0=(2RT/M)^{\frac{1}{2}}, \tag{2.9}$$

and

$$k_0=\frac{\lambda_0^3 N}{8\pi}\frac{g_2}{g_1}\frac{1}{\pi^{\frac{1}{2}}v_0\tau}. \tag{2.10}$$

In (2.9) R is the gas constant per mole, T the absolute temperature, and M the gram-molecular weight of the gas. (2.10) is obtained from (2.8) and (2.5).

(3) Pressure-broadened absorption. This type of absorption arises from the interactions between individual atoms; hence it becomes increasingly important as the pressure is raised. For reviews and literature on this subject the reader is referred to the articles of Weisskopf[6] and Margenau and Watson,[7] and to MZ, Chapter IV, Section II. In many cases the dispersion formula

$$k(\nu)=\frac{C'}{1+[4\pi(\nu-\nu_0)/\gamma_p]^2}, \tag{2.4'}$$

first obtained by Lorentz, is valid. Here γ_p varies directly with the pressure and C' is a constant whose value is determined by (2.5). (2.4') obtains when the main effect of interaction is collision-like, i.e., when atomic frequencies are affected appreciably in a time interval short compared to the average "free" time, during which the atomic frequencies are perturbed negligibly.

At pressures of the order of atmospheres, or for values of $\nu-\nu_0\gg\gamma_p$, the absorption law often departs considerably from (2.4'). These deviations will not be discussed quantitatively in this paper.

(4) A general relation which takes into account the three types of broadening discussed above is (cf. MZ, Chapter III, Section IIc, Eq. (97))

$$k(\nu)=k_0\frac{a}{\pi}\int_{-\infty}^{+\infty}\frac{\exp(-y^2)}{a^2+(x-y)^2}dy. \tag{2.11}$$

Here, k_0 is given by $a=(\gamma+\gamma_p)\lambda_0/4\pi v_0$ and $x\equiv[(\nu-\nu_0)/\gamma_0](c/v_0)$. In many cases a is small compared to unity; for these cases and for $x\gtrsim 2$, (2.4) may be written approximately (cf. MZ, Appendix) as

$$k(\nu)/k_0\approx\exp(-x^2)+a/\pi^{\frac{1}{2}}x^2. \tag{2.12}$$

Equation (2.12) shows that, even for $a\ll 1$, the behavior of the absorption coefficient at large $|x|$, i.e., at the edge of the absorption region, is determined by the dispersion distribution.

We next discuss the frequency spectrum $P(\nu)$ of the radiation emitted from a given volume element. The specification of $P(\nu)$ is not as simple as that of the absorption coefficient $k(\nu)$, since the nature of the excitation is involved. If the system were in temperature equilibrium, the principles of thermodynamics would provide us

[6] V. Weisskopf, Physik. Zeits. **34**, 1 (1933).
[7] H. Margenau and W. W. Watson, Rev. Mod. Phys. **8**, 22 (1936).

with the simple relation

$$P(\nu) \propto k(\nu), \tag{2.13}$$

which is a form of Kirchhoff's law. In the case at hand, the radiation is certainly not in temperature equilibrium with the gas; nevertheless, if the gas were enclosed within perfectly reflecting walls, we would still be able to consider the system of quanta plus atomic excitation as being in a state of *local* thermodynamic equilibrium, with negligible interaction between it and the mass motion of the atoms. Under such conditions, (2.13) would still be valid. However, in view of the circumstance that, in our case, the radiation leaks out through partially reflecting walls, the thermodynamic argument breaks down; the justification of assumption (2.13) thus requires a special treatment. This treatment is presented in the Appendix, wherein it is shown that the assumption applies to the cases of Doppler and pressure broadening; since these two cases are predominantly encountered in practice, we use (2.13) in the evaluation of $T(\rho)$.

The constant of proportionality in (2.13) is determined with the aid of (2.5). We have, since $\int P(\nu)d\nu = 1$,

$$k(\nu) = \frac{\lambda_0^2}{8\pi}\frac{g_2}{g_1}\frac{N}{\tau}P(\nu) \equiv \kappa P(\nu). \tag{2.14}$$

For $T(\rho)$ we then obtain the expression

$$T(\rho) = \int P(\nu)e^{-\kappa\rho P(\nu)}d\nu. \tag{2.15}$$

We now evaluate $T(\rho)$ for the two types of spectral distributions: Doppler and dispersion.

(1) Doppler distribution. It is convenient to represent the frequency in terms of the variable x defined above, *viz*:

$$x = [(\nu-\nu_0)/\nu_0](c/v_0). \tag{2.16}$$

The normalization of $P(x)$ yields

$$P(x) = \frac{1}{\pi^{\frac{1}{2}}}\exp(-x^2). \tag{2.17}$$

We also obtain

$$k(x) = \kappa P(\nu) = \kappa(\nu_0 v_0/c)^{-1}P(x) = k_0\exp(-x^2), \tag{2.18}$$

where k_0 is given by (2.10). Inserting (2.17) and (2.18) into (2.15), we have

$$T(\rho) = \int_{-\infty}^{+\infty}\frac{1}{\pi^{\frac{1}{2}}}e^{-x^2}\exp[-k_0\rho e^{-x^2}]dx. \tag{2.19}$$

To obtain $T(\rho)$ for all values of $k_0\rho$, recourse must be had to numerical integration. However, for many purposes, the asymptotic value of $T(\rho)$ for large $k_0\rho$ suffices. To find this value we first change the variable according to the transformation

$$x = (\log k_0\rho/y)^{\frac{1}{2}} \tag{2.20}$$

and obtain

$$T(\rho) = \frac{1}{k_0\rho\pi^{\frac{1}{2}}}\int_0^{k_0\rho}\frac{e^{-y}dy}{(\log k_0\rho - \log y)^{\frac{1}{2}}}. \tag{2.21}$$

Since the effective region of integration is limited to values of y of the order of magnitude unity, we may, for large values of $k_0\rho$, approximate $(\log k_0\rho - \log y)^{\frac{1}{2}}$ by $(\log k_0\rho)^{\frac{1}{2}}$ and extend the upper limit of integration to infinity. Thus

$$T(\rho) \approx 1/k_0\rho(\pi\log k_0\rho)^{\frac{1}{2}}. \tag{2.22}$$

(2) Dispersion distribution. We associate this distribution with pressure broadening, since natural broadening is in most cases negligible. The normalized distribution may be written as

$$P(u) = \frac{1}{\pi}\frac{1}{1+u^2}, \tag{2.23}$$

where

$$u = 4\pi(\nu-\nu_0)/\gamma_p. \tag{2.24}$$

We have

$$k(u) = \kappa P(\nu) = \frac{4\pi\kappa}{\gamma_p}P(u) = \frac{\lambda_0^2 N}{2}\frac{g_2}{g_1}\frac{\gamma}{\gamma_p}P(u),$$

or

$$k(u) = k_d/(1+u^2), \tag{2.25}$$

with

$$k_d = \frac{\lambda_0^2 N}{2\pi}\frac{g_2}{g_1}\frac{\gamma}{\gamma_p}. \tag{2.26}$$

Inserting (2.23) and (2.25) into (2.15), and transforming the variable of integration according to (2.24), we obtain

$$T(\rho) = \frac{1}{\pi}\int_{-\infty}^{+\infty}\frac{\exp[-k_d\rho/(1+u^2)]}{1+u^2}du. \tag{2.27}$$

The integral of (2.27) can be evaluated for all values of $k_d\rho$ in terms of modified Bessel functions of zero order; however, for our purposes the asymptotic form for large $k_d\rho$ alone is necessary. Now, for $k_d\rho \gg 1$, the effective region of integration is $u^2 \gg 1$, hence

$$T(\rho) \approx \frac{1}{\pi}\int_{-\infty}^{+\infty} \frac{1}{y^2}\exp(-k_d\rho/u^2)du$$

$$= \frac{2}{\pi}\int_0^{\infty} \exp(-k_d\rho y^2)dy,$$

i.e.,

$$T(\rho) \approx 1/(\pi k_d\rho)^{\frac{1}{2}}. \tag{2.28}$$

Equations (2.22) and (2.28) describe the asymptotic variation of $T(\rho)$ for the cases of Doppler and dispersion distributions, respectively. Since both of these forms differ considerably from the exponential variation of Compton's theory, as given by (2.1), it is obvious that the simple kinetic theory concept of mean free path cannot be applied to quanta.

One way of defining the mean free path is via the introduction of the probability, $K(\rho)d\rho$, that the quantum is captured after traversing a distance between ρ and $\rho+d\rho$ from its emission point. The mean free path, λ, may then be defined as

$$\lambda = \int_0^{\infty} \rho K(\rho)d\rho. \tag{2.29}$$

Now, from elementary laws of probability,

$$K(\rho)d\rho = T(\rho) - T(\rho+d\rho) = -d\rho\,\partial T/\partial\rho, \tag{2.30}$$

so that

$$\lambda = -\int_0^{\infty} \rho\frac{\partial T}{\partial\rho}d\rho. \tag{2.31}$$

If we, for instance, insert the exponential form (2.1) into (2.31), we obtain an identity. On the other hand, (2.22) or (2.28) both give divergent results. Thus, in the case of Doppler or dispersion spectral distributions, a mean free path cannot be defined.

It can be shown easily that this conclusion holds for an arbitrary spectral distribution $P(\nu)$ which is related to the absorption coefficient $k(\nu)$ of the medium by the relation (2.14). We have, from (2.31) and (2.15),

$$\lambda = \int\int_0^{\infty} P(\nu)\frac{\partial(e^{-k_\rho P(\nu)})}{\partial\rho}d\nu d\rho = \int \frac{1}{\kappa}d\nu, \tag{2.32}$$

which diverges, q.e.d.

III. TRANSPORT OF EXCITATION BY RESONANCE RADIATION

The impossibility of defining a mean free path for resonance quanta forces us to relinquish the hope of describing the radiative transport of excitation by a diffusion equation. An adequate description, however, can be achieved by a Boltzmann-type integro-differential equation, which we now derive.

We introduce the probability $G(\mathbf{r}', \mathbf{r})d\mathbf{r}$ that a quantum emitted at $\mathbf{r}'$ is absorbed in a volume element $d\mathbf{r}$ around the point $\mathbf{r}$. Denoting the density of excited atoms by $n(\mathbf{r})$, we have, from the law of conservation of particles,

$$dtd\mathbf{r}\partial n(\mathbf{r})/\partial t = a - b, \tag{3.1}$$

where a and b are the increase and decrease in the number of excited atoms in volume element $d\mathbf{r}$ in time dt. For b we have immediately

$$b = \gamma n(\mathbf{r})d\mathbf{r}dt. \tag{3.2}$$

To obtain a, we must sum over the contributions of all other volume elements. The contribution of $d\mathbf{r}'$ is given by the number of quanta emitted therein in time dt, $\gamma n(\mathbf{r}')d\mathbf{r}'dt$, multiplied by the probability of any one of these quanta being captured in $d\mathbf{r}$, $G(\mathbf{r}', \mathbf{r})d\mathbf{r}$. Integrating over these volume elements, we obtain

$$a = \gamma dtd\mathbf{r}\int n(\mathbf{r}')G(\mathbf{r}', \mathbf{r})d\mathbf{r}'. \tag{3.3}$$

In the derivation of (3.3) we have implicitly assumed that the time of flight of quanta, τ', is negligibly small compared to the atomic lifetime, τ (cf. discussion following Eq. (1.3) of text and preceding Eq. (19A) of Appendix). Inserting (3.2) and (3.3) into (3.1), we arrive at the integral equation

$$\partial n(\mathbf{r})/\partial t = -\gamma n(\mathbf{r}) + \gamma\int n(\mathbf{r}')G(\mathbf{r}', \mathbf{r})d\mathbf{r}', \tag{3.4}$$

where the integral is taken over the volume of

the enclosure. (It is here assumed that the walls are non-reflecting.)

Our next step is the specification of $G(\mathbf{r}', \mathbf{r})$ in terms of $T(\rho)$. We require the assumption of isotropic emission. The assumption is valid provided the excited atoms are unpolarized. This situation seems quite likely in view of the large number of absorptions and randomly directed emissions which the average quantum undergoes. In fact, as is stated in MZ, Chapter IV, imprisonment has a strong depolarizing effect on resonance radiation emanating from a region originally excited by a polarized beam. Thus we feel justified in considering polarization effects to be of secondary importance, to be included, perhaps, in a future treatment more refined than that given here.

The assumption of isotropic emission means that the probability of the quantum being propagated in a direction circumscribed by a solid angle $d\omega$ is $d\omega/4\pi$. The probability, then, that it is absorbed in a volume element defined by $d\omega$ and by spheres of radius ρ and $\rho+d\rho$ from the emission point is

$$(1/4\pi)K(\rho)d\omega d\rho,$$

whence we see that, with $\boldsymbol{\rho}=\mathbf{r}-\mathbf{r}'$, $d\mathbf{r}=\rho^2 d\rho d\omega$, $G(\mathbf{r}, \mathbf{r}')d\mathbf{r}'=G(\boldsymbol{\rho})d\boldsymbol{\rho}=(1/4\pi\rho^2)K(\rho)d\rho$, or from (2.30)

$$G(\mathbf{r}, \mathbf{r}')=-(1/4\pi\rho^2)(\partial T/\partial\rho). \tag{3.5}$$

Equation (3.5) shows how the whole problem of the space-time variation of the density of excited atoms is referred back to the nature of the transmission coefficient $T(\rho)$. In this connection it may be pointed out that Compton's diffusion equation can be obtained from (3.4) and (3.5) and the exponential form of $T(\rho)$ given in (2.1) by the Fokker-Planck expansion.[8] In our case, however, in view of the form of $T(\rho)$ as given either by (2.22) or (2.28), we cannot perform this expansion and must hence deal with (3.4) directly.

We first observe that there exist solutions of the type

$$n(\mathbf{r}, t)=n(\mathbf{r})e^{-\beta t}, \tag{3.6}$$

with β and $n(r)$ satisfying the equation

$$(1-\beta/\gamma)n(\mathbf{r})=\int G(\mathbf{r}', \mathbf{r})n(\mathbf{r}')d\mathbf{r}', \tag{3.7}$$

which is a homogeneous integral equation of a standard type treated, e.g., in Courant-Hilbert, Chapter III.[9] We further observe that, in view of (3.5), $G(\mathbf{r}', \mathbf{r})$ is symmetrical in the variables $\mathbf{r}'$ and $\mathbf{r}$, i.e.,

$$G(\mathbf{r}, \mathbf{r}')=G(\mathbf{r}', \mathbf{r}). \tag{3.8}$$

This feature permits us to formulate the problem variationally as is shown in the cited reference.[9] We have, namely,

$$\frac{\beta}{\gamma}=1-\frac{\int\int G(\mathbf{r}, \mathbf{r}')n(\mathbf{r})n(\mathbf{r}')d\mathbf{r}d\mathbf{r}'}{\int n^2(\mathbf{r})d\mathbf{r}}, \tag{3.9a}$$

$$\delta(\beta/\gamma)=0. \tag{3.9b}$$

The application of (3.9b) to (3.9a), with use of (3.8), yields (3.7), as the reader may readily verify.

It can also be shown that β/γ is positive-definite, i.e., its minimum value obtained by applying the variational procedure is positive. One obtains, after some algebraic manipulation,

$$\frac{\beta}{\gamma}=\frac{\int n^2(\mathbf{r})E(\mathbf{r})d\mathbf{r}+\frac{1}{2}\int\int[n(\mathbf{r})-n(\mathbf{r}')]^2G(\mathbf{r}, \mathbf{r}')d\mathbf{r}d\mathbf{r}'}{\int n^2(\mathbf{r})d\mathbf{r}}, \tag{3.10}$$

where

$$E(\mathbf{r})=1-\int G(\mathbf{r}, \mathbf{r}')d\mathbf{r}'; \tag{3.11}$$

[8] A. D. Fokker, Ann. d. Physik **43**, 812 (1914); M. Planck, Sitz. Preuss. Akad. Wiss. 324 (1917); S. Chandrasekhar, Rev. Mod. Phys. **15**, 1 (1943), Chapter II, Section 4.

[9] R. Courant and D. Hilbert, *Methoden der Mathematischen Physik* (Verlag, Julius Springer, Berlin, 1931).

the domain of integration in all cases is the volume of the enclosure. Since $\int G(\mathbf{r},\mathbf{r}')d\mathbf{r}'$ gives the total probability of a quantum emitted at $\mathbf{r}$ being caught somewhere in the enclosure, $E(\mathbf{r})$ is the probability of escape of this quantum. From its definition $E(\mathbf{r})$ is a non-negative quantity. Since $G(\mathbf{r},\mathbf{r}')$ is also non-negative for all values of $\mathbf{r}$ and $\mathbf{r}'$, both terms of (3.10) are non-negative, i.e., β/γ is positive-definite as claimed above.

The eigenvalues of β_n of (3.7) can thus be arranged in an ascending series of positive numbers. (It is also shown in Courant-Hilbert, Chapter III, that these eigenvalues are denumerable, i.e., discrete.) If $n_n(\mathbf{r})$ denotes the solution of (3.7) corresponding to β_n, the most general solution of (3.4) is of the form

$$n(\mathbf{r},t)=\sum_n c_n n_n(\mathbf{r})e^{-\beta_n t}, \tag{3.12}$$

where the c_n are constants depending upon the initial conditions. We observe that, after a sufficiently long time,

$$n(\mathbf{r},t)\approx c_1 n_1(\mathbf{r})e^{-\beta_1 t}, \tag{3.13}$$

i.e., the solution corresponding to the lowest eigenvalues, β_1, determines the behavior of $n(\mathbf{r},t)$ for large t. In what follows, we confine our attention to this solution. We note in passing that $n_1(\mathbf{r})$ must be non-negative for all points $\mathbf{r}$ of the enclosure in order that it may represent a density function.

The method which we employ to obtain the lowest eigenvalue, β, and the corresponding eigenfunction, $n(\mathbf{r})$ (we have dropped the subscript in the notation for both of these quantities) is the Ritz variational procedure. This procedure, in the particular form in which we have applied it, consists in approximating $n(\mathbf{r})$ by a finite series of m terms

$$n(\mathbf{r})=\sum_1^m a_i n_i(\mathbf{r}), \tag{3.14}$$

where the $n_i(\mathbf{r})$ are m known functions of $\mathbf{r}$ and the a_i are to be determined by the minimizing of β. Substituting (3.14) into (3.10), we obtain

$$\frac{\beta}{\gamma}=\sum_{ij} a_i a_j K_{ij}/\sum_{ij} a_i a_j H_{ij}, \tag{3.15}$$

where

$$K_{ij}=\int n_i(\mathbf{r})n_j(\mathbf{r})E(\mathbf{r})d\mathbf{r} + \tfrac{1}{2}\int\int [n_i(\mathbf{r})-n_i(\mathbf{r}')] \times [n_j(\mathbf{r})-n_j(\mathbf{r}')]G(\mathbf{r},\mathbf{r}')d\mathbf{r}d\mathbf{r}', \tag{3.16a}$$

and

$$H_{ij}=\int n_i(\mathbf{r})n_j(\mathbf{r})d\mathbf{r}. \tag{3.16b}$$

We observe that $K_{ij}=K_{ji}$; $H_{ij}=H_{ji}$. β is now a function of the a_i. The minimum conditions are

$$\partial\beta/\partial a_i=0. \tag{3.17}$$

Performing the differentiations, we obtain

$$\sum_{j=1}^m \left[a_j K_{ij}-\frac{\beta}{\gamma}H_{ij}\right]=0; \quad i=1,2,\cdots,m. \tag{3.18}$$

In order for Eqs. (3.18) to be solved by a non-zero set of the a_i, the determinant of the coefficients must be zero, i.e.,

$$\begin{vmatrix} K_{11}-\frac{\beta}{\gamma}H_{11} & \cdots & K_{1m}-\frac{\beta}{\gamma}H_{1m} \\ \vdots & & \vdots \\ K_{1m}-\frac{\beta}{\gamma}H_{1m} & \cdots & K_{mm}-\frac{\beta}{\gamma}H_{mm} \end{vmatrix}=0. \tag{3.19}$$

(3.19) constitutes an algebraic equation of the m'th order in β/γ, and hence possesses m solutions; of these only the lowest one is of interest. Once β/γ has been obtained, any set of $(m-1)$ equations chosen from the m equation of (3.18) can be used to obtain the ratios a_i/a_1, $i=2,\cdots,m$. One thus determines $n(\mathbf{r})$ to within a multiplicative constant.

It is shown in Courant-Hilbert, pages 149–151, that the Ritz variational approach gives values of β and $n(\mathbf{r})$ which converge towards the true solution of (3.7) as the number, m, of independent functions $n_i(\mathbf{r})$ and adjustable constants a_i, increases. In particular, each addition of a new term involving an adjustable constant to the series (3.14) for $n(\mathbf{r})$ brings both β and $n(\mathbf{r})$ closer to the true solution.

The number of terms which must be chosen to obtain accurate results for β and $n(\mathbf{r})$ depends upon the suitability of the $n_i(\mathbf{r})$ with regard to the representation of the true solution. In many cases the use of two well chosen functions suffices to give values of β which are good to one percent.

It is known that $n(\mathbf{r})$ is not determined as accurately as is β by the Ritz method. Nevertheless, if β is accurate to one percent, $n(\mathbf{r})$ is expected not to deviate too radically from the true function. Indications from calculations of specific cases are that this expectation is fulfilled.

IV. DECAY OF EXCITATION IN AN INFINITE SLAB

We now apply the theory presented above to the calculation of the decay of excitation in a one-dimensional enclosure of gas. The enclosure is in the form of a slab of thickness L, with the other two dimensions infinite. The density of excited atoms is now a function $n(z)$ of the coordinate, z, perpendicular to the walls of the slab. We choose the origin to bisect the perpendicular between the walls so that the coordinates of the latter are $z=\pm L/2$. Equation (3.7) can be simplified by integration over the x and y coordinates, both of which are parallel to the walls. We obtain, after some algebraic manipulation,

$$(1-\beta/\gamma)n(z)=\int_{-L/2}^{+L/2} n(z')H(|z-z'|)dz', \quad (4.1)$$

where

$$H(\zeta)=-\partial\mathcal{E}(\zeta)/\partial\zeta, \quad (4.2)$$

and

$$\mathcal{E}(\zeta)=\frac{1}{4\pi}\int_0^{\pi/2}\int_0^{2\pi} T(\zeta\sec\theta)\sin\theta d\theta d\varphi. \quad (4.3)$$

$\mathcal{E}(\zeta)$ is the probability that a quantum, emitted at an arbitrary point, will cross a plane situated at a distance ζ from that point. The integral of (4.3) represents a summation over all directions of propagation; in this case the integration goes over the solid angle subtended by the plane at the point, i.e., half the total solid angle. θ and ϕ are polar and azimuthal angles taken with respect to the perpendicular from point to plane as polar axis. The distance from point to plane in the direction given by θ and ϕ is $\rho=\zeta\sec\theta$.

In (4.1) $H(|z-z'|)dz$ is the probability that a quantum, emitted at z', is absorbed in a layer between the planes z and $z+dz$. Equation (4.2) is then a statement of conservation of probability.

The variational expression for β/γ, corresponding (3.10) reads

$$\frac{\beta}{\gamma}=\frac{\int n^2(z)E(z)dz+\frac{1}{2}\int\int[n(z)-n(z')]^2H(|z-z'|)dzdz'}{\int n^2(z)dz}, \quad (4.4)$$

where

$$E(z)\equiv 1-\int H(|z-z'|)dz'=\mathcal{E}(\tfrac{1}{2}L+z)+\mathcal{E}(\tfrac{1}{2}L-z). \quad (4.5)$$

In these equations, the limits of integration are $z=\pm L/2$.

Calculations have, up to the present, been carried out only for the Doppler spectrum. Here, according to (2.22), the asymptotic form for $T(\rho)$ is

$$T(\rho)\approx 1/k_0\rho(\pi\log k_0\rho)^{\frac{1}{2}}.$$

Inserting this expression into (4.3), we obtain

$$\mathcal{E}(\zeta)=\frac{1}{2}\int_0^{\pi} T(\zeta\sec\theta)\sin\theta d\theta$$

$$\approx\frac{1}{4k_0\zeta(\pi\log k_0\zeta)^{\frac{1}{2}}}\approx\frac{1}{4k_0\zeta(\pi\log k_0L/2)^{\frac{1}{2}}}. \quad (4.6)$$

Applying (4.6) to (4.5) and (4.2), we obtain

$$H(\zeta)\approx\frac{1}{4k_0\zeta^2}\frac{1}{(\pi\log k_0L/2)^{\frac{1}{2}}}, \quad (4.7)$$

and

$$E(z)\approx\frac{1}{4k_0L(\pi\log k_0L/2)^{\frac{1}{2}}}\frac{1}{\frac{1}{4}-(z/L)^2}. \quad (4.8)$$

Inserting (4.7) and (4.8) into (4.4), and changing the variable to $\xi=2z/L$, we obtain

$$\beta'=\frac{\int\frac{n^2(\xi)}{1-\xi^2}d\xi+\frac{1}{4}\int\frac{[n(\xi)-n(\xi')]^2}{(\xi-\xi')^2}d\xi d\xi'}{\int n^2(\xi)d\xi}, \quad (4.9)$$

where

$$\beta' = k_0 L(\pi \log k_0 L/2)^{\frac{1}{2}}\beta/\gamma \tag{4.10}$$

and the limits of integration are $\xi = \pm 1$.

In the variational calculation of β' as given by (4.9), linear combinations of the functions

$$\begin{aligned} n_0(\xi) &= 1/2, \\ n_1(\xi) &= (3/4)(1-\xi^2), \\ n_2(\xi) &= (5/8)(1-\xi^4), \end{aligned} \tag{4.11}$$

were used. (The $n_i(\xi)$ are normalized according to the relation

$$\int_{-1}^{+1} n_i(\xi)d\xi = 1, \tag{4.12}$$

as is customary for probability functions.)

The K_{ij} and H_{ij} are, with the exception of K_{∞}, all readily evaluated from the one-dimensional analogs of (3.16a) and (3.16b), which read

$$K_{ij} = \int_{-1}^{+1} \frac{n_i(\xi)n_j(\xi)}{1-\xi^2}d\xi + \frac{1}{4}\int_{-1}^{+1}\int_{-1}^{+1} \frac{[n_i(\xi)-n_i(\xi')][n_j(\xi)-n_j(\xi')]}{(\xi-\xi')^2}d\xi d\xi', \tag{4.13a}$$

$$H_{ij} = \int_{-1}^{+1} n_i(\xi)n_j(\xi)d\xi. \tag{4.13b}$$

The calculation of K_{00} cannot be carried out in this way since (4.13a) gives a divergent result. This divergence owes its origin to our replacement of $T(\rho)$, $\mathcal{E}(\zeta)$, and $E(z)$ by their asymptotic values. The rigorous expression for K_{00} reads (cf. (4.13a), (4.11), and (4.8))

$$K_{00} = \frac{k_0[\pi \log(k_0 L/2)]^{\frac{1}{2}}}{2}\int_{-L/2}^{+L/2} E(z)dz,$$

which, in view of (4.5), may be written as

$$K_{00} = k_0(\pi \log k_0 L/2)^{\frac{1}{2}}\int_{-L/2}^{+L/2} \mathcal{E}(\tfrac{1}{2}L+z)dz. \tag{4.14}$$

For $\mathcal{E}(\frac{1}{2}L+z)$, we have from (4.3) and (2.19),

$$\mathcal{E}(\tfrac{1}{2}L+z) = \int_0^{\pi/2}\int_0^{\infty} \frac{\exp(-x^2)}{\pi^{\frac{1}{2}}} \times \exp[-k_0 \sec\theta(\tfrac{1}{2}L+z)e^{-x^2}]\sin\theta d\theta dx. \tag{4.15}$$

The insertion of (4.15) into (4.14) gives the complete expression for K_{00}. Integrating this expression with respect to z, we obtain

$$K_{00} = (\log k_0 L/2)^{\frac{1}{2}}\int_0^{\pi/2}\int_0^{\infty} \cos\theta \times\{1-\exp[-k_0 L \sec\theta e^{-x^2}]\}\sin\theta d\theta dx. \tag{4.16}$$

We next consider the integration over x. We perform this operation approximately by taking the factor in curly brackets equal to unity for $x < \log^{\frac{1}{2}}(k_0 L \sec\theta)$ and zero for x greater than this value. Thus,

$$K_{00} \approx (\log k_0 L/2)^{\frac{1}{2}}\int_0^{\pi/2} \cos\theta \log^{\frac{1}{2}}(k_0 L \sec\theta)\sin\theta d\theta.$$

We introduce the further approximations of replacing both $\log k_0 L/2$ and $\log(k_0 L \sec\theta)$ by $\log k_0 L$. These approximations partly cancel each other and are also small in magnitude because of the slow variation of the logarithmic factors. We then obtain

$$K_{00} \approx \tfrac{1}{2}\log k_0 L. \tag{4.17}$$

Once the K_{ij} and H_{ij} have been evaluated, β' and the coefficients a_i in the Ritz approximations of $n(\xi)$ are readily obtained by solution of (3.18) and (3.19).

In the first three calculations $n(\xi)$ was successively equated to $n_1(\xi)$, $n_2(\xi)$, and $n_3(\xi)$; the corresponding eigenvalues, β_0', β_1', and β_2', were found to be $2\log k_0 L$, $15/8$, and $15/8$, respectively.

Next, the two-parameter combinations

$$\begin{aligned} n_{01}(\xi) &= a_0 n_0(\xi) + a_1 n_1(\xi), \\ n_{02}(\xi) &= a_0 n_0(\xi) + a_2 n_2(\xi), \\ n_{12}(\xi) &= a_1 n_1(\xi) + a_2 n_2(\xi) \end{aligned}$$

were tried; these gave the following expressions for β':

$$\begin{aligned} \beta_{01}' &= (15/8)\left(1 - \frac{1/16}{\log k_0 L - 5/4}\right), \\ \beta_{02}' &= (15/8)\left(1 - \frac{1/48}{\log k_0 L - 3/2}\right), \\ \beta_{12}' &= (15/8)(0.986). \end{aligned} \tag{4.18}$$

Taking for $\log k_0 L$ a typical value, say 5, we have

$$\begin{aligned} \beta_{01}' &= (15/8)(0.983), \\ \beta_{02}' &= (15/8)(0.994), \end{aligned} \tag{4.19}$$

whence we see that, although the best two-parameter result is achieved with $n_{01}(\xi)$, the total improvement over the one-parameter value, 15/8, is only 1.7 percent.

In view of the approximations which have already been introduced in the evaluation of $E(z)$ and $H(\zeta)$, discrepancies of this order of magnitude are rather inconsequential. We therefore omit the calculation of β' for three-parameter function

$$n_{012}(\xi)=a_0n_0(\xi)+a_1n_1(\xi)+a_2n_2(\xi),$$

which can only lead to a small additional improvement of the order of a percent.

The coefficients a_i of the function $n_{01}(\xi)$, which gives the best two-parameter result, are found to be

$$a_0=\frac{3/8}{\log k_0L-3/2};\quad a_1=1-a_0, \tag{4.20}$$

which, for $\log k_0L=5$, give $a_0=0.107$; $a_1=0.893$. These numbers correspond to a ratio of density at the edge of the container to that in the center

$$n_{01}(\pm1)/n_{01}(0)=0.071. \tag{4.21}$$

For the comparison of theory with experiment we ignore the 1.7 percent difference between β_{01}' and β_1' and take $\beta'=15/8$. The value of β/γ corresponding to this choice is

$$\beta/\gamma=\frac{1.06}{k_0L(\log k_0L/2)^{\frac{1}{2}}}. \tag{4.22}$$

V. COMPARISON WITH EXPERIMENT

Although the imprisonment of radiation has been observed in a number of ways, the sole reliable, direct measurement known to the author is that of Zemansky,[10] who obtained β for the 2537A line of Hg as a function of gas density, N. The comparison of his results with the theory of this paper encounters a number of complications.

1. Geometry of the enclosure. The experiment consisted in measuring the decay of radiation from two disks of thickness 1.30 cm and 1.95 cm, both of diameter 5.1 cm. It is obvious that the correspondence of this geometry to the one-dimensional idealization of the theory is only approximate.

[10] M. W. Zemansky, Phys. Rev. **20**, 283 (1922).

2. Hyperfine structure. The theoretical calculations are based upon the assumption that the resonance line is simple. Actually, the 2537A line consists of five, hyperfine structure components. The change in β arising from this structure is analyzed immediately below. The main results of the treatment are: (a), $T(\rho)$ may be considered as the average of the transmission functions, $T_i(\rho)$, of the individual components, each taken as an isolated line, and (b), (4.22) is still approximately valid with the sole modification that k_0 is to be replaced by $k_0/5$.

In the evaluation of $T(\rho)$ the first question which arises is whether the absorption bands of the different components overlap. By "absorption band" we mean a continuous aggregate of frequencies which are appreciably absorbed in the traversal of a layer of length L in the gas. If the absorption bands do overlap, it becomes necessary to consider the composite line structure in detail.

The edge of an absorption band is given roughly by the relation

$$k(\nu)L=1. \tag{5.1}$$

For the case of Doppler-broadened spectral distributions, we have

$$k_0Le^{-x^2}=1,$$

or

$$x=(\log k_0L)^{\frac{1}{2}}. \tag{5.2}$$

Combining (5.2) with (2.16), we obtain for the half-breadth of the absorption band in frequency units

$$\Delta\nu=\frac{v_0}{c}\nu_0(\log k_0L)^{\frac{1}{2}}$$

or in wave-length units

$$\Delta\lambda=\frac{c}{\nu_0^2}\Delta\nu=\lambda_0\frac{v_0}{c}(\log k_0L)^{\frac{1}{2}}. \tag{5.3}$$

For mercury at room temperature $v_0=(2RT/M)^{\frac{1}{2}}=1.57\times10^4$ cm/sec.; with $\lambda=2537$A we obtain

$$\Delta\lambda=(\log k_0L)^{\frac{1}{2}}1.33\text{ mA}. \tag{5.4}$$

Now, in Zemansky's experiments, as will be seen below, the maximum value of k_0L, for which quantitative comparison with the theory is at-

tempted, is 1000. Since $(\log 1000)^{\frac{1}{2}} = 2.67$, we have

$$\Delta\lambda_{\max} = 3.5 \text{ mA}.$$

On the other hand, the minimum separation of the hyperfine structure lines is about 10 mA (MZ, p. 38, Fig. 12); hence, there is a band of 3 mA between the two components in which negligible absorption takes place.

Actually, the non-overlap of absorption bands is not a sufficient criterion to permit us to consider the hyperfine components as isolated; this can be seen by consideration of the transmission factor $T(\rho)$. For a line possessing hyperfine structure

$$P(\nu) = \sum_i P_i(\nu) \tag{5.5a}$$

and

$$k(\nu) = \sum_i k_i(\nu), \tag{5.5b}$$

where the P_i's and k_i's are the spectral distribution and absorption coefficients of the individual components. We introduce

$$N_i \equiv \int P_i(\nu)d\nu, \tag{5.6a}$$

$$\sum N_i = 1. \tag{5.6b}$$

N_i gives essentially the intensity of the i'th hyperfine component. We then have, according to (2.3),

$$T(\rho) = \sum_i N_i T_i'(\rho), \tag{5.7a}$$

where

$$T_i'(\rho) = \int [P_i(\nu)/N_i] \exp[-\sum_j k_j(\nu)\rho]d\nu. \tag{5.7b}$$

Now, if over the range in which $P_i(\nu)$ contributes appreciably to $T(\rho)$, all the $k_j(\nu)\rho$, $j \neq i$, are small compared to unity, we obtain

$$T_i'(\rho) = T_i(\rho), \tag{5.8a}$$

where

$$T_i(\rho) = \int [P_i(\nu)/N_i] e^{-k_i(\nu)\rho} d\nu. \tag{5.8b}$$

$T_i(\rho)$ is the transmission coefficient of an isolated line. We thus have

$$T(\rho) = \sum_i N_i T_i(\rho). \tag{5.9}$$

$T(\rho)$ represents a composite or average transmission factor of all the components. Against the introduction of this average transmission, one might raise the objection that each line ought to be treated separately, so that one should obtain different values of β. The answer to this objection is twofold:

(1) All the lines which emanate from a common state of the atom must actually be averaged since their relative intensities are fixed atomic constants. This is the case of the sodium hyperfine structure.

(2) If different excited states or the excited states of different isotopes are involved, radiationless transfers of excitation energy between all such states will take place readily because of the extremely small energy differences between the levels. For pressures of the order of those involved in Zemansky's experiment, this exchange is much more rapid than the decay rates of the individual resonance lines. Hence the relative concentrations of the excited states are in constant thermodynamic equilibrium. We are thus justified in considering $T(\rho)$ to be the common transmission factor for all the components. Now, for the Doppler broadening, we have

$$k_i(\nu) = k_i \exp[-(x-x_i)^2], \tag{5.10}$$

where x_i denotes the frequency center of the i'th component; with use of (2.14), we obtain

$$k_i = k_0 N_i, \tag{5.11}$$

with k_0 given by (2.10). Using the asymptotic formula (2.22) for $T(\rho)$, we find

$$T(\rho) \approx \frac{1}{k_0\rho} \sum_i \frac{1}{(\pi \log N_i k_0 \rho)^{\frac{1}{2}}}. \tag{5.12}$$

Now the logarithmic factor is slowly varying; hence, unless the intensities of the different components are very unequal, we may replace N_i by an average without incurring much error. If the number of components is m, we take $N_i = 1/m$ and obtain

$$T(\rho) \approx \frac{1}{k_e\rho} \frac{1}{(\pi \log k_e\rho)^{\frac{1}{2}}}, \tag{5.13a}$$

where

$$k_e = k_0/m. \tag{5.13b}$$

Since β is determined by $T(\rho)$, we obtain the correct result by replacing k_0 by k_e in (4.22).

This "averaging" procedure of considering the lines to be of equal strength has been used by Zemansky in evaluating Kenty's theory, as well as in other connections (cf., MZ, p. 234, 125).

We now have to show that the fundamental condition for the validity of (5.8a) and hence of (5.13a), namely, the smallness of $k_j(\nu)\rho$, $i \neq j$, in the region in which $P_i(\nu)$ contributes effectively to $T(\rho)$, prevails in the case at hand. Here, as we have found above, there exists a domain of 3mA between absorption bands. This corresponds to a Δx of 2.2. Now, for $k_0L=1000$ (the k_0L of the above numerical estimate should be written k_eL), we have for the edge of the absorption band at $x=2.67$, $\exp(-x^2)=10^{-3}$. At the edge of the adjacent band $x=2.67+2.2=4.89$; the corresponding value of $\exp(-x^2)$ is e^{-24}, which is altogether negligible. The validity of our basic assumption, as expressed by (5.8a), is thus established.

3. Natural broadening. A small correction to (4.22) may arise from natural broadening due to the relatively slow decrease of the dispersion distribution at large x, as is indicated by (2.12) and the discussion immediately following. The correction does not affect the absorption appreciably. Namely, for $k_0\rho$ as high as 1000, the important contributions to $T(\rho)$ come from values of $|x|$ in the neighborhood of $x_1=(\log k_0\rho)^{\frac{1}{2}}=2.67$; taking $a_N=\gamma\lambda_0/4\pi v_0=0.0011$ (Hg at 90°C), we obtain

$$k_0\rho/\pi^{\frac{1}{2}}x_1^2=0.086,$$

which is a small correction to the Doppler absorption, $k_0\rho\exp(-x_1^2)=1$.

However, if we assume (2.13), i.e., $P(x)\propto k(x)$, the change in $T(\rho)$, $\Delta T_N(\rho)$ is not negligible; we have from (2.12), (2.13), and (2.17)

$$\Delta P_N(x)=a_N/\pi x^2,$$

and hence,

$$\Delta T_N(\rho)=\int_{-\infty}^{+\infty}\exp(-k_0\rho e^{-x^2})\frac{a_N}{\pi x^2}dx\approx\frac{2a_N}{\pi(\log k_0\rho)^{\frac{1}{2}}},$$

which, in view of the slow variation of the logarithmic factor, may be approximated by

$$\Delta T_N(\rho)=\frac{2a_N}{\pi(\log k_0L/2)^{\frac{1}{2}}}. \tag{5.14}$$

Since (93) is independent of ρ, $n(z)$ is left unaltered and β is increased by an amount $\Delta\beta_N=\Delta T_N$.

The presence of the hyperfine structure causes a diminution of $\Delta\beta_N$; a rough estimate of this effect gives a reduction factor of 0.8, which, when combined with (5.14), yields

$$\Delta\beta_N\approx\frac{0.5\gamma}{(\log k_0L/2)^{\frac{1}{2}}}. \tag{5.15}$$

With $a_N=0.0011$, $\gamma=10^7$ sec.$^{-1}$, and $\log k_0L/2=4$ (corresponding to $k_0L=110$) we obtain

$$\Delta\beta_N\approx 3\times 10^3 \text{ sec.}^{-1} \tag{5.16}$$

which, although not negligible, is small as far as the comparison between theory and experiment is concerned.

The above analysis is based on assumption (2.13), the validity of which in the case of natural broadening is rather doubtful. However, it seems quite likely that (2.13) gives at least an upper limit for the contribution of natural broadening to $P(x)$. First of all, the radiation from a given volume element contained in the spectral region $|x|\gtrsim x_1$ possesses a preferentially large escape probability. Secondly, as pointed out in the beginning of the Appendix, the absorption-emission process, in the absence of Doppler shift and pressure-broadening interactions, does not alter frequencies and hence cannot contribute to a replenishment of the dispersion component, $\Delta P_N(x)$, in the spectral region $|x|\gtrsim x_1$. Thus, the actual $\Delta P_N(x)$ may be expected to be smaller than $a_N/\pi x^2$; hence, in our opinion, (5.15) represents an upper limit to the natural broadening correction.

4. Pressure broadening. The detailed treatment of the transition from Doppler to pressure broadening in the case of the 2537A line is quite involved due to the hyperfine structure. Here we discuss only the initial manifestation of this transition.

Assuming an absorption law of the form of (2.12), we may take over the results for natural broadening presented immediately above. In the case of pressure broadening we note that: (a), (2.13) is valid as is shown in the Appendix, and (b), a_N is to be replaced by $a_p=a_N\gamma_p/\gamma_N$.

For γ_p we use the result of Furssov and

Vlassov:[11]

$$\gamma_p = \frac{8\pi}{3}\frac{e^2}{m\omega} f N, \tag{5.17}$$

where N is the density of atoms and f the "oscillator" strength for the absorption of the resonance line (cf., MZ, page 96). Equation (5.17) assumes the absence of hyperfine structure.

We also have (cf., MZ, page 97)

$$\gamma = \frac{8\pi e^2}{mc}\frac{g_1}{g_2} f/\lambda_0^2.$$

For the 2537A line $g_2/g_1 = 3$; we thus obtain

$$\gamma_p/\gamma = N\lambda_0^3/2\pi^2 = 0.83\times 10^{-15} N. \tag{5.18}$$

We now consider the effect of hyperfine structure on the magnitude of γ_p. As in the Appendix, we represent the atoms by classical harmonic oscillators whose natural frequencies coincide with those of the actual resonance lines. In this case we must consider oscillators of five different frequencies corresponding to the five hyperfine components; the density of each type of oscillator is proportional to the intensity of the associated component. Now, for collisions between oscillators of the same natural frequency, the usual phase-shift calculation of impact broadening is valid; the contribution of these collisions to γ_p is of the form of (5.17) with the sole modification that f here represents the oscillator strength for the absorption of one hyperfine component. When, on the other hand, oscillators of different natural frequencies collide, the perturbation of the frequencies of both oscillators by the interaction is reduced; in order for a given phase shift to be achieved, the oscillators must approach closer with the result that the rate of effective collision is diminished.

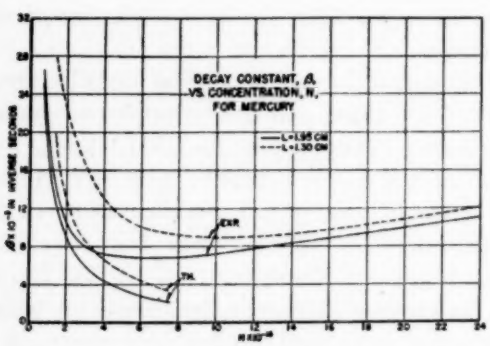

FIG. 1. Decay constant, β, *vs.* concentration, N, for mercury.

A preliminary calculation of this effect indicates that the hyperfine separation cuts down γ_p by a factor of the order of 2. The insertion of this result into (5.18) gives

$$\gamma_p/\gamma \approx \tfrac{1}{2}10^{-15} N. \tag{5.19}$$

Combining (5.19) with (5.15), we obtain for the increase in β due to pressure broadening, $\Delta\beta_p$, the order-of-magnitude estimate

$$10^{-3}\Delta\beta_p \approx 1.5(N\times 10^{-15}) \text{ sec.}^{-1}. \tag{5.20}$$

We now proceed to the comparison of theory with experiment. Since Zemansky has already evaluated $k_e L$ (in his notation, $k_0 l$) as a function of the experimental conditions of gas density, temperature, and slab thickness (MZ, page 234, Table 40), we need only insert these values into (4.22). The resultant theoretical expressions for β are given in Fig. 1 together with Zemansky's experimental results.

We observe that the left-hand portion of the experimental curves agree in order of magnitude with the theoretical prediction. Quantitatively, the agreement for $L = 1.95$ is quite good while that for $L = 1.30$ is not as satisfactory; the reason for the discrepancy in the latter case is not clear.

It should, at this point, be mentioned that Kenty's results show a similar agreement with the left-hand part of the experimental curves (MZ, Table 40).

The slow rise of Zemansky's curves with increasing N for gas densities greater than 10^{16} atoms/cc is not explained by the theory. Two possible causes are: (1) pressure broadening, and (2) non-radiative transitions from the radiating 6^3P_1 state to the metastable 6^3P_0 state 0.218 volt lower.

With regard to the first agency, an order-of magnitude estimate of its initial effect is given by (5.20). According to this equation the increase in β due to pressure broadening becomes appreciable for $N \gtrsim 3\times 10^{15}$/cc. Beyond $N \sim 7\times 10^{15}$/cc we encounter the complications associated with the overlap of the absorption bands of the hyperfine components.

[11] W. Fursov and A. Vlassov, Phys. Zeits. Sowjetunion **10**, 378 (1936).

At densities high enough so that the separation of the components is small compared to the absorption band, we may consider the line to be simple. Assuming a dispersion distribution we have

$$T(\rho) \approx 1/(\pi k_d \rho)^{\frac{1}{2}}, \tag{2.28}$$

where

$$k_d = (\lambda_0^2 N/2\pi)(g_2/g_1)(\gamma/\gamma_p). \tag{2.26}$$

Now, γ_p, the line breadth resulting from pressure broadening, varies linearly with N; hence k_d and $T(\rho)$ become independent of the gas density. Since $T(\rho)$ determines the decay factor, β, the latter should also become independent of the density.

It should be pointed out that, at the high density extreme of absorption band large compared to the separation of the components, the absorption band must cover a spectral range at least of the order of 0.2A. Now according to Kuhn,[12] the pressure-broadened spectrum at distances $\gtrsim$0.6A from the center of the line is no longer of the dispersion type. Since in the determination of $T(\rho)$ the important spectral region is in the neighborhood of the edge of the absorption band $\sim$0.1A from the center of the line, the validity of a treatment based on the dispersion distribution is rather doubtful.

Recently[13] the method of nuclear transmutation has been applied to the production of the pure mercury isotope 198, which by itself shows no hyperfine structure since its spin is zero. Experiments with this isotope should prove quite informative, since the complications due to hyperfine structure do not exist.

In this connection, experiments with the sodium D lines would also be of interest since the element exists in only one isotopic form. Both of the lines are split into only two hyperfine components, the separation of which is small compared to the absorption bands which would be encountered in radiation-decay experiments of the type performed by Zemansky. On the other hand, the 6A separation of the D lines themselves permits the avoidance of overlap complications over a large range of pressure. Whether or not the lines decay independently is an additional question which can be investigated both experimentally and theoretically.

With regard to the second possibility for the rise of Zemansky's curves at higher values of N, namely, the radiationless conversion of the radiating state into the metastable state, the sole evidence known to the present author consists of an experiment performed by Orthmann and Pringsheim.* They find that, as the pressure of mercury is raised to about one atmosphere, the diffuse resonance radiation from a chamber illuminated with the resonance line 2537A is almost completely quenched, whereas the radiation of a small admixture of thallium (2×10^{-3} mm), the atoms of which can be excited upon collision with metastable mercury atoms, loses none of its original intensity. These results indicate that the radiating 6^3P_1 state produced by the incident beam is converted to the 6^3P_0 metastable state, which in turn, lives long enough to make a relatively infrequent collision with a thallium atom.

The conversion from radiating to metastable state should be capable of a more direct and quantitative investigation than that of Orthmann and Pringsheim. However, this has not yet to our knowledge been achieved.

In the light of the above discussion, a further advantage of experiments with sodium vapor is that non-radiative quenching of excitation should not take place in sodium since the only level below the resonance level is the ground state 2.1 volts lower in energy. The conversion of this amount of energy into kinetic energy of nuclear motion is extremely unlikely; hence, the decay should be due entirely to the escape of resonance radiation.

VI. ADDITIONAL PROBLEMS

In conclusion we present a brief discussion of additional problems suggested by the theory.

1. Lines of various spectral distributions. The above theory may be amplified to include various types of spectral distributions arising both from pressure broadening and the existence of hyperfine structure. Concerning the dispersion distribution, the first step has already been taken in the derivation of (2.28). As we have remarked above, in the discussion of pressure broadening,

[12] H. Kuhn, Proc. Roy. Soc. **A158**, 230 (1937).
[13] J. H. Wiens, Phys. Rev. **70**, 910 (1946).

* W. Orthmann and P. Pringsheim, Zeits. f. Physik **35**, 626 (1926).

distributions other than the dispersion distribution occur. Probably the most important is the "statistical" distribution[14] which for large $(\nu_0-\nu)$ is given by the formula

$$P(\nu)=\frac{\frac{2}{3}\pi(-b)^{\frac{1}{2}}N}{(\nu_0-\nu)^{\frac{1}{2}}},$$

in which the sign of $(\nu_0-\nu)$ is opposite to that of b (for $(\nu_0-\nu)b$ positive, $P(\nu)=0$).

The presence of hyperfine structure will, as we have seen above, also give rise to new effects, particularly when the absorption bands overlap.

2. Equilibrium between an excited radiating state and electrons. Here two additional processes must be included.

(a). The creation of excited atoms by electron collision with normal atoms. The contribution of this process to the rate of increase of excitation is given by

$$An_e(\mathbf{r}),$$

where $n_e(\mathbf{r})$ is the electron density and A a constant proportional to the density of normal atoms and otherwise dependent on the cross section for excitation of the level and the energy distribution of the electrons.

(b). The destruction of excited atoms by collisions of the second kind with electrons. The rate of decrease of excitation due to this cause is represented by the term

$$-Bn(\mathbf{r})n_e(\mathbf{r}),$$

where B is a function of the cross section for such collisions and the electron-energy distribution.

The equation describing the equilibrium set up by these two collision processes, together with the radiative transport of excitation, reads

$$0=An_e(\mathbf{r})-Bn_e(\mathbf{r})n(\mathbf{r})-\gamma n(\mathbf{r})+\gamma\int G(\mathbf{r},\mathbf{r}')n(\mathbf{r}')d\mathbf{r}'. \quad (6.1)$$

We observe two limiting cases:

(a). At very low electron densities the second term becomes negligible and we have approximately

$$0\approx An_e(\mathbf{r})-\gamma n(\mathbf{r})+\gamma\int G(\mathbf{r},\mathbf{r}')n(\mathbf{r}')d\mathbf{r}',$$

from which we see that $n(\mathbf{r})$ is proportional to the number of electrons.

(b). At very large electron densities, the last two terms may be neglected and we have

$$n(\mathbf{r})=A/B, \quad (6.2)$$

i.e., $n(\mathbf{r})$ is independent of electron density. We observe here that, if the electron energy distribution is Maxwellian, with a temperature T_e, we must have in case (b)

$$n(\mathbf{r})=Ne^{-\epsilon/kT_e}g_2/g_1, \quad (6.3)$$

where N is the normal atom density, ϵ the excitation energy, and g_2/g_1 the ratio of the statistical weights of the excited and ground states. Equation (6.3) follows from thermodynamic principles which apply to case (b), since the only processes involved are reversible exchanges of energy between free electrons and bound atomic electrons. Now (6.2) and (6.3) must be identical; hence,

$$A/B=(g_2/g_1)e^{-\epsilon/kT_e},$$

when the electrons have a Maxwell distribution in energy.

In order to obtain quantitative results for the general case, we must solve (6.1). This problem was attacked a number of years ago by de Groot,[15] who erroneously assumed the transmission function $T(\rho)$ for light quanta to be exponential; the results were retracted in a subsequent paper.[16]

The approach which seems most feasible at present is the variational method. The application of this method to the solution of linear inhomogeneous integral equations is indicated in Courant-Hilbert[9] (Chapter IV, page 176).

(3) Decay of excited states in noble gases: In noble gases (and to some extent in metallic vapors such as cadmium and mercury) radiating and metastable states are separated by small energy differences. Hence, the conversion from one to the other upon collision with normal atoms, with simultaneous change in the kinetic energy of nuclear motion, may take place readily. It has often been tacitly assumed that once a metastable atom is converted into a radiating atom, the excitation energy is immediately radi-

[14] Reference 7, Section 8, Eq. (2).

[15] W. de Groot, Physica **12**, 289 (1932), (old series).

[16] W. de Groot, Physica **1**, 28 (1934).

ated from the enclosure. Because of the long lifetimes of radiating states caused by imprisonment of radiation, this assumption must be revised. A schematic treatment of the decay problem from the new point of view has been given by de Groot and Penning in their *Handbuch* article. A more accurate analysis will require the solution of integral equations of the type encountered above.

(4) The Penning effect. This phenomenon is the ionization of impurity atoms by excited atoms of the main constituent of a gas mixture; the most notable example is the ionization of argon atoms by excited neon atoms.[17] Since the ionization process must complete with other forms of destruction of excited atoms, the radiative transport of excitation is of crucial importance. A correct treatment of the problem must therefore consider imprisonment of resonance radiation.

APPENDIX I

The purpose of this appendix is the justification of the assumption

$$P(\nu) \propto k(\nu). \tag{1A}$$

The validity of (1A) is by no means universal; one can readily imagine cases for which it fails. For instance, let us suppose that "monochromatic" radiation (whose spectral width is small compared to the natural width) is incident on a medium whose absorption coefficient is characterized by natural broadening, i.e., the atoms are at rest and do not interact with each other. Then it is well known[18] that the spectrum of the emitted radiation is identical with that of the incident beam.

A similar, though less drastic situation prevails in the case of Doppler broadening. Here, a monochromatic beam excites only those atoms whose velocity component in the direction of the incident beam satisfies the Doppler relation (2.7). Since these atoms emit radiation in all directions, the spectral distribution of this radiation is obviously not monochromatic; nevertheless, it will certainly deviate greatly from the Doppler form as given by (2.17).

Since, as these examples demonstrate, (1A) is not universal, its applicability must be examined for the particular situations of interest. In this appendix we show that (1A) may be used in the cases of pressure and Doppler broadening; the case of natural broadening presents difficulties which have not yet been overcome.

A. Pressure Broadening

For this case we demonstrate that atoms, even when excited by a monochromatic beam, emit radiation whose spectral distribution is essentially proportional to $k(\nu)$. For the sake of simplicity the treatment will be classical throughout; i.e., the atoms are considered to be classical harmonic oscillators whose resonance frequency is identical with that of the resonance line; the corresponding quantum-mechanical approach does not present any essentially new features and will hence not be given here.

We first assume that the interaction of a given oscillator with its environment may be represented by quenching collisions, after each of which the oscillator is de-excited, i.e.,

$$\mathbf{u}(t_c) = \dot{\mathbf{u}}(t_c) = 0, \tag{2A}$$

where $\mathbf{u}$ is the oscillator displacement and t_c the time at which the collision takes place. This assumption will later be modified to deal with the actual case of non-quenching collisions. In the time between collisions, the oscillator does not interact with its neighbors; hence, in the presence of an incident field, $Ee^{i\omega t}$, the displacement $\mathbf{u}$ obeys the well-known oscillator equation, which, with neglect of radiation damping, reads

$$\ddot{\mathbf{u}} + \omega_0^2 \mathbf{u} = -(eE/m)e^{i\omega t}, \tag{3A}$$

where $\omega_0 = 2\pi\nu_0$ and the other symbols have their conventional significance.

It is permissible to neglect the damping term in (3A) because of the circumstance that when pressure broadening predominates the mean free time between collisions, τ_p, is much smaller than the radiative lifetime, $\tau = 1/\gamma$; since we integrate (3A) only over times of the order of τ_p, the effect of the damping term, $\gamma\dot{\mathbf{u}}$, can easily be shown to be negligible.

[17] M. J. Druyvesteyn and F. M. Penning, Rev. Mod. Phys. 12, 87 (1940).

[18] Max Born, *Optik* (Verlag, Julius Springer, Berlin, 1933), Chapter VIII, Section 91.

The solution of (3A) subject to (2A) is

$$\mathbf{u}=-\frac{eE}{m}\frac{e^{i\omega t}}{\omega_0^2-\omega^2}\left[1-\frac{1}{2}\left(1+\frac{\omega}{\omega_0}\right)e^{-i(\omega-\omega_0)(t-t_i)}-\frac{1}{2}\left(1-\frac{\omega}{\omega_0}\right)e^{-i(\omega+\omega_0)(t-t_i)}\right], \quad (4A)$$

where t_i is the time at which the last collision previous to time t has occurred. In the neighborhood of resonance (4A) may be approximated by the expression

$$\mathbf{u}=-(Ee/m)\frac{e^{i\omega t}}{2\omega_0(\omega_0-\omega)}[1-e^{-i(\omega-\omega_0)(t-t_i)}]. \quad (5A)$$

Because of the random nature of the collision process, $\mathbf{u}(t)$ is only partly coherent with the impressed field. The coherent component is gotten by averaging $\mathbf{u}(t)$ over all collision times $t_i=t-\theta$ with the weight factor

$$W(\theta)=e^{-\theta/\tau_p}. \quad (6A)$$

We then obtain the well-known result

$$\langle\mathbf{u}\rangle_{Av}=-(eE/m)\frac{e^{i\omega t}}{2i\omega_0}\frac{1}{1/\tau_p+i(\omega_0-\omega)}. \quad (7A)$$

The incoherent component of $u(t)$ is given by

$$\Delta\mathbf{u}\equiv\mathbf{u}-\langle\mathbf{u}\rangle_{Av}. \quad (8A)$$

Now, the field of the emitted radiation has the same time dependence as $\mathbf{u}(t)$; hence, to obtain the spectral distribution of the emitted radiation, it is sufficient to perform a Fourier analysis of $u(t)$. This analysis, which involves the evaluation of the Fourier components of $\mathbf{u}(t)$ for specified times of collision, $t_1, t_2, \cdots, t_i, \cdots$, and the averaging of these components and their absolute squares over all properly weighted values of $t_1, t_2, \cdots, t_i, \cdots$, will not be presented here; we confine oursevles to stating the results.

1. The coherent component, $\langle\mathbf{u}\rangle_{Av}$, obviously has a non-zero Fourier amplitude for only one frequency, the impressed frequency ω, i.e., the spectrum of $\langle\mathbf{u}\rangle_{Av}$ is a line spectrum.

2. The incoherent component, $\Delta\mathbf{u}$, possesses non-vanishing Fourier amplitudes for all frequencies, ω'. These amplitudes are uncorrelated with each other. The average spectral distribution, $P(\omega')$, which is proportional to the average absolute square of the Fourier amplitude at ω', varies with frequency according to the relation

$$P(\omega')\sim\frac{1}{1+(\omega'-\omega_0)^2\tau_p^2}, \quad (9A)$$

which, if we define $\gamma_p=2/\tau_p$, is identical with (2.4'), i.e., the spectrum of the incoherent component obeys (1A).

We now show that the average magnitudes of the coherent and incoherent components of the total displacement are equal. With the aid of (6A) we readily obtain

$$\langle|\mathbf{u}|^2\rangle_{Av}=\left|\frac{eE}{2m\omega_0}\right|^2\frac{2}{(1/\tau_p)^2+(\omega_0-\omega)^2}. \quad (10A)$$

From (10A) and (7A) we then find that

$$\langle|\Delta\mathbf{u}|^2\rangle_{Av}=\langle|\mathbf{u}|^2\rangle_{Av}-|\langle\mathbf{u}\rangle_{Av}|^2=|\langle\mathbf{u}\rangle_{Av}|^2. \quad (11A)$$

Thus, the spectrum of the total displacement, and hence of the emitted radiation, may be resolved into two equal parts of which one is a line spectrum whose frequency is equal to that of the incident beam, whereas the other obeys (1A).

The above result is obtained on the basis of assumption (2A), which states that every collision quenches the oscillation. Since the quenching action of collisions is by no means universal, and, in fact, is very rarely observed if only one type of atom is present, the assumption requires modification. According to the present point of view,[19] a collision need not extinguish the motion of the classical oscillator; in the absence of quenching its chief effect is the introduction of a random phase shift into this motion with the consequence that immediately after collision the phase of the oscillator displacement is uncorrelated with that of the incident field. Thus, at any time t the total displacement $\mathbf{u}(t)$ may be written as

$$\mathbf{u}(t)=\mathbf{u}_1(t)+\mathbf{u}_2(t), \quad (12A)$$

where $\mathbf{u}_1(t)$ is given by (4A) or (5A), and $\mathbf{u}_2(t)$ is uncorrelated in phase with the incident field or with $\mathbf{u}_1(t)$. The coherent part of the total oscillation is thus left unaltered, whereas the intensity of the incoherent component is increased by

[19] V. Weisskopf, Physik. Zeits. **34**, 1 (1933); H. Margenau and W. W. Watson, Rev. Mod. Phys. **8**, 22 (1936).

$|\mathbf{u}_2(t)|^2$. Now, the time dependence of $\mathbf{u}_2(t)$ is that of free oscillation interspersed with the random phase shift due to collisions; as is demonstrated in standard texts,[18] the spectrum associated with this time variation is given by (9A) and, hence, by (1A). Therefore, if we are able to show that

$$\langle|\mathbf{u}_2|^2\rangle_{Av}\gg\langle|\mathbf{u}_1|^2\rangle_{Av}, \tag{13A}$$

we shall have established the validity of (1A) for the case of pressure broadening.

Two processes enter into the determination of $\langle|\mathbf{u}_2|^2\rangle_{Av}$. One of these is the relatively slow decrease due to radiation damping, heretofore neglected in our treatment. The rate of decrease per unit time arising from this mechanism is

$$-\gamma\langle|\mathbf{u}_2|^2\rangle_{Av}.$$

The other process is the transformation of $\mathbf{u}_1$ to $\mathbf{u}_2$ which takes place with each collision because of the introduction of the random phase shift; the rate of the resultant increase of $\langle|\mathbf{u}_2|^2\rangle_{Av}$ is

$$\frac{1}{\tau_p}\langle|\mathbf{u}_1|^2\rangle_{Av}.$$

Equating these two rates, we have

$$\langle|\mathbf{u}_2|^2\rangle_{Av}=\frac{1}{\gamma\tau_p}\langle|\mathbf{u}_1|^2\rangle_{Av},$$

which, in view of the inequality $\gamma\tau_p\ll 1$, immediately gives (13A).

The above treatment establishes the validity of (1A) for the "impact" type of pressure broadening associated with the dispersion-type absorption law (2.4′). As stated in the text, deviations from impact broadening may occur at pressures above 1 mm and for frequency differences $\nu-\nu_0\gg\gamma_p$. Since these cases have not been treated in the text, we shall not analyze the applicability of (1A) to them.

B. Doppler Broadening

From the standard treatments of Doppler-broadened emission spectra it is apparent that the validity of (1A) requires the velocity distribution of the excited atoms to be Maxwellian. In the investigation of this velocity distribution two cases are of interest.

1. Non-radiative transfer of excitation between atoms takes place before radiation. This transfer owes its origin essentially to dipole-dipole interaction between an excited and a normal atom. The cross sections for such reactions, classified as collisions of the second kind, are generally much larger than kinetic cross sections, because of the fact that no energy transfer between electronic excitation and nuclear motion is required. It has been shown, first by Fursov and Vlassov[20] and later by Houston,[21] that the non-radiative exchange of excitation is connected quite intimately with pressure broadening; in fact, at the pressure such that the mean free time between exchanges is equal to the radiative lifetime, pressure broadening is of the same order of magnitude as natural broadening. Another characteristic of the collisions is that the radius of collision varies inversely with the square root of the relative velocity of the colliding atoms, with the result that the mean free time is independent of the relative velocity.

If, now, pressure broadening exceeds natural broadening, both remaining small compared to Doppler broadening, non-radiative exchange of excitation takes place with equal likelihood between atoms of arbitrary velocities in preference to radiation. Hence the velocity distribution of the emitting atoms approaches that of the normal atoms, which is Maxwellian.

2. The radiative time is short compared to the mean free time between excitation transfers. In this case we cannot assume *a priori* that the velocity distribution of the excited atoms is Maxwellian and must, therefore, fall back on a more general formulation of the problem which presents both this velocity distribution and the frequency spectrum of the radiation as unknowns to be solved by analysis.

In describing the frequency spectrum of the radiation we introduce the frequency variable $x=(\nu-\nu_0/\nu_0)c/v_0$. The energy in a positional volume element, $d\mathbf{r}$, radiation whose direction of propagation is contained in an element of solid angle $d\omega$ and whose frequency lies in a range between x and $x+dx$, is represented by

$$h\nu f(\mathbf{r}, x, \mathbf{n})d\mathbf{r}dxd\omega,$$

[20] W. Furssov and A. Vlassov, Physik. Zeits. Sowjetunion **10**, 378 (1936).
[21] W. V. Houston, Phys. Rev. **54**, 884 (1938).

where $\mathbf{n}$ is a unit vector in the direction of propagation. $f(\mathbf{r}, x, \mathbf{n})d\mathbf{r}dxd\omega$ may be regarded as the number of quanta in the positional volume element $d\mathbf{r}$ and within the specified range of solid angle and frequency. Furthermore, we designate by $N(\mathbf{r}, \mathbf{v})$ the density of excited atoms in six-dimensional, velocity-position space. We may then describe the time variation of $f(\mathbf{r}, x, \mathbf{n})$ and $N(\mathbf{r}, \mathbf{v})$ by two "probability-conservation" integro-differential equations. The first reads

$$\partial f/\partial t = -c\mathbf{n}\cdot\mathrm{grad}_r f - ck(x)f + (\gamma/4\pi)\int N(\mathbf{r}, \mathbf{v})\delta\left(\frac{\mathbf{n}-\mathbf{v}}{v_0}-x\right)d\mathbf{v}. \quad (16A)$$

Here $k(x)$ is the absorption coefficient of quanta of frequency x, dv an element of volume in velocity space, and δ the Dirac delta-function, defined by the equations

$$\delta(x-x_1)=0;\ x\neq x_1, \qquad \int_{x_1-a}^{x_1+b}\delta(x-x_1)dx=1. \quad (17A)$$

Equation (17A) describes the generation, transport, and absorption of light quanta. The transport and absorption are obviously given by the first and second terms of the right-hand side. To see that the integral term represents the generation of quanta, we note the following:

(a). The integral is proportional to the density of emitting atoms, $N(\mathbf{r}, \mathbf{v})$.

(b). The delta-function restricts the emissive contribution to those atoms for which $x=\mathbf{n}\cdot\mathbf{v}/v_0$, which, in view of the definition of x, is the Doppler equation.

(c). If we integrate the term over all values of x and $\mathbf{n}$, i.e., over all possible emission frequencies and directions, we should obtain the total rate of emission per unit positional volume. Performing this integration we find for this rate the expression $\gamma N(\mathbf{r}, \mathbf{v})d\mathbf{v}$ which is obviously valid.

(d). Finally, it should be remarked that isotropic emission is assumed. This assumption is discussed in the text.

The second equation reads

$$\frac{\partial N(\mathbf{r}, \mathbf{v})}{\partial t}+\gamma N(\mathbf{r}, \mathbf{v}) = \frac{k_0\exp(-v^2/v_0^2)}{\pi v_0^2}\times\int\delta\left(\frac{\mathbf{n}\cdot\mathbf{v}}{v_0}-x\right)f(r, x, \mathbf{n})d\omega dx. \quad (18A)$$

Here, k_0 represents, as in the text, the absorption coefficient at the center of the Doppler line, $x=0$. In (18A) the transport of excitation due to the velocities of the excited atoms is neglected so that the equation represents the change in N due to absorption and emission of radiation alone. The emission is obviously given by the second term of the left; to show that the term on the right describes the absorption process, we note that (a), the integrand is proportional to the density of quanta, $f(\mathbf{r}, x, \mathbf{n})$, and of normal atoms $\propto \exp(-v^2/v_0^2)$, (b), the delta-function takes care of the Doppler effect, and (c), integration over all velocities gives the total rate per unit volume of absorption of light quanta, i.e.,

$$\int k_0\exp(-x^2)f(\mathbf{r}, x, \mathbf{n})d\omega dx = \int k(x)f(\mathbf{r}, x, \mathbf{n})dxd\omega.$$

In proceeding further we find it convenient to neglect the retardation effect arising from the finite velocity of propagation of light. This effect is contained analytically in the $\partial f/\partial t$ term on the left-hand side of (16A). As we shall show in detail below, the neglect of this term gives $f(\mathbf{r}, x, \mathbf{n})$ at time t as an integral involving $N(\mathbf{r}', \mathbf{v})$ the "source" function, evaluated at the same time, t; on the other hand, consideration of the $\partial f/\partial t$ term would give $f(\mathbf{r}, x, \mathbf{n})$ as an integral containing $N(\mathbf{r}', \mathbf{v})$ evaluated at the retarded time, $t'=t-(|\mathbf{r}-\mathbf{r}'|)/c$. The neglect of retardation is permissible because of the circumstance that as long as we deal with enclosures whose dimensions are of the order of centimeters and radiative lifetimes, $\tau\gtrsim 10^{-8}$ sec, the time of flight of the quanta is much smaller than τ; we may therefore, to a good approximation, regard their motion within the enclosure as instantaneous.

With neglect of the $\partial f/\partial t$ term, we integrate (15A), obtaining

$$f(\mathbf{r}, x, \mathbf{n}) = \frac{\gamma}{4\pi c}\int_0^{\rho_m}\int N(\mathbf{r}-\mathbf{n}\rho, \mathbf{v}') \times\delta\left(\frac{\mathbf{n}\cdot\mathbf{v}'}{v_0}-x\right)e^{-k(x)\rho}d\rho d\mathbf{v}', \quad (19A)$$

where ρ_m corresponds to a point $r-\mathbf{n}\rho_m$ situated

on the boundary of the enclosure. Inserting (19A) into (18A) and introducing the "source-point" vector, $\mathbf{r}'=\mathbf{r}-\mathbf{n}\rho$, with $d\mathbf{r}'=\rho^2 d\rho d\omega$ representing the positional volume element around the source point, we obtain

$$\frac{\partial N}{\partial t}+\gamma N(\mathbf{r},\mathbf{v})=\gamma\exp(-v^2/v_0^2)\times\int\int K(\mathbf{r},\mathbf{v};\mathbf{r}',\mathbf{v}')N(\mathbf{r}',\mathbf{v}')d\mathbf{r}'d\mathbf{v}', \quad (20A)$$

where

$$K(\mathbf{r},\mathbf{v};\mathbf{r}',\mathbf{v}')=\int_{-\infty}^{+\infty}\frac{k_0 e^{-k(x)|\mathbf{r}-\mathbf{r}'|}}{4\pi c\pi v_0^2|\mathbf{r}-\mathbf{r}'|^2}\times\delta\left(\frac{\mathbf{v}\cdot\mathbf{n}}{v_0}-x\right)\delta\left(\frac{\mathbf{v}'\cdot\mathbf{n}}{v_0}-x\right)dx. \quad (21A)$$

We observe in passing that

$$K(\mathbf{r},\mathbf{v};\mathbf{r}',\mathbf{v}')=K(\mathbf{r}',\mathbf{v}';\mathbf{r},\mathbf{v}). \quad (22A)$$

Also, in (20A) the integrations go over all velocities and over the volume of the enclosure.

As in the text treatment, we are interested in steady-state solutions of the form $N(\mathbf{r},\mathbf{v},t)\sim e^{-\beta t}N(\mathbf{r},\mathbf{v})$, which satisfy the equation

$$(-\beta+\gamma)N(\mathbf{r},\mathbf{v})=\gamma\exp(-v^2/v_0^2)\times\int\int K(\mathbf{r},\mathbf{v};\mathbf{r}',\mathbf{v}')N(\mathbf{r}',\mathbf{v}')d\mathbf{r}'d\mathbf{v}'. \quad (23A)$$

Furthermore, we confine our attention to the solution of (23A) which gives the smallest value of β, since, after a sufficiently long time, that solution alone is capable of experimental observation. We note that (23A) is equivalent to the following variational problem

$$\frac{\beta}{\gamma}=1-\frac{\int\int\int\int K(\mathbf{r},\mathbf{v};\mathbf{r}',\mathbf{v}')N(\mathbf{r},\mathbf{v})N(\mathbf{r}',\mathbf{v}')d\mathbf{r}'d\mathbf{v}'d\mathbf{r}d\mathbf{v}}{\int\int\exp(+v^2/v_0^2)N^2(\mathbf{r},\mathbf{v})d\mathbf{r}d\mathbf{v}};\quad \delta(\beta/\gamma)=0, \quad (24A)$$

as can easily be verified with use of (22A). Our problem is then to find the minimum of β/γ as given by (24A).

To solve this problem we have at our disposal the Ritz variational procedure. The value of β obtained by this method is always higher than the true value, and converges towards it as the number of variable parameters increases.

We now try a solution of the form $N(\mathbf{r},\mathbf{v})=N(\mathbf{r})\exp(-v^2/v_0^2)$; inserting this expression into (24A), we obtain

$$\frac{\beta}{\gamma}=1-\frac{\int\int G(\mathbf{r},\mathbf{r}')N(\mathbf{r})N(\mathbf{r}')d\mathbf{r}'d\mathbf{r}}{\int N^2(\mathbf{r})d\mathbf{r}}, \quad (25A)$$

where

$$G(\mathbf{r},\mathbf{r}')=\frac{\int\int K(\mathbf{r},\mathbf{v};\mathbf{r}'\mathbf{v}')\exp[-(v^2+v'^2)/v_0^2]d\mathbf{v}d\mathbf{v}'}{\int\exp(-v^2/v_0^2)d\mathbf{v}}. \quad (26A)$$

The evaluation of (26A) yields

$$G(\mathbf{r},\mathbf{r}')=\int_{-\infty}^{+\infty}\frac{k(x)\exp(-x^2)e^{-k(x)|\mathbf{r}-\mathbf{r}'|}}{\pi^{\frac{1}{2}}4\pi|\mathbf{r}-\mathbf{r}'|^2}dx, \quad (27A)$$

which is easily seen to be equivalent to (3.5) and (2.19). For the determination of $N(r)$ and β we now apply the variational method to (25A); since this form is identical with (3.9a) the

further analysis is the same as that of the text problem.

The above treatment shows that the assumption of a Maxwellian distribution for the velocities of the excited atoms leads to a variational approximation of the exact solution. In particular, the value of β obtained with the Maxwell distribution is always higher than the true value. Thus the text calculation gives an upper limit for β.

Unfortunately, this procedure cannot give quantitative information as to how far off the upper limit is until other more general forms for $N(\mathbf{r}, \mathbf{v})$ have been tried. Such calculations are rather tedious. Another possible approach is that of iteration. One inserts an assumed function for $N(\mathbf{r}, \mathbf{v})$, e.g., the Maxwellian form, into the right-hand side of (23A); the evaluation of the integral gives a new value of $N(\mathbf{r}, \mathbf{v})$, which may be substituted into (14A) for a repetition of the process. The correspondence of the new $N(\mathbf{r}, \mathbf{v})$ to the original function gives an indication as to the validity of the latter as a solution of the problem. Using this approach, we have made some preliminary semiquantitative studies; the essential physical picture which emerges from these studies may be described as follows.

For an infinite vessel, in which $N(\mathbf{r}, \mathbf{v})$ is rigorously Maxwellian (as can be verified by substitution into 23A), the radiation density function, $f(\mathbf{r}, x, \mathbf{n})$ as determined from (19A) is independent of frequency and propagation direction (as well as of position). This independence is linked up with the circumstance that, with increasing x, the diminution in the emissivity of each volume element is compensated by a longer free path, $1/k(x)$, which permits more volume elements to contribute to the radiation density at $\mathbf{r}$. For the finite case this behavior is still realized for those frequencies x such that $1/k(x)$ is much smaller than the linear dimensions of the enclosure; furthermore, in its $\mathbf{r}$ variation $f(\mathbf{r}, x, \mathbf{n})$ is proportional to the density of excited atoms at $\mathbf{r}$.

However, when $1/k(x)$ approaches the linear dimensions of the enclosure, this picture changes. In the central region the radiation density drops, since contributions from outlying regions diminish because of the lower density of excited atoms in those regions. When $1/k(x)$ exceeds the dimensions of the container, no new volume elements are brought into play with the result that the decrease in the emissivity of individual volume elements is now uncompensated; hence the radiation density drops off rapidly with further increase of x.

In the outer portion of the enclosure the x dependence of the radiation is somewhat more complicated. Here, as $1/k(x)$ gets large enough so that quanta emitted in the central regions can penetrate to the boundary, the radiation density at first *increases* with frequency; when, however, $1/k(x)$ exceeds the dimensions of the container, no new volume elements can contribute and the radiation density drops rapidly to zero. The phenomenon of enhanced intensity in the wings of the frequency distribution of the radiation density is often encountered in spectroscopy, where it is designated by the term "self-reversal."

As a result of the above described behavior of $f(\mathbf{r}, x, \mathbf{n})$, it turns out that in the central region the wings of the velocity distribution of excited atoms drop below the Maxwell form. It is also probable, though at the present time not definitely established, that in the boundary regions the self-reversal of the radiation density is duplicated to a certain extent in the velocity distribution of the excited atoms.

Here it should be pointed out that the behavior in the central region is of decisive importance in the estimation of the error in β. Namely, a deficiency of high velocity excited atoms gives rise to a cutting off of the wings of the emission spectrum from the individual volume elements and hence leads to a reduction $T(\rho)$ and β. On the other hand, by an analogous chain of events, the self-reversal, characteristic of the outer regions, may be expected to provide an increase in β. Now, the variational theory states that the true eigenvalue is lower than that obtained from the Maxwell distribution. Hence, in obtaining an upper limit for the error we neglect the possible increase in β due to the self-reversal in the periphery and confine our attention solely to the central region, where the correction results in a diminution.

Preliminary iteration-type calculations following this approach indicate that the emission spectrum of individual volume elements closely ap-

proximates the Doppler distribution, e^{-x^2}, up to a value x_1 such that

$$x_1 \sim (\log(k_0 L/2))^{\frac{1}{2}}.$$

For $x > x_1$ the Doppler distribution is to be multiplied by a factor roughly of the form x_1/x.

These results may now be introduced into (2.3) to calculate, e.g., $T(L/2)$; it is then found that the new value is smaller than the text value

$$T_1(L/2) = \frac{1}{k_0 \rho (\pi \log(k_0 L/2))^{\frac{1}{2}}},$$

by an amount

$$\Delta T \sim \frac{T_1(L/2)}{2 \log(k_0 L/2)},$$

which, for $k_0 L \sim 200$, is of the order of 10 percent.

We may thus expect that the error in β arising from the use of (1A) is less than, say, 20 percent. On the other hand, the error in the functional form of $N(\mathbf{r}, \mathbf{v})$, or even of $N(\mathbf{r})$, is undoubtedly much greater; in particular, for these quantities the contrast between the central region and the periphery of the enclosure is more significant.

PHYSICAL REVIEW VOLUME 72, NUMBER 12 DECEMBER 15, 1947

Paramagnetic Resonance Absorption in Salts of the Iron Group*

R. L. CUMMEROW,** D. HALLIDAY, AND G. E. MOORE
University of Pittsburgh, Pittsburgh, Pennsylvania

(Received August 29, 1947)

When a paramagnetic salt is placed in a high frequency alternating magnetic field which is perpendicular to a static magnetic field, energy may be absorbed by the salt in a resonant fashion for a range of values of the steady field. These paramagnetic losses have been investigated for three manganous, two cupric, and one chromic salt at a frequency of 9375 mc/sec. Well-defined absorption maxima were obtained in all cases, and absolute values of χ'', the imaginary part of the high frequency magnetic susceptibility, are presented.

I. INTRODUCTION

ABSORPTION of energy from a high frequency alternating magnetic field by a paramagnetic salt placed in the field was first demonstrated by Gorter[1] in 1936. He found that this absorption can be influenced by the application of a static magnetic field either parallel or perpendicular to the alternating field. He and his colleagues have carried on an extensive investigation of both types of absorption during the last decade.[2,3] The perpendicular field case has been further investigated by Zavoisky[4,5] and by two of the present authors.[6]

Purcell and co-workers[7] have recently demonstrated that when paraffin is put into a cavity resonator and a static magnetic field of the correct magnitude is applied perpendicularly to the high frequency magnetic field in the paraffin-filled cavity, energy is absorbed from the alternating field. This absorption shows sharp resonance characteristics and is associated with reorientations of the magnetic moments of the protons in the paraffin. Such nuclear absorptions are several orders of magnitude smaller than the absorptions referred to above, which are ionic in character.

In the earlier experiments[2-4] which were limited by the unavailability of oscillators of sufficiently high frequency,*** the strength of the static magnetic field corresponding to the maximum absorption was less than the absorption half-width, so that the maxima were not very clearly

* This work was supported in part by the Office of Naval Research under Contract N6ori-43 Task Order III and in part by the Army Air Forces, Air Materiel Command, under Contract W28-099-ac-238.

** Submitted in partial fulfillment of the requirements for the degree of Doctor of Philosophy at the University of Pittsburgh.

[1] C. J. Gorter, Physica **3**, 503 (1936).
[2] C. J. Gorter, Physica **3**, 1006 (1936).
[3] F. Brons and C. J. Gorter, Physica **5**, 999 (1938).
[4] E. Zavoisky, J. Phys. U.S.S.R. **9**, 211 (1945).
[5] E. Zavoisky, J. Phys. U.S.S.R. **10**, 197 (1946).
[6] R. L. Cummerow and D. Halliday, Phys. Rev. **70**, 433 (1946).
[7] E. M. Purcell, H. C. Torrey, and R. V. Pound, Phys. Rev. **69**, 37 (1946).

*** Zavoisky's most recent work,[5] carried out at 3000 mc/sec., has only recently been available to us.

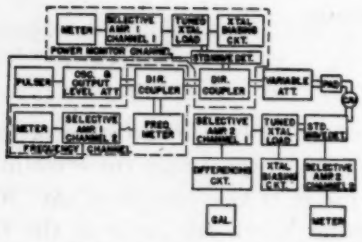

FIG. 1. A block diagram of the apparatus.

defined. In the present experiments, conducted at 9375 mc/sec., the maxima are well defined. Absolute values of χ'' (an absorption parameter to be defined later) are reported in all cases but one. We have adopted the technique of Purcell *et al.* of using a resonant cavity.

We are concerned here with the resonance absorption, associated with reorientations of the magnetic moments of the metallic ions of a paramagnetic salt, which occurs when the salt is placed in fields that are mutually perpendicular only. As a first approximation let us assume that the ions are nearly free, as is the case for the proton spins mentioned above. In the absence of an external magnetic field, all the ions will then exist in a common ground state. When a static external magnetic field is applied, they will be distributed among $2J+1$ equally-spaced levels according to the Boltzmann distribution. It is necessary to assume a slight interaction with the lattice to insure that this equilibrium distribution will be reached in a finite time (spin-lattice relaxation time). The difference in energy between any two adjacent levels is given by

$$\Delta E = g\beta B, \tag{1}$$

where g is the gyromagnetic ratio, β is the Bohr magneton, and B is the strength of the applied field. When the high frequency perpendicular magnetic field of frequency ν is introduced, the transition probability of an ion from the level it occupies to an adjacent level is a maximum when

$$h\nu = g\beta B, \tag{2}$$

the familiar magnetic resonance condition. The transition probability to a higher level is identical with that to a lower level, but the Boltzmann distribution insures that the lower levels are slightly more densely populated than the higher, and a net absorption of energy from the alternating field occurs. In order for the rate of energy absorption at resonance to remain constant with time, the amplitude of the high frequency magnetic field must not be so great that the Boltzmann distribution cannot be continually reestablished. Such a condition would lead to the equalization of the level populations and hence to a disappearance of the absorption effect. In this work no such saturation effects were observed.

TABLE I. Results of measurements to test Eq. (9).

$MnSO_4 \cdot 4H_2O$ mass percent	χ''_{max} 10^{-28} cm³/ion
100	2.31
80	2.32
63	2.21
37	2.34
20	2.44
mean	2.34
mean deviation	0.06

The treatment outlined above is satisfactory for the case of nuclear magnetic moments since here the nuclear magnetic dipolar interaction is relatively small. Expressed differently, the spin-spin relaxation time is relatively great or, still differently, the r.m.s. internal magnetic field at an average nuclear dipole caused by remaining dipoles is much smaller than the applied steady magnetic field at resonance. In the case of magnetic ions in salts, however, internal fields of several hundred gauss are common. This means that resonance-absorption peaks with this order of half-width are to be expected.

The interaction of a magnetic ion with its surroundings is made up of at least two parts: (1) the magnetic-dipolar interaction of the ion with neighboring magnetic ions, mentioned above, and (2), the interaction of the ion with the local electric field in the crystal. Frequently, exchange interactions must also be considered. The magnetic-dipolar interaction is usually treated from the point of view of internal magnetic fields; the distribution of ions-in-internal-field, is generally assumed to be Gaussian. The magnetic interaction alone would thus remove the ground-state degeneracy and would cause the ions to be distributed over numerous closely lying levels, rather than to occupy a single ground level.

The electric fields influence only that component of the ionic magnetic moment caused by

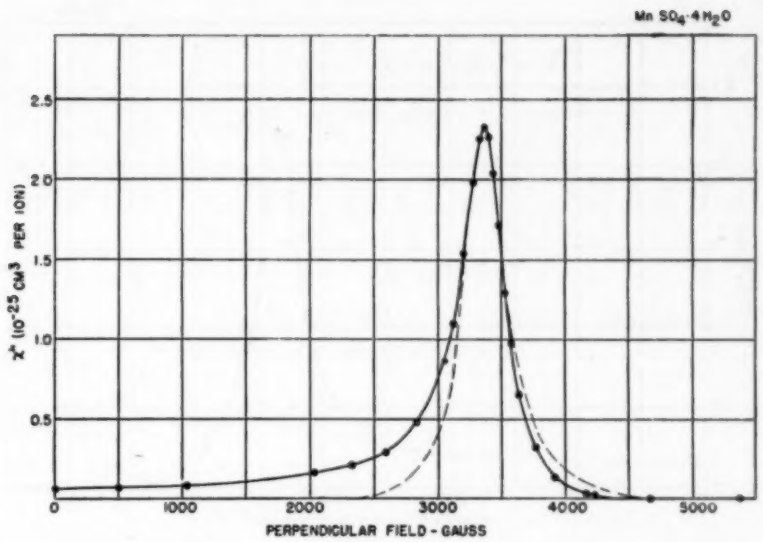

FIG. 2. Paramagnetic absorption in $MnSO_4 \cdot 4H_2O$ at 9375 mc/sec. The dashed curve is Frenkel's theoretical relationship for $\tau = 2.0 \times 10^{-9}$ sec.

orbital electronic motions and do not affect the component caused by spin.[8] The normal space quantization of the magnetic moment of the ion is so altered on this account in the salts of the iron group that the orbital momentum makes almost no contribution to the macroscopic susceptibility, and that part of the ionic magnetic moment is said to be quenched. This quenching action is associated with a splitting of the normal ground level, in a way that depends on the ion and on the symmetry and other characteristics of the electric field.

The manganous (Mn^{++}) ion is in an S state with $J=S=5/2$, but even so has a second-order resultant orbital angular momentum. The internal electric field is able on this account to split the ground level through spin-orbit coupling.[9] With the application of a sufficiently strong external magnetic field, however, the energy-level structure changes in such a way as to approach that expected for an ion with $J=5/2$ in a magnetic field alone.

A free cupric (Cu^{++}) ion is in a $^2D_{5/2}$ state. However, in most cupric salts the orbital contribution to the magnetic moment is almost entirely quenched by the electric fields, and the ground level is split in a way that depends on the salt. The degeneracies of these sublevels are removed by internal and externally applied magnetic fields. The case of $CuSO_4 \cdot 5H_2O$ has been described by Polder,[10] who calculates a splitting of the order of 20,000 cm^{-1}.

A free chromic ion is in a $^4F_{3/2}$ state. The splittings caused by the internal electric fields and also by externally applied magnetic fields have been calculated by Broer[11] for the chromic salt investigated by us, namely, chrome alum ($CrK(SO_4)_2 \cdot 12H_2O$).

II. APPARATUS

A block diagram of the microwave and associated measuring apparatus is shown in Fig. 1. There are three microwave channels: the main channel which includes the salt-filled cavity resonator, a channel for monitoring the power output of the microwave oscillator, and a frequency-monitoring channel. The microwave oscillator

TABLE II. Paramagnetic-absorption characteristics of manganous and cupric salts at 9375 mc/sec.

Salt	χ''_{max} 10^{-25} cm³/ion	B for χ''_{max} gauss	Width for χ_3'' gauss	Free-ion value of B for χ''_{max} gauss
$MnSO_4 \cdot 4H_2O$	2.32	3370	415	3348
$MnC_2O_4 \cdot 2H_2O$	2.24	3353	380	3348
$MnCl_2 \cdot 4H_2O$	0.395	3274	2300	3348
$CuCl_2 \cdot 2(NH_4Cl) \cdot 2H_2O$	0.230	3137	285	—
$CuSO_4 \cdot 5H_2O$	0.287	3039	318	—
$CuSO_4 \cdot 5H_2O$*	0.445	3065	285	—

* Measurement made at 193°K.

[8] J. H. Van Vleck, *The Theory of Electric and Magnetic Susceptibilities* (Clarendon Press, Oxford, 1932), p. 294.
[9] J. H. Van Vleck and W. G. Penney, Phil. Mag. 17, 961 (1934).
[10] D. Polder, Physica 9, 709 (1942).
[11] L. J. F. Broer, Physica 9, 547 (1942).

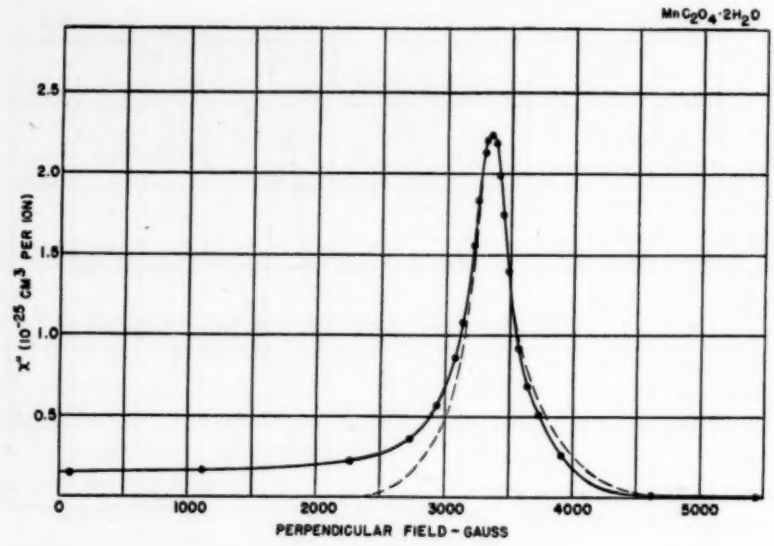

FIG. 3. Paramagnetic absorption in $MnC_2O_4 \cdot 2H_2O$ at 9375 mc/sec. The dashed curve is Frenkel's theoretical relationship for $\tau = 1.9 \times 10^{-9}$ sec.

was a navy 3-cm test set, type AN/APM-3A, modified so that the reflector electrode of the 723 A/B oscillator tube could be pulsed. The applied wave form was a 1300 c/sec. symmetrical square wave, which provided an a. c. output from the crystal detectors in the various channels. This a. c. output was easily amplified and, further, permitted d. c. biasing of the crystal detectors in the main channel and the power-monitoring channel in order to help match the impedance of each crystal and its holder closely to that of the connecting wave guide. The crystal holders for these two channels were mechanically tunable in order to further insure a satisfactory match. Standing-wave detectors were placed ahead of each of these crystal holders to check the impedance match. The crystals in the standing-wave detectors and the frequency-monitoring channel were not biased, since a good termination is not necessary in these channels.

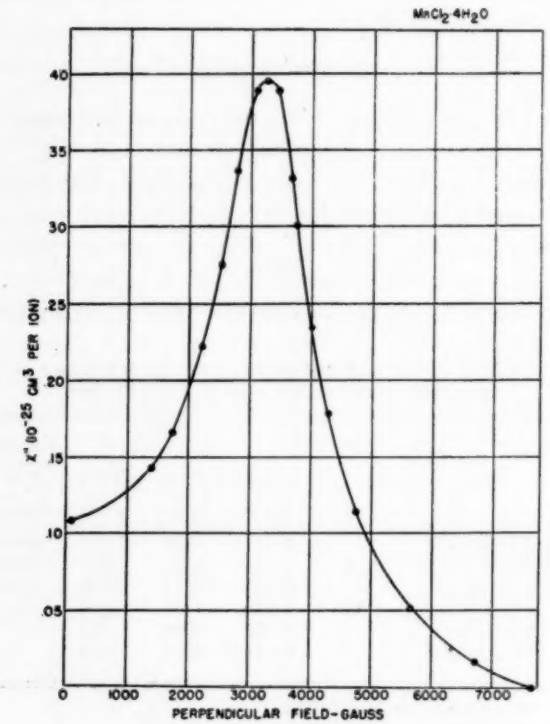

FIG. 4. Paramagnetic absorption in $MnCl_2 \cdot 4H_2O$ at 9375 mc/sec.

The outputs of all crystals were amplified by means of double-channel selective amplifiers tuned to the square-wave fundamental frequency. The rectified output, corresponding to the signal from the main channel, was fed to a differencing circuit in which a comparison was made with a stable variable d. c. voltage obtained from a battery-potentiometer system. The difference signal was then led to a galvanometer. Thus small changes in the power output of the cavity could easily be detected. The measuring system was calibrated by introducing known absorptions by means of a calibrated variable attenuator in the main r-f channel.

III. MEASUREMENTS

In characterizing the absorption of a paramagnetic salt it is desirable to use a quantity which is dependent only on the kind of salt and

the independent variables, such as the frequency of the high frequency magnetic field, the strength of the static perpendicular magnetic field, etc. The imaginary part of the complex high frequency susceptibility, χ'', is such a quantity. It is related to the magnetic power absorption in a particular specimen of salt by

$$M = 2\pi N \chi'' \nu \langle B_0^2 \rangle_{Av}, \tag{3}$$

when N is the number of magnetic ions in the sample, and $\langle B_0^2 \rangle_{Av}$ is the average over the volume of the sample of the mean-squared magnetic field.† The measurement of magnetic losses is further complicated by the electric losses which are unavoidably present in the cavity walls and in the salt itself. The magnitude of the electric loss is not constant but depends on the value of the magnetic loss.

Of the quantities in Eq. (3), $\langle B_0^2 \rangle_{Av}$ and M are not readily measurable so that we must obtain expressions for them in terms of measurable quantities. We now define a Q associated *only* with the energy dissipated magnetically in the cavity

$$Q_m' = \frac{2\pi \text{ (mean-stored energy in cavity)}}{\text{energy dissipated per cycle magnetically}}. \tag{4}$$

Then

$$Q_m' = \omega(\text{mse})/M. \tag{5}$$

The mean-stored energy is given by

$$\text{mse} = \langle B_0^2 \rangle_{Av} V/4\pi, \tag{6}$$

where V is the volume of the cavity (and of the salt). Then

$$Q_m' = V/4\pi N \chi''. \tag{7}$$

By an extension of methods developed by Holstein,[12] one can show that

$$Q_m' = \frac{Q_e}{(P_e/P_{em})^{\frac{1}{2}} - 1}, \tag{8}$$

where Q_e is the loaded Q of the cavity measured with *only electric* losses occurring, and P_e/P_{em} is the ratio of the power output of the cavity with *only electric* losses occurring to that with *both* electric and magnetic losses occurring. Combining Eqs. (7) and (8), one obtains an expression for χ'' in terms of measurable quantities

$$\chi'' = \frac{V[(P_e/P_{em})^{\frac{1}{2}} - 1]}{4\pi N Q_e}. \tag{9}$$

The measurement of Q_e was made with an externally applied field large compared to the field for maximum absorption. This was to insure that there were no transitions of magnetic ions and hence no magnetic absorption. Q_e values of about

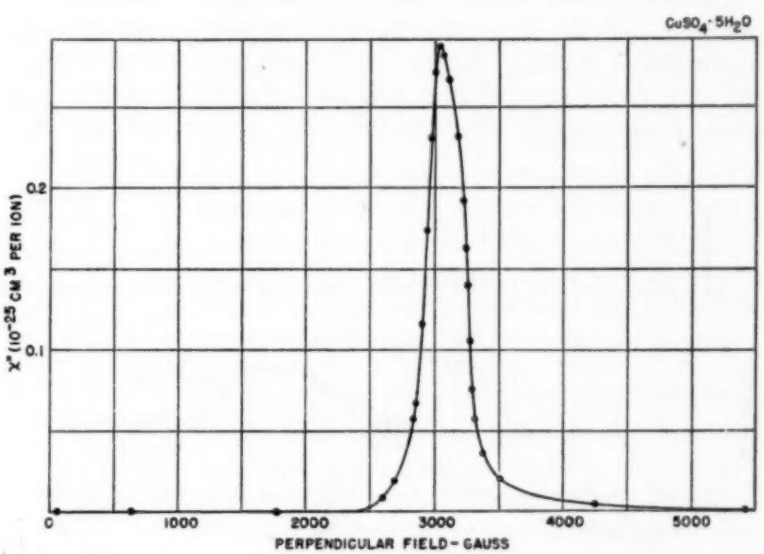

FIG. 5. Paramagnetic absorption in $CuSO_4 \cdot 5H_2O$ at 9375 mc/sec.

† Throughout the following discussion we assume the high frequency permeability to be unity, a good approximation for paramagnetic salts.

[12] T. Holstein, Westinghouse Research Report No. R-94318-F.

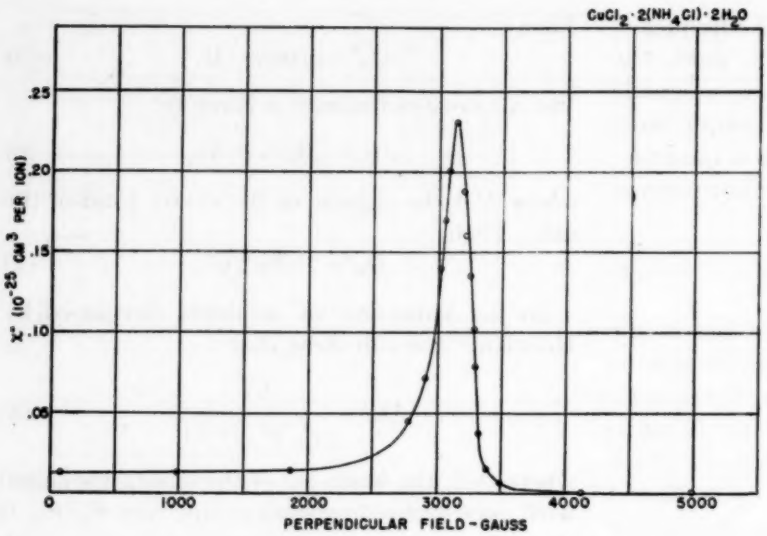

FIG. 6. Paramagnetic absorption in $CuCl_2 \cdot 2(NH_4Cl) \cdot 2H_2O$ at 9375 mc/sec.

140 were obtained, the cavity being singly reentrant, about 0.83/cm³ in volume, and filled completely with salt. The quantity P_e/P_{em} is, then, the ratio of the power output at large externally applied fields to the power output at any other value of static field where both magnetic and electric losses occur. For $MnSO_4 \cdot 4H_2O$, for example, the value of P_e/P_{em} at the absorption maximum was about 4.5. Knowing these two data and V and N of Eq. (9), one may compute χ'' as a function of the value of the applied external field.

Equation (9) was tested by preparing five mixed powdered samples of $MnSO_4 \cdot 4H_2O$ and the nonparamagnetic $BaSO_4$, with the relative masses of the former varying from 20 to 100 percent of the total. These samples were placed in the cavity and χ''_{max} was measured, with the results given in Table I. For comparison, four separate measurements on powdered samples of pure $MnSO_4 \cdot 4H_2O$ yielded a mean χ''_{max} of 2.32×10^{-25} cm³/ion with a mean deviation of 0.04×10^{-25} cm³/ion. The good agreement of all these results, considering that the measurements were made under different conditions as to Q_e, P_e/P_{em}, and N, allows some confidence to be placed in the measuring procedure.

The magnetic field was determined by measuring the commutated output voltage of a small spinning coil placed in the field. The size of this coil was adjusted so that for the range of fields used a type-K potentiometer and standard cell could be conveniently employed to measure the voltage. The spinning coil was calibrated by using

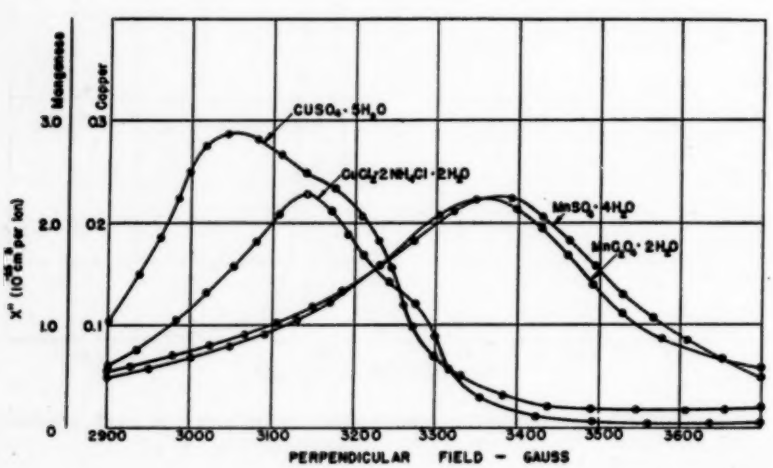

FIG. 7. Paramagnetic absorption for two manganous and two cupric salts at 9375 mc/sec.

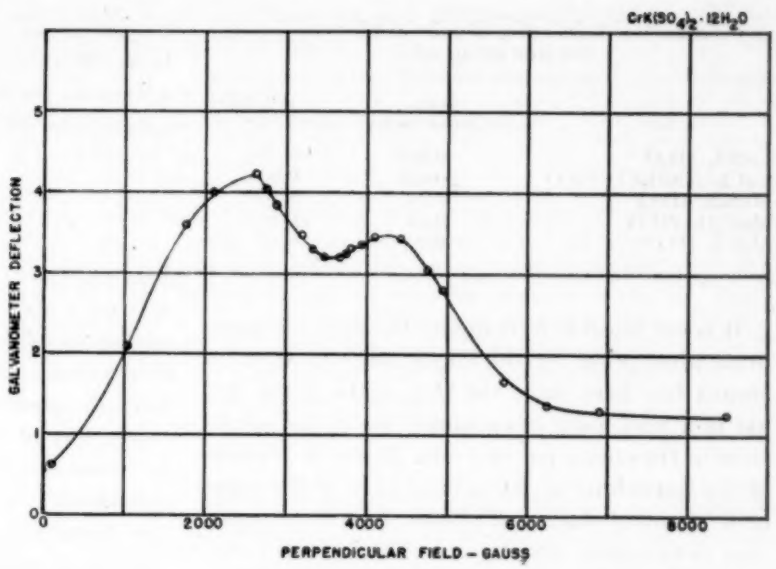

FIG. 8. Paramagnetic absorption in $CrK(SO_4)_2 \cdot 12H_2O$ at 9375 mc/sec. The ordinate is proportional to χ''.

conventional search coil, galvanometer, and standard solenoid techniques. We believe the reported fields to be accurate to about 0.5 percent.

IV. RESULTS AND DISCUSSION

Figures 2 to 6 show χ'' *versus* the perpendicular magnetic field at a frequency of 9375 mc/sec. for three manganous and two cupric salts. Figure 7 shows the curves for four of these salts replotted for better delineation of such characteristics as shape and half-width. Figure 8 shows a curve for chrome alum in which a quantity proportional to χ'' is plotted against B. In Table II some important features of these curves are noted. In addition, data are given for a determination of χ'' of $CuSO_4 \cdot 5H_2O$ made at 193°K (dry-ice temperature). All other determinations were made at room temperature.

A glance at Figs. 2–4 shows that there is a finite amount of magnetic absorption with zero external field. This zero-field absorption indicates, in the usual case, that a certain number of the ions are normally subjected to an internal magnetic field of the correct magnitude to satisfy Eq. (2). At sufficiently high external fields the resultant B for all ions is too great for any transitions to occur, and hence the absorption is zero.

According to Eq. (2), the maximum absorption for almost free manganous ions should occur at 3348 gauss, that for $MnC_2O_4 \cdot 2H_2O$ occurs at 3353 gauss. The difference between these values is not significant. The value for $MnSO_4 \cdot 4H_2O$, 3370 gauss, does seem to be significantly higher than the free-ion value. The shift of the maximum for the manganous chloride curve is in the opposite direction and much larger (74 gauss). The absorption curve for $MnCl_2 \cdot 4H_2O$ is five times wider than the curves for the oxalate and the sulfate.

Frenkel[13] has proposed a theory of paramagnetic-resonance absorption which gives an explicit relationship between χ'' and B provided the spin-spin relaxation time τ is known. A comparison with experiment, however, is hindered by the fact that the dependence of τ on B is not known. Assuming a constant value of 2.0×10^{-9} sec. for $MnSO_4 \cdot 4H_2O$ and of 1.9×10^{-9} sec. for $MnC_2O_4 \cdot 2H_2O$, we obtain the dashed curves of Figs. 2 and 3, respectively. These relaxation times are of the expected order of magnitude. It should be noted that Frenkel's expression for χ'' vanishes for $B=0$, that is, no zero-field absorption is permitted. For the broad $MnCl_2 \cdot 4H_2O$ curve no very good fit for a single value of τ seems possible.

The half-widths of all of the absorption peaks for manganous salts are somewhat narrower than might be expected from the known magnitudes of the internal fields involved. Professor C. J. Gorter has suggested in a private discussion that an exchange interaction may be responsible.

[13] J. Frenkel, J. Phys. U.S.S.R. 9, 299 (1945).

TABLE III. Values of χ in units of 10^{-25} cm³/ion for iron group salts.

Salt	Direct measurement	Area under absorption curve
$CuSO_4 \cdot 5H_2O$	0.028	0.024
$CuCl_2 \cdot 2(NH_4Cl) \cdot 2H_2O$	0.028	0.024
$MnSO_4 \cdot 4H_2O$	0.24	0.30
$MnC_2O_4 \cdot 2H_2O$	0.24	0.29
$MnCl_2 \cdot 4H_2O$	0.24	0.32

It is not feasible to compare the field for maximum absorption for the cupric salts to that for almost free ions, since the $^2D_{5/2}$ state of the free ion is a very poor approximation to the actual state of the cupric ion in a salt. This is so because of the quenching of the orbital part of the magnetic moment discussed above. It will be noted that both cupric salts give indications of structure in the absorption curves. The reasons for this structure are not known. The calculated splittings of Polder[10] seem to offer no ready explanation. It is hoped that absorption measurements in $CuSO_4 \cdot 5H_2O$ single crystals now in progress will help to explain this phenomenon.

The half-widths for the two copper curves agree fairly well with the known internal fields. However, Professor C. J. Gorter has suggested that this agreement is fortuitous, being associated with the known magnetic anisotropy, and that the half-widths for single crystals would be narrower. This is to be expected because of the narrowing arising from exchange interaction mentioned earlier.

The curve for chrome alum (Fig. 8) can be qualitatively explained by considering the splittings calculated by Broer.[11] In zero external magnetic field the ground level is split into two doubly degenerate levels 0.17 cm^{-1} apart. As the strength of the external magnetic field is increased, the degeneracies are removed in a way that depends on the orientation. By considering Fig. 1 of Broer's paper the existence of two absorption maxima is not surprising since, for a given orientation, transitions between levels in each degenerate set will occur at different external fields, corresponding to a level separation of 0.31 cm^{-1} (9375 mc/sec).

A semiquantitative check on the experimental results can be obtained by computing the normal paramagnetic susceptibility of the various salts from the areas under the absorption curves, using a formula presented by Gorter and Kronig.[14] The special case of this formula that is of interest is

$$\chi = \frac{2}{\pi} \int_0^\infty \frac{\chi'' d\nu}{\nu}. \tag{10}$$

Unfortunately, χ'' is given as a function of B for a fixed ν and not the reverse, so that Eq. (10) cannot be evaluated as it stands. An approximate evaluation, valid for very narrow absorption lines, is possible from the following considerations. Any of the absorption peaks reported may be viewed—if only magnetic interactions be considered—as indicating roughly the nature of the distribution of internal magnetic fields for various external fields. What is wanted, however, is the distribution of internal fields for a fixed external field corresponding to the value B_0 at the absorption maximum. Such a distribution may be approximated by multiplying every ordinate of the absorption curve by the ratio B/B_0. By use of the differential form of Eq. (2), namely,

$$d\nu/\nu = dB/B,$$

we are finally led to

$$\chi = 2A/\pi B_0,$$

where A is the area under the absorption curves of Figs. 2 to 6. Table III shows the results.

Considering the assumptions made in the application of Eq. (10), the agreement is perhaps all that can be expected. Well-known experimental difficulties stand in the way of obtaining data suitable for direct verification by Eq. (10).

The authors are very greatly indebted to Professors C. J. Gorter and J. H. Van Vleck for their many indispensable suggestions in connection with the interpretation of the results. We are also thankful to Dr. A. J. Allen for his active interest and encouragement during the course of this research. We further wish to thank Mr. T. Miller of the Westinghouse Research Laboratories for providing the accurately calibrated attenuator used in this work.

[14] C. J. Gorter and R. de L. Kronig, Physica **3**, 1009 (1936).

The Effect of Annealing and Gas Content on the Superconducting Properties of Tantalum*

ROBERT T. WEBBER**
*Sloane Physics Laboratory, Yale University,*** *New Haven, Connecticut*

(Received August 22, 1947)

The superconducting transition temperatures and critical fields of three wires of 99.9+ percent pure tantalum, taken from the same spool, have been investigated to find the effect of annealing and gas content. Annealing the metal at very high temperatures raised the transition temperature from 4.156 to 4.32°K and lowered the initial slope of the critical magnetic field from 1360 to 600 gausses per degree. Much sharper transitions were observed for the annealed specimens. The effect of absorbed gas was slight. Spontaneous fluctuations of resistance on the transition into superconductivity were observed. The effect of the specimen current on the critical field was studied in one of the annealed specimens.

I. INTRODUCTION

EXPERIMENTS on the transition temperatures and critical fields of superconducting tantalum have been noted for their failure to give consistent results for different specimens.[1–5] Transition temperatures have been reported between the extremes of 3.96°K and 4.4°K. The initial slopes of the critical field curves have varied from 310 to 1250 gausses per degree. A more complete summary of the results of the previous investigations will be found in Table I.

In addition to the lack of consistency, tantalum, with one partial exception,[1] has shown considerable evidence of alloy behavior in the form of broad transitions and magnetic hysteresis.

It has generally been supposed that the inconsistencies in the reported superconducting properties of tantalum were due to the presence of small amounts of impurities or to the presence of mechanical strains.[6] There is no question that impurities in the metal have a considerable influence on its behavior. That strains also appear to have some effect was demonstrated by Meissner, Steiner, and Grassman,[7] who lowered the transition temperature of a tantalum wire in zero-magnetic field by 0.017°K by sharply kinking it in many places. A similar conclusion can be drawn from the observation of Brucksch and his co-workers[8] that very fine hard-drawn wires of tantalum have much lower transition temperatures than do larger wires.

The effect of tensile stress was quantitatively studied by Alekseyevski,[9] who found that severely strained wires of tantalum showed sharper zero-field transitions at slightly higher temperatures, and smaller critical field slopes than did the unstrained wires.

The purpose of the work reported here is to investigate the effect of annealing and the effect of gas content on the superconducting properties of tantalum. It is known that tantalum becomes very brittle when heated in high vacuum at temperatures approaching the melting point.[10] The length of the sample under such treatment increases as much as 6 percent, corresponding to the growth of large crystallites. Tantalum also has the property of absorbing gases in large

* This is part of a dissertation presented to the faculty of the Graduate School of Yale University in candidacy for the Degree of Doctor of Philosophy.

** Sterling Fellow in Physics.

*** This work was assisted by the Office of Naval Research under Contract N6ori-44.

[1] J. G. Daunt and K. Mendelssohn, Proc. Roy. Soc. **A160**, 127 (1937).

[2] W. H. Keesom and M. Désirant, Physica **8**, 273 (1941).

[3] W. Meissner, Zeits. f. Physik **61**, 191 (1930).

[4] K. Mendelssohn and J. R. Moore, Phil. Mag. **21**, 532 (1936).

[5] Francis B. Silsbee, Russell B. Scott, and Ferdinand G. Brickwedde, J. Research Nat. Bur. Stand. **18**, 295 (1937).

[6] For example, D. Shoenberg, *Superconductivity* (Cambridge University Press, Teddington, England, 1938), pp. 89–90, references 1–5 also contain speculations on this matter.

[7] W. Meissner, K. Steiner, and P. Grassman, Physik. Zeits. **36**, 519 (1935).

[8] W. F. Brucksch, Jr., W. T. Ziegler, F. H. Horn, and Donald H. Andrews, Phys. Rev. **60**, 170 (1941); W. T. Ziegler, W. F. Brucksch, Jr., and J. W. Hickman, Phys. Rev. **62**, 354 (1942).

[9] N. E. Alekseyevski, J. Phys. U.S.S.R. **3**, 443 (1940).

[10] B. A. Mrowca, J. App. Phys. **14**, 684 (1943). It is likely that the brittleness is caused by precipitation of impurities at the crystallite boundaries.

quantity.[11] The absorption of these gases causes a slight expansion of the lattice and an appreciable increase in the room temperature resistance.

II. PREPARATION OF SPECIMENS

The three specimens used in this investigation were taken from the same spool of wire supplied by Fansteel Metallurgical Corporation (North Chicago, Illinois). The manufacturer produced the wire by cold rolling, swaging, and, finally, cold drawing down to a diameter of 0.0039 in. The cold working was followed by an "anneal" in high vacuum at about 1000°C. This temperature is well below that necessary for any appreciable recrystallization.[10] An analysis of the product by Fansteel gives a purity of 99.9+ percent, with less than 0.01 percent iron and 0.03 percent carbon present. The wire also contained a small amount (less than 0.1 percent) absorbed gas. The specimens, each about 4 inches long, were treated and mounted by us in the following ways:

Specimen I was taken directly from the spool and mounted without further treatment. The potential and current leads of No. 40 copper wire were attached by means of small clamps.

Specimen II was copper plated on the ends which were then soldered to insulating supports mounted on the brass strip. The distance between the insulating supports was made adjustable to allow compensation for the permanent lengthening of the wire caused by heat treatment. The potential and current leads were soldered to the copper plate.† The whole assembly was then inserted in a vacuum system and heated to extremely high temperatures (2200 to 2500°C) for two hours by passing a direct current through the wire. The heating was then continued at intervals (to allow the pumps to take away the evolved gas) until the room temperature resistance of the specimen reached a minimum. This minimum was about 4 percent below the original resistance of the specimen and indicated[11] a relatively gas-free condition in the metal. The heat treatment resulted in a 2 percent permanent elongation of the sample.

Specimen III was mounted and annealed in the same manner as specimen II. At the conclusion of the anneal the sample was heated for a few minutes at 1200°C in air at a pressure of 10^{-3} mm Hg, causing the specimen to absorb gas. At the end of the treatment the room temperature resistance was 37 percent higher than the resistance of the original hard-drawn specimen. This would indicate [11] the absorption of about 9 volumes of oxygen, a quantity much less than that necessary to cause the formation of the oxide. The wire lengthened slightly over 1 percent as result of the treatment. Specimens II and III were somewhat brittle.

III. APPARATUS

The specimens were mounted vertically in a soft glass Dewar flask 18 in. long and $1\frac{1}{4}$ in. in inner diameter. The space between the walls of this flask contained air at a pressure of about 1 mm of mercury at room temperature. This air

TABLE I. Summary of experimental conditions and results of these and previous investigations of tantalum.

	Measurement method	Purity percent	Annealed	$R_{4.2}/R_{273}$	T_c (°K)	dH_c/dT (gauss/°K)	Tension (kg/cm²)
Specimen I	resistance	99.9+	no	0.152	4.156	1360	
Specimen II	resistance	99.9+	yes	0.07	4.30	600	
Specimen III	resistance	99.9+	yes	0.105	4.32	600	
Daunt and Mendelssohn[1]	susceptibility	99.95+	?	—	4.38	310	
Keesom and Désirant[2]	specific heat	99.95+	?	—	4.075	1230	
Meissner[3] I	resistance	?	yes	0.035	4.38	—	
Meissner[3] II	resistance	?	yes	0.0098	4.36	—	
Meissner[3] III	resistance	?	yes	0.050	4.37	—	
Mendelssohn and Moore[4]	resistance	?	?	0.052	4.4	980	
Silsbee and I	resistance	99+	no	0.26	3.961	1250	
co-workers[5] II	resistance	99+	no	0.26	4.068	1080	
Alekseyevski[9]	resistance	?	?	?	4.250	810	0
					4.375	680	18,000

[11] Mary Andrews, J. Am. Chem. Soc. **54**, 1845 (1932).

† This technique did not prove completely satisfactory as a small contact resistance developed at low temperatures.

allowed the contents of the flask to reach temperature equilibrium with the surrounding bath of liquid nitrogen in a short time. On admitting the liquid helium, the air in the annular region is instantly condensed.

After being filled with the liquid helium, the flask and its shield were placed in the center of a large water-cooled solenoid which supplied a longitudinal magnetic field of intensity up to 1600 gausses. This solenoid consisted of a total of 805 turns of $\frac{5}{16}$-inch hollow copper tubing wound in 9 concentric layers and set in insulating plaster. The nine layers were connected in series electrically, and in parallel, for the purpose of cooling, by means of rubber tubing. The total resistance was 0.4 ohms, and the field homogeneity over the region used was 99.8 percent. The solenoid was 24 inches long, with an outer diameter of 12 inches and an inner diameter of $4\frac{3}{4}$ inches. As far as limited by heating, the solenoid is capable of carrying over 200 amperes, which would yield a field of 3200 gausses. Lack of an adequate current supply limited our investigations to fields of half this intensity.

Fluctuations in this current formed the largest source of error, amounting to a little over 1 percent.

The temperature was measured to an accuracy of 0.002°K by determining the vapor pressure of the liquid helium with a Wallace and Tiernan precision mercury manometer. The 1937 Leiden determinations of the vapor pressures[12] were used.

The potential drop across the specimens was continuously measured with a Brown "Electronik" high speed recording potentiometer. This instrument has a range of 0–50 mv, with an accuracy of 0.125 mv and a sensitivity of 0.06 mv. It proved particularly valuable in this work as it allowed a large quantity of data to be taken with great rapidity.

The specimen current in all cases was 25-ma d.c., except in the case of specimen II where data was also secured for a current of 100 ma.

IV. RESULTS AND DISCUSSION

The resistance of specimen I was observed to fluctuate markedly as the temperature was lowered slowly through the transition point in zero field. The fluctuations were completely irregular, and their maximum amplitude was about 5 percent of the total resistance. These fluctuations are similar to, but much smaller than, those reported by Silsbee, Scott, and Brickwedde.[5] The amplitude of the fluctuations in our annealed samples was smaller still (maximum of $1\frac{1}{2}$ percent), lending support to the

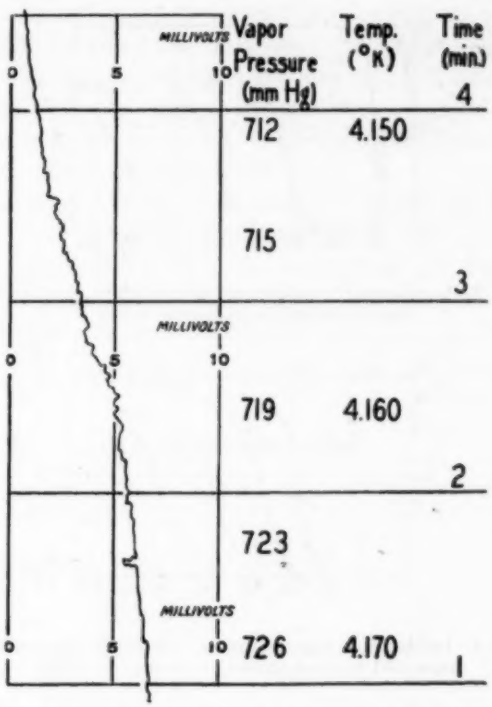

FIG. 1. Potentiometer record of the zero-field transition of tantalum specimen I, showing spontaneous fluctuations of resistance as the temperature is slowly lowered.

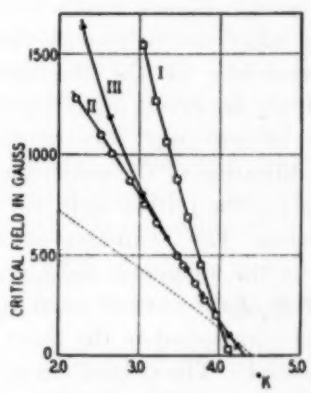

FIG. 2. Critical field curves of the three tantalum specimens. The numbering of the curves corresponds to the specimens as described in the text.

[12] G. Schmidt and W. H. Keesom, Physica **4**, 971 (1937).

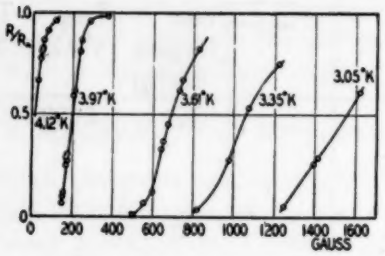

FIG. 3. Isothermal transitions of tantalum specimen I (hard drawn) in magnetic fields.

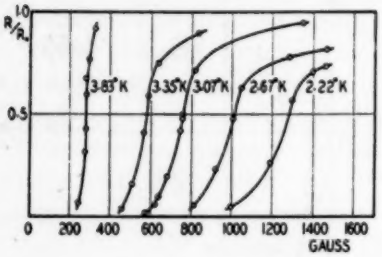

FIG. 4. Isothermal transitions of tantalum specimen II (annealed and outgassed) in magnetic fields.

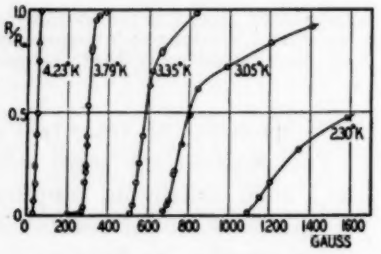

FIG. 5. Isothermal transitions of tantalum specimen III (annealed and gassy) in magnetic fields.

contention of Misener[13] that the phenomenon is of a secondary nature associated with imperfections in the metal. Figure 1 may be of interest as it shows what we believe to be the first published recording of the fluctuations. The square-sided dip occurring at a vapor pressure of 724 mm of mercury was caused by the automatic calibration of the potentiometer.

Figure 2 gives the critical field curves for the three specimens. The ordinates of the points correspond to the magnetic field necessary to restore one-half of the normal resistance. Curves I through III correspond to the three specimens as described above. The dotted curve represents the data of Daunt and Mendelssohn.[1]

[13] A. D. Misener, Proc. Camb. Phil. Soc. **34**, 465 (1938).

Figures 3, 4, and 5 show some of the isothermal transition curves for the three specimens at various temperatures. The ordinates give the ratio of the resistance, R, to the resistance just above the normal transition temperature, R_n. All three specimens exhibited fairly sharp transitions at temperatures near the zero-field transition temperature. At lower temperatures the transitions become increasingly broad, indicating the existence of a considerable amount of intermediate state. A comparison of the isothermal transitions of the three specimens at a given temperature (at 3.35°K, for example) shows that the two annealed specimens have much sharper transitions at lower magnetic fields than those exhibited by the hard-drawn specimen. No hysteresis was observed in any of the specimens.

Specimen III (annealed and gassy) proved to be somewhat anomalous. At temperatures above 3°K it exhibited the sharpest transitions of the three specimens. Below this temperature, however, the transitions degenerate rapidly, corresponding to the break upward of curve III of Fig. 2. Whether this difference in the behavior of specimens II and III is due to the difference in gas content, or to minor differences in annealing technique, is impossible to say. In any case, we can conclude that gas content is not a major factor contributing to the diversity in the properties of superconducting tantalum reported previously.

A summary of the numerical results of these and previous investigations is given in Table I.

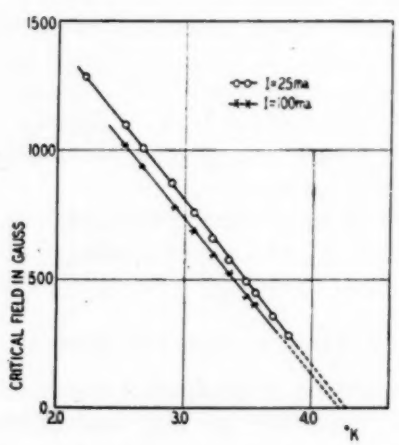

FIG. 6. Critical field curves of tantalum specimen II for currents of 25 and 100 milliamperes.

In the cases where information on annealing is given it is clear that the ratio of the resistance at helium temperatures to that at 0°C (R_n/R_{273}), the transition temperature and the initial critical field slope are strongly affected by the heat treatment. In view of this, the poor characteristics of the sample of Keesom and Désirant[2] are probably explained as being due to severe strains in their specimen. The influence of kinking the tantalum wire[7] and reducing the wire diameter[8] on the superconducting characteristics are probably similarly explained.

The influence of current on the critical fields of the annealed and outgassed specimen is shown in Fig. 6. The critical fields are 50 to 70 gausses lower for the higher current, an amount considerably in excess of what would be expected from the hypothesis of Silsbee.[14]

The author is particularly indebted to Professor C. T. Lane for his frequent advice and encouragement. He is also indebted to Dr. Henry A. Fairbank and Mr. William Fairbank for their assistance in the collection of data.

[14] F. B. Silsbee, Sci. Pap. Bur. Stand. 14, 301 (1917).

PHYSICAL REVIEW VOLUME 72, NUMBER 12 DECEMBER 15, 1947

Ultrasonic Velocity and Absorption in Liquid Helium*

JOHN R. PELLAM** AND CHARLES F. SQUIRE***
Research Laboratory of Electronics, Massachusetts Institute of Technology, Cambridge, Massachusetts

(Received August 7, 1947)

Measurements are given on the velocity and attenuation of ultrasonic energy in liquid helium at a frequency of 15 megacycles per second as a function of temperature from 1.57°K to 4.5°K. The velocity at 15 Mc/sec. was found to agree with results obtained at 1.3 Mc/sec. by previous investigators, and hence there is no dispersion in this frequency range. The attenuation measurements exhibit three important features: (a) in the upper temperature range of He I the measurements agree very well with classical theory, (b) at the λ-point the attenuation coefficient rises abruptly, presumably to infinity, indicating complete absorption of the ultrasonic energy, (c) just below the λ-point the attenuation (first sound in He II) has its smallest value and with lowering temperature the attenuation increases.

I. INTRODUCTION

THE experiments described in this paper give the velocity and attenuation of sound in liquid helium at a frequency of 15 megacycles per second as a function of temperature from 1.57°K to 4.5°K. The object of these experiments is twofold: (a) to check experimentally the theory of sound absorption for a monatomic liquid, and (b), to probe into the nature of liquid helium in its low temperature phase and at the transition point. The experiments were made possible by two recent developments: the ultrasonic pulse technique which grew out of radar research[1] and the Collins Cryostat[2] which can produce relatively large amounts of liquid helium.

II. EXPERIMENTAL

The special advantages and capabilities of the pulse technique originally developed for radar have made measurements of the type conducted in this research possible. By using short pulses absorption measurements may be conducted at relatively high frequencies (15 Mc/sec. in this case), for which the attenuation is sufficient to

FIG. 1. Transducer-reflector system.

* This research has been supported in part through the joint service contract No. W-36-039 sc-32037.
** Submitted in partial fulfillment for the degree of Doctor of Philosophy from Massachusetts Institute of Technology.
*** Now at The Rice Institute, Houston, Texas.

[1] Radiation Laboratory, Massachusetts Institute of Technology Report 963, March 1946.
[2] S. C. Collins, Rev. Sci. Inst. 18, 3 (1947).

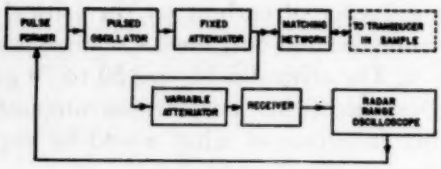

FIG. 2. Block diagram.

make quite accurate measurements possible. As will be seen, the method is direct and straightforward both for obtaining velocity and attenuation; absorption measurements thus obtained[3] are usually superior to those of older, continuous wave methods.

The scheme is essentially to use the liquid sample as a "storage medium" for the short sound pulses and to measure the time delay and attenuation undergone by the sound in traveling a known path length. The acoustical pulses, after being generated from electrical pulses by the transducer, travel through the liquid to a plane reflector (shown purely schematically in Fig. 1) and back again to re-excite the crystal at a later time.

The transducer-reflector distance is variable, so that the increased delay produced by an increase in path length is a direct measure of wave velocity. The attenuation which must be removed from the electrical circuit to balance the acoustical losses in the additional distance provides a measure of absorption.

The timing sequence is as follows (Fig. 2). A crystal-controlled circuit in the oscilloscope starts the scope sweep and simultaneously sends a trigger to the pulse generator. The pulse formed by the generator passes through an impedance-matching network to the transducer. When the resulting sound pulse returns to the transducer after its round trip within the liquid, the delayed electrical pulse is formed and returns through the matching network. Since the transmitter is off when the echo signal arrives, very little leakage loss occurs and the main portion travels through the variable attenuator to the receiver.

Both triggering and time measurements are accomplished by means of the crystal-controlled circuit in the oscilloscope (DuMont type 256B A/R range scope), so that automatic synchronization occurs. In addition to setting off the pulse generator and starting the sweep, this circuit also provides marker pips spaced every 10,000 yards of radar range. An expanded sweep with variable delay is used for examination of the front edge of the echo signal. Crystal control is necessary primarily for accurate timing of the marker pips; one pip is developed for each oscillation, and since the crystal frequency is accurate to better than 1 part in 10,000 the same holds for range marker positions.

Concerning measurement procedures, velocity is obtained directly from the slope of *distance travelled* plotted *versus pulse delay*, and absorption is obtained from the slope of *compensating electrical attenuation versus distance*. Since the method depends only upon observing the effects of differences in acoustical path length, knowledge of exact distance traveled by the sound is unnecessary.

Velocity readings are taken for helium at 10,000-yard (radar) range intervals by placing the returned signal pip at definite positions with respect to successive scope-range markers, and recording the transducer-reflector distance. By adjusting the scope properly these markers appear as very short (dark) breaks in the sweep, and, if consistent criteria are adopted, accurate range difference readings result. Since the echo signal is adjusted to a predetermined level on the scope for each range position (by means of attenuators, without disturbing the gain of the remainder of the system), absorption data are obtained directly. Figure 3 gives an example of excellent data for attenuation in liquid helium at 3.08°K; the attenuation is plotted against the

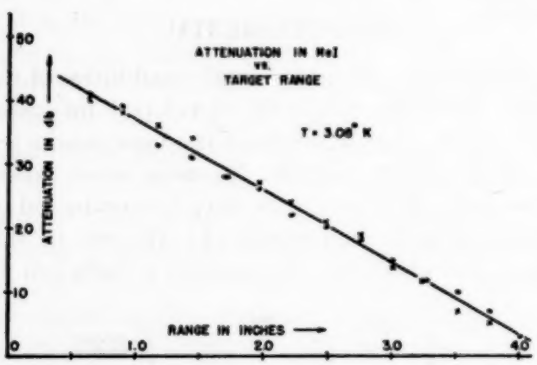

FIG. 3. Sample plot of receiver attenuation *versus* target range at constant temperature.

[3] J. R. Pellam and J. K. Galt, J. Chem. Phys. 14, 608 (1946).

transducer-reflector distance, and the slope of the straight line is a measure of absorption.

Results obtained by such measurements may be regarded as physically equivalent to those obtained by continuous wave methods. It may be shown that differences in behavior between pulsed sound and continuous sound in liquids should produce negligible effects. For example, no significant dispersion in liquids has been detected in the 15 Mc/sec. range (nor pulse distortion) so that the group velocities measured by pulsing should not differ measurably from the phase velocities ordinarily determined. Similarly, although attenuation within liquids varies as frequency squared, the band width associated with the pulses is too narrow for a measurable effect to result.

The velocity of ordinary sound in liquid helium is about 2×10^4 cm/sec., corresponding to a wave-length at 15 Mc/sec. of roughly 1.3×10^{-3} cm. Since the crystal radiating and receiving surface is about 1 cm across, this diameter corresponds to about 750 wave-lengths. Accordingly, the pulses travel out within a very narrow beam (0.1° when computed on the basis of Fraunhofer diffraction to obtain an order of magnitude). Therefore, the pulses retain nearly their exact size and shape throughout their travel, so that any geometrical attenuations caused by spreading are completely overshadowed by true liquid absorption. Therefore, attenuation data may be converted directly to absorption coefficients by applying a numerical factor; thus from the linearity of the curve of Fig. 3 one obtains db/inch = 11.1, and $\alpha = 11.1/44.3 = 0.25$ is the absorption coefficient, in (cm^{-1}).

In the classical theory of sound[4] the α is commonly referred to as the coefficient of pressure attenuation and enters into the solution of the wave equation as

$$P = P_0 e^{-2\pi i\nu[t-(x/v)]-\alpha x}, \qquad (1)$$

where P is the pressure, ν the frequency, v the wave velocity, and x the coordinate of distance along which the wave travels. In Fig. 3 the exponential decay is experimentally verified, and it is understood that the α determined from the slope of data such as in Fig. 3 is the composite attenuation caused by viscosity and heat conduction. For liquids containing polyatomic molecules an additional attenuation involving internal molecular vibrations would also be included.

In discussing the equipment for these experiments no detailed information (such as circuit diagrams) is included concerning the standard electronic elements of pulse power, transmitter, and the receiver. The ultrasonic equipment in the bath of liquid helium requires some discussion and is illustrated in Fig. 4. The entire ultrasonic equipment is placed in a Collins Cryostat[2] (A) where as much as 5 liters of liquid helium may be produced for experiments. The ultrasonic equipment and its associated helium vapor pressure thermometer, (T), pumping tubes, (P), and vacuum jacket, (V), underwent

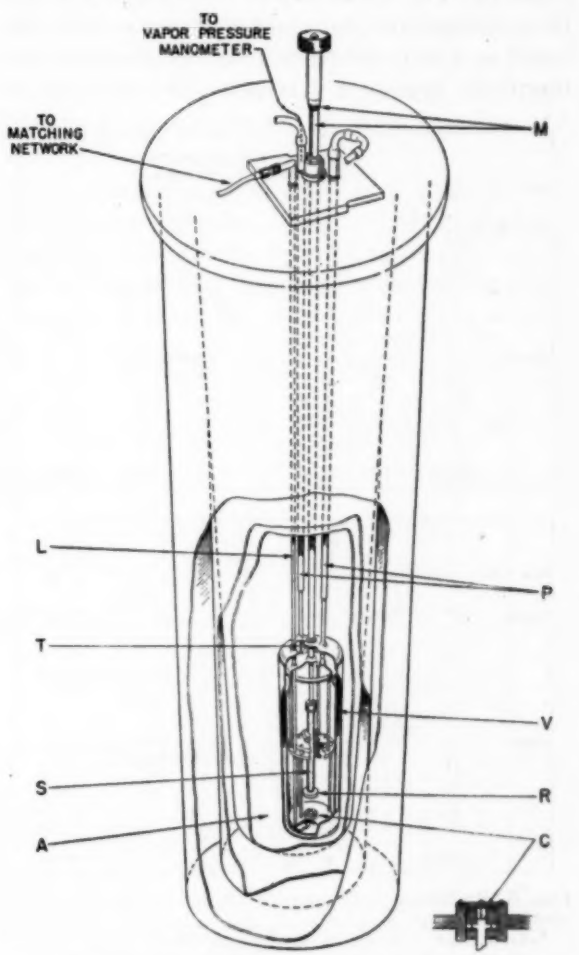

FIG. 4. Composite isometric view of transducer-reflector equipment within cryostat.

[4] Lord Rayleigh, *Theory of Sound* (Dover Publications, New York, 1945), Vol. 2.

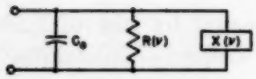

FIG. 5. Equivalent matching network.

continuous development* during the course of the research program. The crystal (C) was driven by electrical pulses, arriving through the coaxial line (L) at a frequency of 15 Mc/sec. The resulting sound waves traveled out from the crystal to the reflecting target (R). This mirror could be placed at any desired range by means of the screw (S). This precision screw was driven by a steel rod extending from the top of the equipment, and was equipped with a micrometer vernier scale (M) for precise distance readings. Liquid helium was allowed to condense in the innermost container until it covered the crystal transducer to a height of approximately 15 centimeters. The intermediate chamber (V) was then pumped out to a high vacuum so that the liquid in which the measurements are made was thermally insulated. Except at the very lowest

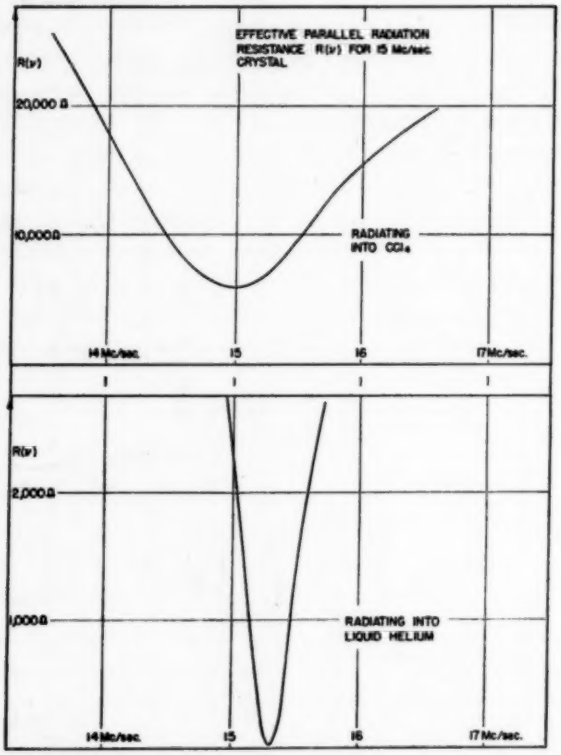

FIG. 6. Radiation resistance of crystal *versus* frequency.

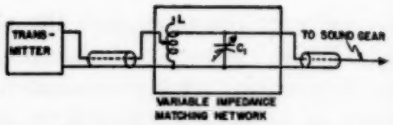

FIG. 7. Impedance-matching network.

temperatures (below 2°K) the liquid in the outer cyrostat was kept at a slightly lower temperature than the liquid covering the crystal. These conditions permitted excellent temperature control and avoided rapid boiling which could have been detrimental to accurate readings.

The transducer consisted of a thin x cut quartz crystal one centimeter in diameter. Such a crystal undergoes thickness vibrations when an oscillating voltage is applied across its thin dimension. The crystal was cut to the proper thickness (about 0.018 cm) for its fundamental resonance to occur at approximately 15 Mc/sec.

The upper (and radiating) surface was completely silvered and was grounded to the housing cartridge. On the other hand, the silver plating on the lower surface did not extend quite to the crystal circumference, thus forming an insulated electrode to which the r-f signal could be fed from the pulser. This transducer had two separate effects on the electrical properties of the system. First of all the geometry of the crystal provided a certain fixed capacity between its electrodes, amounting to about 25 $\mu\mu$f.

A more important effect of the transducer upon the system was a marked narrowing of the band width, especially for the case when the crystal was in contact with liquid helium. This may be illustrated by means of the equivalent transducer circuit, Fig. 5. This particular equivalent form for representing the crystal has been chosen as convenient for the present discussion. Here C_0 is the fixed crystal capacity (25 $\mu\mu$f) in parallel with a frequency-dependent radiation resistance $R(\nu)$ and a frequency-dependent reactance $X(\nu)$.

The band width of the transducer may be determined by measuring the radiation resistance $R(\nu)$ *vs.* frequency and obtaining the half-power points. Sample Q-meter measurements of $R(\nu)$, given in Fig. 6 for CCl_4 and liquid helium, illustrate the sensitivity of the electrical properties of the crystal to the medium into which it radiates. It is noted that, whereas for CCl_4 the band width $\Delta\nu$ is about 1.7 Mc/sec.,

* An earlier version of low temperature sound gear is described by Dr. J. Galt in a paper "Sound Absorption and Velocity in Liquefied Argon, Oxygen, Nitrogen, and Hydrogen" to be published shortly.

the band width for liquid helium is only about 0.2 Mc/sec.

The characteristic impedance of most ordinary liquids such as CCl_4 is about one-tenth that for crystalline quartz, and this provides sufficient damping (through radiation) to reduce the crystal Q to the neighborhood of 10 or less. On the other hand, the characteristic acoustical impedance for liquid helium being only about one-thousandth that for quartz, the band width of 0.2 Mc/sec. corresponds to a Q of about 75, since

$$Q=\nu/\Delta\nu=15/0.2\simeq 75. \quad (2)$$

The band width $\Delta\nu=0.2$ Mc may be converted directly to the corresponding acceptable pulse length $\Delta\tau$ by the relationship

$$\Delta\tau=(\Delta\nu)^{-1}=5\times 10^{-6}\ \text{sec}. \quad (3)$$

It is therefore evident that pulse-lengths of at least 5 μsec. duration were required. This corresponded to about 75 complete oscillations per pulse, also numerically equal to the Q of the system. These are merely quantitative ways of expressing the fact that helium is a most difficult liquid in which to generate sound pulses.

It is necessary to match the impedance presented by the crystal system to that of the coaxial line reading from the pulser. At resonance the impedance presented by the crystal is complex, and ordinarily the impedance level is different from that of the line. Therefore a matching network was essential, and was placed directly outside the cryostat. This is illustrated in Fig. 7.

The effect of the fixed capacity of the crystal (25 $\mu\mu$f) plus the capacity of the internal coaxial line (100 $\mu\mu$f) was tuned out by means of the coil L. The fixed tap from the coaxial line into this coil was positioned to provide somewhat more inductance than actually necessary for this purpose. The excess was available for adjustment during operation (using the echo signal as a guide) by tuning out with the variable capacity C_1.

The input signal from the transmitter entered coil L a *via* variable tap T. A sliding contact was provided to make the turns ratio continuously variable, and the setting was obtained by maximizing the returned echo signal.

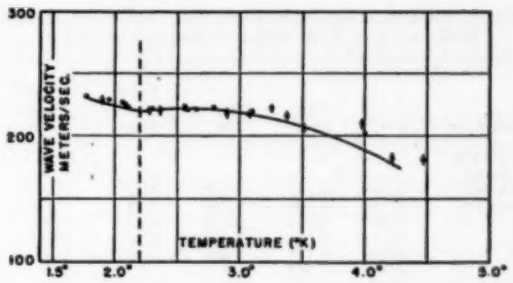

FIG. 8. Ultrasonic wave velocity *versus* temperature in liquid helium. —— Toronto data (1.3 Mc/sec.); ···· Massachusetts Institute of Technology data (15 Mc/sec.)

III. RESULTS

The velocity of first sound (meter/sec.) is plotted *versus* temperature (degrees Kelvin) in Fig. 8. The circles represent individual values at 15 Mc/sec. and are determined by the pulse method described. These are compared with results of previous investigators[5] obtained interferometrically at 1.3 Mc/sec. and indicated by the solid line. The general correlation shows the absence of any dispersive effects within this frequency range. All of the above data refer to liquid helium under its own vapor pressure. The investigation by the Toronto Laboratory[5] revealed a discontinuity in velocity at the λ-point under conditions of increased pressure. The conclusion was that whatever discontinuity existed

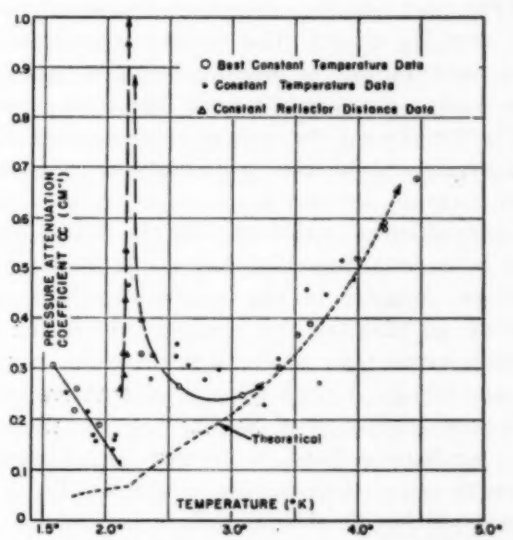

FIG. 9. Ultrasonic pressure attenuation coefficient α *versus* temperature.

[5] Findlay, Pitt, Grayson Smith, and Wilhelm, Phys. Rev. **54**, 506 (1938); *ibid.* **56**, 122 (1939).

TABLE I. Values of α, the attenuation coefficient and the ratio of c_p/c_v from which α was calculated.

Temperature	$\gamma-1$	$\alpha_{\text{vis-cosity}}$	$\alpha_{\text{ther-mal}}$	Total $\alpha_{\text{theo-retical}}$	Total $\alpha_{\text{experi-mental}}$
5.10±0.1°K					(1.78 cm^{-1})
4.47±0.01					0.68
4.22±0.01	1.35	0.244	0.382	0.62	0.58
4.00±0.01	1.14	0.200	0.260	0.46	0.52
3.62	0.80	0.131	0.198	0.33	0.39
3.52	0.72	0.122	0.184	0.30	0.37
3.38	0.58	0.114	0.164	0.28	0.30
3.08	0.38	0.103	0.122	0.22	0.25
2.58	0.14	0.087	0.055	0.14	0.27
2.28	0.03	0.079	0.015	0.09	0.33
λ-point (2.19)	0	0.077	0	0.077	(∞)
2.11		0.071	0	0.071	0.11
1.94		0.061	0	0.061	0.15
1.76		0.050	0	0.050	0.24
1.57		0.042	0	0.042	0.30

under its own vapor pressure conditions was too small for measurement by that method. Similarly, the present technique was incapable of detecting such an effect.

Attenuation

The pressure attenuation coefficient α in cm^{-1} is plotted as a function of temperature in degrees Kelvin in Fig. 9 and represents the essentially new information resulting from this investigation. Each point represents a separate series of electrical attenuation *versus* range readings at constant temperature. These db *versus* range data were graded according to linearity of the plots, and the most reliable results from this standpoint indicated by circles. The results of remaining runs contributing significant but less reliable values are represented by dots. The solid curves of Fig. 9 represent the composite average for the measurements. In the region above 3°K the solid curve is omitted since it merges with the theoretical curve represented by the dotted line.

It is evident from Fig. 9 that the absorption changes abruptly in the neighborhood of the λ-point, so that for this temperature region it proved impractical to conduct db *versus* range measurements. Accordingly, an alternative procedure was adopted of holding the transducer-reflector distance fixed and noting receiver signal strength *versus* temperature as the λ-point was passed. Although this technique is inadequate for detailed measurements in the low attenuation ranges, it is suitable for mapping out large scale, rapid changes. This is represented by the triangles and dashed line of Fig. 9. Such a procedure yields only differences in α after one has obtained the shape of the curve; the absolute magnitude of α is adjusted to fit the true values of the solid line curve of Fig. 9.

Several significant features are revealed. Beginning with the highest temperatures in the He I domain, the attenuation falls steadily as temperature is decreased. A minimum is reached in the 2.8°K region below which the attenuation increases, finally to rise sharply in the immediate vicinity of the λ-point. It was not possible to determine whether α actually became infinite, but on the basis of signal strengths at temperatures of known attenuation it is clear that values of at least 3.5 cm^{-1} occur for α.

Lowest attenuations occur immediately below the λ-point where values of about 0.1 cm^{-1} were observed. However, at lower temperatures the attenuation again increases in a steady manner. This trend appears to continue even to the lowest temperature at which measurements were conducted (1.57°K).

Numerical values of attenuation coefficient α, including one at 5.1°K, are given in Table I for runs indicated by circles in Fig. 9. Numerical values for the computed α are given at corresponding temperatures where data exist for such computations. The ratio of the specific heat capacities $\gamma=c_p/c_v$ can be computed from data in Keesom's recent book[6] by means of the thermodynamic relationship

$$\gamma-1=-\frac{T}{\rho^2 c_v}\left(\frac{\partial P}{\partial T}\right)_\rho\left(\frac{\partial \rho}{\partial T}\right)_P,$$

where ρ is the density, P the pressure, and T the temperature. Values of $(\gamma-1)$ are included with the theoretical and experimental results of Table I.

IV. DISCUSSION

He I

One of the revealing features of the attenuation measurements is the manner in which classical theory completely accounts for the absorption in He I at temperatures above about 3°K. Values computed on the basis of classical theory are represented by the dotted curve of Fig. 9, which

[6] W. H. Keesom, *Helium* (Elsevier Publishing Company, Inc., Amsterdam, 1942), p. 244.

above 3°K also represents the best experimental curve. This is significant, since for ordinary liquids (with the exception of Hg) the measured values consistently exceed[7] the amounts expected on the basis of classical viscosity and heat-conduction losses. This is presumably attributable to the monatomic nature of helium, which precludes the type of relaxation phenomena associated with the inner degrees of vibration of polyatomic molecules. Moreover, He I presents a situation in which the relative contributions to absorption between viscosity and heat conductivity vary over a large range as temperature is varied. Numerical values for these two classical contributions to absorption,

$$\alpha = \alpha_{\text{viscosity}} + \alpha_{\text{thermal}}, \tag{4}$$

are given in Table I and were computed according to the well-known formulas[8]

$$\alpha_{\text{viscosity}} = \frac{8\pi^2}{3}\frac{\eta}{\rho c_1^3}\nu^2, \tag{5}$$

$$\alpha_{\text{thermal}} = \frac{2\pi^2(\gamma-1)}{\rho c_1^3}\frac{K}{c_p}\nu^2. \tag{6}$$

In the above, ν is the ultrasonic frequency in cycles per second, c_1 the ultrasonic velocity in cm/sec., η the coefficient of viscosity in poise, ρ the liquid density in g/cc, K the heat conductivity coefficient in cal./deg. cm sec., c_p the specific heat at constant pressure in cal./g deg., and γ the ratio of specific heats. With the exception of heat conductivity K, each of these quantities is a known function of temperature. In the case of K results are published[9] only for 3.3°K, so that this value of 6.0×10^{-5} cal./cm sec. was of necessity used throughout the temperature range of the He I calculations. It is noteworthy that the magnitude of the ultrasonic absorption places He I in the category of relatively high absorption liquids (in spite of its low viscosity). This behavior is accounted for by the occurrence in the denominator of Eqs. (5) and (6) of ρ and c_1^3, both of which are extremely low for helium.

In the general region of 3°K the experimental results of α begin to exceed considerably the classical theoretical values. Finally, the sharp peak occurs at the λ-point, whereas the predicted value for that temperature is only 0.07 cm^{-1}. Clearly, the inadequacy of the classical theory points to some other mechanism. Possibly a discontinuity in velocity such as suggested by the Toronto investigations might account for this effect. Another more general explanation of the complete absorption of ultrasonic energy at the λ-point is possible. The energy of transition from He II phase to He I phase is vanishingly small as the system approaches the λ-point (because the phase transition is of the second order—i.e., no latent heat at the λ-point). In just this region such transitions might be forced by the ultrasonic energy.

He II

The mechanism and formulas of classical absorption are not directly applicable to the case of He II since this liquid obeys a special system of complex hydrodynamics. Discussion of attenuation is rendered difficult because the complex hydrodynamics has been developed only to the first approximation. The main characteristic of He II is the possibility of a heat transfer as a first-order hydrodynamical process. The only dissipative process considered so far in the literature is the damping of an oscillating disk through viscosity. It appears that the classical formula (5) may be applied below the λ-point as long as the appropriate value of η is used. It turns out that this proper quantity is the effective viscosity, η_n referred to the normal fluid only (η_s for superfluid is taken as zero). Since for first sound, which we are considering, the two fluid components vibrate in phase with essentially identical particle excursions, the fluids are effectively locked together. Therefore, in setting up a wave equation the differential acceleration force on a thin layer involves the total density ρ, exactly as for the classical case (see footnote of Eq. (5)). However, the viscous retarding forces opposing the expansion and contraction of the layer are dependent upon the only existent vis-

[7] The discrepancy ranges to an extreme factor of 800 in the case of liquid H_2S.

[8] The expression for $\alpha_{\text{viscosity}}$ may be derived from the wave equation $\rho\ddot{\xi} - \rho c^2\nabla^2\xi = (4/3)\eta\nabla^2\dot{\xi}$, where the last term involves viscosity (here ξ is the particle displacement). A similar formulation involving heat flow leads to (6); L. Bergman, *Ultrasonics* (John Wiley and Sons, Inc., New York, 1939), p. 128.

[9] W. H. Keesom, Physica **5**, 281 (1938).

cosity present, namely, η_n for the normal fluid component. Accordingly, for He II this becomes

$$\alpha_{\text{viscosity}} = \frac{8\pi^2}{3}\frac{\eta_n}{\rho c_1^3}\nu^2, \tag{7}$$

which is the quantity plotted in Fig. 9 for points below the λ-point. The curve falls only gradually with lowering temperature, since the viscosity coefficient η_n is given by a smooth extension†† of η for He I into the He II region. The effect of heat conductivity on ultrasonic absorption is more complicated. The ordinary diffusion type of heat transfer must exist also in He II, but is completely masked by the first-order (reversible) heat transfer. The latter manifests itself in the so-called second sound,[10,11] which has been verified experimentally by Peshkov[12] and by Lane.[13] The α-thermal of Eq. (6) would be of the same order of magnitude in He II as it is in He I close to the λ-point and would not essentially change the total theoretical α plotted in Fig. 9 below the λ-point.

One might expect other dissipation effects which are peculiar to He II and which would give ultrasonic absorption of the relaxation type. Tisza[10] has suggested non-adiabatic transitions between the normal and superfluid component induced by ultrasonic waves. Other relaxation mechanisms such as between the ultrasonic energy and the zero-point energy may also appear. Finally, the coupling between first and second sound might give rise to dissipation effects. It does not seem possible at present to compute these effects without making arbitrary assumptions.

V. ACKNOWLEDGMENTS

Professor S. C. Collins has given this research a great deal of enthusiastic and technical support, and the authors are most pleased to acknowledge his generosity. There have been many fruitful discussions with Professor J. C. Slater and with Professor J. A. Stratton. Finally, the authors wish to express their thanks for the interest shown in this work by Professor F. Bitter and especially to Professor L. Tisza for many valuable discussions concerning the theory of liquid helium.

†† Viscosity measurements in He II made by use of the oscillating-disk method[6] were originally taken to indicate a coefficient falling sharply with temperature from the λ-point. A subsequent reinterpretation of the viscosity data by Tisza leads to a normal value of η for the normal fluid and an essentially zero value of η for the superfluid.

[10] L. Tisza, J. de phys. et rad. **8**, 1 (1940), Phys. Rev. **72**, 838 (1947).

[11] L. Landau, J. Phys. U.S.S.R. **5**, 71 (1941).

[12] Peshkov; J. Phys. U.S.S.R. **8**, 381 (1944).

[13] C. T. Lane, H. Fairbank, and W. Fairbank, Phys. Rev. **71**, 9 (1947).

Letters to the Editor

PUBLICATION of brief reports of important discoveries in physics may be secured by addressing them to this department. The closing date for this department is five weeks prior to the date of issue. No proof will be sent to the authors. The Board of Editors does not hold itself responsible for the opinions expressed by the correspondents. Communications should not exceed 600 words in length.

On the Application of Captive Balloons to Carry Photographic Emulsions

NIELS ARLEY
Institute of Theoretical Physics, University of Copenhagen, Copenhagen, Denmark
October 29, 1947

BY the recent discovery of Powell and his co-workers of a new meson about twice as heavy as the usual one, the great value of the photographic emulsion as a tool for the investigation of cosmic rays has been further stressed. It seems certain that this tool will in the future compete most favorably with the ionization chamber, the Wilson chamber, and the G-M counter. However, the photographic emulsion method has at present two drawbacks. The first one is the long time of several weeks required for the exposure of the emulsions. This drawback is very serious because it has hitherto excluded the applicability of this method in that part of cosmic-ray investigations which are at the present time of greatest importance, *viz.*, high altitude investigations. The second drawback is that for intensity reasons the emulsions cannot be exposed at sea level but have to be placed at the top of high mountains, often far away from the laboratories.

To overcome these two difficulties we would like to suggest the application of captive balloons to carry the emulsions. With present day technique, using, e.g., the light and very strong nylon strings already used in deep sea explorations, it seems not impossible to make a captive balloon carrying photographic emulsions stay at very high altitudes for a sufficiently long time to allow the exposure of the emulsions. Since this method would obviously overcome both of the above-mentioned drawbacks, thereby greatly increasing the value of the photographic emulsion method, it would be extremely important to investigate more closely the possibility of realizing it.

Statistical Geometry and Fundamental Particles

NATHAN ROSEN
University of North Carolina, Chapel Hill, North Carolina
November 3, 1947

IN connection with my recent paper of the above title,[1] I have learned of a paper by de Broglie,[2] in which he proposed introducing a Gaussian error function in the interaction between the electron and the electromagnetic field. The constant (having dimensions of length) which appeared in this function was considered by de Broglie as a measure of the uncertainty in the position of the point of application of the field to the charge (or inversely). Since these ideas are essentially the same as some of those forming the basis of my paper, I regret having failed to make a reference there to the work of de Broglie.

[1] Nathan Rosen, Phys. Rev. **72**, 298 (1947).
[2] Louis de Broglie, C. R. Acad. Sci. Paris **200**, 361 (1935).

Velocity Dependence of Nuclear Forces

H. SNYDER
Brookhaven National Laboratory, Upton, New York
AND
R. E. MARSHAK
University of Rochester, Rochester, New York
November 3, 1947

NEUTRON–PROTON scattering experiments at 90 Mev are being carried out in Berkeley at the present time. As proton beams of several hundred Mev become available, both neutron-proton and proton-proton scattering experiments will be performed at even higher energies. We wish to underline the great care which must be exercised in using high energy scattering experiments to draw precise conclusions about the nature of nuclear forces. If the meson field-theoretic origin of nuclear forces is taken seriously, the static potential description must of necessity breakdown for relativistic energies of the nucleons. This fact has been recognized by previous authors[1] who found the velocity dependent corrections to the nuclear interaction to terms of order $(v/c)^2$ (v is the velocity of the nucleon) and then solved the approximate Dirac equation for the two nucleons to the same order. This type of procedure corresponds to Breit's treatment of the two-electron problem[2] and suffers from the defect that it is only valid to order $(v/c)^2$.

In the Born approximation, one can obtain a complete relativistic expression for the nucleon-nucleon scattering cross section. In analogy with Møller's treatment of the scattering of fast electrons by electrons, one only considers the virtual emission and re-absorption of *one* meson quantum (Born approximation!), but otherwise takes rigorous account of the retardation of the meson field and the recoil of the nucleons. In this method of calculation, one foregoes explicit knowledge of the nuclear interaction in configuration space and finds directly the scattering cross section.

We have performed a Møller-type calculation for the scalar and vector meson fields, assuming in each case the type of coupling which leads to a convergent static potential (scalar coupling for the scalar theory, vector coupling for the vector theory). These meson theories do not lead to tensor forces (the scalar theory even leads to a repulsive potential!); however, they illustrate the error introduced into the high energy scattering cross section through the use of static potentials. All meson theories which yield tensor forces also lead to divergent static potentials (e.g., the pseudoscalar meson with pseudovector coupling) and hence cannot be calculated with the present method. Our

calculations only apply to neutron-proton scattering since we have not considered the identity of the two nucleons.

Our results are:

Scalar theory-neutral meson

$$\sigma(\theta)=\frac{M^2g^4[1-(v^2/c^2)\cos^2(\theta/2)]^2}{[(\mu c)^2+4p^2\sin^2(\theta/2)]^2[1-(v^2/c^2)]}. \quad (1)$$

Vector theory-neutral meson

$$\sigma(\theta)=\frac{M^2g^4\{1+2(v^2/c^2)\cos\theta+(v^4/c^4)[1+2\sin^2(\theta/2)]\}}{[(\mu c)^2+4p^2\sin^2(\theta/2)]^2[1-(v^2/c^2)]}. \quad (2)$$

In Eqs. (1) and (2), g is the coupling constant, M is the mass of a nucleon, μ that of the meson, p is the momentum, v the velocity, and θ the scattering angle, all in the center-of-mass system. The static potential in the scalar theory is $(g^2e^{-\mu cr/\hbar})/r$, in the vector theory $(-g^2e^{-\mu cr/\hbar})/r$; both theories lead to the same "static" cross section in the Born approximation, namely:

$$\frac{M^2g^4}{[(\mu c)^2+4p^2\sin^2(\theta/2)]^2}.$$

If charged mesons are emitted, the corresponding scattering cross sections are obtained from (1) and (2) by replacing θ by $\pi-\theta$.

Equations (1) and (2) show that the "non-static" forces alter both the angular distribution and the total scattering cross section, and that their effect is appreciable (a factor 2) in the several hundred Mev region. It is interesting to note that the vector theory leads to a much larger effect than does the scalar theory. We reiterate that our calculations are intended only to illustrate the magnitude of the effect of the "velocity-dependence" of nuclear forces so as to engender the proper amount of skepticism about too close an evaluation of high energy scattering experiments.

The above calculations were started last summer at the Brookhaven National Laboratory during the second author's stay as a consultant.

[1] G. Breit, Phys. Rev. **51**, 248 (1937); E. Feenberg, Phys. Rev. **55**, 602 (1939); C. Møller and L. Rosenfeld, Kgl. Danski Vid. Sels. Math.-Fys. Medd. **17**, 8 (1940); L. Hulthen, Ark. f. Mat. Astr. och. Fys. **30A**, 9 (1943), **31A**, 15 (1944).
[2] G. Breit, Phys. Rev. **34**, 553 (1929).
[3] C. Møller, Zeits. f. Physik **70**, 786 (1931).

Interaction of Neutrons with Electrons

J. M. Jauch and K. Watson
Department of Physics, The State University of Iowa, Iowa City, Iowa
October 27, 1947

EVEN without the assumption of a specific nuclear interaction, an electron may interact with a neutron by purely electromagnetic effects for two reasons. In the first place, the magnetic moment of the neutron interacts with the magnetic moment of the electron. An additional interaction of the electron with the neutron is predicted by the meson theory. According to this theory the neutron is part of the time decomposed into a proton and a meson thus causing the time average of the charge to be spread over a finite region in space. In a strong electric field this charge cloud around the proton is partly polarized, thus giving rise to a van der Waal's type of force.

In an interesting experiment Havens, Rabi, and Rainwater[1] have interpreted the apparent decrease of the total cross section for slow neutrons with increasing energy in lead as caused by the second of the above-mentioned effects. The purpose of this letter is to point out that their estimation of 4×10^{-31} cm^2 for the cross section of the scattering due to polarization is at variance with the value calculated from the meson theory by a factor $\sim10^4$.

Watson[2] finds for the potential of a charged particle in the neighborhood of a neutron the expression (units $\hbar$ c and cm)

$$V(r)\sim-1/10(e^4g^2/\mu^2)1/r^4 \quad (\text{for } \mu r\geq1),$$

$e^2\sim1/137$, $g^2\sim1/10$ (dimensionless coupling constant) μ = meson mass in cm^{-1}. The formula does not hold for $\mu r\ll1$. Instead the potential is expected to reach a finite value for $r\to0$. Apart from numerical factors of order ~1 $V(r)$ is the same for scalar, pseudoscalar, and vector theories. The low energy cross section for the scattering of neutrons on bound electrons with this potential turns out to be $\sim10^{-25}$ cm^2.

From this result we must conclude that either the interpretation of the experimental results given by Havens, Rabi, and Rainwater is incorrect or that there exists an additional interaction between electrons and neutrons which does not follow from meson theory.

[1] W. W. Havens, Jr., I. I. Rabi, and L. J. Rainwater, Phys. Rev. **72**, 634 (1947).
[2] K. Watson, Ph.D. Thesis, University of Iowa (Phys. Rev. **72**, 1060 (1947)).

Relative Cross Sections of Reactions Induced by High Energy Neutrons in C, N, O, and F

William J. Knox
Radiation Laboratory, Department of Physics, University of California, Berkeley, California
October 30, 1947

WHEN a nucleus is bombarded with very high energy neutrons a large variety of nuclear reactions can occur, resulting in the formation of most, if not all, the radioactive species below the bombarded nucleus. However, in the region of light elements such as C, N, O, and F the activities of suitable half-life for easy detection are few enough that relative cross sections for the reactions producing these activities can be obtained from simple analysis of decay curves taken on the bombarded substance.

Various samples of carbon, Be_3N_2, BeO, and LiF have been bombarded with high energy neutrons[1,2] from the 184-in. cyclotron in order to determine the relative cross sections of certain nuclear reactions which occur. Beryllium and lithium compounds were used because these elements give no interfering activities in the range of half-lives investigated. The neutrons used were produced by the action of 190-Mev deuterons on a $\frac{1}{4}$-in. Be target. These neutrons

have an energy distribution with a peak at about 90 Mev and a width at half-maximum of about 27 Mev. The samples were placed on the wall of the cyclotron tank where the neutron beam emerges, bombarded for times ranging from 5 to 30 minutes, and then spread in thin layers and measured on a G-M counter.

The activities observed in these samples after bombardment were the well-known isotopes C^{11} (20.5 min.), N^{13} (9.93 min.), O^{15} (2.1 min.), F^{17} (70 sec.), and F^{18} (112 min.). Observed half-lives agreed closely with reported values. (In the case of F^{17} the resolution of the curve was not good enough to check the half-life accurately.) For comparison of cross sections of different reactions occurring in a single element a single sample was bombarded, and its decay curve was resolved into the component activities. For comparison of cross sections of reactions occurring in different elements samples of two elements were bombarded simultaneously in the same beam, and decay curves were taken on weighed samples. Each bombardment was repeated several times. In calculation of the relative cross sections corrections were made for self-absorption of samples in counting and for length of bombardment. The relative activation cross sections found are given in Table I. The reproducibility of

TABLE I.

Product	Bombarded element C	N	O	F
C^{11}	1.00	0.40	0.31	*
N^{13}		0.32	0.12	*
O^{15}			0.90	*
F^{17}				*
F^{18}				1.7

* Observed but not quantitatively resolvable.

the results is within a range of about 10 percent of the values given.

Because high energy neutron cross sections are of interest theoretically, further work is being done in the range of light elements to determine as many of these cross-section ratios as is readily possible.

The author wishes to express his appreciation to Professor Edwin M. McMillan for proposing this problem. This work was done under the auspices of the Atomic Energy Commission under Contract No. W-7405-eng-48.

[1] A. C. Helmholz, E. M. McMillan, and D. Sewell, Phys. Rev. **72**, 1003 (1947).
[2] R. Serber, Phys. Rev. **72**, 1114 (1947).

Interval Formula for Multiplets of Atomic Energy Levels

GENTARO ARAKI
Department of Industrial Chemistry, Kyoto Imperial University, Kyoto, Japan
October 27, 1947

THERE are many cases in which intervals of multiplets do not satisfy the Landé rule; nevertheless the arrangement of the levels shows the Russell-Saunders coupling. The cause of such phenomena for lighter atoms was found to be due to spin-spin interactions between atomic electrons by detailed researches for triplets of the He atom, Be atom, and Be-like ions.[1] It was also shown that spin-spin interactions can give rise to a deviation from the Landé rule even if the atomic number is large, because the effect of the atomic number is considerably reduced by spin-orbit interactions between atomic electrons.[1]

From the results of these researches one may imagine that a spin-spin part of a multiplet-interval becomes, under certain circumstances, comparable with its spin-orbit part also for atoms with larger atomic numbers, although it is often accepted that the former is negligibly small compared with the latter. It is thus quite probable that some of irregular or even partly inverted multiplets of complex atoms belong to the Russell-Saunders case and that their deviations from the Landé rule can be attributed to spin-spin interactions as is in the case of lighter atoms. I have quantitatively verified this expectation. A brief account of the calculated result will be given in the following.

Spin-orbit and spin-spin interactions between atomic electrons were given by Breit.[2] We can calculate diagonal elements of these operators in L, S, J, M scheme using commutation relations satisfied by the operators which are involved in these interactions. An interval formula, for multiplets of atomic energy levels in the Russell-Saunders case, can be obtained from these diagonal elements. It is given by

$$^{2S+1}L_{J-1}-{}^{2S+1}L_J=2\zeta J+12\eta J\{J^2-L(L+1)-S(S+1)+\tfrac{1}{2}\},$$

where $^{2S+1}L_J$ denotes a spectral term, L, S, *and* J are, respectively, azimuthal, spin, and inner quantum numbers of the atom, ζ and η depend on λ, L, and S, and λ stands for quantum numbers other than L, S, and J. The former term including ζ is due to spin-orbit interactions, and it satisfies the Landé rule. The latter term including η comes from spin-spin interactions and it causes a deviation from the Landé rule. This general formula completely agrees with my previous results[1,2] for the special cases of doublets and triplets.

All observed values of multiplets, which are registered in Bacher-Goudsmit's table and have multiplicities greater than three, are numerically examined by this formula. Many irregular and partly inverted multiplets are in good agreement with this formula. In these cases, contributions

TABLE I.

Atom and Z	Configuration and symbol		Observed interval in cm^{-1}	Interval ratio	Spin-orbit part in cm^{-1}	Spin-spin part in cm^{-1}	Empirically determined value source	ζ	η
BrIII	$4p^35d$	A	808	3.01	688	+120	AB	76.4	0.44
		B	479	1.79	531	− 52	BC	75.8	0.41
35	^4F	C	268	1	384	−116	CA	76.8	0.43
ZrII	$4d^2(^3F)5p$	A	285	1.03	393	−108	AB	56.1	−0.86
		B	358	1.30	282	+ 76	BC	56.4	−0.84
40	$^4D^0$	C	275	1	168	+107	CA	56.0	−0.85
FII	$2s^22p^3(^3P)3d$	A	132.7	3.31	64.5	+ 68.2	AB	9.22	0.541
		B	− 2.6	−0.065	45.6	− 48.2	BC	9.12	0.536
9	^4D	C	−40.1	−1	27.8	− 67.9	CA	9.26	0.539

$A=^4F_{7/2}-{}^4F_{9/2}$, $B=^4F_{5/2}-{}^4F_{7/2}$, $C=^4F_{3/2}-{}^4F_{5/2}$

or

$A=^4D_{5/2}-{}^4D_{7/2}$, $B=^4D_{3/2}-{}^4D_{5/2}$, $C=^4D_{1/2}-{}^4D_{3/2}$

from spin-spin interactions are by no means negligibly small compared with those from spin-orbit interactions. In some cases the former is even larger than the latter. Three examples are given in Table I.

The detailed report will shortly be published in *Progress of Theoretical Physics*.

[1] G. Araki, Proc. Phys. Math. Soc. Japan, 19, 128, 592 (1937).
[2] See reference 1; 21, 508 (1939).
[3] G. Breit, Phys. Rev. 34, 553 (1929); 36, 383 (1930); 39, 616 (1932).
[4] R. F. Bacher and S. Goudsmit, *Atomic Energy States* (McGraw-Hill Book Company, New York, 1932).

The Self-Diffusion Coefficient of Argon

FRANKLIN HUTCHINSON*
*Sloane Physics Laboratory, Yale University,**
New Haven, Connecticut
November 6, 1947

THE diffusion coefficient for the diffusion of A^{41} into normal argon (99.6 percent A^{40}) has been measured, using the beta- and gamma-radiation from A^{41} to determine the amount of that isotope diffused. This coefficient should be close to the self-diffusion coefficient of A^{40}.

The apparatus consists of two brass tubes 45 cm long and 1.2 cm i.d., mounted with their axes horizontal and in line with each other, and connected by a suitable valve.[1] One side was filled with argon containing A^{41} made by bombarding tank argon with deuterons, the other side with tank argon to the same pressure, and the gases allowed to interdiffuse for a known time through the valve. The radioactivity of the gas in either side could be determined by Lauritsen quartz fiber electroscopes, one mounted on each tube over a "window" made by thinning the tube wall to 0.005 cm. From measurements of the activities in both tubes before and after diffusion, properly corrected for A^{41} decay, the fraction of A^{41} transferred from one tube to the other by diffusion could be determined, and from this figure and the geometry the diffusion coefficient D could be calculated. The weighted mean of six runs gives

$$D=0.423\pm0.003 \text{ cm}^2/\text{sec.},$$

corrected to 32 cm Hg and 22°C. The error is the probable error calculated from the scatter of the data.

Kinetic theory gives the relation $\rho D=\epsilon\eta$, ρ being the gas density, η the viscosity, and ϵ a number which depends on the forces between two colliding molecules. Taking ρ of argon at 22°C, 32 cm Hg to be $(0.6947\pm0.0003)\times10^{-3}$ g/cm³, η at 22°C to be $(0.225\pm0.001)\times10^{-3}$ poise, we find $\epsilon=1.31\pm0.01$. Assuming that the force between two molecules varies as r^{-n}, Chapman and Cowling[2] give a method of calculating a first approximation to ϵ. Fitting the calculated dependence of viscosity on temperature to the experimental data, they find $n=7.36$, which gives $\epsilon=1.47$. The discrepancy between this value and the experimental value is larger than can be accounted for by experimental error.

Table I. Reported values of ϵ.

Gas	Temp., °C	
H_2	20	$1.37_0\pm0.003$[4]
	−188	1.32 ±0.06[4]
	−252.8	1.28 ±0.02[4]
Ne	20	$1.27_8\pm0.006$[5]
A	22	1.31 ±0.01
Kr	20	1.30 ±0.06[5]
Xe	20	1.24 ±0.06[5]
CH_4	20	1.33[6]
UF_6	30	1.31[7]

Table I is a summary of measured values of ϵ collected from the literature. Amdur[3] has pointed out that knowing the value of ϵ will not permit an unambiguous determination of intermolecular forces. However, the small variation in ϵ shown in the table is rather unexpected, and must have some significance.

I would like to thank Professor E. C. Pollard for suggesting the problem and for many valuable discussions during the work.

* Coffin Fellow.
** Assisted in part by the Office of Naval Research under Contract N6ori-44.
[1] L. E. Boardman and N. E. Wild, Proc. Roy. Soc. 162A, 511 (1937).
[2] S. Chapman and T. G. Cowling, *Mathematical Theory of Non-uniform Gases* (Cambridge University Press, 1939), pp. 172, 198.
[3] I. Amdur, Phys. Rev. 72, 642 (1947).
[4] P. Harteck and H. W. Schmidt, Zeits. f. physik. Chemie 21B, 447 (1933).
[5] From a paper by W. Groth and E. Sussner, Zeits. f. physik. Chemie 193, 296 (1944).
[6] E. B. Winn and E. P. Ney, Phys. Rev. 72, 77 (1947).
[7] E. P. Ney and F. C. Armistead, Phys. Rev. 71, 14 (1947).

Precision Measurement of the Ratio of the Atomic 'g Values' in the $^2P_{3/2}$ and $^2P_{1/2}$ States of Gallium*

P. KUSCH AND H. M. FOLEY
Columbia University, New York, New York
November 3, 1947

THE measurement of the frequencies associated with the Zeeman splittings of the energy levels in two different atomic states in a constant magnetic field permits a determination of the ratio of the g_J values of the atomic states. This determination involves only an accurate measurement of the frequencies, and does not require a knowledge of the value of the constant magnetic field.

Using the atomic beam magnetic resonance technique we have measured six lines in the Zeeman spectrum of the $^2P_{1/2}$ state, and five lines of the $^2P_{3/2}$ state of gallium at a field strength of 380 gauss. The spectrum is, of course, complicated by the level splittings produced by the nuclear magnetic moments and electric quadrupole moments. At the field strength employed in this experiment the nuclear energy level pattern is of an intermediate Paschen-Back character.

The procedure employed in the observations was to make a series of alternate measurements of the frequencies of the lines in the $^2P_{1/2}$ and $^2P_{3/2}$ states. In this way the effect of a drift in magnetic field was minimized.

Becker and Kusch[1] have recently determined with high precision the nuclear magnetic moment and electric quadrupole moment coupling coefficients as well as the nuclear g values of Ga^{69} and Ga^{71} in both states. Their determinations are independent of any knowledge of g_J in either state.

Their results are consistent with the less accurate values obtained by Renzetti[2] by the zero moment deflection method.

With the constants given by Becker and Kusch and with assumed values for g_J it is possible to determine the magnetic field from the observed frequencies. The field values obtained from either of the groups of lines in the $^2P_{1/2}$ or the $^2P_{3/2}$ states are constant within the experimental uncertainty. What is more, there is excellent consistency of the results obtained from the data on the two isotopes. The mean value of magnetic field determined from the $^2P_{1/2}$ lines is less than the mean field value for the $^2P_{3/2}$ lines by 0.65 ± 0.02 gauss when the g_J values for the $^2P_{3/2}$ and $^2P_{1/2}$ states are taken to be 4/3 and 2/3, respectively. To remove this discrepancy we must assume for the ratio of the g_J values

$$\frac{g3/2}{g1/2}=2.00344\pm0.00012=2+\Delta.$$

If the electronic configuration in these states is accurately described by Russell-Saunders coupling the above discrepancy must be assigned to a change in the g value of the intrinsic moment of the electron or of the orbital moment from their accepted values. If the electron spin g value $g_S=2+\delta_S$ and the orbital g value $g_L=1+\delta_L$, then $\Delta=\frac{1}{2}\delta_S-3\delta_L$. Our present experiments, even assuming Russell-Saunders coupling, do not permit any evaluation of δ_S and δ_L. However, the discrepancy could be accounted for by taking $g_S=2.00229\pm0.00008$ and $g_L=1$, or alternatively $g_S=2$ and $g_L=0.99886\pm0.00004$.

The experiments reported in this note are of a preliminary nature. It is our intention to continue these studies with other atomic systems to clarify the role of the coupling in this phenomenon.

The authors are grateful to Professors G. Breit and I. I. Rabi for suggestions which stimulated these experiments.

* Publication assisted by the Ernest Kempton Adams Fund for Physical Research of Columbia University.

[1] To be published.

[2] N. A. Renzetti, Phys. Rev. **57**, 753 (1940).

On the Tripartition of Heavy Elements

TSIEN SAN-TSIANG*

Laboratoire de chimie Nucléaire, Collège de France, Paris, France

October 21, 1947

AFTER our experimental proof of the existence of tripartition and quadripartition of the compound nucleus of U^{236} by means of photographic emulsion,[1] I have discussed the mechanism of the first phenomenon and concluded, from the direction of the light third fragment, that the three fission fragments are emitted very probably in the same instant of separation.[2] This point of view is supported by other independent investigators.[3,4]

From the successively published results[1,4-9] on tripartition of Th^{232}, U^{236}, U^{239}, Pu^{240}, it is established that: (*A*) In 1–2 percent of all fissions, a light fragment is liberated in connection with the two heavy fragments, a part of them might be He^4. (*B*) These light fragments can be

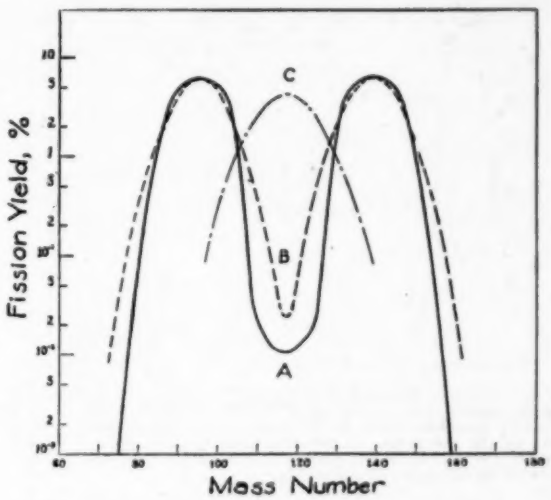

FIG. 1. The simplified model of tripartition. For the compound nucleus U^{236}, $R_1\sim8.4\times10^{-13}$ cm, $R_2\sim7.8\times10^{-13}$ cm, and $R_3\sim2\times10^{-13}$ cm, $Z_1\sim50$ and $Z_3\sim40$. In *A*, $H=6\times10^{-13}$ cm; in *B*, $H=0.1\times10^{-13}$ cm.

divided into two groups according to their range: the more frequent short range group ($L<3$ cm in air) exists in fissions of all elements, whereas the less frequent long range group (10 cm $<L<$45 cm) occurs only in the case of fissions by slow neutrons, its frequency varies with the element (that of U^{235} is twice that of Pu^{240}), and it depends probably on the degree of excitation of the compound nucleus, the low lying levels favoring this phenomenon. (*C*) The light fragment is emitted preferentially in a direction perpendicular to that of two main heavy fragments. Let α_1 be the angle made by the light fragment (M_3) with the heaviest fragment (M_1) and α_2 that with the lighter heavy fragment (M_2); in general, $\alpha_1>\alpha_2$, which means that M_1 takes more momentum than M_2. In the case of U^{236}, $\theta=\frac{1}{2}\Delta\alpha=\frac{1}{2}(\alpha_1-\alpha_2)$ has a value of 8° and 20° for the long and short range groups, respectively.

Let us take the simplified model of tripartition just before the moment of separation of 3 fragments (Fig. 1*A*, *B*),[2,10] one can calculate the direction and the velocity of M_3 as a function of time by taking into account the electrostatic repulsions due to M_1 and M_2. The result depends upon the choice of the value of nuclear radius R. It is well established that with $R\backsimeq1.5\times A^{\frac{1}{3}}\times10^{-13}$ cm, the deduced total kinetic energy of the two bipartition fragments ($\backsimeq$electrostatic potential energy just before the separation) is much higher than the experimental value,[11,12] while with the new value[12] of $R=(1.52\times A^{-\frac{1}{3}}+0.696)\times10^{-13}$ cm, the agreement between the theoretical and the maximum experimental values is satisfactory. By using the observed distribution of the total kinetic energy[14] of bipartition fragments of U^{236}, one can deduce the corresponding distribution of the nuclear radii $R'=KR$ (with the new value of R) of the heavy fragments in excited state, where K varies from 1 to 1.5 with the maximum frequency at 1.23.

(1) Assuming that the initial velocity of M_3 is zero (Fig. 1, *A*), for each value of A_3/Z_3, one can deduce the asymptotic velocity (V) and angle of emission (θ) of M_3

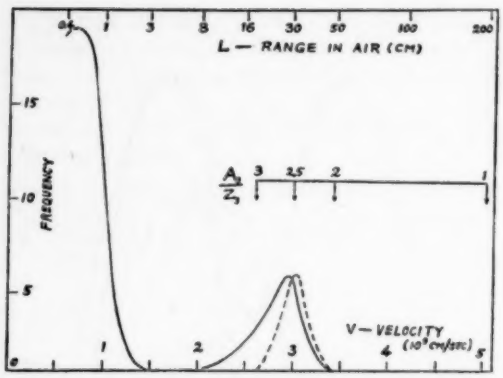

FIG. 2. Velocity distribution of M_3 of U^{235}. Full curve: experimental values. Dashed curve: theoretical velocity distribution of M_3 with $A_3/Z_3=2$ (position: Fig. 1, A), its maximum intensity is taken to be the same as the maximum of the experimental curve near $V\sim3\times10^9$ cm/sec. The arrows on the scale of A_3/Z_3 indicate the maximum velocity of M_3 for each value of A_3/Z_3.

for different values of K. The theoretical frequency-velocity curve of M_3 for $A_3/Z_3=2$ corresponding to the given distribution of K is shown in Fig. 2 (dashed curve), its maximum velocity, corresponding to a range about 47 cm in air, is in good agreement with the observation. For $A_3/Z_3=1$, 2.5, or 3, the maximum velocities are also indicated in Fig. 2, their absolute values are insensitive with respect to the mass value of M_3 (4 to 12). The comparison with the experimental curve (full curve) shows that A_3/Z_3 must be equal to or greater than 2 (therefore H^1 and He^3 are excluded). In combining the mass determination of M_3 in our experiments ($M_3=4\rightarrow7$, except one case in which $M_3=32$),[6] one can conclude that the third fragment group is composed of He^4, Li^6, He^6, etc.

(2) The velocity and angle of emission vary with the position of M_3. An example of their relation with H (Fig. 1A, B) for $K=1$ and $A_3/Z_3=2$ is given in Fig. 3. The theoretical mean value of θ for the long range and short range groups is 6° and 19°, respectively, in good agreement with the experimental values: 8° and 20°. The spread of θ from the mean value is partly due to different mass and charge distributions of the two heavy fragments and partly due to the possibility that the third fragment is emitted a little later than the separation of the two main fragments.[10] Detailed calculations show that the upper limit of this delay is 10^{-21} sec.

(3) The short range group is connected with the case in which the three fragments are almost collinear at the moment of separation (Fig. 1, B) ($H<0.15\times10^{-13}$ cm) while the long range group corresponds to the case in which the central third fragment shifts away from the axis of deformation (Fig. 1, A) (0.5×10^{-13} cm $<H<6\times10^{-13}$ cm). When the compound nucleus is in a highly excited state, its lifetime is so short that the separation of the three fragments may take place immediately when the deformation reaches the form of 3 collinear droplets. But if the excitation of the compound nucleus is just sufficient to overcome the fission threshold, the lifetime is a little longer and there may be a certain possibility, due to asymmetric effect or strong vibration, that the third fragment shifts away from the axis of deformation before the separation of 3 fragments. Therefore one can conclude tentatively that the ratio of the frequency of tripartition to that of bipartition is nearly constant for all fissions (1–2 percent), but the percentage of tripartition with emission of a long range third fragment varies with the degree of excitation of the compound nucleus above the fission threshold, the lower the excitation, the greater the percentage.

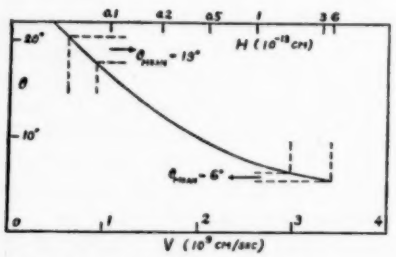

FIG. 3. The relations between the velocity V, the angle of emission θ, and the position H of M_3 (for $K=1$).

With the simplified model of tripartition, all the main experimental facts can be explained in a satisfactory way. The detailed discussions will be published shortly in the Journal de Physique et le Radium.[15]

* On leave from The National Tsinghua University, Peiping, China.

[1] Tsien San-Tsiang, Ho Zah-Wei, R. Chastel, and L. Vigneron, Comptes Rendus **223**, 986, 1119 (1946) and **224**, 272 (1947); Phys. Rev. **71**, 382 (1947).
[2] Tsien San-Tsiang, Comptes Rendus **224**, 1056 (1947).
[3] N. Feather, Nature **159**, 607 (1947).
[4] E. O. Wollan, C. D. Moak, and R. B. Sawyer, Phys. Rev. **72**, 447 (1947).
[5] Tsien San-Tsiang and H. Faraggi, Comptes Rendus **225**, 294 (1947).
[6] Tsien San-Tsiang, Ho Zah-Wei, R. Chastel, and L. Vigneron, Nature **159**, 773 (1947); J. de phys. et rad. **8**, June and July (1947).
[7] P. Demers, Phys. Rev. **70**, 974 (1946).
[8] L. L. Green and D. L. Livesey, Nature **159**, 332 (1947).
[9] G. Farwell, E. Segrè, and C. Wiegand, Phys. Rev. **71**, 327 (1947).
[10] R. D. Present, Phys. Rev. **59**, 566 (1941).
[11] N. Bohr and J. A. Wheeler, Phys. Rev. **56**, 426 (1939).
[12] A. J. Dempster, Phys. Rev. **72**, 431 (1947).
[13] E. Amaldi and B. N. Cacciopuoti, Phys. Rev. **71**, 739 (1947).
[14] A. Flammersfeld, P. Jensen, and M. Gentner, Zeits. f. Physik **120**, 450 (1943).
[15] Tsien San-Tsiang, J. de phys. et rad. **8**, Sept. (1947).

Preliminary Data on Absorption of High Energy Neutrons from the 184-Inch Cyclotron

R. HILDEBRAND AND B. J. MOYER
Radiation Laboratory, Department of Physics, University of California, Berkeley, California
November 7, 1947

WHEN the 190-Mev deuterons produced in the 184-inch cyclotron strike the target they project forward a spray of fast neutrons with a maximum of intensity along an axis tangent to the deuteron orbit at the target. Helmholz, *et al.*,[1] have studied the angular distribution; Serber[2] has calculated a theoretical energy distribution of these neutrons giving a maximum at 95 Mev and a bell-shaped spread from about 30 to 160 Mev.

Early in the work it was desirable to study approximately the absorption of this high energy neutron beam in various materials, particularly in concrete, in order to judge shielding requirements.

Figure 1 shows the arrangement employed in measurement of concrete absorption. The monitor and detector were aluminum-walled ionization chambers with battery-operated electrometer circuits and cables to remote meters. In the study of other materials the monitor and detector were Lauritsen electroscopes placed along the axis of the neutron beam, with broad slabs of the material under test between the electroscopes and close to the detector.

In the region where the absorbing slabs were placed the neutron beam section had a half-intensity diameter of about 3 ft., and the slabs of absorbing material presented an area of about 2 ft.×3 ft. normal to the beam. The dimensions of the slabs varied somewhat depending upon stock available.

Considerable evidence has indicated that the ionizing secondaries arising from the passage of these fast neutrons through matter are projected predominately in the forward direction. Tests by R. Loevinger[3] in related work have shown that ionizing particles effective in the chamber from a thick slab of copper placed immediately following the chamber will increase its reading by about 6 percent. Materials of lower atomic number gave smaller effects, and Pb gave about a 10 percent effect.

It is thus only approximately correct to refer to these measurements with broad beam and broad slabs as absorption measurements. The data are presented graphically in Fig. 2. All curves have been normalized to unity at zero absorber thickness, except in the case of concrete whose zero reading is 10.

The curves display a transition region within which the beam approaches the equilibrium with its ionizing secondaries which is appropriate to the material in question. Materials of atomic number lower than the iron of the cyclotron tank wall yield a positive transition effect, i.e., increase of ionization. Lead with higher atomic number shows a negative effect. The positive effect here shown by copper is geometrical in nature. It is due to the fact that the irradiated portion of the iron tank wall is seen by the detector with rather "good" geometry, whereas the copper absorber slab is seen with "poor" geometry and can make contributions to the detector from a wide-angle scattering. This effect contributes of course to the apparent transition phenomena in each case presented here. When geometry differences were eliminated in a test with Fe and Cu this discrepancy was absent.

Following the transition regions the absorption is exponential over the regions studied and yields the half-value thicknesses shown in Fig. 2.

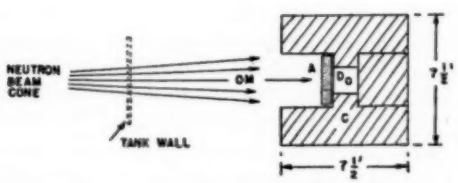

FIG. 1. Arrangement for testing shielding properties of concrete (median plane section). *A*. Slab under test. Dimensions 3′×3′×thickness, *C*. Concrete "Igloo"; *D*. Detector, in cubical cavity 1-1/′ edge; *M*. Beam moniter.

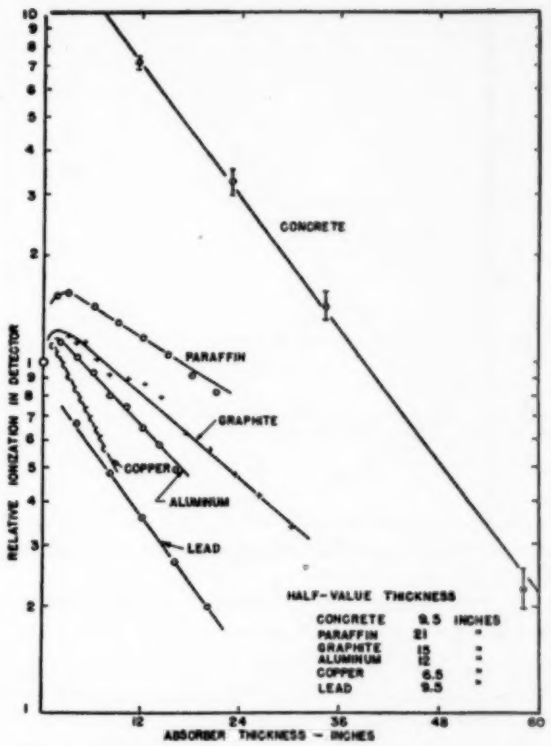

FIG. 2. Absorption of fast neutron beam in various materials (aluminum—wall ionization chamber).

A test by Dr. T. J. Parmley of concrete absorption with carbon disk detectors activated by the $C^{12}(n, 2n)C^{11}$ reaction (20.5-Mev threshold) gave a half-value thickness between 9½ and 10 inches. The absorption per unit length in concrete made from a barite aggregate was not distinguishable from that in ordinary concrete.

Table I summarizes the half-value thicknesses and the mass absorption coefficients for the materials studied. The values for water were obtained by Loevinger[3] in a related experiment. The coefficients for hydrogen and oxygen are calculated from carbon, paraffin, and water data.

TABLE I. Half-value thicknesses and mass absorption coefficients.

Absorber	Half-value thickness	Mass abs. coeff.	Est. P.E.
	(cm)	(cm^2/g)	(%)
Pb	24.1	0.255×10^{-2}	2
Cu	16.5	0.471×10^{-2}	4
Al	30.5	0.841×10^{-2}	4
C	38.1	1.14×10^{-2}	5
Concrete (ordinary)	24.1	1.24×10^{-2}	5
Concrete (barite)	24.1	1.24×10^{-2}	—
H_2O	55.9	1.24×10^{-2}	—
CH_2	53.4	1.43×10^{-2}	5
O	—	1.02×10^{-2}	—
H	—	3.06×10^{-2}	25

In Fig. 3 are plotted the values of μ for the elements vs. atomic number. The large absorption cross section indicated for hydrogen, together with the magnitude of the

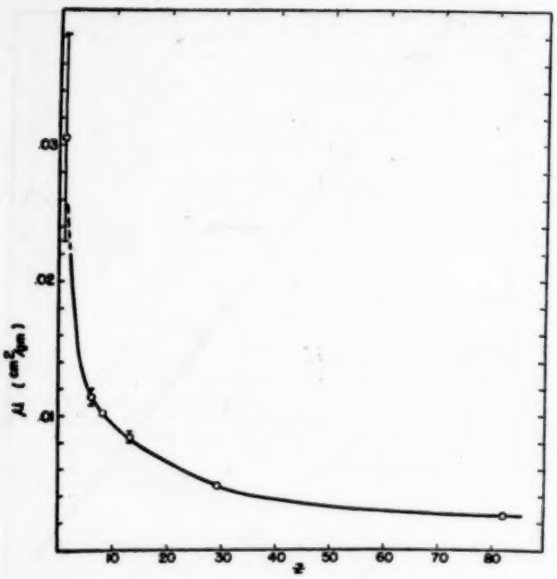

FIG. 3. Mass absorption coefficient *vs.* atomic number.

transition effect observed with paraffin, may lend support to the conception of exchange processes playing a prominent role in the attenuation of the fast neutrons.

The assistance of N. Knable and H. York in a portion of the work is acknowledged. This study was carried out under the auspices of the U. S. Atomic Energy Commission under Contract No. W-7405-eng-48 with the Radiation Laboratory, University of California, Berkeley, California.

[1] A. C. Helmholz, E. M. McMillan, and D. Sewell, Phys. Rev. **72**, 1003 (1947).
[2] R. Serber, Phys. Rev. **72**, 1007 (1947).
[3] To be published.

Further Studies on the Radiations From Ba^{131} and Cs^{131}*

BERNARD J. FINKLE**
Metallurgical Laboratory, University of Chicago, Chicago, Illinois
October 29, 1947

THE radiations of the 12.0*d* Ba^{131} and 10.2*d* Cs^{131} isotopes[1] were examined for positrons by means of magnetic deflection with a magnet whose strength was about 1350 gauss. The experimental set-up is shown in Fig. 1. The sample card, *S*, with the activity mounted at one end was fastened by Scotch Tape to a lead absorber (3.5 g/cm²), *B*, and placed, as shown, with respect to the magnetic field. In this arrangement it is impossible for particles to travel directly from the sample to the counter. The movable lead absorber, *A*, is of the same thickness as *B*, so that counts may be taken with the G-M tube completely shielded (*A* in place), and with *A* removed. Counts with and without *A* were taken for both directions of the magnetic field. The results for Ba^{131} are given in Table I.

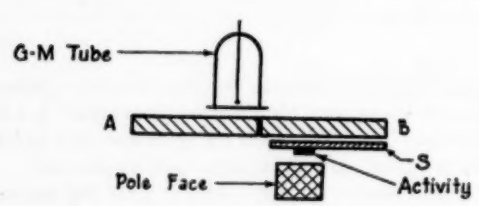

FIG. 1. Experimental arrangement used in the search for positron emission.

TABLE I.

	Absorber *A* in place	Absorber *A* removed
Activity with magnetic field oriented to deflect positrons into G-M tube	706 c/m	951 c/m
Activity with magnetic field oriented to deflect electrons into G-M tube	670 c/m	3556 c/m

The increase in apparent positron count when *A* was removed was caused by scattering, as shown by results obtained without a magnetic field. The large increase in in electron count indicates the presence of conversion electrons. In similar experiments with Cs^{131}, an increase in apparent positron count was entirely attributable to scattering. These experiments, which are rather rough, indicate that neither Ba^{131} nor Cs^{131} emits positrons. The absence of 0.5-Mev gamma-rays from Cs^{131} is additional evidence that this isotope does not decay by positron emission, but the presence of 0.5-Mev gamma-rays in the case of Ba^{131} requires further experimentation to determine whether any of these are positron annihilation radiation.

The tables in Compton and Allison's *X-Rays in Theory and Experiment* give for the energies of the *K* x-rays of Xe, Cs, and Ba the values shown in Table II. The elements which are suitable for use as critical absorbers to measure these energies are Sn, Sb, and Te, with critical absorption energies of 29.11, 30.39, and 31.70 kev, respectively. For the Sn and Sb absorbers, solutions of different concentrations of these elements in 6*N* HCl were used. Activity was measured through a 1-cm depth of each solution in a flat mica-bottomed dish 7.9 cm in diameter and 1.7 cm deep. The Te absorbers consisted of different amounts of powdered Te metal distributed in the same weight of beeswax in as uniform a way as possible. A known weight of Te powder was sprinkled into molten beeswax in a Petri dish (coated with glycerol to prevent sticking) and stirred gently to achieve a uniform distribution. The cooled wax cake was removed from the dish, cut to size, and covered with Cellophane. When some of the Te was found in the glycerol layer after the absorber was removed from the dish, its weight was subtracted from the weight of Te added.

TABLE II. *K* x-rays of Xe, Cs, and Ba.

	$K-L_{II}$		$K-L_{III}$
Xe		29.59 kev	
Cs	30.54		30.88
Ba	31.72		32.10

The half-thickness values found for the x-ray components of the absorption curves are given in Table III.

TABLE III. Half-thickness values for absorption of x-rays from Ba^{131} and Cs^{131}.

Absorbers	Ba^{131} x-rays	Cs^{131} x-rays
Sn	34 mg/cm²	30 mg/cm²
Sb	30	63
Te	144	95

The K_α x-ray of Xe, which arises after the Cs^{131} captures a K electron, should be strongly absorbed by Sn but not by Sb and Te. This general condition is met. However, the half-thicknesses given for Te absorbers are too high. This may be due to insufficiently uniform distribution of the Te powder in the beeswax. Although it can be concluded from these data that the x-rays from Cs^{131} are the K radiations of Xe, the data are inconclusive with respect to Ba^{131}. But since the latter decays to Cs^{131}, the observed x-rays are very probably the K radiations of Cs.

This paper is based on work performed at the Metallurgical Laboratory of the University of Chicago under Contract W-7401-eng-37 for the Manhattan Project, and the information contained therein will appear in Division IV of the Manhattan Project Technical Series.

* This work was originally reported in Manhattan Project Report CC-3148 (June 1, 1945); see also Plutonium Project Record IX B, 12.1.2.

** Now at University of California at Los Angeles.

[1] S. Katcoff, Phys. Rev. **72**, 1160 (1947).

The Conductivity of Metals at Microwave Frequencies*

B. SERIN
Physics Department, Rutgers University, New Brunswick, New Jersey

November 7, 1947

IT is the purpose of this note to point out that the application of the free electron theory to the problem of metallic conductivity at microwave frequencies leads to conclusions about the temperature dependence of r-f conductivity which seem to have been overlooked.

We consider an electromagnetic wave of frequency ν with the electric vector polarized in the x direction incident in the z direction on a metal whose surface lies in x-y plane, so that inside the metal the electric field equals $E(z, t) = Re\{E_{0x}e^{2\pi i\nu(t-Mz/c)}\}$, where E_{0x} = amplitude of the electric vector, t = time, M = complex index of refraction of the metal, and c = velocity of light in vacuum. In the presence of this field, the distribution function, $f(\mathbf{k}, \mathbf{r})$, giving the number of electrons per unit volume at the point $\mathbf{r}$ having momentum $\mathbf{k}$, is a solution of the Boltzmann equation[1],

$$\frac{\partial f}{\partial t} - \frac{e}{\hbar}E(z, t)\frac{\partial f}{\partial k_z} + v_z\frac{\partial f}{\partial z} = -\left(\frac{f-f_0}{\tau}\right),$$

where e = electronic charge, $\hbar$ = Planck's constant/2π, $k_z = x$ component of the electron momentum, $v_z = z$ component of the electron velocity, f_0 = distribution function in the absence of the field, and τ = relaxation time for the collision of an electron with the metal lattice.

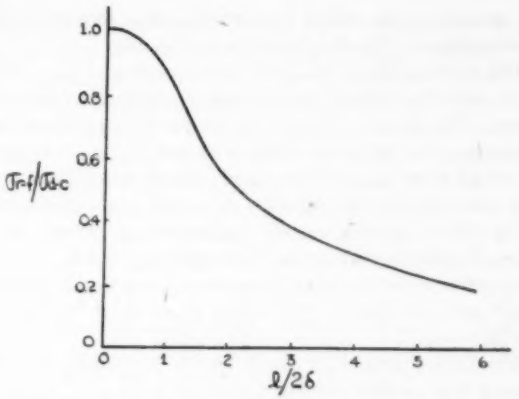

FIG. 1. The ratio of the r-f conductivity to the d.c. conductivity is shown plotted *versus* the ratio of the mean free path to twice the skin depth.

In view of the dependence of the field on z and t, we have attempted to find a solution of this equation without neglecting any of the terms. For the case where the distribution function f differs only slightly from the equilibrium Fermi-Dirac function f_0, the differential equation has a particular solution

$$f = f_0 + \frac{e}{\hbar}\frac{\partial f_0}{\partial k_z}\tau\ Re\left\{\frac{E(z, t)}{1+2\pi i\nu\tau-2\pi i\nu Mv_z\tau/c}\right\}.$$

This solution reduces to the usual solution in the limit $\nu = 0$.

The current density is found by multiplying f by v_z and averaging over momentum space. If this is carried out for the case of free electrons and the conduction current is separated from the displacement current, it is found that the ratio of the r-f conductivity (σr-f) to the d.c. conductivity (σd.c.) in the microwave region is a function only of

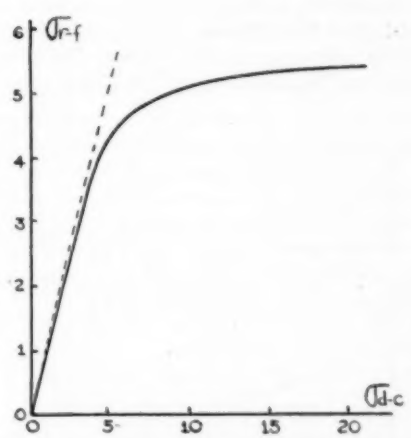

FIG. 2. The theoretical curve of the r-f conductivity *versus* the d.c. conductivity is shown for the metal silver. The r-f frequency was assumed to be 10^4 mc/sec. The σ's are in units of the value at 0°C.

the quantity $l/2\delta$, where l=electron mean free path and δ=skin depth. This function is shown in Fig. 1.

The calculation of $\sigma_{r\text{-}f}/\sigma_{d.c.}$ for any given l (i.e., for a $\sigma_{d.c.}$) must be carried out self-consistently since δ depends on $\sigma_{r\text{-}f}$. The theoretical curve of $\sigma_{r\text{-}f}$ at 10^4 megacycle/sec. *versus* $\sigma_{d.c.}$ for the metal silver is shown in Fig. 2. It is to be noted that $\sigma_{r\text{-}f}/\sigma_{d.c.}$ decreases rapidly with increasing $\sigma_{d.c.}$. $\sigma_{d.c.}$ may be increased by decreasing the temperature.

The above results are in qualitative agreement with recent experiments performed on lead[2,3] at M.I.T.

At infra-red frequencies, the effect of skin depth is again small and one obtains the usual expression[4] for the r-f conductivity.

The author wishes to thank Dr. H. C. Torrey for suggesting this problem to him.

* This work was supported in part by funds provided by the Research Corporation, F. G. Cottrell Grant, and by the Rutgers University Research Fund.

[1] A. H. Wilson, *The Theory of Metals* (Cambridge University Press, 1936), pp. 3, 158.

[2] J. C. Slater, private communication.

[3] J. G. Daunt has recently informed the author that A. B. Pippard of the Royal Society Mond Laboratory, England, has several papers in press in the Proc. Roy. Soc. on both the experimental and theoretical aspects of this subject.

[4] See reference 1, p. 123ff.

Abnormality in Cosmic-Ray Absorption in Lead in Low Latitudes*

W. F. G. Swann and P. A. Morris
Bartol Research Foundation of the Franklin Institute, Swarthmore, Pennsylvania
October 27, 1947

THE apparatus used comprised two cosmic-ray telescopes in parallel, each supplied with five counter trays. Lead could be placed between trays 3 and 4 and between trays 4 and 5. Triple coincidences were observed between trays 3, 4, and 5.[1] Six centimeters of lead were placed above the apparatus to shield out electrons and a shield was also placed around the top tray.

In taking the aforementioned observations, and in order to allow for possible variations of the cosmic-ray intensity throughout those observations which extended over about ten days, the plan was not to complete the observations for any one lead thickness, a, and then pass on to another thickness, b, but to take a few observations for all thicknesses ranging from the smallest to the largest, then another few observations with thicknesses ranging from the largest to the smallest, then another set ranging from the smallest to the largest, and so on. In this manner, each thickness of lead was tested with rays which, on the average, were of exactly the same kind. Also the procedure was to make observations without lead, with 1 cm of lead between trays 3 and 4 and another between trays 4 and 5, then with two 1-cm slabs between trays 3 and 4 and two between trays 4 and 5, proceeding in this way until a totality of 20 cm of lead had been reached. Observations were made with each of the two telescopic units, and the results were combined.

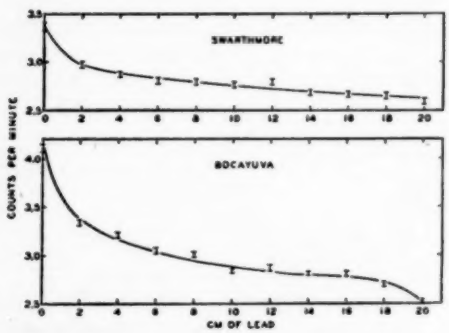

FIG. 1. Coincidence rate *vs.* lead-absorber thickness.

Figure 1 shows the data obtained at Bocayuva (magnetic latitude 7°S) and at Swarthmore (magnetic latitude 51.5°N). The Bocayuva curve shows an approximately 10 percent drop at a total lead thickness of 22 cm. Experiments performed by S. V. Chandrashekhar Aiya at Bangalore show a 5 percent drop at 21 cm of lead. On the other hand, the Swarthmore curve shows no appreciable drop. These facts seem to invite the belief that the phenomenon resulting from a component of the radiation which is present in low latitudes is absent in high latitudes. This aspect is being developed in detail by one of us elsewhere.

One element rather difficult to reconcile is the fact that the altitude at Bocayuva is 2300 feet while that at Bangalore is 3100 feet. The difference in lead absorption is the equivalent of about 7 cm of lead. It is rather surprising, therefore, that the phenomenon seems to take place at approximately the same lead thickness at Bocayuva as at Bangalore, suggesting that it is concerned purely with something happening in the lead as distinct from something depending upon the energy of the rays.

* Supported by funds from Navy Contract N6ori-144 and from the National Geographic Society, also by airplane services from the U. S. Army Air Force.

[1] The other trays were for another purpose.

Microwave Spectra: Methyl Cyanide and Methyl Isocyanide*

Harold Ring,** Howard Edwards, Myer Kessler,** and Walter Gordy
Department of Physics, Duke University, Durham, North Carolina
November 7, 1947

THE first and second rotational transitions of CH_3CN and of CH_3NC have been studied in the microwave region.

Nuclear Effects. The spectrum of CH_3CN shows a definite hyperfine structure which can be attributed to the quadrupole moment effects of the nitrogen nucleus. Figure 1 shows the $J=0$ to $J=1$ transition, which is split into only three components by the nuclear effects. Accurate measurement of the separation of the components was made by a method evolved in this laboratory.[1] The bars give the theoretically predicted hyperfine structure. The magnitude of the coupling coefficient, $eQ(\partial^2 V/\partial z^2)$, thus deter-

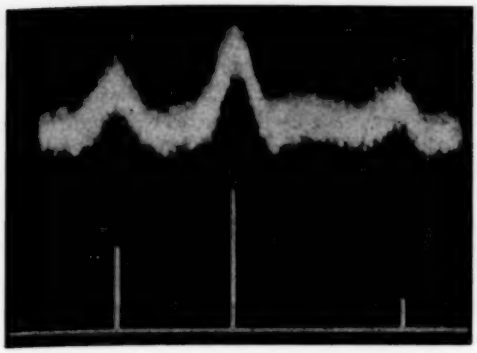

FIG. 1. Theoretical and observed hyperfine structure in the $J=0$ to $J=1$ rotational transition of CH_3CN occurring at 18,400 Mc. Observed spacing of lines are 1.40 Mc/sec. and 2.10 Mc/sec. from central line.

mined is 4.67±0.10 Mc. This differs somewhat from that given by Townes and his co-workers[2] for the nitrogen coupling in ClCN, 3.66±0.15 Mc. This difference is significantly greater than that allowed by the probable experimental errors and must be attributed to differences in the electronic structures of the molecules. An even greater difference is shown for CH_3NC, for which the hyperfine structure could not be resolved. This indicates that the absolute value of the coupling factor $eQ(\partial^2V/\partial z^2)$ must be less than about one megacycle and implies a rather symmetric distribution of electronic charge about the nitrogen nucleus.

In calculating the hyperfine structure, the formula,

$$T_F=\left(eQ\frac{\partial^2V}{\partial z^2}\right)\left(\frac{3K^2}{J(J+1)}-1\right)\frac{\frac{3}{4}C(C+1)-I(I+1)J(J+1)}{2I(2I-1)(2J-1)(2J+3)},$$

where

$$C=F(F+1)-I(I+1)-J(J+1)$$

was used. This formula differs slightly from that given by Coles and Good[3] and that used in previous papers[4] from this laboratory. Though both formulas give correct positions of the lines, they yield different coupling coefficients except when $I=\frac{1}{2}$. The different formulas apparently arise from different definitions of quadrupole coupling existing in the literature. The above formula is used so that the coupling coefficient may be compared with the results of Townes and his associates.

Molecular Properties. The structure of the second rotational line of CH_3CN ($J=1$ to $J=2$ transition), observed at 36,800 Mc, reveals a purely symmetric top configuration for this molecule. The moment of inertia, I_B, determined from the present measurements is 90.9×10^{-40} g cm², compared with 92.8×10^{-40} g cm², computed from the dimensions determined by electron diffraction.[5] For the $J=0$ to $J=1$ transition of CH_3NC a single line was observed at 1.488-cm wave-length. However, in the region of the second rotational transition, about 7.45-mm wave-length, a group of eight lines was observed, dispersed over a region of 330 Mc. These are too widely spaced to represent hyperfine structure caused by the nitrogen nucleus. An attempt is being made to interpret the spectrum on the basis that the molecule is a very slightly asymmetric top, i.e., that the CNC group is not quite linear. Because the compound is rather unstable some of the lines may be due to impurities. We are attempting to determine whether this is true, or if any of the lines arise from molecules in excited vibrational states. Assuming the symmetric top configuration, the moment of inertia is 83.2×10^{-40} g cm², in satisfactory agreement with the most recent electron-diffraction data,[6] from which the moment of inertia, I_B, is determined as 84.8×10^{-40} g cm².

We wish to thank Dr. Walter M. Nielsen for his interest in the project.

* This research was supported by a grant-in-aid from the Research Corporation of New York and by Contract No. W-28-099-ac-125 with the Army Air Forces, Watson Laboratories, Air Materiel Command.

** Frederick Gardner Cottrell Fellow.

[1] R. L. Carter and W. V. Smith (to be published).
[2] C. H. Townes, A. N. Holden, J. Bardeen, and F. R. Merritt, Phys. Rev. 71, 644 (1947).
[3] D. K. Coles and W. E. Good, Phys. Rev. 70, 979 (1946).
[4] W. Gordy, A. G. Smith, and J. W. Simmons, Phys. Rev. 72, 249 (1947); 72, 344 (1947).
[5] L. Pauling, H. D. Springall, and K. J. Palmer, J. Am. Chem. Soc. 61, 927 (1939).
[6] W. Gordy and L. Pauling, J. Am. Chem. Soc. 64, 2952 (1942).

Sea Level Latitude Effect of Cosmic Radiation*

PETER A. MORRIS, W. F. G. SWANN, AND H. C. TAYLOR
Bartol Research Foundation of the Franklin Institute, Swarthmore, Pennsylvania

October 27, 1947

ON a recent voyage from Rio de Janeiro to Boston the vertical intensity of the total and hard components of the cosmic radiation were measured with a Geiger counter telescope apparatus. The hard component was measured both through 8 cm and 16 cm of lead.

The apparatus consisted of two identical units each with five trays of nine Geiger counters in parallel. The individual counting rates of the counters, their dead times, and the resolving time of the circuits were sufficiently small to preclude their contributing to any spurious effects on the coincident rates of the telescopes.

While the vertical intensity of the total and hard components of the radiation are measured directly, the intensity of the soft component must be arrived at by the difference between the other measured quantities. Such a method gives rise to considerably larger probable errors in the determination of the latitude effect, and the method has been criticized for this reason. Certain observers have made an effort to circumvent this difficulty by measuring the radiation underneath from 1 to 2 cm of lead to determine the latitude effect of the soft component. In any event,

TABLE I. Percentage diminution in the vertical intensity.

Telescope	Total radiation No lead	Hard component 8 cm	Hard component 16 cm	Soft component 8-cm diff.	Soft component 16-cm diff.
1 and 2	5.05±0.55	5.26±1.27	5.36±1.33	4.3±4.6	4.5±4.3
1	5.34±0.77	4.96±0.92	6.20±0.97	6.0±2.8	3.7±2.9
2	4.76±0.75	5.56±0.88	4.51±0.91	2.6±3.7	5.3±3.2
Combined		5.32±0.46		4.46±0.61	

previous determinations have been somewhat ambiguous, as is evidenced by the fact that Auger's[1] data have been interpreted to give a ten percent latitude effect for the soft component by Heisenberg[2] and a zero percent latitude effect by Heitler.[3]

We have paid particular attention to the estimates of probable errors in our calculations, based on the individual probable errors of the individual intensities of the components as measured in the high latitudes and at the equator. The probable errors of the intensities are estimated in the usual manner from the total number of counts obtained for a given condition. The probable errors are derived for the determination of the latitude effects using standard statistical concepts.

In Table I we have summarized the results for the separate telescopes and for the combined results. It is interesting to note that the latitude effects for the total radiation and the hard component are smaller than have been reported previously. (Arley[4] summarizes previous results as indicating a sea level latitude effect of from 10 to 20 percent.) Of greater interest, however, is the fact that our data strongly indicate the existence of a sea level latitude effect for the soft component whose magnitude is of the same order as that for the hard and total radiation.

If the soft component is defined as that radiation which is absorbed in 10 cm of lead, the radiation is largely restricted, except for Auger showers, to that which is formed below one kilometer from the earth's surface, by mesotron decay and knock-on processes from the mesotron component existing near sea level, rather than pair formation having to do with primary electrons or with electrons produced near the top of the atmosphere. It is not surprising to us, therefore, to find the latitude effects of the hard and soft components of comparable magnitude.

* Supported by funds from Navy Contract N6ori-144 and from the National Geographic Society, also by airplane services from the U. S. Army Air Force.

[1] P. Auger, Nature 133, 138 (1934).
[2] W. Heisenberg, *Vorträge über Kosmische Strahlung* (1943).
[3] W. Heitler, Nature 140, 235 (1937).
[4] N. Arley, Mat.-Fys. Medd. 23, No. 7.

Total Cross Sections of Nuclei for 90-Mev Neutrons

LESLIE J. COOK, EDWIN M. MCMILLAN, JACK M. PETERSON, AND DUANE C. SEWELL
Radiation Laboratory, University of California, Berkeley, California
October 30, 1947

GOOD geometry neutron attenuation measurements have been made, using the 184-inch cyclotron as a neutron source and carbon disks as detectors. The line-up of equipment was as follows:

1. Source: This was a $\frac{1}{2}$-in. Be target inside the cyclotron traversed by 190-Mev deuterons, giving neutrons of 90-Mev mean energy and an energy distribution having a width of about 27 Mev between points of half-maximum intensity.[1,2]

2. Neutron window in tank wall in line of neutron beam: This window is of spun aluminum, $\frac{1}{8}$ in. thick×32-in. diameter, and its purpose is to reduce the amount of scattering material in the path of the beam.

3. Detector: A carbon disk $\frac{1}{8}$ in. thick×$1\frac{11}{16}$-in. diameter was placed 17 feet from the source. This had the 20.5-min. C^{11} induced in it by the $(n, 2n)$ reaction; the activity was of the order of a few thousand counts per minute after a 1.5-minute exposure.

4. Scattering blocks: These were $2\frac{1}{2}$ in. in diameter and of various lengths and were placed about midway between source and detector.

5. Monitor: A carbon disk similar to the detector was placed between the source and the scattering block.

Source, monitor, scatterer, and detector were lined up accurately with the aid of a cathetometer. Each measurement consisted of a determination of the ratio (detector activity/monitor activity) with G-M counters. This was done with no scatterer (blank), with a very long copper scatterer (background), and with the scatterer whose attenuation was being measured. The background, arising from scattering in the window, sample supports, and other surrounding material, was 6 percent of the blank. Absorption curves were run on paraffin, carbon, aluminum, and copper, and these were exponential as far as they could be followed accurately in the presence of the background (to about 1/20 of the initial intensity). The most accurate cross-section measurements were made with scatterers about one mean free path long, on which repeated measurements were made to improve the statistics. The spread found in these individual measurements was what was expected from the number of counts taken.

Li, Be, C, Mg, Al, Cu, Zn, Sn, Pb, and U were done as the elements. H was done by taking the difference between carbon and paraffin blocks having about the same attenuation, the readings being taken alternately on the two blocks. The difference $D-H$ was found by a similar direct comparison of heavy and light water contained in thin-walled aluminum cells. O, N, and Cl were computed from the attenuations in water, melamine, and carbon tetrachloride. The statistical mean errors in the direct measurements are 1 percent, and greater than this in the difference measurements; the quoted mean errors include an additional 1 percent added to allow for other possible sources of error. A computed correction has been made for the error caused

TABLE I.

Substance	Total cross section (barns) (10^{-24} cm^2)
H	0.083 ±0.004
*D	0.117 ±0.005
Li	0.314 ±0.006
Be	0.431 ±0.008
C	0.550 ±0.011
N	0.656 ±0.021
O	0.765 ±0.020
Mg	1.03 ±0.02
Al	1.12 ±0.02
Cl	1.38 ±0.03
Cu	2.22 ±0.04
Zn	2.21 ±0.04
Sn	3.28 ±0.06
Pb	4.53 ±0.09
U	5.03 ±0.10

* The difference $D-H$, which may be interpreted roughly as the $n-n$ cross section, is good to ±0.003.

by neutrons diffracted into the detector by the scatterers; its greatest value is about 3 percent. The results are given in Table I.

If these cross sections are expressed in terms of a collision radius R, were $\sigma=2\pi R^2$, and plotted against $A^{\frac{1}{3}}$ as done by Sherr,[3] it is seen that the values from Li to U lie on a nearly smooth curve, and are all below Sherr's line [$R=(1.7+1.22A^{\frac{1}{3}})\times10^{-13}$ cm] for 25-Mev neutrons. The difference becomes less for the heavier nuclei, as if the values are tending to approach a line near his. One possible interpretation is to say that the lighter nuclei are partially transparent, and approach opacity with increasing A. Dr. Serber has shown[4] that such an interpretation is well justified. An empirical formula that fits the data from Li to U very well is: $R=(0.5+1.37A^{\frac{1}{3}})[1-\exp(-0.49A^{\frac{1}{3}})]\times10^{-13}$ cm. This formula is not intended to have any theoretical significance, but may be useful for purposes of interpolation. From Li to O, the cross sections are nearly proportional to A. A complete account of this work will be published later.

This paper is based on work performed under Contract No. W-7405-eng-48, with the Atomic Energy Commission in connection with the Radiation Laboratory, University of California, Berkeley, California.

[1] A. C. Helmholz, E. M. McMillan, and D. C. Sewell, Phys. Rev. 72, 1003 (1947).
[2] R. Serber, Phys. Rev. 72, 1007 (1947).
[3] R. Sherr, Phys. Rev. 68, 240 (1945).
[4] R. Serber, Phys. Rev. 72, 1114 (1947).

The Uncertainty Principle and the Yield of Nuclei Formed in Fission

P. F. Gast
The General Electric Company, Hanford Engineer Works, Richland, Washington
September 29, 1947

A RECENT letter by Dempster[1] discussed the yield curve[2] for the nuclei formed in fission from the standpoint of the liquid-drop model. As an alternative, the hypothesis is here advanced that the yield curve is related to the Heisenberg uncertainty principle in much the same ways as the line breadth of atomic spectra.[3]

Just before the moment of separation of the two fragment nuclei, produced by the fission process, nucleons may be pictured as passing through the area of contact caused by the "thermal" agitation of the particles forming the nucleus. The quantum-mechanical waves associated with these particles have an extent comparable with that of the nuclei themselves, and thus the time for a wave to pass the contact surface will be Bethe's[4] "characteristic nuclear time," 3×10^{-22} sec. The uncertainty in the time of final break between the fragments must be of a comparable magnitude.

From the width of the yield curve at half-maximum and Dempster's curve connecting the masses of the fragments with the energy a value, $\Delta E\approx18$ Mev, is obtained for the uncertainty in the energy. The use of the relation

$$\Delta E\Delta t\approx h/2\pi$$

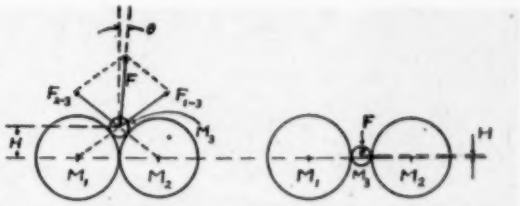

FIG. 1. Curve A gives the experimentally observed fission yields on a logarithmic scale. Curve B is calculated assuming cores of 60- and 16-mass units for the heavy and light fragments, respectively. Curve C gives the calculated yields when all nucleons have equal probability of being in either fragment.

then gives $\Delta t\approx3.6\times10^{-22}$ sec., in reasonably good agreement with the value postulated above.

This suggests the possibility that some of the nucleons, at least, have wave functions giving them an appreciable probability of being in either fragment at the time of fission, and that the yield curve is the net result of the various probabilities for the nucleons involved. The yield curve itself gives a clue as to the number of nucleons involved. Since the difference between the two maxima of the curve is 44 mass units, we assume "cores" for the two fragments differing by that amount, taking for the heavy fragment a core of mass number 60 (the nucleus having the largest known negative packing fraction[5]) and for the light fragment mass number 16. The remaining 158 nucleons are assumed to have equal probability of being in either fragment. Figure 1 shows a curve calculated from the well-known theory of combinations and based on the above assumptions along with the observed curve. The calculated curve gives a value of 6.3 percent at the maxima and underestimates the yield near the maxima while overestimating it in more remote regions. This may arise because neutrons and protons are not distinguished in the calculation. The curve which would be obtained when all nucleons have equal probability of being in either fragment is also shown for comparison.

[1] A. J. Dempster, Phys. Rev. 72, 431 (1947).
[2] The Plutonium Project, Rev. Mod. Phys. 18, 539 (1946).
[3] W. Heitler, *The Quantum Theory of Radiation* (Clarendon Press, Oxford, 1936), p. 113.
[4] H. A. Bethe, Rev. Mod. Phys. 9, 72 (1937).
[5] J. Mattauch, *Nuclear Physics Tables* (Interscience Publishers, Inc., New York, 1946), p. 113.

Microwave Spectrum Frequency Markers*

Robert L. Carter and William V. Smith
Department of Physics, Duke University, Durham, North Carolina
November 8, 1947

MEASUREMENT of the separation of the satellites of NH_3 microwave spectrum lines exhibiting quadrupole splitting has been reported by Strandberg and others,[1] and subsequently by Watts and Williams.[2] In their experiments the microwave oscillator was frequency modulated by the application of a variable intermediate frequency component of known frequency to the reflector voltage. This caused the microwave oscillator simul-

FIG. 1. 3,3 absorption line of $N^{15}H_3$ with superimposed inverted marker ladder just inside inner left-hand fine structure line. Ladder spacing is 267 kilocycles.

taneously to generate appreciable intensities of radiation of three or more frequencies, differing from one another by the frequency of the modulating voltage. The resultant radiation was passed through an absorption cell and slowly swept through the frequency of a spectrum line. The spectrum line then displayed appeared to have been flanked by two or more "ghost" lines, which were separated from the main line by the modulation frequency or a multiple thereof. These "ghosts" were used as calibrated markers with which to measure absolutely the separations of satellite lines.

The former method is difficult to apply when narrow, fairly strong lines cannot be obtained or when there are several closely spaced lines. The method to be described gives a movable marker ladder, of known spacing, independent of the quality of the absorption spectrum being studied. This is achieved through the introduction of the radiation from an auxiliary microwave oscillator into the wave guide leading to the detector crystal. When the main oscillator frequency is swept through the frequency of the auxiliary oscillator, the resultant interference causes a narrow blurred pattern to be displayed on the detector oscilloscope. This pattern is attributable to the audio-frequency noise produced by beating of the radiation from the two oscillators during the moment of near synchronization. Since the relative phases of the two oscillators are random, and since both execute small amplitude, rapid fluctuations in frequency, successive patterns are irregular and dissimilar.

A narrower and more distinct pattern can be obtained if a small amount of power from the auxiliary oscillator is allowed to feed back into the main oscillator. The power fed back results in a pulling of the oscillators into synchronization as they approach the same unperturbed frequency. The relative phases of the two oscillators will be a function of the difference of the unperturbed frequencies so that the same oscilloscope pip pattern is reproduced on successive sweeps. Power can be fed back through the use of a directional coupler and attenuator. The pattern can be made to appear as an increase in signal strength, a decrease in signal strength, or both in succession, by adjustment of the relative oscillator phases by means of a variable length line, or "squeeze section." The pip can be split into a ladder through the application of an intermediate frequency voltage to the reflector of the auxiliary oscillator. The spacing between the pips is the applied intermediate frequency or a multiple thereof. The markers thus obtained have been used with spacings varying from 0.2 to 10 megacycles, and have a width of 50 kilocycles or less. The accompanying photograph (Fig. 1) of a marker ladder displayed with the familiar NH_3 3,3 line and satellites qualitatively illustrates the results obtainable. Visually the marker pips appear sharper than shown in the photograph, which was blurred by small variations during the time of exposure.

It is believed that a similar direct mixing method could be used in the superposition upon microwave spectra of standard frequency markers obtained from frequency multiplier arrays or oscillators stabilized upon standard spectrum lines.

* The research described in this report was supported by Contract No. W-28-099-ac-125 with the Army Air Forces, Watson Laboratories, Air Materiel Command.

[1] Dailey, Kyhl, Strandberg, Van Vleck, and Wilson, Phys. Rev. 70, 984 (1946).
[2] R. J. Watts and D. Williams, Phys. Rev. 72, 263 (1947).

Stark Effect in High Frequency Fields

C. H. TOWNES AND F. R. MERRITT
Bell Telephone Laboratories, Murray Hill, New Jersey
November 8, 1947

STARK effect on molecular absorption lines in the microwave region has been reported in which constant or d.c. Stark fields[1] and a.c. Stark fields of frequency up to several hundred kilocycles are used.[2] It is possible to oscillate the Stark field applied to molecules at such a rapid rate that one or many oscillations occur during a single absorption process. In this case ordinary Stark effect breaks down and a new type of spectrum appears.

A solution of the time-dependent wave equation for a molecule subjected to a varying field $E_0 \cos 2\pi\nu_0 t$ can be obtained by perturbation methods, and the effect of the field on its spectrum shown to be as follows:

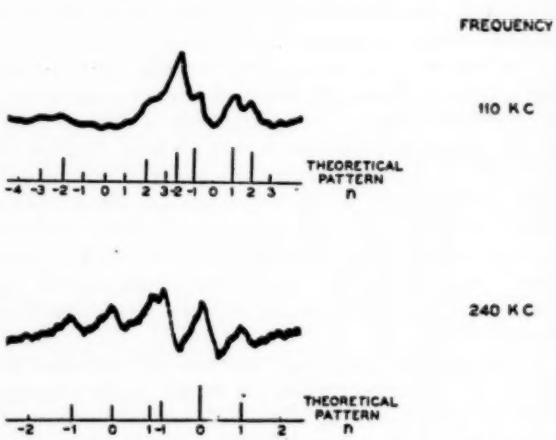

FIG. 1. Stark effect on OCS $J=1 \rightarrow 2$ line (25,326 mc) with applied fields of low and high frequency.

(1) When ν_0 is much smaller than the half-width of the molecular absorption lines, each Stark component appears to follow the oscillating field. Thus if a particular component shows only second-order Stark displacement of magnitude $\Delta\nu = aE^2$ in a static field of strength E, in the a.c. field, its displacement as a function of time will be $aE_0^2 \cos^2 2\pi\nu_0 t$.

(2) When ν_0 is of the same order or larger than the half-width of the absorption line, each Stark component breaks up into a number of fixed lines with spacings determined by the frequency ν_0 and relative intensities by the ratio of ν_0 to the magnitude of the Stark displacement. Thus, assuming only second-order Stark effect as in case (1), frequency shifts of lines produced from a single Stark component are given by $aE_0^2/2 \pm 2n\nu_0$ where n is any integer. Intensity of any line corresponding to a particular value of n is given by $IJ_n^2(aE_0^2)/(4\nu_0)$, where I is the intensity of the Stark component for a static field. Thus if ν_0 is very large, $aE_0^2/4\nu_0$ is small, and all components are of small intensity except the one for $n=0$. Each Stark component appears then as a single line displaced an amount $aE_0^2/2$, the average of its displacement if it "followed" the field. If $aE_0^2/4\nu_0$ is not small, a number of lines corresponding to various values of n may be observed. Similarly, for first-order Stark effect of magnitude bE in a static field, frequency shifts become $\pm n\nu_0$ and corresponding intensities $IJ_n^2(bE_0)/(\nu_0)$.

Figures 1 and 2 show the variation in Stark pattern of the $J=1\rightarrow 2$ line of OCS with variation in frequency ν_0 of the applied field. Stark effect, which in this case is second order, was obtained and observed in the usual way on an oscilloscope trace. The gas OCS was chosen to demonstrate this effect because of its convenience and because no complications arising from nuclear quadrupole effects are present. Part of the gas-absorption path was not subjected to an electric field, which produced a weak undisplaced line as a reference in addition to the two Stark components shown under d.c. field at the top of Fig. 1. All spectra shown are on the same frequency scale and at about the same pressure (6×10^{-3} mm Hg) of OCS. Relative intensities of the spectra for various applied frequencies are not accurately represented. From Fig. 1 it is evident that at 1 kc the two Stark lines simply follow the field, the d.c. field strength and the peak a.c. field for a given displacement being the same. At 1200 kc the pattern resembles the d.c. pattern, peak voltage being $\sqrt{2}$ times the d.c. voltage required for the same displacement. Figure 2 shows intermediate conditions. At 110 k.c. the Stark lines no longer "follow" the field, although the general intensity distribution is similar to that expected for the same field intensity at lower frequency. This is because intensity for the lines for which $n=0$ is small, the main intensity falling at $n=1$ or 2. At 240 kc the lines corresponding to $n=0$ are most intense, although those for $n=1$ are still prominent. Theoretical intensities are plotted below each spectrum for comparison. In every case extra intensity at the center of the pattern is due to the undisplaced line of gas not subjected to a field.

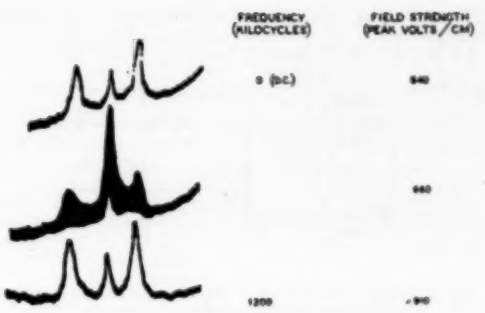

FIG. 2. Stark effect on OCS $J=1\rightarrow2$ line (24,326 mc) showing additional lines produced by fields of intermediate frequencies. Peak field strengths of both fields are 640 volts/cm.

The Stark patterns obtained at any one frequency vary considerably with field strength, some cases displaying several more lines than those shown here. In every case the positions and relative intensities of lines appear to agree well with theoretical expectations described briefly above. This agreement provides a new test of the time-dependent wave equation.

[1] Dakin, Good, and Coles, Phys. Rev. 70, 560 (1946).
[2] R. H. Hughes and E. B. Wilson, Phys. Rev. 71, 562 (1947).

Excess-Defect Germanium Contacts

S. BENZER
Department of Physics, Purdue University, Lafayette, Indiana
October 27, 1947

IN a recent letter,[1] L. Sosnowski describes interesting rectification and photo-voltaic effects in lead sulfide films attributed to an internal potential barrier at the contact between N-type (excess) and P-type (defect) regions of the film. It is also suggested that such effects might be expected to occur in germanium and silicon.

This is indeed the case for germanium. In the course of a NDRC project for the development of germanium point contact rectifiers, photoelectric effects were found[2,3] which were shown to be due to just such internal transitions between N- and P-type regions. Figure 1 illustrates "photo-

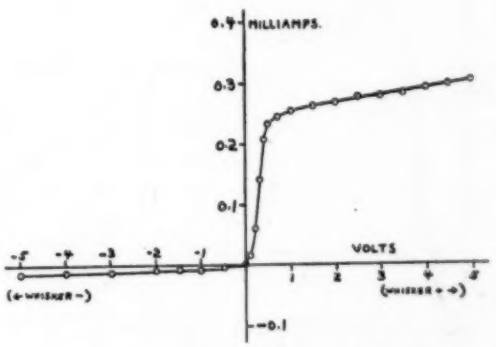

FIG. 1. Current-voltage characteristic of a germanium "photo-diode" (25°C).

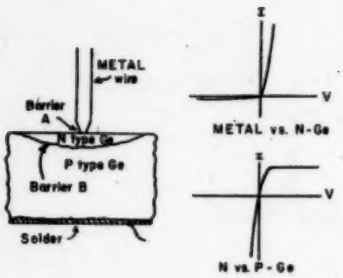

FIG. 2. Structure of a photo-diode and characteristics of the individual rectifying barriers (schematic).

diode" type of characteristic obtained when a metal point contacts certain areas on inhomogeneous germanium crystals. At low voltage, this characteristic is typical of a contact between metal and *N*-type Ge, but a marked saturation occurs in the forward (conducting) direction at higher voltage. Investigation showed that the geometry of Fig. 2 applies to such cases. There are two rectifying barriers involved, one of small area between metal and *N*-type Ge, and one of larger area between *N*- and *P*-type Ge. Figure 2 shows the characteristics for these individual rectifying barriers, which combine in series to produce the curve of Fig. 1, each half of the curve representing the reverse direction of one of the contacts.

If the layer of *N*-type Ge is thin, light can reach the $N-P$ boundary, causing pronounced photo-effects. Figure 3 illustrates the photo-conductive effect. The photo-current is instantaneous (within 10^{-6} sec.), varies linearly with light intensity, but varies little with voltage and temperature, thus appearing to be a primary photo-effect. Sensitivities of several milliamperes per lumen of white light are observed. Maximum sensitivity occurs at around 1.3μ with threshold at 1.5μ, the latter corresponding to an activation energy of 0.8 ev. With no voltage applied, a photo-voltaic effect occurs, the current being enhanced in this case by increasing the size of the metal contact in order to reduce its series resistance.

The saturation current in the dark is extremely sensitive

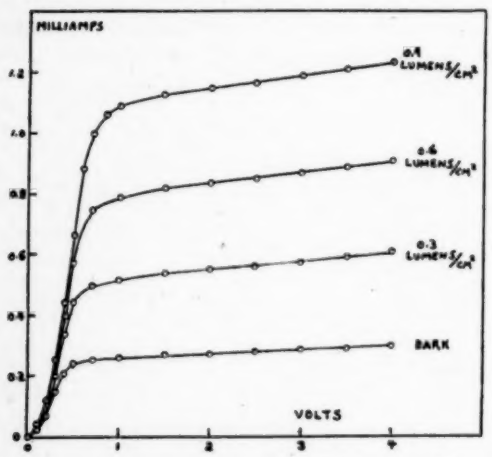

FIG. 3. Effect of illumination on photo-diode characteristic (25°C).

to temperature, changing about a factor of two in a 10°C temperature change. The variation is as $i \sim \exp[-e\phi/kT]$, where ϕ is found to have a value around 0.7 volt. This is the order of the width of the forbidden band in germanium as determined from resistivity *vs.* temperature measurements,[4] and therefore agrees with the barrier height to be expected for a contact between *N*- and *P*-type Ge.

Deliberate contacts between different specimens of germanium, including *N*- and *P*-type, have been tried[5] and give the sign of rectification expected. The geometry of Fig. 2 leads to greater photosensitivity, however, since the sensitive layer is more easily accessible to illumination. Thin films, as in the case of lead sulfide, would probably be most desirable.

In addition to photo-conductive and photo-voltaic effects, there are associated with these barriers negative resistance and self-oscillations.[6] A detailed description of all these phenomena will be published shortly.

[1] L. Sosnowski, Phys. Rev. **72**, 641 (1947).
[2] S. Benzer, "Photoelectric effects in germanium" NDRC report 14-580, Oct. 31, 1945
[3] S. Benzer, Phys. Rev. **70**, 105 (1946).
[4] K. Lark-Horovitz and V. A. Johnson, Phys. Rev. **69**, 258 (1946).
[5] S. Benzer, Phys. Rev. **71**, 141 (1947).
[6] S. Benzer, Phys. Rev. **72**, 531 (1947).

The Microwave Spectrum of Iodine Monochloride at 4½ Centimeters Wave-Length*

RICHARD T. WEIDNER**
Sloane Physics Laboratory, Yale University, New Haven, Connecticut
November 8, 1947

THE $J=0$ to $J=1$ absorption lines of the pure rotational spectra of ICl^{35} and ICl^{37} have been detected with a microwave spectrometer covering the frequency range of 6500 to 7200 megacycles. The absorption was observed as a lowering of the loaded Q, Q_L, of a resonant cavity into which the gas was introduced, the change in Q_L being measured by noting the fractional decrease in power, $\Delta P/P$, transmitted through the cavity at resonance upon introduction of the gas.[1] For a frequency ν the power absorption coefficient, α, in cm^{-1} is given by

$$\alpha = \pi\nu/cQ_L . \Delta P/P,$$

where c is the velocity of light in vacuum.

A Klystron oscillator stabilized in frequency to one part in 10^6 by the Pound[2] circuit and a cavity with $Q_L = 30{,}000$ were used. The rectified current of about one microampere from the crystal detector, which was proportional to the received microwave power, fed into a photo-cell galvanometer amplifier whose output was applied to a recording potentiometer. With the cavity tuned close to its resonance, the frequency of the oscillator was swept through several kilocycles to give a smooth recorder trace of the maximum transmitted power by slightly changing the temperature, and, therefore, the resonance frequency of the wave meter which controlled the frequency in the stabilization circuit. In this way the effect of the dielectric constant of the absorbing gas in shifting the resonance frequency could be easily compensated. The minimum measurable power absorption coefficient was 6×10^{-8} cm^{-1}.

The absorption peaks of the ICl^{35} and ICl^{37} molecules were found at 6980 and 6684 megacycles, respectively, with a possible error of one part in 10^3. The following values for the rotational constants, B_e, moments of inertia, I, and interatomic distances, r_e, have been calculated:

	B_e	I	r_e
ICl^{35}	0.1167 cm^{-1}	2.397×10^{-38} g/cm^2	2.303A
ICl^{37}	0.1118 cm^{-1}	2.502×10^{-38} g/cm^2	2.303A

The value of B_e for ICl^{35} obtained here is in disagreement with that of Curtis and Patkowski,[3] 0.1141 cm^{-1}, obtained from an analysis of the vibration-rotation bands of ICl^{35}.

The absorption peak of 10^{-6} cm^{-1} for ICl^{35} is in agreement with that given by the theory of Van Vleck and Weisskopf[4] for a choice of the line-breadth parameter, $\Delta\nu/c$, at atmospheric pressure of 0.08 cm^{-1} and assuming a linear $\Delta\nu/c$-pressure relationship. The measured half-breadths, linear in pressure over the 2 to 20-mm Hg pressure range investigated, were in harmony with this choice. A preliminary analysis of the line profiles shows the absorption in the wings of the lines to be in excess, by a factor 5 roughly, of that predicted by the Van Vleck-Weisskopf theory.

The author gratefully acknowledges the guidance of Professor R. Beringer in suggesting and supervising this work, and the generous loan of some microwave apparatus from the Radio Frequency Research Section of the Naval Research Laboratory.

* Assisted by the Office of Naval Research under Contract N6ori-44, Task Order II.
** Now at Rutgers University, New Brunswick, New Jersey.
[1] B. Bleaney and R. P. Penrose, Proc. Roy. Soc. 189, 358 (1947).
[2] R. V. Pound, Rev. Sci. Inst. 17, 490 (1946).
[3] W. E. Curtis and J. Patkowski, Phil. Trans. Roy. Soc. 232, 395 (1934).
[4] J. H. Van Vleck and V. F. Weisskopf, Rev. Mod. Phys. 17, 229 (1945).

The Crystal Structure of Element 43

Rose C. L. Mooney
Argonne National Laboratory, Chicago, Illinois
November 8, 1947

THE chemistry of element 43 was first studied by Perrier and Segrè,[1] from samples containing tracer quantities of technetium (Tc) produced by deuteron bombardment of molybdenum. More recently, a long-lived isotope has been found to be one of the products from U^{235} fission.[2] Lately, this long-lived, *beta*-active isotope has been produced by neutron bombardment of Mo.[3]

The material used in this work was a technetium preparation separated from fission products by G. W. Parker, J. W. Ruch, and J. Reed of the Clinton Laboratory. From this original sample, a number of chemical preparations in microgram amounts have been made by Dr. Sherman Fried of the Argonne Laboratory. Two of these proved to be the element itself. The fact that the sample was metallic technetium was shown conclusively by the characteristics of the x-ray pattern itself.

Technetium crystallizes in the hexagonal close-packed arrangement; that is to say, it is isomorphous with rhenium, ruthenium, and osmium. The cell, which contains two atoms of Tc, has the following dimensions:

$$a=2.735\pm0.001\text{A},\quad c=4.391\pm0.001\text{A},\quad c/a=1.604.$$

The calculated density, based on the atomic weight of 99, is 11.487 g/cm^3. Each Tc atom has twelve nearest neighbors. Six are at a distance of 2.735A—the cell translation—and six at a somewhat smaller distance, 2.704A.

[1] C. Perrier and E. Segrè, J. Chem. Phys. 5, 712 (1937).
[2] Plutonium Project Fission Product Survey, Rev. Mod. Phys. 18, 539 (1946).
[3] E. E. Motta, G. E. Boyd, and Q. V. Larson, Phys. Rev. 72, 1270 (1947).

Mass Spectrometric Study of Fission Element 43

Mark G. Inghram, David C. Hess, Jr., and Richard J. Hayden
Argonne National Laboratory, Chicago, Illinois
November 8, 1947

A SAMPLE of element 43 (Tc) separated from uranium fission products by Messrs. G. W. Parker, J. W. Ruch, and J. Reed of the Clinton Laboratories of the Monsanto Chemical Company was analyzed by a mass spectrometer in order to determine which of the possible fission isotopes have long lives. The existence of a Tc^{99} isotope with a half-life greater than forty years was first predicted by Seaborg and Segrè.[1] Glendenin, from experiments with fission products, set the half-life of a long-lived fission isotope of technetium at more than 3000 years.[2] A long-lived technetium activity was found in fission products by Lincoln and Sullivan,[3] and Schuman.[3] Motta, Boyd, and Larson obtained a half-life of 9.4×10^5 years with a sample prepared by neutron bombardment of molybdenum.[3]

The sample of fission technetium used for our work was distilled into the ionization chamber of a Nier-type spectrometer as NH_4TcO_4. The resolved ion currents were recorded by means of a vibrating reed electrometer and a Leeds and Northrup Speedomax recorder. The curves obtained in the Tc^+ ion position are shown in Fig. 1. Curve *a* is the plot of the 98–103 mass range before the technetium was distilled into the source. The six large peaks in the spectrum are due to doubly charged mercury ions which were used as mass standards. Curve *b* is a plot of the same

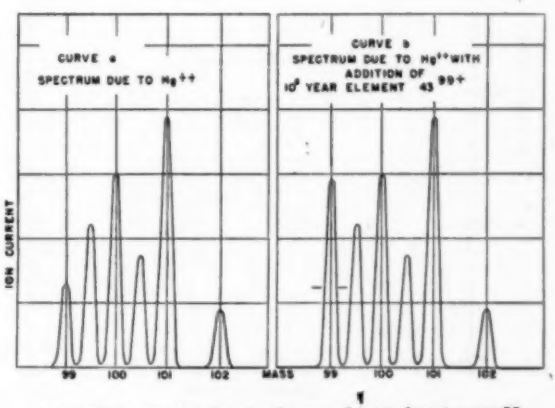

FIG. 1. Mass spectra showing increased intensity at mass 99 when technetium is added.

region obtained while the technetium was distilling into the source. The marked increase at mass 99 is immediately apparent. In addition to the increased peak at mass 99 shown in Fig. 1, new single peaks appeared at masses 115, 131, and 147, due to $Tc^{99}O^+$, $Tc^{99}O_2^+$, and $Tc^{99}O_3^+$, respectively. These results show that the technetium formed in fission contains a long-lived isotope at mass 99, and that all other possible long-lived fission isotopes of technetium are present to less than 3 percent of this value. Making use of the fission yield curve, we may conclude that at least 97 percent of the Tc^{101} nuclei formed in fission decay with a half-life shorter than six months. Assuming a packing fraction of -6×10^{-4}, and a conversion factor of 1.000275, the atomic weight of long-lived fission technetium is found to be 98.913.

[1] G. T. Seaborg and E. Segrè, Phys. Rev. **55**, 808 (1939).
[2] Plutonium Project Fission Product Survey, Rev. Mod. Phys. **18**, 539 (1946).
[3] E. E. Motta, G. E. Boyd, and Q. V. Larson, Phys. Rev. **72**, 1270 (1947).

Production and Properties of a Long-Lived Radio-Isotope of Element 43*

E. E. Motta, G. E. Boyd, and Q. V. Larson
Clinton National Laboratory, Oak Ridge, Tennessee
October 8, 1947

THE possible existence of a long-lived beta-active, or stable isotope of element 43 (Tc) was suggested in the early work of Seaborg and Segrè[1] wherein a 6×10^4-fold decay of an isomeric 6.6-h Tc^{99} was observed without giving rise to a detectable radiation from the ground state. Recently, the presence of a long-lived isotope of Tc among the fission products from U-235 has been established.[2]

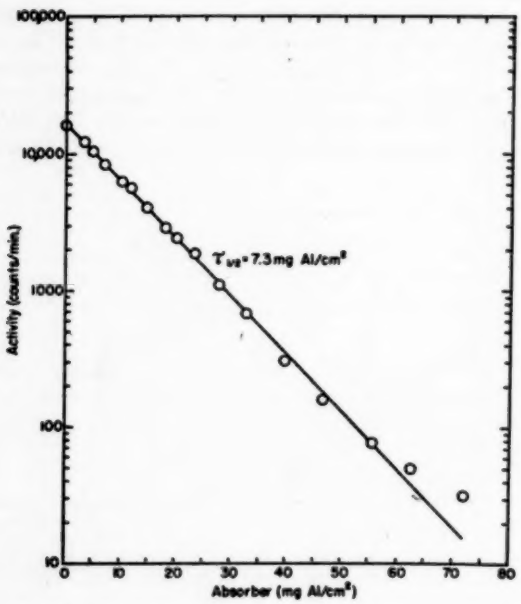

FIG. 1. Aluminum-absorption curve for the beta-radiations of Tc^{99}.

Since the 67-h Mo^{99} parent of Tc^{99} may be formed in appreciable yield by neutron irradiation of stable Mo^{98}, it was decided to attempt to produce the ground state activity by irradiating quantities of pure Mo metal with neutrons from the Clinton pile.

Four forty-gram molybdenum metal samples were irradiated in Stringer 21 for approximately one month each from February to May 1946. After chemical separation from the metal matrix in which it was produced, the Tc activity was purified, coprecipitated with PtS_2 carrier, mounted, and counted. A typical aluminum-absorption curve obtained with the sample placed at 30 percent geometry with respect to a thin mica end-window G-M counting tube is shown in Fig. 1. An average half-thickness of 7.3 mg Al/cm² corresponding to a range of 85 mg Al/cm², and to a maximum beta-energy[3] of 0.32 Mev was observed. A beta:gamma counting ratio in excess of 2000 has been found, and this has been taken to indicate the absence of gamma-radiation more energetic than 0.1 Mev. The foregoing radiation characteristics are virtually identical with those observed for the long-lived Tc isotope produced in fission.

A subsequent neutron irradiation of four kilograms of Mo for 112 days permitted the separation of weighable quantities of element 43 (September 1946). Measurements of the specific activity were conducted as follows: After extensive chemical purification to remove an initial Re and Mo contamination, *ca.* 100-microgram amounts of Tc metal were electroplated on polished copper disks, which then were weighed on a semimicro balance and counted. Uncertainties as to counting efficiency, scattering, etc., were minimized by electroplating a standardized Co^{60} preparation which was counted under identical conditions. The best average value for the half-life of the Tc activity obtained thus far has been 9.4×10^5 years.

The yield of long-lived activity resulting from the neutron irradiation of molybdenum metal is consistent with its production by the reaction, $Mo^{98}(n,\gamma)Mo^{99}$, followed by the radioactive decay of the 67-h Mo^{99} so formed. If the 9.4×10^5-y Tc had been produced by neutron capture in the less abundant stable Mo^{100} isotope followed by the decay of 14-m Mo^{101}, the yield of activity would have been roughly one-third that actually found. Accordingly, a mass of 99 is proposed for this radioactive isotope of element 43.

A few qualitative observations on the macro-chemistry may be of interest. A highly insoluble, dark-brown sulfide, presumably Tc_2S_7, precipitates readily from $4MH_2SO_4$ solutions. The heptavalent oxidation state may give rise to a light pink coloration when present in concentrations above 10^{-3}M. Many of the chemical properties observed at extremely low (i.e., tracer) concentrations by Perrier and Segrè[4], using 88-d Tc^{97}, have been confirmed. Detailed observations on the chemistry of element 43 will be reported elsewhere.

* This document is based on work performed under Contract No. W-35-058-eng-71 for the Atomic Energy Project at the Clinton Laboratories.
[1] G. T. Seaborg and E. Segrè, Phys. Rev. **55**, 808 (1939).
[2] Plutonium Project Fission Product Survey, Rev. Mod. Phys. **18**, 539 (1946).
[3] N. Feather, Proc. Camb. Phil. Soc. **34**, 599 (1938).
[4] C. Perrier and E. Segrè, J. Chem. Phys. **5**, 712 (1937); *ibid.* **7**, 155 (1939).

A Measurement of the Deuteron Proton Magnetic-Moment Ratio[1]

F. BITTER, N. L. ALPERT, D. E. NAGLE, AND H. L. POSS
Research Laboratory of Electronics, Massachusetts Institute of Technology, Cambridge, Massachusetts
November 8, 1947

DURING a recent period of availability of the Massachusetts Institute of Technology cyclotron magnet, measurements were made of the ratio of the magnetic moment of the deuteron to that of the proton in liquid hydrogen and deuterium by means of nuclear-absorption experiments with circuits similar to those previously used.[2]

The resonances were presented simultaneously on an oscilloscope by means of an electronic switch. A sinusoidal sweep was used, so that with proper adjustment the observed patterns could be made symmetrical about the center-line of the oscilloscope. The shapes of the two resonance curves were rather different, and the most prominent maxima of the deuterium resonance were of the order of a half-line width from the hydrogen maxima when the desired symmetry conditions were established. This effect, though not understood in detail, is probably due to the rate of sweep through resonance.

Eleven observations were made, of which three were rejected because the photographs of the oscilloscope traces were found to be unsymmetrical. Half of the remaining eight observations were made with the Dewar containing the resonance coils rotated through 180° so that the effects of a field gradient in the magnet could be eliminated. All eight of these observations fell within the following limits:

$$\mu_D/\mu_H = 0.307021 \pm 0.000005.$$

[1] This work has been supported in part by the Signal Corps, the Air Materiel Command, and O.N.R.
[2] F. Bitter, N. L. Alpert, H. L. Poss, C. G. Lehr, and S. T. Lin, Phys. Rev. 71, 738 (1947).

Multiple Nuclear Isomerism

E. DER MATEOSIAN, M. GOLDHABER,* C. O. MUEHLHAUSE, AND M. MCKEOWN
*Argonne National Laboratory,** Chicago 80, Illinois*
November 8, 1947

IN the course of an investigation of the activity induced in Sb by slow neutrons we noticed three previously unobserved short periods. An analysis of the decay curves obtained under various conditions of bombardment yields the following half-life periods: 1.3 min., 3.5 min., and 21 min. Though a short bombardment brings out these activities quite well relative to the long-lived known Sb^{122} (2.8 d) and Sb^{124} (60 d) activities, the saturation intensities as detected with either an end-window Geiger counter or an ionization chamber are only of the order of a few tenths of one percent of those of the long-lived activities. The new activities were observed with a number of samples of Sb of different origin, including C. P. Sb_2O_3 and Hilger's spectroscopically pure Sb metal. We could observe the activities with epicadmium neutrons as well as thermal neutrons and were able to show that all three activities induced by epicadmium neutrons are strongly

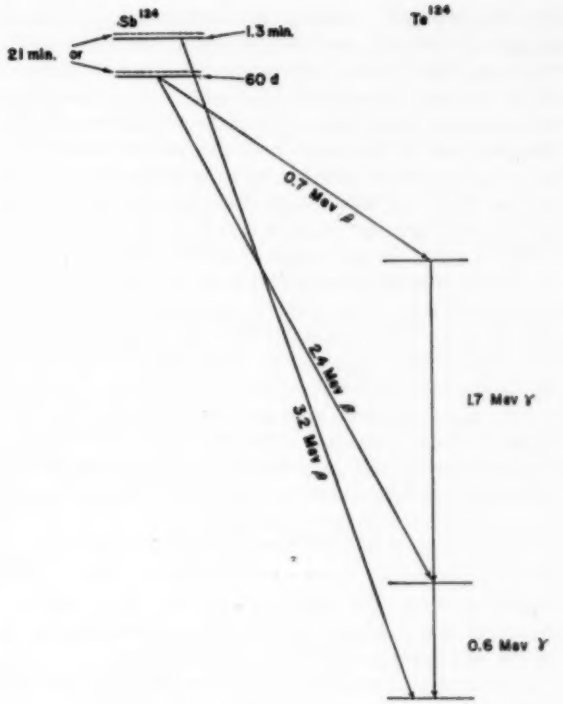

FIG. 1.

"self-absorbed" by Sb, which makes it unlikely that they are due to impurities. In addition, it was found that the short periods along with 2.8-d Sb plated out on Fe from an acid (HCl) solution of freshly bombarded Sb metal powder, whereas Sn, added as a carrier and plated out on Zn after the Sb was removed, proved inactive.

Using a sample of Sb enriched in Sb^{122} (96.3 percent Sb^{123}) we found that the 1.3- and 21-min. periods are due to isomers of Sb^{124} (60 d) and that the 3.5-min. period is due to an isomer of Sb^{122} (2.8 d). Characteristic K α-radiation of Sb was found to be associated with the 3.5-min. period, but not with the 1.3- and 21-min. periods. The 3.5- and 21-min. periods both show intense internal conversion electrons with half-value thicknesses in Al of 1.7 mg/cm²

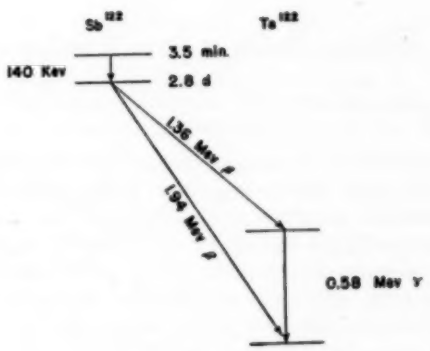

FIG. 2.

and 0.2 mg/cm², respectively, indicating approximate energies of 110 kev and 14 kev, respectively. It appears, therefore, that the energy of the isomeric transition of Sb^{124} (21 min.) is unusually low and smaller than the K work function of Sb (31 kev). If we assume that the 110-kev electrons are K electrons and the 14-kev electrons L electrons, we obtain for the energy of the isomeric transition of Sb^{122} (3.5 min.), approximately 140 kev and for that of Sb^{124} (21 min.) approximately 20 kev.

The 1.3-min. isomer decays with the emission of beta-rays with an absorption coefficient in Al of ~310 mg/cm², corresponding to 3.2+0.2-Mev maximum energy. Softer beta-rays, as well as gamma-rays, are also present. The partial isotopic cross section for the formation of this isomer by thermal neutrons is found to be $\sim 0.03 \times 10^{-24}$ cm².

The decay schemes proposed for Sb^{124} and Sb^{122} are shown in Figs. 1 and 2. The decay scheme of Sb^{124} (60 d) adopted here is that proposed by Meyerhof and Scharff-Goldhaber.[1] Our experiments so far do not decide the question whether the 21-min. transition leads to the 60-d or 1.3-min. level. Besides internal conversion electrons the 21-min. period also shows a beta-transition which is being studied further. The decay scheme for Sb^{122} (2.8 d) is based on the work of Mitchell, Langer, and McDaniel,[2] Miller and Curtiss,[3] and Rall and Wilkinson.[4]

On current theoretical views there would seem to be two possibilities to account for the existence of two metastable states in a nucleus of even mass number: Either there is a spin difference of at least three units between any two of the three states of Sb^{124} (1.3 min., 21 min., and 60 d), or one of the states has a spin $\geqslant 3$ and the other two have each a spin 0 and opposite parity.

Our thanks are due to Dr. Keim's group at Oak Ridge for putting the isotopically enriched antimony sample at our disposal.

* University of Illinois.
** This document is based on work performed under Contract No. W-31-109-eng-38 for the Atomic Energy Project at the Argonne National Laboratory.

[1] W. E. Meyerhof and G. Scharff-Goldhaber, Phys. Rev. **72**, 273 (1947).
[2] A. C. G. Mitchell, L. M. Langer, and P. W. McDaniel, Phys. Rev. **57**, 1107 (1940).
[3] L. C. Miller and L. F. Curtiss, Phys. Rev. **70**, 983 (1940).
[4] W. Rall and R. G. Wilkinson, Phys. Rev. **71**, 321 (1947).

Relative Yields of (γ, n) Reactions

M. L. Perlman and G. Friedlander
Research Laboratory, General Electric Company, Schenectady, New York
November 8, 1947

A NUMBER of elements throughout the periodic system have been irradiated with x-rays generated by the 100-Mev betatron at Schenectady. The amount of product resulting from loss of a single neutron by one of the target isotopes was determined by measurement of its beta-activity, which was distinguished from that of other beta-active isotopes by analysis of the decay curve. Irradiations were made at 50-Mev and 100-Mev maximum x-ray energies.

TABLE I. $(\gamma - n)$ yields relative to $N^{14}(\gamma, n)N^{13}$ yield as unity.

Parent isotope	Relative yield at maximum x-ray energy of 100 Mev	50 Mev
$_6C^{13}$	2.23	2.21
$_7N^{14}$	1.00	1.00
$_8O^{16}$	2.14	2.25
$_9F^{19}$	2.66	2.71
$_{15}P^{31}$	6.95	6.74
$_{17}Cl^{35}$	2.28	2.28
$_{19}K^{39}$	2.55	2.43
$_{28}Ni^{58}$	6.10	5.66
$_{29}Cu^{63}$	32.3	33.8
$_{31}Ga^{69}$	40.5	42.4
$_{31}Ga^{71}$	42.0	42.0
$_{46}Pd^{110}$	32.3	37.3
$_{47}Ag^{109}$	39.5	44.2
$_{51}Sb^{121}$	40.4	44.0
$_{75}Re^{187}$	82.5	82.0

The cases studied were chosen so as to eliminate or minimize the following possibilities: the product might have resulted from x-ray induced reactions on other isotopes present in the target material; an isotope of nearly the same half-life as that of the product sought might have been made; the quantitative result might be in error because of the unknown decay scheme of the product. Measurements were made which showed that $(n, 2n)$ reactions can account only for about one percent of the yields observed in this work.

Irradiations were monitored by measurement of the C^{11} or F^{18} activity induced in a standard piece of polystyrene or lithium fluoride which was bombarded together with each target. For product half-lives of less than one hour polystyrene monitors were used; for all other half-lives the monitors were lithium fluoride. All bombardments and measurements were carried out in standard geometries. Activities were calculated to saturation and were corrected for self-absorption, for absorption in counter windows, and for relative counter efficiencies. Yields were calculated to correspond to one milligram-atom of parent isotope in the target and, in the table below, they are normalized to the yield of the reaction $N^{14}(\gamma, n)N^{13}$, which is arbitrarily taken as unity at each x-ray energy. It is estimated that values in Table I are not in error by more than approximately ±15 percent.

The fact that the relative yields at 50 Mev and at 100 Mev are the same within experimental error suggests either that the cross sections of all the reactions investigated vary with energy in the same way or that the (γ, n) cross section is very small above 50 Mev. The latter conclusion is substantiated by unpublished data of G. C. Baldwin on the reactions $C^{12}(\gamma, n)C^{11}$ and $Cu^{63}(\gamma, n)Cu^{62}$.

Relative yields investigated fall roughly into three groups. The light elements as far as Ni^{58} have (γ, n) yields from 1 to 7. From Ni^{58} to Cu^{63} there is an abrupt and unexpected rise. Cases between Cu^{63} and Sb^{121} have values between 30 and 45. The only case studied above Sb^{121} is Re^{187} with a yield of 82. Additional cases of the (γ, n) reaction are being studied; a similar investigation of (γ, p) reactions is in progress.

These experiments were carried out with the assistance of Mr. G. Jaffe, which we gratefully acknowledge.

The Nuclear Magnetic Moments of Bromine

R. V. POUND*
Jefferson Physical Laboratory, Harvard University, Cambridge, Massachusetts
November 8, 1947

A DETERMINATION of the magnetic moments of the nuclei Br^{79} and Br^{81} by the method of nuclear paramagnetic resonance absorption[1] is of interest in view of the very large electric quadrupole coupling observed for these nuclei in BrCN[2,3] and in CH_3Br.[3] In the determination of the magnetic moments of bromine by the molecular-beam resonance method, using CsBr and LiBr, Brody, Ramsey, and Nierenberg found that a large quadrupole coupling was not evident.[4]

An automatic, recording r-f spectrometer[5] was used to search in samples of liquid Br_2 and $CHBr_3$, a single crystal of KBr, and aqueous solutions of LiBr and NaBr. The lines were found only in the aqueous solutions. The samples were about 1.5 cc in volume in a field of about 3000 gausses, and the lines occurred in the neighborhood of 3 Mc/sec.

Because of the very rapid motions characterizing liquids and solutions, the electric quadrupole moments of the nuclei cannot give rise to splittings of the lines but only to a broadening, through a shortening, of the relaxation time T_1 as was observed for the deuteron in heavy water.[6] The broadening from this cause may be so large as to make the absorption weak enough to account for the failure to find the lines in $CHBr_3$ and Br_2. In the aqueous solutions the lines were about 10 kc/sec. in width between half-power points. The intensities of the bromine lines were unaffected by the addition of paramagnetic Cr^{+++} ions, whereas that of the much narrower Na^{23} line, which occurs between the bromine lines, was considerably enhanced by the addition of the paramagnetic ions. This is in support of the view that the width of the bromine lines is indicative of a very short relaxation time. A value for $T_1=1/\pi\Delta\nu$ of about 3×10^{-5} sec. is indicated.

If the electric quadrupole moment of bromine is assumed to be 0.2×10^{-24} cm^2, the ratio of the relaxation time found for bromine to that found for the deuteron in heavy water is such as to indicate approximately the same intensity for the spectra of the tensor grad E in the two cases. This cannot be considered to be evidence of the correctness of the assumed value for the quadrupole moment of bromine, however, since the bromine nuclei, unlike the deuterons in heavy water, are situated at the centers of negatively charged ions having spherical symmetry.

Of more direct significance is the fact that the two lines for the two equally abundant bromine isotopes have different widths. This allows the assignment of the smaller magnetic moment to the isotope with the larger quadrupole moment, Br^{79},[2,3] since the line occurring at lower frequency was the broader. The lines recorded are derivatives of the absorption curves, for sufficiently small modulation of the strong magnetic field, and therefore the ratio of the recorded amplitudes should be $(Q_{Br^{79}}/Q_{Br^{81}})$.[4] The lines recorded were in a ratio of 1.75/1, which is somewhat smaller than expected, though this can be caused by an insufficiently small modulation amplitude.

The ratios of the frequencies of the two bromine lines and of their frequencies to that of the Na^{23} line, all in the same field, were determined. These results are

$$\nu_{Br^{81}}/\nu_{Br^{79}}=1.0778\pm0.0003,$$

and

$$\nu_{Br^{81}}/\nu_{Na^{23}}=1.0209\pm0.0003.$$

From these, using the known spin of $\frac{3}{2}$ for all three nuclei and the value of 2.217 ± 0.002 for the magnetic moment of Na^{23},[7] after making a correction for the diamagnetism of the electrons in the two kinds of ions,[8] values of

$$\mu_{Br^{81}}=2.2706\pm0.003$$

and

$$\mu_{Br^{79}}=2.1066\pm0.003$$

are obtained. These are in close agreement with the values of 2.271 ± 0.023 and 2.110 ± 0.021 reported by Brody, Nierenberg, and Ramsey.

* Society of Fellows.
[1] E. M. Purcell, H. C. Torrey, and R. V. Pound, Phys. Rev. **69**, 37 (1946).
[2] C. H. Townes, A. N. Holden, J. Bardeen, and F. R. Merritt, Phys. Rev. **71**, 644 (1947).
[3] W. Gordy, W. V. Smith, A. G. Smith, and Harold Ring, Phys. Rev. **72**, 259 (1947).
[4] S. B. Brody, W. A. Nierenberg, and N. F. Ramsey, Phys. Rev. **72**, 258 (1947).
[5] R. V. Pound, Phys. Rev. **72**, 527 (1947).
[6] N. Bloembergen, E. M. Purcell, and R. V. Pound, Nature **160**, 475 (1947).
[7] J. B. M. Kellogg and S. Millman, Rev. Mod. Phys. **18**, 323 (1946).
[8] W. E. Lamb, Jr., Phys. Rev. **60**, 817 (1941).

Erratum: The Arc Spectrum of Silver

[Phys. Rev. **57**, 894 (1940)]

A. G. SHENSTONE
Palmer Physical Laboratory, Princeton University, Princeton, New Jersey

IT has just come to my notice that an inexplicable omission occurred in the above paper. In Table II there should be inserted the level $5s5p^4D_{3-\frac{1}{2}}$ at -666.6. The lines due to this important level are so labeled in Table III of the paper, although the level was omitted from Table II.

Author Index to Volume 72

References with (A) are to abstracts of papers presented at meetings of the American Physical Society. References with (L) are to Letters to the Editor, and those with (T) designate title only.

Abelson, P. H. (see Marton, L.)—161(A)
—— (see Roberts, R. B.)—76(L)
——(see Snell, A. H.)—169(A)
Abraham, Wayne G. Loading of resonant cavities by electron beams—741(A)
Adams, Raymond V. (see Anderson, Carl D.)—724
Adel, Arthur. Near infra-red spectra of the planets—538(A)
—— (see McMath, Robert R.)—644(L)
Adler, Robert (see Cherry, W. L., Jr.)—981(L)
Agnew, H. M., W. C. Bright, and Darol Froman. Distribution of neutrons in the atmosphere—203
Ahearn, A. J., J. A. Burton, and K. G. McKay. Conductivity pulses induced in diamond by alpha-particles—524(T)
Alburger, D. E. (see Pollard, Ernest)—1196
—— **and E. C. Pollard.** An automatically recording gamma-ray scattering apparatus—169(A)
Aldrich, L. T. (see Daunt, J. G.)—502
—— (see McInteer, B. B.)—510(L)
Alfvén, H. Solar magnetic field and diurnal variation of cosmic radiation—88(L)
Alpert, N. L. Studies of the solid state by means of nuclear magnetism—637(L)
—— (see Bitter, F.)—1271(L)
Altar, William, M. Garbuny, and J. W. Coltman. Speed gauge for HV-ion beams—528(A)
Alvarez, Luis W. Measurement of short time intervals—741(A)
Amdur, I. Determination of the molecular law of force and self-diffusion coefficients—642(L)
Anderson, B. L. (see Weisz, Paul B.)—431(L)
Anderson, Carl D., Raymond V. Adams, Paul E. Lloyd, and R. Ronald Rau. On the mass and the disintegration products of the mesotron—724
Anderson, E. C., W. F. Libby, S. Weinhouse, A. F. Reid, A. D. Kirshenbaum, and A. V. Grosse. Natural radiocarbon from cosmic radiation—931
Anderson, E. E. (see McDaniel, B. D.)—729(L)
—— (see Sutton, R. B.)—1147
Anderson, H. L., E. Fermi, A. Wattenberg, G. L. Weil, and W. H. Zinn. Method for measuring neutron-absorption cross sections by the effect on the reactivity of a chain-reaction pile—16
Andrews, Donald H. and Chester W. Clark. Radiofrequency and detection by superconductivity—161(A)
Anfinsen, C. B. (see Solomon, A. K.)—1097
Antonoff, George. Conductivity of aluminum sulphate with aluminum electrodes in magnetic field—183(A)
Apker, Le Roy, E. Taft, and J. Dickey. External photoelectric effect at semi-conductor surfaces—153(T)
Araki, Gentaro. Interval formula for multiplets of atomic energy levels—1255(L)
Arley, Niels. On the application of captive balloons to carry photographic emulsion—1253(L)
Arnold, W. (see Langsdorf, A. S., Jr.)—167(A)
Arons, A. B., R. H. Cole, W. D. Kennedy, E. B. Wilson, Jr. Design and use of Tourmaline gauges for piezoelectric measurement of explosion phenomena—176(A)
Atherton, Ralph. An experiment in acoustical resonance—150(T)
Austern, N. (see Mack, J. E.)—972
Austin, Pauline (see Spencer, Roy C.)—186(A)

Babcock, Horace W. Magnetic fields of astronomical bodies—83(L)
Bailey, C. L. (see Sherr, R.)—662
Barber, W. C. Search for positron-electron branching in certain beta-emitting isotopes—1156
Bachman, C. H. (see Johnson, W. E.)—174(A)
Baer, W. (see Hull, G. F., Jr.)—522(A), 532(A)
Bardeen, John. Surface states and space charge layers in semi-conductors—153(T)
—— Theory of crystal rectifiers with application to copper oxide—524(T)
Barkas, Walter H. Note on the disintegration energies of Na^{24} and Al^{28}—346(L)
Barker, Edgar C. Average gamma-energy emitted per beta particle for several radioactive isotopes—167(A)
Barrett, Charles S. Low temperature transformation in lithium—245(L)
Barschall, H. H. (see Seagondollar, L. W.)—439
——, **M. E. Battat, W. C. Bright, E. R. Graves, T. Jorgensen, and J. H. Manley.** Measurement of transport and inelastic scattering cross sections for fast neutrons. Part II. Experimental results—881
—— **J. H. Manley, and V. F. Weisskopf.** Measurement of transport and inelastic scattering cross sections for fast neutrons. I. Method—875
Bartlett, James H. Vector mesotron—219
Battat, M. E. (see Barschall, H. H.)—881
Bauer, Carl August. Production of helium in meteorites by cosmic radiation—354(L)
Beams, J. W. Radial density variation of gases and vapors in a centrifugal field—433(L)
—— Rotors driven by light pressure—987(L)
Beaumont, D. W. (see Mathias, B. T.)—532(A)
Beeman, W. W. Neutron scattering cross section at the cadmium resonance—986(L)
—— **and Paul Kaesberg.** X-ray scattering at very small angles—512(L)
Belinfante, F. J. Interaction between electrons and radiation—524(T)
Bell, P. R., S. De Benedetti, and J. E. Francis, Jr. Fast coincidence circuit with pulse height selection—160(A)
Bell, R. E. (see Elliott, L. G.)—979(L)

Benson, Bruce B. Proton-gamma coincidence counting —162(A)
Benzer, S. Excess-defect germanium contacts—1267(L)
—— Spontaneous electrical oscillations in germanium crystals—531(A)
Bergmann, Peter G. Fluctuation of transmitted sound —738(T)
Beringer, R. (see Schultz, H. L.)—346(L)
Bernstein, S. (see Sawyer, R. B.)—109
Berry, Chester Riddon. Shape of x-ray diffraction lines from colloidal magnesium oxide—942
Bethe, H. A. Electromagnetic shift of energy levels—339(L)
—— Shock wave conditions—171(T)
—— Theoretical considerations on large air showers—172(A)
——(see Marshak, R. E.)—506
Beyer, Robert T. Use of magnetic amplifiers in computing circuits—522(A)
Birch, Francis. Radioactivity of potassium and geophysics —1128(L)
Bitter, F., N. L. Alpert, D. E. Nagle, and H. L. Poss. Measurement of deuteron-proton magnetic moment ratio—1271(L)
Blair, J. M. (see Sherr, R.)—662
Blair, John S. (see Zilsel, Paul R.)—155(A), 225
Blatt, John M. On the Heitler theory of radiation damping —466
Bleakney, Walker (see Mariner, Thomas)—792, 807
—— **and Richard G. Stoner.** Attenuation of a spherical shock wave—170(A)
Blifford, I. H. and H. Friedman. Voltage stabilization properties of the continuous corona discharge—185(A)
Blitzer, L. (see Cady, W. M.)—159(A)
Bloch, F., E. C. Levinthal, and M. E. Packard. Relative nuclear moments of H^1 and H^2—1125(L)
Bloch, Felix. Nuclear radiospectroscopy—738(T)
—— Some theoretical considerations about Einstein-Bose degeneracy and its possible connection with the superconductivity of metal-ammonia solutions—153(T)
Bloch, I. (see Breit, Gregory)—135
Bohm, D. and L. L. Foldy. Theory of the synchro-cyclotron —649
Bonner, T. W., J. E. Evans, C. W. Malich, and J. R. Risser. Study of the break-up of Li^8—163(A)
Boyd, G. E. (see Motta, E. E.)—1270(L)
Bozorth, R. M. (see Yager, W. A.)—80(L), 529(A)
Bradt, H. L. (see Tendam, D. J.)—527(A), 1118(L)
—— **and D. J. Tendam.** Relative yields of (α, n) and $(\alpha, 2n)$ reactions with 15-20-Mev alpha-particles—527(A), 1117(L)
Brady, Edward L. and Martin Deutsch. Angular correlation of successive gamma-ray quanta—870(L)
Branch, G. M. (see Snell, A. H.)—169(A)
Branson, Herman. On the theory of the use of isotopes as tracers—533(A)
Bratenahl, A. (see Leith, C. E.)—732(L), 745(A)
Brattain, W. H. Evidence for surface states on semiconductors from change in contact potential on illumination —345(L)
—— **and H. B. Briggs.** Refractive index of germanium films—174(A)
—— **and W. Shockley.** Density of surface states on silicon deduced from contact potential measurements—345(L)
Bray, Ralph, K. Lark-Horovitz, and R. N. Smith. Spreading resistance discrepancies and field effects in germanium—530(A)
Breckenridge, R. G. (see Mathias, B. T.)—532(A)
Breit, G. Does the electron have an intrinsic magnetic moment?—984(L)
—— (see Barschall, H. H.)—881
—— (see Zilsel, P. R.)—576
—— **and I. Bloch.** Relativistic correction to the magnetic moment of the deuteron—135
—— **and R. E. Meyerott.** Effect of nuclear motion on the hyperfine structure of the ground term of hydrogen—1023
Brentano, J. C. M. Converter for obtaining micro-densitometer tracings in which the ordinates are proportionate to the energy values received by the photographic pattern—166(A)
Bridge, H. Interpretation of cosmic-ray ionization bursts in cylindrical chambers by pulse shapes—172(A)
—— (see Sutton, R. B.)—1147
——, **Bruno Rossi, and Robert Williams.** Burst production by penetrating cosmic-ray particles—257(L)
Bridgman, P. W. New results at pressures up to 100,000 kg-cm^2—533(A)
Briggs, H. B. (see Brattain, W. H.)—174(A)
Bright, W. C. (see Agnew, H. M.)—203
—— (see Barschall, H. H.)—881
Brill, T. and H. V. Lichtenberger. Neutron cross-section studies with the rotating shutter mechanism—585
Brinkley, Stuart R., Jr. (see Kirkwood, John G.)—171(A)
—— **and John G. Kirkwood.** Theory of the propagation of shock waves from infinite cylinders of explosive—1109
Brode, R. B. Cosmic rays—738(T)
Brody, S. B., W. A. Nierenberg, and N. F. Ramsey. Nuclear moments of the bromine isotopes—258(L)
Brown, B. W. (see Curtiss, L. F.)—643(L)
Brown, F. W. and M. A. Greenfield. Calculation of index of refraction of water vapor in the far infra-red—534(A)
Brown, Harrison. Experimental method for the estimation of the age of the elements—348(L)
—— **and M. G. Inghram.** Isotopic composition of meteoric copper—347(L)
—— **and Claire Patterson.** Relative abundance of some light nuclear species as determined from the composition of stony meteorites—456
Brown, V. A. and B. P. Ramsay. Maxwell bridge at low frequencies—528(A)
Broxon, James W. Further investigation of frequency of occurrence of small cosmic ray bursts—525(A)
—— Relation of frequency of occurrence of small cosmic-ray bursts to areas of sunspots and other variables—1187
Broyles, Arthur A. and John L. Powell. Coulomb functions for heavy nuclei—155(A)
Brubaker, W. M. (see Slepian, J.)—185(A)
Brulin, O. and S. Hjalmars. On the symmetrical vector meson pair theory of nuclear interaction—1126(L)

Buechner, W. W., R. J. Van de Graaff, A Sperduto, E. A. Burrill, Jr., and H. Feshbach. Further experiments on the elastic single scattering of electrons by nuclei—678
Burrill, E. A., Jr. (see Buechner, W. W.)—678
Burton, J. A. Photoelectric and optical properties of cesium-antimony films—531(A)
Burton, J. A. (see Ahearn, A. J.)—524(T)

Cady, W. M., B. Cassen, and L. Blitzer. Remarks on the spectra of electroplated electrodes—159(A)
Cahn, A. (see Spatz, W. D. B.)—163(A)
Cannon, Walter F. (see Pond, T. Alexander)—1121(L)
Carmichael, H. "Fragmentation" bursts at sea level—525(A)
—— Review of the topic of cosmic-ray bursts—524(T)
—— (see Smith, B. S.)—527(A)
Carr, J. W., Jr. Permeameter for magnetic measurements on high permeability material—530(A)
Carter, Robert L. and William V. Smith. Microwave spectrum frequency markers—1265(L)
—— (see Smith, William V.)—638(L)
Cassen, B. (see Cady, W. M.)—159(A)
—— **and J. Stanton.** Theory of non-steady shock waves—180(A)
Castleman, R. A., Jr. On the independence of energy released from the atom surrounding atmospheric conditions—182(A)
Chao, C. Y. (see Pi, T. H.)—639(L)
Chapman, Seville. Sensitive d.c. current-amplifier operated from a.c.—745(A)
Cheney, Ruth K. (see Wacker, Paul F.)—182(A)
Cherry, W. L., Jr. and Robert Adler. Piezoelectric effect in polycrystalline barium titanate—981(L)
Christian, Richard S. (see Wouters, Louis F.)—1127(L)
Christy, R. F. (see Cohen, E. Richard)—738(A)
——, **E. R. Cohen, W. A. Fowler, C. C. Lauritsen, and T. Lauritsen.** Conservation of momentum in the disintegration of Li^8—698
Chu, K. Y. (see Wiedenbeck, M. L.)—1164, 1171
Chupp, Warren, W. and Edwin M. McMillan. Excitation curve for the reaction $C^{12}(p, pn)C^{11}$ up to 140 Mev—873(L)
Clark, Chester W. (see Andrews, Donald H.)—161(A)
Clark, J. C. Ultra-short duration flash radiographs—741(A)
Clarke, C. L. (see Schultz, H. L.)—346(L)
Clearman, H. E. (see Wolf, H. E.)—528(A)
Clement, Evans. Cloud-chamber study of the ionization by high energy cosmic-ray electrons—742(A)
Cleveland, Forrest F. (see Meister, Arnold G.)—157(A)
Cocconi, Giuseppe. Extensive air showers and the cascade theory—964
—— Theoretical evaluation of the size-frequency curve of extensive cosmic-ray showers—350(L)
Cohen, E. R. (see Christy, R. F.)—698
—— **and R. F. Christy.** Conservation of momentum in the disintegration of Li^8—738(A)
—— **and William F. Hornyak.** Least squares fit of the fundamental mass doublets—1127(L)
Cole, R. H. Spherical shock waves from underwater explosions—177(A)
—— (see Arons, A. B.)—176(A)
—— (see Coles, J. S.)—177(A)
Coleman, K. D., R. Nudenberg, and M. L. Pool. X-ray emission from radioactive tin, antimony, and tungsten—164(A)
—— **and M. L. Pool.** X-ray emitting isotopes of radioactive Sb and Sn—1070
Coles, D. K. (see Good, W. E.)—157(A)
——, **E. S. Elyash, and J. G. Gorman.** Microwave absorption spectra of N_2O—973(L)
—— **and W. E. Good.** Stark and Zeeman effects in microwave spectroscopy—156(A)
Coles, J. S. (see Cross, Paul C.)—179(A)
——, **P. C. Cross, and R. H. Cole.** Underwater shock-wave parameters measured off the ends and perpendicular bisectors of line charges—177(A)
Collins, C. B. Inelastic scattering of protons—521(T)
Coltman, J. W. (see Altar, William)—528(A)
—— (see Marshall, Fitz-Hugh)—528(A)
—— **and Fitz-Hugh Marshall.** Some characteristics of the photo-multiplier radiation detector—528(A)
Cook, C. S. (see Langer, L. M.)—355(L)
Cook, J. W. (see Scott, R. B.)—161(A)
Cook, Leslie J., Edwin M. McMillan, Jack M. Peterson, and Duane C. Sewell. Total cross sections of nuclei for 90 Mev neutrons—1264(L)
Cook, Richard K., Martin Greenspan, and Pearl G. Weissler. Thermal voltage of a quartz crystal—175(A)
Corben, H. C. Generalization of general relativity theory—156(A)
—— **and Mulaika Corben.** Motion of a particle in an electromagnetic and gravitational field—434(L)
—— **and Mulaika Corben.** Range of nuclear forces—526(A)
Corben, Mulaika (see Corben, H. C.)—434(L), 526(A)
Cork, J. M. Gamma-radiation from tantalum, iridium, and gold—581
——, **R. G. Schreffler, and A. Weaver.** Internally converted gamma-rays from the heavy elements—186(A)
——, **R. G. Schreffler, and C. M. Fowler.** Internally converted radiation from europium, hafnium, and osmium—1209
Correll, Malcolm. Positive excess of slow mesotrons at an altitude of 11,500 feet—171(A), 1054
Corruccini, R. J. and D. C. Ginnings. Heat capacities of some solids and liquids at high temperatures using an ice calorimeter—183(A)
Cosby, C. B. Simple electrical stimulator producing the several clinically useful currents—160(A)
Courant, E. D. and P. R. Wallace. Fluctuations of neutron intensity in a chain reacting pile—526(A), 1038
Cox, Everett F. Microbarographic waves at great distances from explosions—180(A)
Craggs, J. D. and A. A. Jaffe. Discharge spread in Geiger counters. Part I. With self-quenching gases—784
Cragoe, C. S. (see Stimson, H. F.)—183(A)
Craig, D. S. (see Smith, B. S.)—527(A)
Cranshaw, T. E. (see English, A. C.)—253(L)
Crawford, F. H. Calculation of thermodynamic first derivatives from Jacobians—521(A)
Crawford, M. F. (see Welsh, H. L.)—524(T)

Crittenden, E. C. New basis for photometric units—166(A)
Cross, P. C. (see Coles, J. S.)—177(A)
—— **and J. S. Coles.** Underwater shock wave interactions with the ocean surface—179(A)
Cummerow, R. L., D. Halliday, and G. E. Moore. Paramagnetic resonance absorption at 9000 mc/sec. for five salts of the iron group—173(A), 1233
Cunningham, B. B. (see Seaborg, G. T.)—740(A)
——, **H. H. Hopkins, M. Lindner, D. R. Miller, P. R. O'Connor, I. Perlman, G. T. Seaborg, and R. C. Thompson.** Transmutations with high-energy deuterons in the 184-inch cyclotron—739(A)
Curtiss, L. F. and B. W. Brown. Diamond as a gamma-ray counter—643(L)

Dailey, B. P. First-order Stark effect in the microwave spectrum of methyl alcohol—84(L)
——, **S. Golden, and E. Bright Wilson, Jr.** Preliminary analysis of the microwave spectrum of SO_2—871(L)
—— **and E. B. Wilson, Jr.** Microwave spectra of several polyatomic molecules—522(A)
Dancoff, S. M. Disintegration of the deuteron in flight—163(A), 1017
—— (see Lichtenberger, H. V.)—164(A)
Darling, B. T. (see Zilsel, P. R.)—576
Daunt, John G. Magnetic threshold curves of superconductors—89(L)
—— Properties of helium II—153(T)
—— **and H. L. Johnston.** A new liquid helium cryostat—161(A)
——, **R. E. Probst, H. L. Johnston, L. T. Aldrich, and Alfred O. Nier.** A new method of separation of the isotopes of He^3 and He^4—502
Davidson, W. L., G. A. Morton, C. G. Shull, and E. O. Wollan. Diffraction of neutrons by hydrogen and deuterium containing crystals—168(A)
Davis, Leverett, Jr. Stellar electromagnetic fields—632
Davison, Perry W. (see Pollard, Ernest)—736(L)
—— **and E. C. Pollard.** Cyclotron bombardment of gaseous targets—162(A)
Dearnley, I. H., C. L. Oxley, and J. E. Perry, Jr. Proton-proton scattering—169(A)
De Benedetti, S. (see Bell, P. R.)—160(A)
De Bretteville, A. P., Jr. (see Field, Norman J.)—1119(L)
Decius, J. C. Rigorous theory of dimensional analysis and model experiments—178(A)
—— (see Swift, Elijah, Jr.)—177(A)
Deeds, Edward. Isochronization of simple and physical pendulums—150(T)
De Hoffman, F. and B. T. Feld. Delayed neutrons from Pu^{239}—525(A), 567
De Launay, Jules and Richard L. Dolocek. Superconductivity and the Debye characteristic temperature—141
Demers, Pierre. Radioactive stars showing migration of single nuclei in the photographic emulsion—536(A)
—— (see English, A. C.)—253(L)
—— (see La Palme, J.)—536(A)
— **and V. Fredette.** New autoradiographic method—538(A)
Dempster, A. J. Yield of nuclei formed by fission—431(L)
Dennison, David M. (see Nielsen, Harald H.)—86(L), 1101
—— (see Shull, Franklin B.)—180(A), 256(L)
DePackh, David C. and Andrew V. Haeff. On-orbit injector for betatrons and synchrotrons—247(L)
Der Mateosian, E., M. Goldhaber, C. O. Muelhause, and M. McKeown. Multiple nuclear isomerism of Sb—1271(L)
Deutsch, Martin. Beta- and gamma-ray level schemes—521(T)
—— Decay of Ag^{110} (200 day)—527(A)
—— Gamma-rays from Cu^{64}, annihilation of swift positrons, and experiments on orbital-electron capture—729(L)
—— (see Brady, Edward L.)—870(L)
—— (see Miller, Arthur E.)—527(A)
Devaney, Richard (see Kaye, Wilbur)—165(A)
DeWire, J. W. (see Sutton, R. B.)—1147
Dibeler, Vernon H. (see Mohler, Fred L.)—158(A)
Dickey, Fred P. (see Lagemann, Robert T.)—284
Dickey, J. (see Apker, LeRoy)—153(T)
Dolocek, Richard L. (see de Launay, Jules)—141
Duell, Bernhard. An observed relationship between solar and ionospheric activity and sea-level pressure—153(T)
DuMond, Jesse W. M. Method of correcting low angle x-ray diffraction curves for the study of small particle sizes—83(L)
—— Solid state interpretation of the structure near the limit of the continuous x-ray spectrum—276

Eckart, Carl. Coherence of scattered sound—738(T)
Edwards, Howard (see Ring, Harold)—1262(L)
Edwards, J. E. and M. L. Pool. Radioactive isotopes of Mo and Tc—384
Edwards, R. L. Proposed additions to the list of standard algebraic operations—150(T)
Eggler, C. (see Hughes, D. J.)—646(L), 892
Eisenbud, L. (see Wigner, E. P.)—29
—— **and E. P. Wigner.** General basis for the resonance formula—155(A)
Eisenstein, A. Some electrical properties of an oxide cathode interface—531(A)
Eisner, E. and R. G. Sachs. Note on angular distributions in nuclear reactions—680
Elliott, L. G. and R. E. Bell. Disintegration scheme of 1.7-year Cs^{134}—979(L)
Elsasser, Walter M. Induction effects in terrestrial magnetism. Part III. Electric modes—821
Elyash, E. S. (see Coles, D. K.)—973(L)
English, A. C., T. E. Cranshaw, P. Demers, J. A. Harvey, E. P. Hincks, J. V. Jelley, and A. N. May—$(4n+1)$ radioactive series—253(L)
English, W. N. Corona from water drops—741(A)
Epstein, S. (see Lounsbury, M.)—517(L)
Estermann, I., A. Foner, and J. A. Randall. Resistivity and Hall constant of germanium samples at low temperatures—530(A)
Evans, J. E. (see Bonner, T. W.)—163(A)
Eyring, Carl F. Reverberation in the sea—738(T)

Fairbank, Henry A. (see Fairbank, William M.)—645(L)
—— (see Lane, C. T.)—1129(L)
Fairbank, William M. (see Lane, C. T.)—1129(L)
——, **Henry A. Fairbank, and C. T. Lane.** Conversion of ordinary sound into second sound—645(L)
Fano, U. Ionization yield of radiations II. Fluctuations of the number of ions—26
Feld, B. T. On the nuclear electric quadrupole interaction in molecular spectra—1116(L)
—— (see de Hoffman, F.)—525(A), 567
Fermi, E. (see Anderson, H. L.)—16
—— **and L. Marshall.** On the interaction between neutrons and electrons—1139
—— **and L. Marshall.** Spin dependence of scattering of slow neutrons by Be, Al, and Bi—408
——, **J. Marshall, and L. Marshall.** Thermal neutron velocity selector and its application to the measurement of the cross section of boron—193
—— **and E. Teller.** Capture of negative mesotrons in matter—399
Feshbach, H. (see Buechner, W. W.)—678
—— (see McKinley, W.)—155(A)
—— **and L. I. Schiff.** Thresholds for creation of particles —254(L)
Field, Norman J. and A. P. de Bretteville, Jr. Phase change in barium titanate crystals induced by infra-red radiation absorption—1119(L)
Finkle, Bernard. Further studies on the radiations from Be^{121} and Ca^{121}—1260(L)
Finkelstein, R. J. γ-instability of mesons—415, 746(A)
—— Scattering of neutrons in polycrystals—907
Fisher, Leon H. An attempt to verify the theory of the long spark of Loeb and Meek—423
Fisher, Russell A. (see Meeks, Wilkison)—169(A), 451
Fitzgerald, J. W. (see Ringo, G. R.)—87(L)
Fock, V. Note on the paper "Second quantization and representation theory" by E. M. Corson—737(L)
Foldy, Leslie, L. On the meson theory of nuclear forces —125
—— Proton-proton scattering at 10 Mev—731(L)
—— (see Bohm, D.)—649
Foley, H. M. Second-order magnetic perturbations in nuclear quadrupole spectra and the "pseudo-quadrupole" effect in diatomic molecules—504
—— (see Kusch, P.)—1256(L)
Follin, James W., Jr. Propagation of cosmic rays through interstellar space—743(A)
Foner, A. (see Esterman, I.)—530(A)
Forrester, A. Theodore. Noise in electrometer tubes— 747(A)
—— (see Smith, Lloyd P.)—989
——, **William E. Parkins, and Edward Gerjuoy.** On the possibility of observing beat frequencies between lines in the visible spectrum—728(L)
Forró, M. Temperature effect of cosmic radiation at 1000-m water equivalent depth—868(L)
Forster, Harriet H. Cosmic ray tracks in photographic emulsions at high altitudes—742(A)
Foster, J. S. Progress report and plans for the McGill University cyclotron—524(T)
Fountain, C. R. Basic optical formula—166(A)
Fowler, C. M. (see Cork, J. M.)—1209
Fowler, J. L. and Louis Rosen. Energy distribution of the fragments resulting from the fission of U^{235} and Th^{232} by slow and fast neutrons—926
Fowler, W. A. (see Christy, R. F.)—698
—— (see Lauritsen, C. C.)—739(A)
—— (see Lauritsen, T.)—746(A)
——, **C. C. Lauritsen, and T. Lauritsen.** Conservation of momentum in the disintegration of Li^8—738(A)
Francis, J. E., Jr. (see Bell, P. R.)—160(A)
Frank, J. M., W. S. Huxford, and W. R. Wilson. Modulation of the resonance lines in a cesium arc—156(A)
Frankel, S. (see Metropolis, N.)—186(A)
—— **and N. Metropolis.** Calculations in the liquid drop model of fission—914
Fraser, L. W., R. P. Petersen, H. E. Tatel, and J. A. Van Allen. Methods in cosmic-ray measurement in rockets—173(A)
Fredette, V. (see Demers, P.)—538(A)
Frerichs, Rudolf. Photo-conductivity of "incomplete phosphors"—594
Fretter, W. B. Penetrating showers produced in lead at sea-level—743(A)
Friedlander, G. (see Perlman, M. L.)—1272(L)
Friedlander, Herbert N. (see Seren, Leo)—163(A), 888
——, **L. Seren, and S. H. Turkel.** Evidence for the cross section of 115-day Se^{75}—23
Friedman, B. Behavior of bubbles produced by underwater explosions—177(A)
Friedman, H. (see Blifford, I. H.)—185(A)
Friedrichs, K. O. On the determinancy of gas flows involving reaction fronts—171(A)
Fröberg, Carl-Erik. Calculation of the interaction between two particles from the asymptotic phase—519(L)
Froman, Darol (see Agnew, H. M.)—203
——, **Louis Rosen, and Bruno Rossi.** Cosmic-ray induced fission—525(A)
Froslie, Harold M. and J. G. Winans. Absorption spectrum of InCl—481
Frost, Robert H. Specific ionization of 25- to 300-Kv electrons—747(A)
Frye, Paul M. Underwater photography of explosion phenomena—170(A)
—— (see Wilson, E. B., Jr.)—178(A)
Furry, W. H. Discussion of a possible method for measuring masses of cosmic-ray mesotrons—171(A)

Galvin, J. A. (see Shaw, T. M.)—537(A)
Gamble, Edward H. High frequency response of thermionic diodes—160(A)
Gamow, G. Problem of explosive initiation—170(A)
Garbuny, M. (see Altar, William)—528(A)
Gardner, Eugene. Stars in photographic emulsions produced by particles accelerated by the cyclotron—743(A)
Gast, P. F. Uncertainty principle and yield of nuclei formed in fission—1265(L)
Geisler, A. H., J. K. Hill, and J. B. Newkirk. Divergent beam x-ray photography of metallic single crystals— 983(L)

Gerjuoy, E. Sound pressure in water resulting from a point source in air—745(A)
—— (see Forrester, A. Theodore)—728(L)
Ghiorso, A. (see Hagemann, F.)—252(L)
Gibbs, Leigh (see Gibbs, Norman)—160(A)
Gibbs, Norman, Leigh Gibbs, and E. W. Pike. Coding radiosonde of rational design—160(A)
Gibney, R. B. and G. L. Pearson. Magnetic susceptibility of sodium in liquid ammonia solutions at low temperatures—76(L)
Gill, Piara Singh (see Schein, Marcel)—171(A)
——, **Marcel Schein, and Victor Yngve.** Latitude effect of the hard component as a function of altitude—733(L)
Ginnings, D. C. (see Corruccini, R. J.)—183(A)
—— **and N. S. Osborne.** Measurements of heat of vaporization and heat capacity of a number of hydrocarbons—182(A)
Givens, M. P. An experimental study of the quantum nature of x-rays—186(A)
Gleditsch, E. and T. Gráf. On the gamma-rays of K^{40}—640(L)
—— **and T. Gráf.** Significance of the radioactivity of potassium in geophysics—641(L)
Glover, Clyde P. and K. S. Van Dyke. Variations in crystal quartz—175(A)
Goeckermann, R. H. (see Perlman, I.)—352(L)
Goertzel, G. (see Rose, M. E.)—162(A), 749
Goldberg, Leo (see McMath, Robert R.)—644(L)
Goldblatt, M., E. S. Robinson, and R. W. Spence. Half-life of tritium—973(L)
Golden, S. (see Dailey, B. P.)—871(L)
Goldfarb, E. (see Hughes, D. J.)—646(L)
Goldhaber, M. (see Der Mateosian, E.)—1271(L)
Goldman, J. E. Magneto-striction of annealed and cold worked nickel rods—529(A)
Golian, S. E. (see Krause, E. H.)—173(A)
Gombás, P. On the pressure volume and pressure compressibility relation of metals—1123(L)
Good, W. E. (see Coles, D. K.)—156(A)
—— **and D. K. Coles.** Precision frequency measurements of microwave absorption lines and their fine structure—157(A)
Goodman, C. D. (see Snell, A. H.)—169(A)
Gordy, Walter and Myer Kessler. New electronic system for detecting microwave spectra—644(L)
——, **James W. Simmons, and A. G. Smith.** Nuclear and molecular constants from microwave spectra: Methyl chloride and methyl bromide—344(L)
——, **A. G. Smith, and James W. Simmons.** Analysis of the hyperfine structure in the microwave spectrum of the symmetric top molecule CH_3I—249(L)
——, **William V. Smith, A. G. Smith, and Harold Ring.** Millimeter-wave spectra: hyperfine structure of BrCN and ICN—259(L)
—— (see Ring, Harold)—1262(L)
Gorman, J. G. (see Coles, D. K.)—973(L)
Gorter, C. J. and J. H. VanVleck. Role of exchange interaction in paramagnetic absorption—1128(L)
Goudsmit, S. A. Why Germany did not get the atomic bomb—153(T)
Gould, R. G. (see Solomon, A. K.)—1097
Gráf, T. (see Gleditsch, E.)—640(L), 641(L)
Grahame, D. C. New techniques in the measurement of the capacity of the electrical double layer—522(A)
Graves, E. R. (see Barschall, H. H.)—881
Grayson-Smith, H. Supraconductivity—153(T)
Green, Alex E. S. Self-energy and interaction energy in Podolsky's generalized electrodynamics—628
Gregory, Christopher. Non-linear invariants and the problem of motion—72
Greenblatt, M. H. and P. H. Miller, Jr. Microwave secondary electron multiplier—160(A)
Greenfield, M. A. (see Brown, F. W.)—534(A)
Greenspan, Martin (see Cook, Richard K.)—175(A)
Griesheimer, Rudolph N. Rheological concepts in industry—150(T)
Grosse, A. V. (see Anderson, E. C.)—931
Guth, Eugene (see James, Hubert M.)—537(A)
Guindon, William G., S.J. Radial dependence of the tensor force in the deuteron—526(A)

Haeff, Andrew W. (see DePackh, David C.)—247(L)
Hagemann, F., L. I. Katzin, M. H. Studier, A. Ghiorso, and G. T. Seaborg. $(4n+1)$ radioactive series: the decay products of U^{233}—252(L)
Hagstrum, Homer D. On the dissociation energy of CO—158(A), 947
Hale, Donald H. High frequency-excited spectra of A, Kr, and Xe in the near infra-red—156(A)
Hall, D. (see Hughes, D. J.)—646(L)
Hall, H. J. Notes on impulse corona studies in air—185(A)
Hall, Leonard. Structural absorption of sound in water—537(A)
Hall, T. (see Sutton, R. B.)—1147
Hall, T. A. and P. G. Koontz. Scattering of fast neutrons by helium—196
Halliday, D. (see Cummerow, R. L.)—173(A), 1233
—— (see Quade, E.)—181(A)
Halpern, Otto. On the hyperfine structure of the ground state of H and D atoms—245(L)
—— On the inelastic scattering of neutrons in crystals—260(L)
—— On the scattering of neutrons by O_2 molecules—746(A)
—— **and Norman M. Kroll.** On scattering processes of higher order—82(L)
Halverson, R. R. Photographic method of measuring the peak pressure and duration of the shock wave from an underwater explosion—179(A)
Hannay, N. B. Electrical conductivity and thermionic emission of oxide coated cathodes—153(T)
Hansen, James W. Dust electrostatics—741(A)
Hansen, Jay M. and Harold W. Webb. Specular reflection from mercury vapor—332
Hanson, A. O. and J. L. McKibben. Neutron detector having uniform sensitivity from 10 kev to 3 Mev—673
Hardy, A. E. Application of the I.C.I. color system to the development of the all sulfide television white screen—166(A)

—— (see Johnson, R. E.)—165(A)
Harris, S. P. (see Seidl, F. G. P.)—168(A)
——, **A. S. Langsdorf, Jr., and F. G. P. Seidl.** Resonance scattering of neutrons by cobalt—866
Hartmann, G. K. Remarks on some underwater explosion phenomena and measurements—170(A)
Harvey, J. A. (see English, A. C.)—253(L)
Hass, Georg. Studies on the structure and behavior of thin evaporated films of silver, aluminum, silicon, and germanium—174(A)
Havens, W. W., Jr., I. I. Rabi, and L. J. Rainwater. Interaction of neutrons with electrons in lead—634
Hayden, Richard J. (see Hess, David C., Jr.)—730(L)
—— (see Inghram, Mark G.)—349(L), 515(L), 967, 1269(L)
—— (see Parker, G. W.)—85(L)
Hayward, Evans. Ionization of high energy cosmic-ray electrons—937
Hees, George (see Jacobs, Harold)—174(A)
Heitler, W. and S. Power. On the origin of the soft component of cosmic radiation—266
Helmholtz, A. C., Edwin M. McMillan, and Duane Sewell. Angular distribution of neutrons from targets bombarded by 190-Mev deuterons—740(A), 1003
Henrich, L. (see Sewell, D. C.)—739(A)
Henry, Hugh F. Importance of potential in maintaining a luminous spark in $CuSO_4$ solutions—184(A)
Hereford, Frank L. Specific primary ionization of 1-Mev electrons relative to sea level cosmic radiation—982(L)
Hereford, Frank L., Jr. Acceleration of electrons by a single resonant cavity—159(A)
Herring, Conyers. Survey of the theory of bubble pulsations—170(A)
Hess, David C., Jr. (see Inghram, Mark G.)—349(L), 515, 967, 1269(L)
—— (see Parker, G. W.)—85(L)
——, **Richard J. Hayden, and Mark G. Inghram**—730(L)
Hess, Victor Francis. Further experiments on the surplus gamma-radiation from granite—609
Hessaby, M. Continuous particles—536(A)
Heydenburg, N. P. and D. R. Inglis. Angular distribution of both proton ranges from $O^{16}(d, p)O^{17}$—186(A)
Hicks, Bruce L. On explicit solutions of the equations for steady compressible flow—433(L)
—— Simple diabatic flows of elliptic type—179(A)
Hildebrand, R. (see Moyer, B. J.)—744(A)
—— **and B. J. Moyer.** Preliminary data on absorption of high energy neutrons from the 184-inch cyclotron—1258(L)
Hill, E. L. On the kinematics of uniformly accelerated motions and classical electromagnetic theory—143
—— Relativistic clock problem—236
Hill, J. K. (see Geisler, A. H.)—983(L)
Hillger, R. E., M. W. P. Strandberg, T. Wentink, and R. L. Kyhl. Microwave absorption spectrum of carbonyl sulfide—157(A)
Hincks, E. P. (see English, A. C.)—253(L)
Hjalmars, S. (see Brulin, O.)—1126(L)
Hodge, Mary W. (see Wulf, O. R.)—153(T)
Hoffmann, Banesh. Vector meson and projective relativity—154(A), 458
Hofstadter, Robert. Rise time of pulses in silver chloride crystal counters—747(A)
—— Thallium halide crystal counter—1120(L)
——, **J. C. D. Milton, and S. L. Ridgway.** Behavior of silver chloride crystal counters—977(L)
Hoge, Harold J. Circuits for controlling the power supplied to a calorimeter—182(A)
Hogg, Benjamin G. Vacuum properties of some synthetic dielectrics—522(A)
Hogg, C. C. Secondary recovery in the oil industry—150(T)
Hok, Gunnar. Response of linear resonant system to excitation of a frequency varying linearly with time—159(A)
Holden, A. N. (see Townes, C. H.)—513(L), 740(A)
Holstein, T. Imprisonment of resonance radiation in gases—1212
Holtzman, R. H. (see Hughes, D. J.)—168(A)
—— (see Wallace, J. R.)—168(A)
Hopkins, H. H. (see Cunningham, B. B.)—739(A)
—— (see Seaborg, G. T.)—740(A)
Hornig, Donald F. Method of measuring the thickness of a shock front—179(A)
Horning, W. and M. Weinstein. Meson production 251(L)
Hornyak, William F. (see Cohen, E. Richard)—1127(L)
Horton, C. W. (see Watson, R. B.)—159(A)
Howland, B. (see Shipman, J. D., Jr.)—181(A)
Howland, J. J. (see Perlman, I.)—352(L)
—— (see Templeton, D. H.)—758, 766
Hsiang, Jen-Sen (see Weiss, P. R.)—975(L)
Hudson, George E. Impulsive motion of a thin diaphragm in the plastic range—178(A)
Hughes, D. J. (see Spatz, W. D. B.)—163(A)
—— (see Wallace, J. R.)—168(A)
—— **and C. Eggler.** Cloud-chamber energy measurement of photo-neutron sources—902
——, **D. Hall, C. Eggler, and E. Goldfarb.** Formation and properties of radioactive lithium—646(L)
—— **J. R. Wallace, and R. H. Holtzmann.** Neutron polarization—168(A)
Hughes, Harold Kenneth. Electric resonance method of radiofrequency spectroscopy. Moment of inertia and electric dipole moment of CsF—614
Hulburt, E. O. and R. Tousey. Visibility of stars in daytime—167(A)
Hull, G. F., Jr. and W. Baer. Characteristics of bridges between metallic contacts—532(A)
——, **W. Baer, and H. Saltzman.** Apparatus for the study of bridges and arcs between metallic contacts—522(A)
Huntington, H. B. Ultrasonic measurements on single crystals—321
Hurdle, B. G. (see Ringo, G. R.)—87(L)
Hutchinson, Franklin. Self diffusion coefficient of argon—1256(L)
Hutner, Reina A. (see Saxon, David S.)—744(A)
Huxford, W. S. (see Frank, J. M.)—156(A)
—— (see Sittner, W. R.)—535(A)

Ibser, H. W. (see Snell, Arthur H.)—541
Infeld, L. Recurrence formulas for Coulomb wave function—1125(L)
— Theory of radioactivity in the momentum space—154(A)
Inghram, M. G. (see Brown, Harrison)—347(L)
—— (see Hess, David C., Jr.)—730(L)
—— (see Parker, G. W.)—85(L)
——, **Richard J. Hayden, and David C. Hess, Jr.** Isotopic constitution of lanthanum and cerium—967
——, **Richard J. Hayden and David C. Hess, Jr.** New naturally occurring lanthanum isotope at mass 138—349(L)
——, **David C. Hess, Jr., and Richard J. Hayden.** Mass spectrometric study of fission element 43—1269(L)
——, **A. E. Shaw, D. C. Hess, Jr., and R. J. Hayden.** Nuclear isomerism in dysprosium 165—515(L)
Inglis, D. R. (see Heydenberg, N. P.)—186(A)
Iskraut, Richard W. On the restricted 5-dimensional treatment of wave theories—154(A)
Ives, Herbert E. Physical significance of Birkhoff's gravitational equations—229
Ivey, Henry F. Spectral location of the absorption due to color centers in alkali halide crystals—341(L), Errata—873(L)

Jacobs, Harold and George Hees. Variations in the constants of Richardson's equation as a function of life for the case of oxide coated cathodes on nickel—174(A)
—— **and Armand P. LaRocque.** Minimum sparking potentials of barium, magnesium, and aluminum in xenon—537(A)
Jacobs, S. J. Studies pertaining to the measurement of temperature in a detonating explosive—176(A)
Jacobson, Louis (see Overstreet, Roy)—349(L)
Jaffe, A. A. (see Craggs, J. D.)—784
James, Hubert M. and Eugene Guth. Theory of the increase in rigidity of rubber during cure—537(A)
Jamison, D. E. (see Shaw, T. M.)—537(A)
Jarmotz, P. (see Pepinsky, R.)—529(A)
Jauch, J. M. Hyperfine structure of the ammonia inversion spectrum in an electric field—535(A), 712
—— and K. Watson. Interaction of neutrons with electrons—1254(L)
Jelley, J. V. (see English, A. C.)—253 (L)
Jen, C. K. Microwave spectra and Zeeman effect in a resonant cavity absorption cell—986(L)
Jenkins, F. A. Nuclear spins of the carbon isotopes—169(A)
Jnanananda, Swami. The β-radiations of antimony^{124}, tantalum^{182}, tungsten^{184}, and iridium^{192}—1127(L)
Johnson, M. H., G. T. Rado, and M. Maloof. Complex permeability of Permalloy—173(A)
Johnson, R. E. and A. E. Hardy. Performance characteristics of long-persistence screens, their measurement and control—165(A)
Johnson, Robert C., Roy C. Weidler, and Dudley Williams. Inter-molecular vibration spectrum of water—158(A)
Johnson, Thomas H. Pressure coefficient of surface tension and the expansion ratio of high pressure cloud chambers—86(L)
Johnson, Vivian and Karl Lark-Horovitz. From classical statistics to quantum statistics in germanium semiconductors—153(T)
—— **and Karl Lark-Horovitz.** Theory of low temperature semiconductor resistivity—531(A)
Johnson, W. E., C. H. Bachman, and I. Zaleon. Structure of evaporated copper films—174(A)
Johnston, H. L. (see Daunt, J. G.)—161(A), 502
Jones, R. Clark. X-ray diffraction by randomly oriented line gratings—175(A)
Jones, Wm. B., Jr. On the slow neutron absorption resonances in iodine—362
Jorgenson, T. (see Barschall, H. H.)—881
Jost, Res. Compton scattering and emission of low frequency photons—815
Julian, Renne S. (see Nagle, Darragh E.)—971(L)

Kaesberg, Paul (see Beeman, W. W.)—512(L)
Kaplan, J. Composition of the upper atmosphere—153(T)
—— (see Penn, H. S.)—165(A)
Kaplan, Nathan (see Yagoda, Herman)—356(L)
Katcoff, Seymour. New barium and cesium isotopes: 12.0d Ba^{131}, 10.2d Cs^{131}, and long-lived Ba^{132}—1160
Kaufman, H. and A. Norman Shaw. Further simplifications in the derivation of thermodynamical relations—537(A)
Katzin, L. I. (see Hagemann, F.)—252(L)
Kaye, Wilbur and Richard Devaney. Apparatus for the observation of the Kerr effect with microsecond electrical pulses—165(A)
Kê, T'ing-Sui. Atomic vacancy and the viscosity of grain boundaries in metals—534(A)
—— Effect of grain size and frequency of measurement upon internal friction and rigidity modulus of aluminum—174(A)
—— Stress relaxation across grain boundaries in metals—41
Kelley, Elmer L. and E. Segrè. Some excitation functions of alphas and deuterons on Bi—746(A)
Kennard, E. H. Shock waves on a partly submerged plate—178(A)
Kennedy, W. D. (see Arons, A. B.)—176(A)
Kerr, George P., Jr. (see Olsen, Leonard O.)—115
Kessler, Myer (see Gordy, Walter)—644(L)
—— (see Ring, Harold)—1262(L)
Kidnapillai, M. Note on the barometer coefficient of cosmic-ray intensity—518(L)
Kinsey, B. B. 40-kev transition of ThC″—526(A)
Kirchner, F. Effect of a direct current potential on the initiation of a radiofrequency discharge—348(L)
Kirkwood, John G. (see Brinkley, Stuart R., Jr.)—1109
—— **and Stuart R. Brinkley, Jr.** Theory of the propagation of shock waves—171(A)
Kirshenbaum, A. D. (see Anderson, E. C.)—931
Kittel, Charles. Relaxation effects in paramagnetic and ferromagnetic resonance—529(A)
Klema, Ernest D. Fission cross section of Np^{237}—88(L)

Klick, C. C. and R. J. Maurer. Optical absorption bands in alkali halide crystals—165(A)
Knable, N. (see Moyer, B. J.)—744(A)
Knight, G. B. (see Macklin, R. L.)—435(L)
Knowles, W. Silver bromide grain of special photographic emulsions—535(A)
Knox, William J. Relative cross sections of reactions induced by high energy neutrons in C, N, O, and F—1254(L)
Knudsen, Vern O. Sounds in the ocean—738(T)
Kohman, Truman P. General method for determining coincidence corrections of counting instruments—181(A)
Konopinski, Emil J. H^3 and the mass of the neutrino—518(L)
Koomen, M. J. and R. Tousey. Optical aberrations of the eye and night myopia—534(A)
Koontz, P. G. (see Hall, T. A.)—196
Korff, S. A. On the rise of the wire-potential in counters—477
Kratz, H. R. (see Sherr, R.)—662
Krause, E. H. and S. E. Golian. Further cosmic-ray experiments above the atmosphere—173(A)
Kraybill, Henry L. (see Ovrebo, Paul J.)—172(A)
—— **and Paul J. Ovrebo.** Altitude dependence of high energy atmospheric showers—351(L)
Kroll, Norman M. (see Halpern, Otto)—82(L)
Kruger, P. Gerald (see Phillips, J. A.)—164(A)
—— (see Smith, Lyle W.)—357
—— **and Lyle W. Smith.** Cloud-chamber search for a low mass neutral particle—360
—— **and Lyle W. Smith.** Study of electron tracks in a cloud chamber—167(A)
Kubitschek, H. (see Lichtenberger, H. V.)—164(A)
Kundu, D. N. and M. L. Pool. Results of H^3 bombardment of Ag leading to Pd^{109}—101
Kusch, P. and H. M. Foley. Precision measurement of the ratio of the atomic 'g values' in the $^2P_{\frac{1}{2}}$ and $^2P_{\frac{3}{2}}$ states of gallium—1256(L)
Kyhl, R. L. (see Hillger, R. E.)—157(A)

Labaw, L. W. An "inside" counter for soft beta-emitters—187(A)
Lagemann, Robert T., Alvin H. Nielsen, and Fred P. Dickey. Infra-red spectrum and molecular constants of $C^{13}O^{16}$ and $C^{13}O^{18}$—284
Lamb, Willis E., Jr. and Robert C. Retherford. Fine structure of the hydrogen atom by a microwave method—241
Lampson, C. W. Subsurface phenomena near an exploding charge—170(A)
Lane, C. T. (see Fairbank, William M.)—645(L)
——, **Henry A. Fairbank, and William M. Fairbank.** Erratum: Second sound in liquid He II—1129(L)
Langer, L. M., C. S. Cook, and M. B. Sampson. Erratum: On the alleged gamma-ray of N^{13}—355(L)
Langille, R. C. (see Marshall, J. S.)—538(A)
Langsdorf, A. S., Jr. (see Harris, S. P.)—866
—— (see Seidl, F. G. P.)—168(A)
—— **and W. Arnold.** Simple demonstration of resonance scattering—167(A)
Lantz, P. M. (see Parker, G. W.)—85(L)
La Palme, J. and P. Demers. Regression of the latent image of nuclear tracks in the photographic emulsion—536(A)
Lark-Horovitz, K. (see Bray, Ralph)—530(A)
—— (see Johnson, V. A.)—153(T), 531(A)
—— (see Scanlon, Wayne)—530(A)
——, **J. R. Risser, and R. N. Smith.** Alpha-2 neutrons nuclear research—1117(L)
LaRocque, Armand P. (see Jacobs, Harold)—537(A)
Larson, Q. V. (see Motta, E. E.)—1270(L)
Lauer, James L. and P. H. Miller, Jr. An instrument for the measurement of the index of refraction of liquids in the wave-length range, 200 mμ to 1000 mμ—166(A)
Lauritsen, C. C. (see Christy, R. F.)—698
—— (see Fowler, W. A.)—738(A)
—— (see Lauritsen, T.)—746(A)
——, **T. Lauritsen, and W. A. Fowler.** Gamma-radiation from Be^9+H^1—739(A)
Lauritsen, T. (see Christy, R. F.)—698
—— (see Fowler, W. A.)—738(A)
—— (see Lauritsen, C. C.)—739(A)
——, **W. A. Fowler, and C. C. Lauritsen.** Electrostatic analyzer for 1.5-Mev protons—746(A)
Lavatelli, Leo S. (see McDaniel, B. D.)—729(L)
—— (see Sutton, R. B.)—1147
Law, H. B. Surface tension of glass in the neighborhood of the strain point—184(A)
Lawrence, R. W. Low velocity of detonation in nitroglycerin and other liquid nitric esters—180(A)
Lawson, A. W. Solubility gaps in simple binary systems—533(A)
Lax, Melvin. Absolute sensitivity of a graphite ionization chamber—61
LeCaine, J. Application of a variational method to Milne's problem—564
Leith, C. E., A. Bratenahl, and B. J. Moyer. Radioactivity of Cu^{60}—732(L), 745(A)
Levine, Harold and Julian Schwinger. On the radiation of sound from an unflanged circular pipe—742(A)
Levinger, J. S. (see Snell, Arthur H.)—541, 545
Levinthal, E. C. (see Bloch, F.)—1125(L)
Levy, Paul W. Beta-ray spectrum of C^{14}—248(L)
—— Radiations from 60-day Ir^{192} and 27-day Pa^{232}—352(L)
Lewis, Margaret N. (see Stephens, W. E.)—526(A)
Libby, W. F. (see Anderson, E. C.)—931
Lichtenberger, H. V. (see Brill, T.)—585
——, **R. G. Nobles, G. D. Monk, H. Kubitschek, and S. M. Dancoff.** Boron absorption of resonance activation—164(A)
Lichtenstein, Roland M. Electromechanical properties of rochelle salt at the lower Curie point—492
Liebson, S. H. Discharge mechanism of self-quenching G-M counters—187(A), 602
—— Low voltage self-quenching counters—181(A)
Lindner, M. (see Cunningham, B. B.)—739(A)
—— (see Seaborg, G. T.)—740(A)
Lloyd, Paul E. (see Anderson, Carl D.)—724
Lockwood, J. A. (see Schultz, H. L.)—346(L)

Lodge, J. I. (see Stewart, R. W.)—537(A)
Lofgren, Edward J. (see Wilson, Robert R.)—1131
Long, E. A. (see Sutton, R. B.)—1147
Longini, R. L. Motion of low pressure arc spots in magnetic fields—184(A)
Lonsdale, Kathleen. Diffuse scattering of x-rays—153(T)
Lopes, J. Leite. On the high energy neutron-proton scattering—355(L)
—— **and J. Tiomno.** On the proton-proton scattering at 14.5 Mev—731(L)
Loughridge, D. H. and F. M. Millican. Temperature coefficients of cosmic-ray components—743(A)
Lounsbury, M., S. Epstein, and H. G. Thode. Isotopic composition of normal krypton and xenon—517(L)
Luttinger, J. M. and L. Tisza. Erratum: Theory of dipole interaction in crystals—257(L)

Ma, S. T. Relativistic invariance of the quantum theory of radiation—1090
MacDougall, D. P. Experimental studies of detonation velocities in high explosives—176(A)
Mack, J. E. and N. Austern. Newly observed structure in HeλII 4686—972(L)
Macklin, R. L. and G. B. Knight. X-rays associated with U^{234}—435(L)
MacNair, D. and A. H. White. Electrical conductivity of alkaline earth oxides—153(T)
Madansky, Leon and M. L. Wiedenbeck. Measurement of the decay time of short lived metastable states—185(A)
Majumdar, Sudhansu Datta. Class of exact solutions of Einstein's field equations—390
Malich, C. W. (see Bonner, T. W.)—163(A)
Malone, T. F. Meteorology of the atmosphere between 10 and 20 kilometers—153(T)
Maloof, M. (see Johnson, M. H.)—173(A)
Mandeville, C. E. and Morris Scherb. A coincidence study of Ga^{72}—520(L)
Manley, J. H. (see Barschall, H. H.)—875, 881
Marcus, Jules A. deHaas-van Alphen effect in a single crystal of zinc—162(A)
Mariner, Thomas and Walker Bleakney. Ionization and dissociation of formic acid monomer by electron impact—792
—— **and Walker Bleakney.** Note on the significance of appearance potentials of ions in a mass spectrometer 807
Mark, C. Neutron density near a plane surface—558
Marshak, R. E. Milne problem for a large plane slab with constant source and anisotropic scattering—47
—— (see Snyder, H.)—1253(L)
—— **and H. A. Bethe.** On the two-meson hypothesis—506
Marshall, Fitz-Hugh (see Coltman, J. W.)—528(A)
—— **and J. W. Coltman.** Photo-multiplier radiation detector—528(A)
Marshall, F. R. (see Zarem, A. M.)—158(A)
Marshall, J. (see Fermi, E.)—193
Marshall, J. S., R. C. Langille, W. M. Palmer, and D. W. Perrie. Measurement of rainfall by radar—538(A)
Marshall, L. (see Fermi, E.)—193, 408, 1139
Martin, A. B. Energy levels in the nucleus Mn^{56}—378
Marton, L. and P. H. Abelson. Tracer micrography—161(A)
Mason, F. D. (see Stephenson, S. T.)—744(A)
Mason, W. P. Comments on "Theory of the ferroelectric effect and clamped dielectric constant of rochelle salt" —976(L)
—— Electrostrictive effect in barium titanate—869(L)
—— Theory of the ferroelectric effect and clamped dielectric constant of rochelle salt—854
Mathias, B. T., R. G. Breckenridge, and D. W. Beaumont. Single crystals of barium titanate—532(A)
Matthews, David E. and M. L. Pool. X-ray emission from radioactive Ce, Pd, and Ca—163(A)
Maurer, R. J. (see Klick, C. C.)—165(A)
May, A. N. (see English, A. C.)—253(L)
McCarthy, R. L. (see Schultz H. L.)—346(L)
McDaniel, B. D., R. B. Sutton, Leo S. Lavatelli, and E. E. Anderson. Absorption cross section of gold for neutrons of energies from 0.01 to 0.3 ev—729(L)
——, **Guy von Dardel, and Robert L. Walker.** Absorption of 17-Mev gamma-rays in lead and aluminum—985(L)
McFee, R. H. Foreign ion rejection in the growth of sodium chloride single crystals from the melt—176(A)
McInteer, B. B., L. T. Aldrich, and Alfred O. Nier. Thermal diffusion constant of helium and the separation of He^3 by thermal diffusion—510(L)
McKay, K. G. (see Ahearn, A. J.)—524(T)
McKeehan, L. W. Magnetic dipole fields in unstrained cubic crystals—78(L)
McKeown, M. (see Der Mateosian, E.)—1271(L)
McKibben, J. L. (see Hanson, A. O.)—673
McKinley, W. and H. Feshbach. Elastic Coulomb scattering of electrons at relativistic energies—155(A)
McMath, Robert R., Arthur Adel, Leo Goldberg, and Orren C. Mohler. New atomic lines in the infra-red solar spectrum—644(L)
McMillan, Edwin M. Energy and half-life of the Be^{10} radioactivity—591
—— (see Chupp, Warren W.)—873(L)
—— (see Cook, Leslie J.)—1264(L)
—— (see Helmholtz, A. C.)—740(A), 1003
McMillan, W. G. and E. Teller. On the production of mesotrons by nuclear bombardment—1
—— **and E. Teller.** Theoretical mesotron production by nuclear bombardment—155(A)
Meeks, Wilkison and Russell A. Fisher. Hyperfine structure and nuclear moments of columbium^{93}—451
—— **and Russell A. Fisher.** Nuclear magnetic moment of columbium from hyperfine structure—169(A)
Meem, J. Lawrence, Jr. (see Ramsey, Margaret M.)—639(L)
Meiners, E. P., Jr. (see Snell, Arthur H.)—545
Meissner, K. W. and L. G. Mundie. Structure of the *D*-terms of Li^7—535(A)
Meister, Arnold G. and Forrest F. Cleveland. Nondegenerate vibrations of diacetylene, dimethylacetylene, and dimethyldiacetylene—157(A)
Mendenhall, H. E. Secondary emission from conducting films of tin oxide—532(A)

Merchant, M. Eugene. Studies in friction II. Maximum shear strength of solids in relation to thermodynamics of melting—534(A)
Merritt, F. R. (see Townes, C. N.)—513(L), 740(A), 1266 (L)
Metropolis, N. (see Frankel, S.)—914
—— **and S. Frankel.** Calculations in the liquid drop model of fission—186(A), 914
Meyerhof, Walter E. and Gertrude Scharff-Goldhaber. Decay-scheme for Sb^{124}—164(A), 273
Meyerott, R. E. (see Breit, G.)—1023
—— (see Setlow, R. B.)—186(A)
Miller, Arthur E. and Martin Deutsch. Decay scheme of Sc^{48}—527(A)
Miller, D. R. (see Cunningham, B. B.)—739(A)
—— (see Seaborg, G. T.)—740(A)
Miller, P. H., Jr. (see Greenblatt, M. H.)—160(A)
—— (see Lauer, James L.)—166(A)
Millican, F. M. (see Loughridge, D. H.)—743(A)
Millikan, R. A., H. V. Neher, and W. H. Pickering. Primary cosmic-ray protons and the atom annihilation hypothesis—513(L)
Milone, Carmel and Vanna Tongiorgi. On the generation in paraffin of ionizing penetrating particles by a neutral component of the cosmic radiation—735(L)
Milton, J. C. D. (see Hofstadter, R.)—977(L)
Mitchell, Allan C. G. (see Ramsey, Margaret M.)—639(L)
Mitchell, F. H. and L. B. Snoddy. Ionization processes in in a long discharge tube with application to lightning mechanism—1202
Moak, Charles D. (see Wollan, E. O.)—447
Mohler, Fred L. and Vernon H. Dibeler. Mass spectrometer analysis of C_2H_2, C_2D_2, and C_2DH—158(A)
Mohler, Orren C. (see McMath, Robert R.)—644(L)
Mohr, E. I. (see Weissler, G. L.)—289
—— **and G. L. Weissler.** Positive corona in Freon-air mixtures—294
Monk, G. D. (see Lichtenberger, H. V.)—164(A)
Montgomery, C. G. (see Schultz, H. L.)—346(L)
—— **and D. D. Montgomery.** Atmospheric showers of cosmic rays—173(A)
—— **and D. D. Montgomery.** Transition effect for large bursts of cosmic-ray ionization. II—131
Montgomery, D. D. (see Montgomery, C. G.)—131, 173(A)
Mooney, Rose C. L. Crystal structure of element 43—1269(L)
Moore, G. E. (see Cummerow R. L.)—173(A), 1233
Morris, P. A. (see Swann, W. F. G.)—1262(L)
—, **W. F. G. Swann, and H. C. Taylor.** Sea level latitude effect of cosmic radiation—1263(L)
Morse, P. M. Plans for Brookhaven National Laboratory —521(T)
Morton, G. A. (see Davidson, W. L.)—168(A)
Motta, E. E., G. E. Boyd, and Q. V. Larson. Production and properties of a long-lived radio-isotope of element 43—1270(L)
Moyer, B. J. (see Hildebrand, R.)—1258(L)
—— (see Leith, C. E.)—732(L), 745(A)
—— (see Parmley, Thomas J.)—82(L), 746(A)
—, **R. Hildebrand, N. Knable, T. J. Parmley, and H. York.** Character of the radiation field and shielding at the 184-inch cyclotron—744(A)
Mrozowski, S. On the $^2\pi_u \rightarrow {}^2\pi_g$ bands of CO_2^+. Parts III and IV—682, 691
Muelhause, C. O. (see Der Mateosian, E.)—1271(L)
Mundie, L. G. (see Meissner, K. W.)—535(A)
Munk, M. M. Substitution flows in theoretical gas flow —176(A)
Murphey, Byron F. Temperature variation of the thermal diffusion factors for binary mixtures of hydrogen, deuterium, and helium—834
Mutter, W. E. Rectification characteristics of an oxide cathode interface—531(A)

Nagle, Darragh E., Renne S. Julian, and Jerrold R. Zacharias. Hyperfine structure of atomic hydrogen and deuterium—971(L)
—— (see Bitter, F.)—1271(L)
Neddermeyer, S. H. Ultra-fast counters—741(A)
Nedzel, V. A. (see Snell, Arthur H.)—541
Neher, H. V. (see Millikan, R. A.)—513(L)
Newkirk, J. B. (see Geisler, A. H.)—983(L)
Newton, R. R. Positive ion transient in Townsend discharge tubes—184(A)
Ney, E. P. (see Winn, E. B.)—77(L)
Nielsen, Alvin H. (see Lagemann, Robert T.)—284
Nielsen, Harald H. and David M. Dennison. Anomalous values of certain of the fine structure lines in the ammonia microwave spectrum—86(L), 1101
Nier, Alfred O. (see Daunt, J. G.)—502(L)
—— (see McInteer, B. B.)—510(L)
Nierenberg, W. A. (see Brody, S. B.)—258(L)
—— **and N. F. Ramsey.** Radiofrequency spectra of the sodium halides—1075
Nobles, R. G. (see Lichtenberger, H. V.)—164(A)
Nolle, A. W. Temperature dependence of the dynamic modulus of rubber—184(A)
Nottingham, Wayne B. Crystallographic non-uniformity and its influence on the thermionic emission properties of clean surfaces—153(T)
Novic, Aaron. Half-life of tritium—972(L)
Nudenberg, R. (see Coleman, K. D.)—164(A)

O'Connor, P. R. (see Cunningham, B. B.)—739(A)
—— (see Seaborg, G. T.)—740(A)
Olsen, Leonard O. and George P. Kerr, Jr. Quenching and depolarization of mercury resonance radiation by nitrogen and oxygen—115
Omer, Guy C., Jr. Non-homogeneous cosmological model —744(A)
Ore, Aadne. Binding energy of the quadrielectron—521(A)
Osborne, N. S. (see Ginnings, D. C.)—182(A)
Oughton, C. D. (see Schaffert, R. M.)—535(A)
Overstreet, Roy and Louis Jacobson. On the existence of a calcium isotope with an 8.5 day period—349(L)
Ovrebo, Paul J. (see Kraybill, Henry L.)—351(L)
—— **and Henry L. Kraybill.** High energy cosmic-ray air showers—172(A)
Oxley, C. L. (see Dearnley, I. H.)—169(A)

Packard, M. E. (see Bloch, F.)—1125(L)
Palmer, W. M. (see Marshall, J. S.)—538(A)
Parker, G. W., P. M. Lantz, M. G. Inghram, D. C. Hess, Jr., and R. J. Hayden. The 5.3 day isotope in element 61—85(L)
Parkins, William E. (see Forrester, A. Theodore)—728(L)
—— (see Smith, Lloyd P.)—989
Parmley, T. J. (see Moyer, B. J.)—744(A)
—— **and Burton J. Moyer.** Cobalt 61 radioactivity—82(L), 746(A)
Patterson, Claire (see Brown, Harrison)—456
Peabody, C. O. (see Smith, B. S.)—527(A)
Peacock, Charles and Roger G. Wilkinson. Disintegration scheme of Sc^{46}—251(L)
Peacock, W. C. Decay scheme of $_{45}Rh^{106}$—1049
Pearson, G. L. (see Gibney, R. B.)—76(L)
Peck, R. A., Jr. Calibration for Eastman proton plates—1121(L)
Peierls, R. E. and M. A. Preston. Proton-proton scattering at 10 Mev—250(L)
Pellam, John R. and Charles F. Squire. Ultrasonic velocity and absorption in liquid He—1245
Penn, H. S. and Joseph Kaplan. Fluorescence of cancerous and non-cancerous lipoids—165(A)
Pepinsky, R. An electronic computer for crystal structure analyses—175(A)
—— **and P. Jarmotz.** Inductively coupled degenerative high voltage stabilizer—529(A)
Perlman, I. (see Cunningham, B. B.)—739(A)
—— (see Seaborg, G. T.)—740(A)
—— (see Templeton, D. H.)—758, 766
——, **R. H. Goeckermann, D. H. Templeton, and J. J. Howland.** Fission of bismuth, lead, thallium, platinum, and tantalum with high energy particles—352(L)
Perlman, M. L. and G. Friedlander. Relative yields of (γ, n) reactions—1272(L)
Perlow, Gilbert J. V-2 cosmic-ray experiment—173(A)
Perls, Thomas A. Quantitative experiment on the rotation of electrolytes in a magnetic field—183(A)
Perrie, D. W. (see Marshall, J. S.)—538(A)
Perry, J. E., Jr. (see Dearnley, I. H.)—169(A)
Petersen, R. P. (see Fraser, L. W.)—173(A)
Peterson, Jack M. (see Cook, Leslie J.)—1264(L)
Peterson, K. C. (see Sawyer, R. B.)—109
Phillips, J. A. and P. Gerald Kruger. Energy of gamma-rays emitted during the reaction $F(p, \alpha)O$—164(A)
Phillips, T. D. Miniature demonstration for the physics museum—150(T)
Pi, T. H. and C. Y. Chao. On the positively charged particles accompanying the beta-rays of P^{32}—639(L)
Pickering, W. H. (see Millikan, R. A.)—513(L)
Pike, E. W. (see Gibbs, Norman)—160(A)
Pincherle, L. Refraction of plane non-uniform electromagnetic waves between absorbing media—232
Placzek, G. Angular distribution of neutrons emerging from a plane surface—556
—— Diffusion of neutrons—524(T)
—— **and W. Seidel.** Milne's problem in transport theory—550
Plyler, E. K. Infra-red spectroscopy beyond 15μ—165(A)
Podolsky, Boris. On the Lorentz transformation of charge and current densities—624
Polachek, Harry. Underwater explosion of a cylindrical charge—177(A)
Pollard, E. Proton groups in transmutations—521(T)
—— (see Alburger, D. E.)—169(A)
—— (see Davison, P. W.)—162(A)
—— **and D. E. Alburger.** Gamma-rays from the alpha-particle bombardment of Na, Mg, Al, Si, P, S—1196
—— **and Perry W. Davison.** Energy levels of O^{17} obtained from $O^{16}(d, p)O^{17}$ and $N^{14}(\alpha, p)O^{17}$—736(L)
Pond, T. Alexander and Walter F. Cannon. Saturation effect in microwave spectrum of ammonia—1121(L)
Pontecorvo, B. Nuclear capture of mesons and the meson decay—246(L)
Pool, M. L. (see Coleman, K. D.)—164(A), 1070
—— (see Edwards, J. E.)—384
—— (see Kundu, D. N.)—101
—— (see Matthews, David E.)—163(A)
Poole, F. L. (see Zarem, A. M.)—158(A)
Poss, H. L. Magnetic moment of Tl^{205}—637(L)
——(see Bitter F.)—1271(L)
Pound, R. V. Nuclear magnetic moments of bromine—1273(L)
—— Radiofrequency spectrometer for the detection of resonance absorption—527(A)
Powell, John L. Recurrence formulas for Coulomb wave functions—626
—— (see Broyles, Arthur A.)—155(A)
—— (see Zilsel, Paul R.)—155(A), 225
Powell, Wilson M. Cloud chamber study of the particles in the neutron beam of the 184-inch cyclotron—739(A)
Power, S. (see Heitler, W.)—266
Present, R. D. On self-quenching halogen counters—243
—— On the division of nuclear charge in fission—7
Preston, M. A. (see Peierls, R. E.)—250(L)
Price, W. J. Calculation of the shear elastic constants of the alkali halides—514(L)
Primakoff, H. Long range tensor forces and the magnetic moment of the deuteron—118
Probst, R. E. (see Daunt, J. G.)—502
Purcell, E. M. Nuclear magnetic resonance absorption in solids and liquids—524(T)
—— Recent results in nuclear magnetic resonance absorption—521(T)

Quade, E. and D. Halliday. Magnetic lens beta-ray spectrometer—181(A)

Rabi, I. I. (see Havens, W. W., Jr.)—634
Rado, G. T. (see Johnson, M. H.)—173(A)
Rainwater, L. J. (see Havens, W. W., Jr.)—634
Raitt, R. W. Vertical reflection of supersonic sound from the sea bottom—745(A)
Ramsay, B. P. (see Brown, V. A.)—528(A)
Ramsay, Margaret M., J. Lawrence Meem, Jr., and Allan C. G. Mitchell. Radiations from K^{38}—639(L)
Ramsey, N. F. (see Brody, S. B.)—258(L)
—— (see Nierenberg, W. A.)—1075
Randall, J. A. (see Estermann, I.)—530(A)

Rapuano, Robert A. Ultrasonic absorption from 75 to 280 Mc/sec.—78(L).
—— Ultrasonic absorption in liquids from 100 to 225 Mc/sec.—184(A)
Rau, R. Ronald (see Anderson, Carl D.)—724
Redman, W. C. and D. Saxon. Delayed neutrons in plutonium and uranium fission—570
Reid, A. F. (see Anderson, E. C.)—931
Retallack, J. G. Further measurements on the mass of the mesotron—742(A)
Retherford, Robert C. (see Lamb, Willis E.)—241(L)
Rice, P. J. (see Schultz, H. L.)—346(L)
Richardson, J. Reginald (see Wilson, Robert R.)—1131
Ridgway, S. L. (see Hofstadter, R.)—977(L)
Ring, Harold, Howard Edwards, Myer Kessler, and Walter Gordy. Microwave spectra: methyl cyanide and methyl isocyanide—1262(L)
——(see Gordy, Walter)—259(L)
Ringo, G. R., J. W. Fitzgerald, and B. G. Hurdle. Propagation of U.H.F. sound in mercury—87(L)
Risser, J. R. (see Bonner, T. W.)—163(A)
—— (see Lark-Horovitz, K.)—1117(L)
Roberts, Arthur. Magnetic moment of the deuteron—979(L)
—— Two new methods for observing nuclear radiofrequency resonance absorption—182(A)
Roberts, R. B. and P. H. Abelson. $(d-n)$ reactions at 15 Mev—76(L)
Robertson, J. K. (see Stewart, R. W.)—537(A)
Robinson, E. S. (see Goldblatt, M.)—973(L)
Rogers, F. T., Jr. Calculation of XR for a high energy particle from its deflection in a uniform electrostatic field—161(A)
Rose, Albert. Electron optical aspects of surface problems—153(T)
Rose, M. E. and G. Goertzel. High energy photo-disintegration of the deuteron—162(A), 749
Rosen, Louis (see Fowler, J. L.)—926
—— (see Froman, Darol)—525(A)
Rosen, Nathan. An attempt at a statistical theory of space-time—156(A)
—— Statistical geometry and fundamental particles—298, 1253(L)
Rosenblum, Earl S. On the double focusing beta-ray spectrometer—731(L)
Rossi, Bruno (see Bridge, Herbert)—257(L)
—— (see Froman, Darol)—525(A)
—— (see Williams, R. W.)—172(A)
——, **Matthew Sands, and Robert F. Sard.** Measurement of the slow meson intensity at several altitudes—120
—— **and R. W. Williams.** Cosmic-ray induced nuclear disintegrations at 11,500 feet—172(A)
Rubin, Sylvan. Photographic apparatus for angular distribution measurements—1176
—— Proton scattering from Be^9—739(A)
Ruedy, R. Wiedemann-Franz-Lorenz ratio for copper alloys—533(A)

Sachs, R. G. Interpretation of the triton moment—312
—— On the magnetic moment of the deuteron—91
—— (see Eisner, E.)—680
Saibel, Edward. Speed of propagation of a fracture crack in metals—534(A)
Saltzman, H. (see Hull, G. F., Jr.)—522(A)
Sampson, M. B. (see Langer, L. M.)—355(L)
—— (see Snell, Arthur H.)—541, 545
Sands, Matthew (see Rossi, Bruno)—120
San-Tsiang, Tsien. On the tripartition of heavy elements—1257(L)
Sard, Robert F. (see Rossi, Bruno)—120
Sawyer, R. B. (see Wollan, E. O.)—447
——, **E. O. Wollan, S. Bernstein, and K. C. Peterson.** Bent crystal neutron spectrometer and its application to neutron cross-section measurements—109
Saxon, D. (see Redman, W. C.)—570
Saxon, David S. and Reina A. Hutner. Electronic energy levels in simple crystal models—744(A)
Scalettar, R. (see Snell, A.)—169(A)
Scanlon, Wayne and K. Lark-Horovitz. Electrical behavior of vacuum evaporated tellurium—530(A)
Schaffert, R. M. and D. C. Oughton. Electrophotography—535(A)
Scharff-Goldhaber, Gertrude (see Meyerhof, Walter E.)—164(A), 273
Schein, Marcel (see Gill, Piara Singh)—733(L)
—— (see Ticho, Harold K.)—248(L)
—— **and J. Steinberger.** On the production of cosmic-ray mesotrons by primary protons—734(L)
——, **Piara Singh Gill, and Victor Yngve.** Latitude effect of the mesotron component up to elevations of 35,000 feet—171(A)
Scherb, Morris (see Mandeville, C. E.)—520(L)
Schiff, L. I. (see Feshbach, H.)—254(L)
Schreffler, R. G. (see Cork, J. M.)—186(A)
Schroeder, C. A. (see Shipman, J. D., Jr.)—181(A)
Schultz, H. L., R. Beringer, C. L. Clarke, J. A. Lockwood, R. L. McCarthy, C. G. Montgomery, P. J. Rice, and W. W. Watson. Cavity accelerator for electrons—346(L)
Schwarzmann, Gertrude. Composite non-Keplerean orbits—154(A)
—— Cosmic rays as products of radioactivity—744(A)
—— On the nuclear mass defect—536(A)
Schwinger, Julian. Variational principle for scattering problems—742(A)
—— (see Levine, Harold)—742(A)
Scott, Russell B. (see Wacker, Paul F.)—182(A)
—— **and J. W. Cook.** Simon-type helium liquefier with provision for withdrawing the liquid—161(A)
Seaborg, G. T. (see Cunningham, B. B.)—739(A)
—— (see Hagemann, F.)—252(L)
——, **B. B. Cunningham, H. H. Hopkins, M. Lindner, D. R. Miller, P. R. O'Connor, I. Perlman, and R. C. Thompson.** Transmutations with high-energy helium ions in the 184-inch cyclotron—740(A)
Seagondollar, L. W. and H. H. Barschall. Total cross section of aluminum for fast neutrons—439
Seall, Robert. Simple proof of the existence of minimum deviation of a prism—150(T)
Seaton, S. L. Rate of electron production in the ionosphere—720

Segrè, E. (see Kelly, Elmer, L.)—746(A)
Seidel, W. (see Placzek, G.)—550
Seidl, F. G. P. (see Harris, S. P.)—866
——, **S. P. Harris, and A. S. Langsdorf, Jr.** Resonance scattering of neutrons by Mn^{55}—168(A)
Seitz, F. Diffraction of neutrons in crystals—524(T)
Senseman, Richard W. (see Thornton, R. L.)—872(L)
Serber, R. Nuclear reactions at high energies—1114
—— Production of high energy neutrons by stripping—740(A), 748(A), 1007
Serin, B. Conductivity of metals at microwave frequencies—1261(L)
Seren, L. (see Friedlander, H. N.)—23
—— (see Vought, R. H.)—164(A)
——, **Herbert N. Friedlander, and Solomon Turkel.** New radio isotopes of tantalum produced by slow neutron irradiation—163(A)
——, **Herbert N. Friedlander, and Solomon H. Turkel.** Thermal neutron activation cross section—888
Setlow, R. B. and Roland Meyerott. The *b'* and *c* states of N_2—186(A)
Sewell, D. C., L. Henrich, and J. Vale. Some operating phenomena associated with the 184-inch cyclotron—739(A)
—— see Cook, Leslie J.)—1264(L)
—— (see Helmholtz, A. C.)—740(A), 1003
Shaler, A. J. and J. Wulff. Rate of sintering of copper powder—79(L)
Shankland, Robert S. (see Wilson, Robert R.)—1131
Shaw, A. E. (see Inghram, M. G.)—515(L)
Shaw, A. Norman (see Kaufman, H.)—537(A)
Shaw, T. M., D. E. Jamison, and J. A. Galvin. Impedance of biological cells at microwave frequencies—537(A)
Shearer, Robert E. Metallic rectifiers, a review—150(T)
Shenstone, A. G. ^5S state of carbon—411
—— Erratum: Arc spectrum of silver—1273(L)
Sherr, R., J. M. Blair, H. R. Kratz, C. L. Bailey, and R. F. Taschek. Scattering of protons by deuterons—662
Shipman, J. D., Jr., B. Howland, and C. A. Schroeder. Diode coincidence circuit—181(A)
Shockley, W. (see Brattain, W. H.)—345(L)
Shreffler, R. G. (see Cork, J. M.)—186(A), 1209
Shull, C. G. (see Davidson, W. L.)—168(A)
——, **and E. O. Wollan.** Diffraction of neutrons by crystalline powders—168(A)
Shull, Franklin B. and David M. Dennison. Double focusing beta-ray spectrometer—180(A); Errata; 256(L).
Siegert, A. J. F. On the recurrence-time probability for the harmonic oscillator in the limit of vanishing mass—537(A)
Silsbee, F. B. Impending change in the electrical units—159(A)
Simmons, James W. (see Gordy, Walter)—249(L), 344(L)
Simpson, J. A., Jr., Properties of ion counters operating at low potentials—181(A)
Sittner, W. R., and W. S. Huxford. Infra-red spectra of argon, krypton, and xenon between 1.15 and 2.25 microns—535(A)
Skellett, A. M. Palletron, a new electron resonator and its proposed application to the generation of potentials in the million volt range—180(A)
Slater, J. C. Some applications of microwaves to physics—738(T)
—— Theoretical foundations of low-temperature physics—153(T)
Slawson, I. E. (see Snell, A. H.)—169(A)
Sleator, William, Jr. Collision cross sections of carbon and hydrogen for fast neutrons—207
Slepian, J. and W. M. Brubaker. Ambipolar diffusion of ions and electrons—185(A)
Smith, A. G. (see Gordy, Walter)—249(L), 259(L), 344(L)
Smith, B. S., H. Carmichael, J. F. Steljes, C. O. Peabody, and D. S. Craig. Design and performance of two of the Chalk River ion-chambers—527(A)
Smith, Lloyd P. Mass spectrographic investigations of solid surfaces—153(T)
——, **W. E. Parkins, and A. T. Forrester.** On the separation of isotopes in quantity by electromagnetic means—989
Smith, Lyle W. (see Kruger, P. Gerald)—167(A), 360
—— **and P. Gerald Kruger.** Multiple scattering of electrons in the gas of a Wilson cloud chamber—357
Smith, R. N. (see Bray, Ralph)—530(A)
—— (see Lark-Horovitz, K.)—1117(L)
Smith, William V. (see Carter, Robert L.)—1265(L)
—— (see Gordy, Walter)—259(L)
—— **and R. L. Carter.** Saturation effect in microwave spectrum of ammonia—638(L)
Smoluchowski, R. Impingement and stimulation in grain growth—533(A)
—— Reglarities in the properties of metallic elements—538(A)
Smythe, W. R. Double current sheet in diffraction—1066
Snell, A. H., C. D. Goodman, P. H. Abelson, R. Scalettar, G. M. Branch, I. E. Slawson, and W. E. Stanley. Criticality studies of the enriched-uranium heavy-water chain-reacting system—169(A)
——, **J. S. Levinger, E. P. Meiners, Jr., M. B. Sampson, and R. G. Wilkinson.** Studies of the delayed neutrons II. Chemical isolation of the 56-second and the 23-second activities—545
——, **V. A. Nedzel, H. W. Ibser, J. S. Levinger, R. G. Wilkinson, and M. B. Sampson.** Studies of the delayed neutrons I. Decay curve and the intensity of the delayed neutrons—541
Snoddy, L. B. (see Mitchell, F. H.)—1202
Snyder, Hartland S. Electromagnetic field in quantized space-time—68
—— Fluctuations for proportional counters—181(A)
—— **and R. E. Marshak.** Velocity dependence of nuclear forces—1253(L)
Snyder, T. (see Sutton, R. B.)—1147
Solomon, A. K., R. G. Gould, and C. B. Anfinsen. Energy of beta-radiation from S^{35} and C^{14}—1097
Sosnowski, L. Excess-defect semiconductor contacts—641(L)

Spatz, W. D. B., D. J. Hughes, and A. Chan. Photo-neutrons produced in D_2O and beryllium by fission product gamma-rays—163(A)
Spence, R. W. (see Goldblatt, M.)—973(L)
Spencer, Roy C. and Pauline Austin. Methods of calculation of radiation patterns of line sources—186(A)
Sperduto, A. (see Buechner, W. W.)—678
Spitzer, R. W. (see Wilson, E. B., Jr.)—178(A)
Squire, Charles F. (see Pellam, John R.)—1245
Stanley, W. E. (see Snell, A. H.)—169(A)
Stanton, J. (see Cassen, B.)—180(A)
Steinberger, J. (see Schein, Marcel)—734(L)
Steljes, J. F. (see Smith, B. S.)—527(A)
Stephens, W. E. and Margaret N. Lewis. High energy limit of the C^{14} beta-ray spectrum—526(A)
Stephenson, S. T. and F. D. Mason. Vacuum x-ray spectrometer—744(A)
Stewart, R. W., J. I. Lodge, and J. K. Robertson. Interference patterns on the walls of tubes carrying high frequency discharges—537(A)
Stimson, H. F. and C. S. Cragoe. Triple point of water as a fixed point on the international temperature scale—183(A)
Stoner, Richard G. (see Bleakney, Walker)—170(A)
Strandberg, M. W. P. (see Hillger, R. E.)—157(A)
Studier, M. H. (see Hagemann, F.)—252(L)
Sutton, R. B. (see McDaniel, B. D.)—729(L)
——, **T. Hall, E. E. Anderson, H. S. Bridge, J. W. DeWire, L. S. Lavatelli, E. A. Long, T. Snyder, and R. W. Williams.** Scattering of slow neutrons by *ortho-* and *para*-hydrogen—1147
Swann, W. F. G. (see Morris, Peter A.)—1263(L)
—— **and P. A. Morris.** Abnormality in cosmic-ray absorption in lead in low latitudes—1262(L)
Swift, Elijah, Jr. and John C. Decius. Energy parameters of explosion product bubbles in free water—177(A)

Taft, E. (see Apker, LeRoy)—153(T)
Taschek, R. F. (see Sherr, R.)—662
Tatel, H. E. (see Fraser, L. W.)—173(A)
Taub, A. H. Refraction of plane shock waves—51
Taylor, H. C. (see Morris, Peter A.)—1263(L)
Taylor, Robert B. Glass and physics in Scandanavia—150(T)
Teller, E. (see Fermi, E.)—399
—— (see McMillan, W. G.)—1, 155(A)
Templeton, D. H. (see Perlman, I.)—352(L)
——, **J. J. Howland, and I. Perlman.** Artificial radioactive isotopes of bismuth and lead—766
——, **J. J. Howland, and I. Perlman.** Artificial radioactive isotopes of polonium—758
Tendam, D. J. (see Bradt, H. L.)—527(A), 1117(L)
—— **and H. L. Bradt.** Indium isotopes produced by bombardment of silver with 20-Mev alpha-particles—527(A)
—— **and H. L. Bradt.** Radioactive indium isotopes of mass numbers 111 and 112—1118(L)
Thayer, R. N. Laboratory exercises and thesis possibilities using standard fluorescent lamps—150(T)
Thode, H. G. (see Lounsbury, M.)—517(L)
Thompson, R. C. (see Cunningham, B. B.)—739(A)
—— (see Seaborg, G. T.)—740(A)
Thornton, R. L. and Richard W. Senseman. Excitation curves for the reactions $C^{12}(d, dn)C^{11}$ and $C^{13}(d, dn)C^{13}$ at high energies—872(L)
Ticho, Harold K. Mean life of mesotrons at an altitude of 11,500 ft.—255(L)
—— **and Marcel Schein.** On the change of the mean life of negative mesotrons—248(L)
Tiomno, J. (see Lopes, J. Leite)—731(L)
Tisza, Laszlo. On a connection between the fountain effect, second sound, and thermal conductivity in liquid helium II—353(L)
—— On the classification of phase transitions—532(A)
—— Phase transition in the hydrogen halides—161(A)
—— Theory of liquid helium—838
—— (see Luttinger, J. M.)—257(L)
Tongiorgi, Vanna (see Milone, Carmel)—735(L)
Torrey, H. C. (see Weiss, P. R.)—975(L)
Tousey, R. (see Hulburt, E. O.)—167(A)
—— (see Koomen, M. J.)—534(A)
Townes, C. H., A. N. Holden, and F. R. Merritt. Microwave spectra of linear molecules—513(L)
——, **A. N. Holden, and F. R. Merritt.** Nuclear and molecular information from microwave spectra—740(A)
—— **and F. R. Merritt.** Stark effect in high frequency fields—1266(L)
Turkel, S. H. (see Friedlander, H. N.)—23
—— (see Seren, Leo)—163(A), 888
Turkevich, John. Chemical aspects of surfaces—153(T)
Turner, H. Compatibility of primary protons with the atom-annihilation hypothesis—512(L)

Urick, R. J. Acoustic interferometer for the measurement of sound velocity in the ocean—746(A)

Vale, J. (see Sewell, D. C.)—739(A)
Vallarta, Manuel S. On the magnetic field of the milky way and its effect on cosmic radiation—519(L)
Valley, G. E. Radioactive decay of slow positive and negative mesons—772
Van Allen, J. A. (see Fraser, L. W.)—173(A)
Van de Graaff, R. J. (see Buechner, W. W.)—678
Van Dyke, K. S. (see Clyde, P.)—175(A)
Van Vleck, J. H. (see Gorter, C. J.)—1128(L)
Victoreen, John A. Atomic absorption coefficient for x-rays—869(L)
Villars, Felix. On the magnetic exchange moment for H^3 and He^3—256(L)
von Dardel, Guy (see McDaniel, Bryce D.)—985(L)
Vought, R. H. and Leo Seren. Positron analysis of high energy gamma-ray spectra—164(A)

Wacker, Paul F., Ruth K. Cheney, and Russell B. Scott. Precision calorimeter for gaseous heat capacities—182(A)
Wait, G. R. Ion-content of air irradiated by ultra-violet light—158(A)
Walker, Robert L. (see McDaniel, Boyce D.)—985(L)
Wallace, J. R. (see Hughes, D. J.)—168(A)
——, **D. J. Hughes, and R. H. Holtzman.** Polarization of neutrons in different materials—168(A)

Wallace, P. R. Erratum. The Band theory of graphite—258(L)
—— On the asymptotic distribution of diffusion monoenergetic neutrons—525(A)
—— (see Courant, E. D.)—526(A), 1038
Wannier, Gregory H. Deflection of charged particles in a ferromagnetic medium—304
Warburton, F. W. Stability of a reciprocating electron—747(A)
Ward, A. G. Ion sources—524(T)
Watson, K. (see Jauch, J. M.)—1254(L)
Watson, K. M. Polarization of the neutron in an electrostatic field—526(A)
—— Production of a positron-electron pair in the electrostatic field of an electron—1060
Watson, R. B. and C. W. Horton. Radiation patterns of dielectric rods—experiment and theory—159(A)
Watson, W. W. (see Schultz, H. L.)—346(L)
Wattenberg, A. (see Anderson, H. L.)—16
Watts, Richard J. and Dudley Williams. Double modulation detection method for microwave spectra—1122(L)
—— **and Dudley Williams.** Hyperfine structure in the microwave spectrum of ammonia—157(A)
—— **and Dudley Williams.** Modified Stark-effect modulation spectrograph for microwaves—980(L)
—— **and Dudley Williams.** Nuclear quadrupole moment effects in the inversion spectrum of ammonia—263
Weaver, A. (see Cork, J. M.)—186(A)
Webb, Harold W. (see Hansen, Jay M.)—332
Webber, Robert T. Effect of annealing and gas content on the super-conducting properties of tantalum—1241
Weidler, Roy C. (see Johnson, Robert C.)—158(A)
Weidner, Richard T. Microwave spectrum of iodine monochloride at 4½ cm wavelength—1268(L)
Weil, G. L. (see Anderson, H. L.)—16
Weinhouse, S. (see Anderson, E. C.)—931
Weinstein, M. (see Horning, W.)—251
Weiss, P. R., C. A. Whitmer, H. C. Torrey, and Jen-Sen Hsiang. Magnetic resonance absorption of chromic ammonium alum—975(L)
Weisskopf, Victor F. On the interaction of mesons with nuclei—155(A)
—— On the production process of mesons—510(L)
—— (see Barschall, H. H.)—875
Weissler, G. L. (see Mohr, E. I.)—294
—— **and E. I. Mohr.** Negative corona in Freon-air mixture—289
Weissler, Pearl G. (see Cook, Richard K.)—175(A)
Weisz, Paul B. and B. L. Anderson. Geiger-Mueller counter detection of light radiation from the paths of high energy particles—431(L)
Welsh, H. L. and M. F. Crawford. Methods in raman spectroscopy—524(T)
Wentink, T. (see Hillger, R. E.)—157(A)
White, A. H. (see MacNair, D.)—153(T)
Whitmer, C. A. (see Weiss, P. R.)—975(L)
Widerøe, Rolf. The "Gigator"—a proposed new circular accelerator for heavy particles—978(L)
Wiedenbeck, M. L. Absolute strength of radioactive sources—974(L)
—— γ-radiation of Na^{24} and the energy level scheme of Mg^{24}—429
—— (see Madansky, Leon)—185(A)
—— **and K. Y. Chu.** Coincidence measurements. Part I. Beta-spectra—1164. Part II. Internal conversion—1171
Wiegand, Clyde. Balanced ionization chamber for differtial measurements of gamma-rays—743(A)
Wigner, E. P. (see Eisenbud, L.)—155(A)
—— **and L. Eisenbud.** Higher angular momenta and long range interaction in resonance reactions—29
Wilchinsky, Zigmond W. Random-absorption effect in diffraction of x-rays from coarse powders—511(L)
Wilkinson, R. G. (see Snell, Arthur H.)—541, 545
—— (see Peacock, Charles)—251(L)
Williams, Dudley. Further work on satellites in the microwave spectrum of ammonia—1122(L)
—— (see Johnson, Robert C.)—158(A)
—— (see Watts, Richard J.)—157(A), 263, 980(L), 1122(L)
Williams, H. J. Direction of magnetization in powder patterns—529(A)
Williams, Robert (see Bridge, Herbert)—257(L)
Williams, R. W. (see Rossi, Bruno)—172(A)
—— (see Sutton, R. B.)—1147
—— **and Bruno Rossi.** Study of the structure of air showers at 11,500 feet—172(A)
Wilson, Donald A. Experimental measurement of the upward velocity of the spray dome resulting from an underwater explosion—178(A)
Wilson, E. B., Jr. (see Arons, A. B.)—176(A)
—— (see Dailey, B. P.)—522(A), 871(L)
——, **Paul M. Frye, and R. W. Spitzer.** Cavitation produced by shock waves in sea water—178(A)
Wilson, Robert R. Directional properties of fission neutrons—189
—— On the time required for the fission process—98
——, **Edward J. Lofgren, J. Reginald Richardson, Byron T. Wright, and Robert S. Shankland.** Proton-proton scattering at 14.5 Mev—1131
Wilson, W. R. Two amplifiers for PbS photo-cells used in recording infra-red spectra—156(A)
—— (see Frank, J. M.)—156(A)
Winans, J. G. Nucleus as a crystalline solid—435(L)
—— (see Froslie, Harold M.)—481
Wineland, W. C. (see Wolf, H. E.)—528(A)
Winn, E. B. and E. P. Ney. Determination of the self-diffusion coefficient of methane—77(L)
Wintner, Aurel. On the normalization of characteristic differentials in continuous spectra—516(L)
—— Stability and spectrum in the wave-mechanics of lattices—81(L)
Witmer, Enos E. Integral and rational numbers in the nuclear domain—154(A), 536(A)
Wolf, H. E., H. E. Clearman, and W. C. Wineland. Fluxmeter in the fluxbridge circuit—528(A)
Wollan, E. O. Upper limit for the cross section for scattering of neutrinos by hydrogen—445
—— (see Davidson, W. L.)—168(A)
—— (see Sawyer, R. B.)—109

—— (see Shull, C. G.)—168(A)
——, **Charles D. Moak, and R. B. Sawyer.** Alpha-particles associated with fission—447
Wood, Elizabeth Armstrong. X-ray wave-length standards—436(L)
Woolley, Harold W. Effect of Fermi resonance on the thermodynamic functions of gaseous CO_2—183(A)
Worrell, Francis T. Structure of manganese-rich alloys of copper and manganese—533(A)
Wouters, Louis F. and Richard S. Christian. Effects of space charge on the detection of high energy particles by means of silver chloride crystal counters—1127(L)
Wright, Byron T. (see Wilson, Robert R.)—1131
Wright, Ray H. Application of the hydraulic analogy to the study of transonic flow—176(A)
Wu, Ta-You. A suggested experiment to detect the shift of 1^3S_1 level of H and He^+—976(L)
Wulf, O. R. Terrestrial influences in the lunar and solar tidal motions of the air—153(T)
—— **and Mary W. Hodge.** Comparison of the monthly average pressure patterns near the base of the stratosphere (10 km) over the United States during the year 1945 with the patterns seasonally indicated—153(T)
Wulff, John (see Shaler, A. J.)—79(L)
Yager, W. A. and R. M. Bozorth. Ferromagnetic resonance at microwave frequencies—80(L), 529(A)
Yagoda, Herman and Nathan Kaplan. Quantitative alpha-particle counting by the emulsion technique—356(L)
Yang, C. N. On quantized space-time—874(L)
Yngve, Victor (see Gill, Piara Singh)—733(L)
—— (see Schein, Marcel)—171(A)
York, H. (see Moyer, B. J.)—744(A)
Young, Louis B. Instrumentation in the paper industry—150(T)
Young, R. W. Transmission of sound in the sea—738(T)

Zacharias, Jerrold R. (see Nagle, Darragh E.)—971(L)
Zaleon, I. (see Johnson, W. E.)—174(A)
Zarem, A. M., F. R. Marshall, and F. L. Poole. Transient electrical discharges: disintegration of fine wires—158(A)
Zener, Clarence. Relaxation spectrum of metals—524(T)
Zilsel, P. R., B. T. Darling, and G. Breit. Scattering of slow neutrons by bound protons. III. Intermediate energies—576
——, **John S. Blair, and John L. Powell.** Effect of "*f*-interaction" of Pais on symmetry of nuclear Hamiltonian—155(A), 225
Zinn, W. H. (see Anderson, H. L.)—16

Analytic Subject Index to Volume 72

References with (A) are to abstracts of papers presented at meetings of the American Physical Society. References with (L) are to Letters to the Editor.

Absorption of radiation
Of 17 Mev gamma-rays in Pb and Al, Boyce D. McDaniel, Guy von Dardel, and Robert L. Walker—985(L)

Acoustics
Absorption in liquids from 100 to 225 Mc/sec, Robert A. Rapuano—184(A)
Absorption of sound in water, Leonard Hall—537(A)
Producing "second sound" in He, William M. Fairbank, Henry A. Fairbank, and C. T. Lane—645(L)
Propagation of U.H.F. in Hg, G. R. Ringo, J. W. Fitzgerald, and B. G. Hurdle—87(L)
Radiation from unflanged circular pipe, end connection, Harold Levine and Julian Schwinger—742(A)
Reflection of supersonic sound from sea bottom, R. W. Raitt—745(A)
"Second sound" in liquid He II, Erratum, C. T. Lane, Henry A. Fairbank, and William M. Fairbank—1129(L)
Sound pressure in water, point source in air, E. Gerjuoy—745(A)
Sound velocity in the ocean, R. J. Urick—746(A)
Ultrasonic absorption in liquids, Robert A. Rapuano—78(L)
Ultrasonic measurements on single crystals, H. B. Huntington—321
Ultrasonic velocity and absorption in liquid He, John R. Pellam and Charles F. Squire—1245

Astrophysics
Infra-red solar lines, Robert R. McMath, Arthur Adel, Leo Goldberg, and Orren C. Mohler—644(L)
Infra-red spectra of planets, Arthur Adel—538(A)
Magnetic fields of astronomical bodies, Horace W. Babcock—83(L)
Visibility of stars in daytime, E. O. Hulburt and R. Tousey—167(A)

Atomic structure (see also **Spectra**)
Atomic 'g values' in $^3P_{3/2}$ and $^3P_{1/2}$ states of Ga, P. Kusch and H. M. Foley—1256(L)
Composite non-Keplerean orbits, Gertrude Schwarzmann—154(A)
^5S state of C, A. G. Shenstone—411

Biophysics
Aberrations of eye, night myopia, M. J. Koomen and R. Tousey—534(A)
Autoradiographic method, P. Demers and V. Fredette—538(A)
C^{14} in biological materials, E. C. Anderson, W. F. Libby, S. Weinhouse, A. F. Reid, A. D. Kirshenbaum, and A. V. Grosse—931
Electrical stimulator, C. B. Cosby—160(A)
Fluorescence of cancerous and non-cancerous lipoids, H. S. Penn and Joseph Kaplan—165(A)
Impedance of biological cells, T. M. Shaw, D. E. Jamison, and J. A. Galvin—537(A)
"Inside" counter for soft beta-emitters, L. W. Labaw—187(A)
Tracer micrography, L. Marton and P. H. Abelson—161(A)

Constants, physical, standards
Electrical units, F. B. Silsbee—159(A)
Photometric units, E. C. Crittenden—166(A)
Triple point of water as a fixed point, H. F. Stimson and C. S. Cragoe—183(A)
X-ray wave-length standards, Elizabeth Armstrong Wood—436(L)

Contact potentials
Surface states of silicon, W. H. Brattain and W. Shockley—345(L)

Cosmic Radiation
Abnormality in absorption, W. F. G. Swann and P. A. Morris—1262(L)
Altitude dependence of high energy atmospheric showers, Henry L. Kraybill and Paul J. Ovrebo—351(L)
Atmospheric showers; shielded, C. G. Montgomery and D. D. Montgomery—173(A)
Barometer coefficient, M. Kidnapillai—518(L)
Burst production by penetrating particles, Herbert Bridge, Bruno Rossi, and Robert Williams—257(L)
Captive balloons to carry photographic emulsions, Niels Arley—1253(L)
Čerenkov radiation from high energy particles, Paul B. Weisz and B. L. Anderson—431(L)
Cloud-chamber study of ionization by high energy cosmic-ray electrons, Evans Clement—742(A)
Cosmic rays as products of radioactivity, Gertrude Schwarzmann—744(A)
Decay of slow mesons, G. E. Valley—772
"Fragmentation" bursts at sea level, H. Carmichael—525(A)
Generation of ionizing particles by neutral component, Carmel Milone and Vanna Tongiorgi—735(L)
High energy air showers, Paul J. Ovrebo and Henry L. Kraybill—172(A)
Induced fission, Darol Froman, Louis Rosen, and Bruno Rossi—525(A)
Interpretation of ionization bursts, H. Bridge—172(A)
Ionization of high energy electrons, Evans Hayward—937
Large air showers, H. A. Bethe—172(A)
Latitude effect, hard component, altitude, Piara Singh Gill, Marcel Schein, and Victor Yngve—733(L)
Latitude effect of the mesotron component, Marcel Schein, Piara Singh Gill, and Victor Yngve—171(A)
Lead-shielded counters at 96 miles, E. H. Krause and S. E. Golian—173(A)

Cosmic Radiation (continued)
Magnetic field of milky way, effect on radiation, Manuel S. Vallarta—519(L)
Mass and disintegration products, Carl D. Anderson, Raymond V. Adams, Paul E. Lloyd, and R. Ronald Rau—724
Mass of mesotron, W. H. Furry—171(A); J. G. Retallack—742(A)
Measurement in rockets, L. W. Fraser, R. P. Petersen, H. E. Tatel, and J. A. Van Allen—173(A)
Nuclear disintegrations at 11,500 feet, Bruno Rossi and R. W. Williams—172(A)
Origin of soft component, W. Heitler and S. Power—266
Positive excess of slow mesotrons, Malcolm Corell—171(A), 1054
Primary protons, atom-annihilation hypothesis, H. Turner—512(L); R. A. Millikan, H. V. Neher, and W. H. Pickering—513(L)
Production of C^{14}, E. C. Anderson, W. F. Libby, S. Weinhouse, A. F. Reid, A. D. Kirschenbaum, and A. V. Grosse—931
Production of He in meteorites, Carl August Bauer—354(L)
Production of mesotrons, Marcel Schein and J. Steinberger—734(L); Victor F. Weisskopf—510(L)
Propagation through interstellar space, James W. Follin, Jr.—743(A)
Sea level latitude effect, Peter A. Morris, W. F. G. Swann, and H. C. Taylor—1263(L)
Showers and cascade theory, Giuseppe Cocconi—964
Showers in lead at sea-level, W. B. Fretter—743(A)
Size-frequency curve of showers, G. Cocconi—350(L)
Slow meson intensity, Bruno Rossi, Matthew Sands, and Robert F. Sard—120
Small bursts, sunspots, James W. Broxon—525(A), 1187
Solar magnetic field and diurnal variation, H. Alfvén—88(L)
Stellar electromagnetic fields, Leverett Davis, Jr.—632
Structure of air showers, R. W. Williams and Bruno Rossi—172(A)
Temperature coefficients of components, D. H. Loughridge and F. M. Millican—743(A)
Temperature effect at 1000 m water equivalent depth, M. Forró—868(L)
Tracks in photographic emulsions at high altitudes, Harriet H. Forster—742(A)
Transition effect for large bursts, C. G. Montgomery and D. D. Montgomery—131
Vector meson pair theory, O. Brulin and S. Hjalmars—1126(L)
V-2 experiment, Gilbert J. Perlow—173(A)

Cosmology
Non-homogeneous model, Guy C. Omer, Jr.—744(A)

Cross section, measurements, theory
Of Al for fast neutrons, L. W. Seagondollar and H. H. Barschall—439
Bent crystal neutron spectrometer cross section measurements, R. B. Sawyer, E. O. Wollan, S. Bernstein, and K. C. Peterson—109
Of C and H for fast neutrons, William Sleator, Jr.—207
Cross sections for fast neutrons, experimental results, H. H. Barschall, M. E. Battat, W. C. Bright, E. R. Graves, T. Jorgensen, and J. H. Manley—881
Cross sections for fast neutrons, method, H. H. Barschall, J. H. Manley, and V. F. Weisskopf—875
Of Au for neutrons, B. D. McDaniel, R. E. Sutton, Leo S. Lavatelli, and E. E. Anderson—729(L)
Interaction of neutrons with electrons in Pb, W. W. Havens, Jr., I. I. Rabi and L. J. Rainwater—634
Of iodine for neutrons, Wm. B. Jones, Jr.—362
Long range interaction in resonance reactions, E. P. Wigner and L. Eisenbud—29
Neutron-absorption cross sections, reactivity of chain-reaction pile, H. L. Anderson, E. Fermi, A. Wattenberg, G. L. Weil, and W. H. Zinn—16
Neutron cross section of boron, E. Fermi, J. Marshall, and L. Marshall—193
Neutron cross sections, Cd resonance, W. W. Beeman—986(L)
Neutron cross section studies with rotating shutter, T. Brill and H. V. Lichtenberger—585
Of nuclei for 90-Mev neutrons, Leslie J. Cook, Edwin M. McMillan, Jack M. Peterson, and Duane C. Sewell—1264(L)
Relative cross sections of reactions, William J. Knox—1254(L)
Scattering of neutrinos by hydrogen, E. O. Wollan—445
Of Se^{75} for neutrons, H. N. Friedlander, L. Seren, and S. H. Turkel—23
Thermal neutron activation, Leo Seren, Herbert N. Friedlander, and Solomon H. Turkel—888
Velocity dependence of nuclear forces, H. Snyder and R. E. Marshak—1253(L)

Crystal structure
Of alloys of Cu and Mn, Francis T. Worrell—533(A)
Of barium titanate, B. T. Mathias, R. G. Breckenridge, and D. W. Beaumont—532(A)
Diffraction by randomly oriented line gratings, R. Clark Jones—175(A)
Diffraction of neutrons by crystalline powders, C. G. Shull and E. O. Wollan—168(A)
Diffraction of neutrons by hydrogen and deuterium containing crystals, W. L. Davidson, G. A. Morton, C. G. Shull, and E. O. Wollan—168(A)
Electronic computer for crystal structure analyses, R. Pepinsky—175(A)
Of element 43, Rose C. L. Mooney—1269(L)
Foreign ion, growth of NaCl crystals, R. H. McFee—176(A)
Impingement in grain growth, R. Smoluchowski—533(A)
Variations in quartz, Clyde P. Glover and K. S. Van Dyke—175(A)
X-Ray photography of metallic single crystals, A. H. Geisler, J. K. Hill, and J. B. Newkirk—983(L)

Crystalline state
Absorption due to color centers in crystals, spectral location, Henry F. Ivey—341(L); Errata—873(L)
Absorption bands in alkali halide crystals, C. C. Klick and R. J. Maurer—165(A)

Band theory of graphite, Erratum, P. R. Wallace—258(L)
Compressibility of metals, P. Gombás—1123(L)
DeHaas-van Alphen effect, Jules A. Marcus—162(A)
Dipole interaction in crystals, Errata, J. M. Luttinger and L. Tisza—257(L)
Energy levels in simple crystal models, David S. Saxon and Reina A. Hutner—744(A)
Ferroelectric effect and dielectric constant of rochelle salt, W. P. Mason—854, 976(L)
Low temperature transformation in Li, Charles S. Barrett—245(L)
Nuclear magnetism, solid state, N. L. Alpert—637(L)
Paramagnetic resonance absorption at 9000 mc/sec, salts of iron group, R. L. Cummerow, D. Halliday, and G. E. Moore—173(A), 1233
Phase change in barium titanate, Norman J. Field and A. P. deBretteville—1119(L)
Phase transition in hydrogen halides, L. Tisza—161(A)
Piezoelectric effect in barium titanate, W. L. Cherry, Jr. and Robert Adler—981(L)
Properties of metallic elements, R. Smoluchowski—538(A)
Properties of rochelle salt at lower Curie point, Roland M. Lichtenstein—492
Rigidity modulus of Al, grain size, T'ing-Sui Kê—174(A)
Self-diffusion of argon, Franklin Hutchinson—1256(L)
Silver chloride crystal counters, R. Hofstadter, J. C. D. Milton, and S. L. Ridgway—977(L); Louis F. Wouters and Richard S. Christian—1127(L)
Sintering of copper powder, A. J. Shaler and J. Wulff—79(L)
Stress relaxation across grain boundaries, T'ing-Sui Kê—41
Structure of Cu films, W. E. Johnson, C. H. Bachman, and I. Zaleon—174(A)
Structure of evaporated films, Georg Hass—174(A)
Thallium halide crystal counter, Robert Hofstadter—1120(L)
Thermal voltage of quartz crystal, Richard K. Cook, Martin Greenspan, and Pearl G. Weissler—175(A)
Transitions in uranium, R. J. Corruccini and D. C. Ginnings—183(A)
Wave-mechanics of lattices, Aurel Wintner—81(L)

Dielectrics and dielectric properties
Ferroelectric effect and dielectric constant of rochell salt, W. P. Mason—854, 976(L)

Diffraction of radiation
Double current sheet in diffraction, W. R. Smythe—1066
Radiation patterns of line sources, Roy C. Spencer and Pauline Austin—186(A)

Diffusion (see also **Thermal diffusion**)
Law of force and self-diffusion coefficients, I. Amdur—642(L)
Milne's problem, neutron diffusion, G. Placzek and W. Seidel—550
Milne's problem, variational method, J. LeCaine—564
Neutron angular distribution from a plane, G. Placzek—556
Neutron density near a plane, C. Mark—558
Self-diffusion coefficient of methane, E. B. Winn and E. P. Ney—77(L)

Discharge of electricity in gases
Arcs between metallic contacts, G. F. Hull, Jr., W. Baer, and H. Saltzman—522(A)
Arc spots in magnetic fields, motion, R. L. Longini—184(A)
Continuous corona discharge, I. H. Blifford and H. Friedman—185(A)
Corona from water drops, W. N. English—741(A)
Diffusion of ions and electrons, J. Slepian and W. M. Brubaker—185(A)
Discharge mechanism of self-quenching counters, S. H. Liebson—187(A), 602
Discharge spread in Geiger counters, J. D. Craggs and A. A. Jaffee—784
Disintegration of fine wires by electrical discharges, A. M. Zarem, F. R. Marshall, and F. L. Poole—158(A)
Impulse corona in air, H. J. Hall—185(A)
Initiation of a radiofrequency discharge, F. Kirchner—348(L)
Interference patterns on walls of discharge tubes, R. W. Stewart, J. I. Lodge, and J. K. Robertson—537(A)
Negative corona in freon-air mixtures, G. L. Weissler and E. I. Mohr—289
Positive corona in freon-air mixtures, E. I. Mohr and G. L. Weissler—294
Positive ion transient, Townsend discharge, R. R. Newton—184(A)
Processes in discharge tube, lightning mechanism, F. H. Mitchell and L. B. Snoddy—1202
Rise of wire-potential in counters, S. A. Korff—477
Sparking potentials of Ba, Mg, and Al in Xe, Harold Jacobs and Armand P. LaRocque—537(A)
Theory of long spark, verification, Leon H. Fisher—423

Disintegration and excitation of nucleus (see also **Nuclear structure, Radioactivity**)
$(\alpha, 2n)$ reaction, K. Lark-Horovitz, J. R. Risser, and R. N. Smith—1117(L)
Angular distribution of protons from $O^{16}(d, p)O^{17}$, N. P. Heydenburg and D. R. Inglis—186(A)
Angular distributions, E. Eisner and R. G. Sachs—680
Of Ba and Cs isotopes, Seymour Katcoff—1160
$(d-n)$ reactions, R. B. Roberts and P. H. Abelson—76(L)
Of deuterons in flight, S. M. Dancoff—163(A), 1017
Disintegration energies of Na^{24} and Al^{28}, Walter H. Barkas—346(L)
Disintegration of the deuteron, M. E. Rose and G. Goertzel—162(A), 749
Electron tracks in cloud chamber, P. Gerald Kruger and Lyle W. Smith—167(A)
Energy of gamma-rays from $F(p, \alpha)O$, J. A. Phillips and P. Gerald Kruger—164(A)
Energy of photo-neutrons, D. J. Hughes and C. Eggler—892
Excitation curves for $C^{12}(d, dn)C^{11}$ and $C^{12}(d, dn)C^{11}$, R. L. Thornton and Richard W. Senseman—872(L)

Disintegration and excitation of nucleus (continued)
Excitation curve for $C^{12}(p, pn)C^{11}$, Warren W. Chupp and Edwin M. McMillan—873(L)
Excitation functions of α and d on Bi, Elmer L. Kelly and E. Segrè—746(A)
Gamma-energy emitted per beta-particle, Edgar C. Barker—167(A)
Gamma-radiation from Be^9+H^1, C. C. Lauritsen, T. Lauritsen, and W. H. Fowler—739(A)
High energy neutrons by stripping, R. Serber—740(A), 748(A), 1007
Of Li^8, T. W. Bonner, J. E. Evans, C. W. Malich, and J. R. Risser—163(A)
Of Li^8, Conservation of momentum, E. Richard Cohen and R. F. Christy—738(A); W. A. Fowler, C. C. Lauritsen, and T. Lauritsen—738(A); R. F. Christy, E. R. Cohen, W. A. Fowler, C. C. Lauritsen, and T. Lauritsen—698
Of N^{14}, P. W. Davison and E. C. Pollard—162(A)
Of 1.7-year Cs^{134}, L. G. Elliott and R. E. Bell—979(L)
Of oxygen by neutrons; recoil protons, Wilson M. Powell—739(A)
Photo-disintegration of deuteron, M. E. Rose and G. Goertzel—162(A), 749
Photographing angular distribution, Sylvan Rubin—1176
Photo-neutrons produced in D_2O, W. D. B. Spatz, D. J. Hughes, and A. Cahn—163(A)
Positron analysis of gamma-ray spectra, R. H. Vought and Leo Seren—164(A)
Reactions at high energies, R. Serber—1114(L)
Relative yields of (α, n) and $(\alpha, 2n)$ reactions, H. L. Bradt and D. J. Tendam—527(A), 1117(L)
Relative yields of (γ, n) reactions, M. L. Perlman and G. Friedlander—1272(L)
Stars in photographic emulsions in cyclotron beam, Eugene Gardner—743(A)
Thresholds for creation of particles, H. Feshbach and L. I. Schiff—254(L)
Transmutations with high-energy deuterons, B. B. Cunningham, H. H. Hopkins, M. Lindner, D. R. Miller, P. R. O'Connor, I. Perlman, G. T. Seaborg, and R. C. Thompson—739(A)
Transmutations with high-energy helium ions, G. T. Seaborg, B. B. Cunningham, H. H. Hopkins, M. Lindner, D. R. Miller, P. R. O'Connor, I. Perlman, and R. C. Thompson—740(A)
H^3 bombardment of Ag, D. N. Kundu and M. L. Pool—101

Dissociation
Of formic acid monomer, Thomas Mariner and Walker Bleakney—792

Dissociation energy (see also **Molecular structure and constants**)
Of CO, Homer D. Hagstrum—158(A), 947

Dynamics
Response to excitation of a frequency varying linearly with time, Gunnar Hok—159(A)

Elasticity
Compressibility of metals, P. Gombás—1123(L)
Dynamic modulus of rubber, temperature dependence, A. W. Nolle—184(A)
Propagation of fracture crack, Edward Saibel—534(A)
Rigidity of rubber during cure, Hubert M. James and Eugene Guth—537(A)
Of rochelle salt, Roland M. Lichtenstein—492
Shear constants of alkali halides, W. J. Price—514(L)
Shear strength, thermodynamics of melting, M. Eugene Merchant—534(A)
Stress relaxation across grain boundaries, T'ing-Sui Kê—41
Ultrasonic measurements on single crystals, H. B. Huntington—321
Viscosity of grain boundaries, T'ing-Sui Kê—534(A)

Electrical conductivity and resistance
Aluminum electrodes in magnetic field, George Antonoff—183(A)
Bridges between metallic contacts, G. F. Hull, Jr. and W. Baer—532(A)
Of Ge at low temperatures, I. Estermann, A. Foner, and J. A. Randall—530(A)
Of Ge contacts, S. Benzer—1267(L)
Low temperature semiconductor resistivity, theory, V. A. Johnson and K. Lark-Horovitz—531(A)
Magnetic threshold curves of superconductors, John G. Daunt—89(L)
Of metals at microwave frequencies, B. Serin—1261(L)
Photoconductivity of "incomplete phosphors", Rudolf Frerichs—594
Rectification by oxide cathode, W. E. Mutter—531(A)
Semiconductor contacts, L. Sosnowski—641(L)
Semiconductors, surface states, W. H. Brattain—345(L)
Of sodium ammonia solutions, R. B. Gibney and G. L. Pearson—76(L)
Spontaneous electrical oscillations in Ge crystals, S. Benzer—531(A)
Spreading and field effects in Ge, Ralph Bray, K. Lark-Horovitz, and R. N. Smith—530(A)
Superconductivity and Debye characteristic temperature, Jules de Launay and Richard L. Dolocek—141
Superconductivity of Ta, annealing, Robert T. Webber—1241
Of Te films, Wayne Scanlon and K. Lark-Horovitz—530(A)
Wiedemann-Franz-Lorenz ratio for Cu alloys, R. Ruedy—533(A)

Electrolysis
Rotation in magnetic field, Thomas A. Perls—183(A)

Electromagnetic theory
Deflection of a high energy particle, calculation of XR, F. T. Rogers, Jr.—161(A)
Deflection of particles in a ferromagnetic medium, Gregory H. Wannier—304
Double current sheet in diffraction, W. R. Smythe—1066
Field in quantized space-time, Hartland S. Snyder—68
Kinematics of uniformly accelerated systems, E. L. Hill—143

Radiation patterns of dielectric rods, experiment and theory, R. B. Watson and C. W. Horton—159(A)
Radiation patterns of line sources, Roy C. Spencer and Pauline Austin—186(A)
Refraction of plane non-uniform waves between absorbing media, L. Pincherle—232
Self-energy and interaction energy in generalized electrodynamics, Alex E. S. Green—628
Stellar electromagnetic fields, Leverett Davis, Jr.—632

Electron optics
Observation of Kerr effect, Wilbur Kaye and Richard Devaney—165(A)

Electronic tubes
High frequency response of thermionic diodes, Edward H. Gamble—160(A)

Electrons (see also **Positrons**)
Cloud-chamber search for a low mass neutral particle, P. Gerald Kruger and Lyle W. Smith—360
Intrinsic magnetic moment, G. Breit—984(L)
Stability of reciprocating electron, F. W. Warburton—747(A)

Electrons, secondary
From films of tin oxide, H. E. Mendenhall—532(A)
In resonant cavities, Wayne G. Abraham—741(A)

Electrostatics
Dust electrostatics, James W. Hansen—741(A)

Electrostriction
In barium titanate, W. P. Mason—869(L)

Elements
Estimation of age, Harrison Brown—348(L)

Errata:
On the alleged gamma-ray of N^{13}, L. M. Langer, C. S. Cook, and M. B. Sampson—355(L)
Arc spectrum of silver, A. G. Shenstone—1273(L)
Band theory of graphite, P. R. Wallace—258(L)
Double focusing beta-ray spectrometer, Franklin B. Shull and David M. Dennison—180(A), 256(L)
Magnetic dipole fields in unstrained cubic crystals, L. W. McKeehan—78(L)
Saturation effect in microwave spectrum of ammonia, William V. Smith and R. L. Carter—638(L)
"Second sound" in liquid He II, C. T. Lane, Henry A. Fairbank, and William M. Fairbank—1129(L)
Spectral location of the absorption due to color centers in alkali halide crystals, Henry F. Ivey—873(L)
Theory of dipole interaction in crystals, J. M. Luttinger and L. Tisza—257(L)

Explosion phenomena (see also **Shock waves**)
Attenuation of a shock wave, Walker Bleakney and Richard G. Stoner—170(A)
Bubble pulsations, Conyers Herring—170(A)
Bubbles, energy parameters, Elijah Swift, Jr. and John C. Decius—177(A)
Bubbles, underwater explosions, B. Friedman—177(A)
Cylindrical charge underwater, Harry Polachek—177(A)
Determinacy of gas flows involving reaction fronts, K. O. Friedrichs—171(A)
Detonation velocities, D. P. MacDougall—176(A)
Initiation of explosive, G. Gamow—170(A)
Microbarographic waves at distances from explosions, Everett F. Cox—180(A)
Shock waves from underwater explosions, R. H. Cole—177(A)
Subsurface phenomena near exploding charge, C. W. Lampson—170(A)
Temperature in detonating explosive, S. J. Jacobs—176(A)
Tourmaline gauges for piezoelectric measurement, A. B. Arons, R. H. Cole, W. D. Kennedy, E. B. Wilson, Jr.—176(A)
Underwater explosion measurements, G. K. Hartmann—170(A)
Underwater measurement, J. S. Coles, P. C. Cross, and R. H. Cole—177(A)
Underwater photography, Paul M. Frye—170(A)
Upward velocity, underwater explosion, Donald A. Wilson—178(A)
Velocity of detonation, R. W. Lawrence—180(A)

Films, properties of
Of Ag, Al, Si, and Ge, Georg Hass—174(A)
Refractive index of films, W. H. Brattain and H. B. Briggs—174(A)
Structure of Cu films, W. E. Johnson, C. H. Bachman, and I. Zaleon—174(A)

Fission of nucleus
Associated alpha particles, E. O. Wollan, Charles D. Moak, and R. B. Sawyer—447
Of Bi, Pb, Tl, Pt, and Ta, I. Perlman, R. H. Goeckermann, D. H. Templeton, and J. J. Howland—352(L)
Cosmic-ray induced fission, Darol Froman, Louis Rosen, and Bruno Rossi—525(A)
Cross section of Np^{237}, Ernest D. Klema—88(L)
Delayed neutrons, chemical isolation of activities, Arthur H. Snell, J. S. Levinger, E. P. Meiners, Jr., M. B. Sampson and R. G. Wilkinson—545
Delayed neutrons from Pu^{239}, F. de Hoffman and B. T. Feld—525(A), 567
Delayed neutrons from Pu and U, W. C. Redman and D. Saxon—570
Delayed neutrons, intensity, Arthur H. Snell, V. A. Nedzel, H. W. Ibser, J. S. Levinger, R. G. Wilkinson, and M. B. Sampson—541
Direction properties of neutrons, Robert R. Wilson—189
Division of nuclear charge, R. D. Present—7
Energy distribution of fragments, J. L. Fowler and Louis Rosen—926
Enriched-uranium heavy-water chain-reacting system, A. H. Snell, C. D. Goodman, P. H. Abelson, R. Scalettar, G. M. Branch, I. E. Slawson, and W. E. Stanley—169(A)
Fluctuations of neutrons in a pile, E. D. Courant and P. R. Wallace—526(A), 1038
Liquid drop model, N. Metropolis and S. Frankel—186(A), 914
Time required for fission, Robert R. Wilson—98
Tripartition of heavy elements, Tsien, San-Tsiang—1257(L)

Fission of nucleus (continued)
Uncertainty principle and yield in fission, P. F. Gast—1265(L)
Yield of nuclei by fission, A. J. Dempster—431(L)
Fluid dynamics (see also **Hydrodynamics**)
Cavitation by shock waves in water, E. B. Wilson, Jr., Paul M. Frye, and R. W. Spitzer—178(A)
Diabatic flows of elliptic type, Bruce L. Hicks—179(A)
Fluorescence
Of cancerous and non-cancerous lipoids, H. S. Penn and Joseph Kaplan—165(A)

Geophysics
He in meteorites, Carl August Bauer—354(L)
Induction effects in terrestrial magnetism, Walter M. Elsasser—821
Radioactivity of K in geophysics, E. Gleditsch and T. Gráf—641(L)
Radioactivity of K^{40}; geophysics, Francis Birch—1128(L)
Gravitation
Birkhoff's gravitational equations, Herbert E. Ives—229

Hall effect
Of Ge at low temperatures, I. Estermann, A. Foner, and J. A. Randall—530(A)
Of Te films, Wayne Scanlon and K. Lark-Horovitz—530(A)
Heat of combustion
Energy released, atmospheric conditions, R. A. Castleman, Jr.—182(A)
Heat of vaporization
Of hydrocarbons, D. C. Ginnings and N. S. Osborne—182(A)
High pressure phenomena
Results at pressures up to 100,000 kg-cm^2, P. W. Bridgman—533(A)
High voltage tubes and machines (see also **Methods and instruments**)
Palletron, a new electron resonator, A. M. Skellett—180(A)
Hydrodynamics (see also **Fluid dynamics**)
Dimensional analysis and model experiments, J. C. Decius—178(A)
Explicit solutions for steady compressible flow, Bruce L. Hicks—433(L)
Hydraulic analogy, transonic flow, Ray H. Wright—176(A)
Hyperfine structure (see also **Atomic spectra, nuclear moments and spin**)
Ammonia inversion spectrum, J. M. Jauch—535(A), 712
Of BrCN and ICN, Walter Gordy, William V. Smith, A. G. Smith, and Harold Ring—259(L)
Ground term of H, G. Breit and R. E. Meyerott—1023

Ionization in gases
Appearance potentials of ions, Thomas Mariner and Walker Bleakney—807
Of CO, Homer D. Hagstrum—158(A), 947
Dissociation of formic acid monomer, Thomas Mariner and Walker Bleakney—792
By high energy cosmic-ray electrons, Evans Clement—742(A)
Ionization of high energy electrons, Evans Hayward—937
1-Mev electrons relative to sea level cosmic radiation, Frank L. Hereford—982(L)
Specific ionization for electrons, Robert H. Frost—747(A)
Ionosphere
Electron production, S. L. Seaton—720
Ions, mobility
Diffusion of ions and electrons, J. Slepian and W. M. Brubaker—185(A)
Isomers, nuclear
Multiple isomerism, of Sb, E. Der Mateosian, M. Goldhaber, C. O. Muelhause, and M. McKeown—1271(L)
Isotopes
Abundance of nuclear species, Harrison Brown and Claire Patterson—456
Of Ba and Cs, Seymour Katcoff—1160
Constitution of La and Ce, Mark G. Inghram, Richard J. Hayden, and David C. Hess, Jr.—349(L), 967
Of fission element 43, Mark G. Inghram, David C. Hess, Jr., and Richard J. Hayden—1269(L)
Of In, D. J. Tendam and H. L. Bradt—527(A)
Isotopes as tracers, Herman Branson—533(A)
Of Kr and Xe, M. Lounsbury, S. Epstein, and H. G. Thode—517(L)
Mass doublets, E. Richard Cohen and William F. Hornyak—1127(L)
In meteoritic copper, Harrison Brown and M. G. Inghram—347(L)
Separation by electro-magnetic means, Lloyd P. Smith, W. E. Parkins, and A. T. Forrester—989
Separation of He^3, B. B. McInteer, L. T. Aldrich, and Alfred O. Nier—510(L)
Separation of He^3 and He^4, J. G. Daunt, R. E. Probst, H. L. Johnston, L. T. Aldrich, and Alfred O. Nier—502

Kinetic theory
Bubble pulsations, Conyers Herring—170(A)
Radial density of gases in centrifugal field, J. W. Beams—433(L)

Liquids (see also **Hydrodynamics**)
Converting sound waves into "second sound" in He, William M. Fairbank, Henry A. Fairbank, and C. T. Lane—645
Properties and theory of liquid He, Laszlo Tisza—353(L), 838
Low temperature phenomena
Helium liquefier, R. B. Scott and J. W. Cook—161(A)
Liquid helium cryostat, J. G. Daunt and H. L. Johnston 161(A)
Phase transition in hydrogen halides, L. Tisza—161(A)
Properties and theory of liquid He, Laszlo Tisza—353(L), 838
"Second sound" in liquid He II, Erratum, C. T. Lane, Henry A. Fairbank, and William M. Fairbank—1129(L)

Magnetic fields
Induction effects in terrestrial magnetism, Walter M. Elsasser—821
Magnetic properties (see also **Nuclear moments and spin**)
Deflection of particles in a ferromagnetic medium, Gregory H. Wannier—304
de Haas-van Alphen effect in Zn, Jules A. Marcus—162(A)
Dipole fields in cubic crystals, L. W. McKeehan—78(L)
Exchange interaction in paramagnetic absorption, C. J. Gorter and J. H. Van Vleck—1128(L)
Ferromagnetic resonance at microwave frequencies, W. A. Yager and R. M. Bozorth—80(L), 529(A)
Intrinsic magnetic moment of electron, G. Breit—984(L)
Magnetic fields of astronomical bodies, Horace W. Babcock—83(L)
Magnetization in powder patterns, H. J. Williams—529(A)
Magneto-striction of nickel, J. E. Goldman—529(A)
Moment of deuteron, R. G. Sachs—91
Paramagnetic resonance absorption at 9000 mc/sec., R. L. Cummerow, D. Halliday, and G. E. Moore—173(A), 1233
Permeability of permalloy, M. H. Johnson, G. T. Rado, and M. Maloof—173(A)
Permeameter, W. J. Carr, Jr.—530(A)
Relativistic correction to magnetic moment of deuteron, Gregory Breit and I. Bloch—135
Relaxation effects, Charles Kittel—529(A)
Resonance absorption of chromic ammonium alum, P. R. Weiss, C. A. Whitmer, H. C. Torrey, and Jen-Sen Hsiang—975(L)
Of sodium ammonia solutions at low temperatures, R. B. Gibney and G. L. Pearson—76(L)
Threshold curves of superconductors, John G. Daunt—89(L)
Mass spectroscopy (see also **Isotopes**)
Analysis of C_2H_2, C_2D_2, and C_2DH, Fred L. Mohler and Vernon H. Dibeler—158(A)
Dissociation of formic acid monomer, Thomas Mariner and Walker Bleakney—792
Mechanics, quantum—general
Basis for resonance formula, L. Eisenbud and E. P. Wigner—155(A)
Electromagnetic field in quantized space-time, Hartland S. Snyder—68
Five-dimensional wave theories, Richard W. Iskraut—154(A)
Heitler theory of radiation damping, John M. Blatt—466
Integral and rational eigenvalues, Enos E. Witmer—536(A)
Interaction between two particles from asymptotic phase, Carl-Erik Fröberg—519(L)
Long range interaction in resonance reactions, E. P. Wigner and L. Eisenbud—29
Note on the paper "Second Quantization and Representation Theory," V. Fock—737(L)
Pair production in field of electron, K. M. Watson—1060
Quantized space-time, C. N. Yang—874(L)
Quantum theory of radiation, relativistic invariance, S. T. Ma—1090
Recurrence formulas for Coulomb wave functions, John L. Powell—626
Self-energy and interaction energy in generalized electrodynamics, Alex E. S. Green—628
Statistical geometry and fundamental particles, Nathan Rosen—298, 1253(L)
Mechanics, quantum—of solid bodies
Wave-mechanics of lattices, Aurel Wintner—81(L)
Mesotrons (see also **Cosmic radiation**)
Capture of negative mesotrons, E. Fermi and E. Teller—399
Decay of slow mesons, G. E. Valley—772
Excess of positive mesotrons in cosmic radiation, Malcolm Correll—171(A), 1054
γ-instability, R. J. Finkelstein, 415, 746(A)
Interaction with nuclei, Victor F. Weisskopf—155(A)
Latitude effect in cosmic rays, Marcel Schein, Piara Singh Gill, and Victor Yngve—171(A)
Mass and disintegration products, Carl D. Anderson, Raymond V. Adams, Paul E. Lloyd, and R. Ronald Rau—724
Masses of cosmic-ray mesotrons, W. H. Furry—171(A); J. G. Retallack—742(A)
Mean life at 11,500 ft., Harold K. Ticho—255(L)
Mean life of negative mesotrons, Harold K. Ticho and Marcel Schein—248(L)
Meson field and projective relativity, Banesh Hoffmann—154(A), 458
Meson production, W. Horning and M. Weinstein—251(L)
Meson theory of nuclear forces, Leslie L. Foldy—125
Nuclear capture and meson decay, B. Pontecorvo—246(L)
Production by nuclear bombardment, W. G. McMillan and E. Teller—1, 155(A)
Production process of mesons, Victor F. Weisskopf—510(L)
Slow mesotrons at an altitude of 11,500 feet, Malcolm Correll—171(A), 1054
Symmetry of meson field part of nuclear Hamiltonian, proton-proton, proton-neutron interaction, P. R. Zilsel, J. S. Blair, and J. L. Powell—155(A), 255
Two-meson hypothesis, R. E. Marshak and H. A. Bethe—506
Vector meson pair theory, O. Brulin and S. Hjalmars—1126(L)
Vector mesotron, James H. Bartlett—219
Meteorology
Coding radiosonde, Norman Gibbs, Leigh Gibbs, and E. W. Pike—160(A)
Electron production in the ionosphere, S. L. Seaton—720
Measurement of rainfall by radar, J. S. Marshall, R. C. Langille, W. M. Palmer, and D. W. Perrie—538(A)
Microbarographic waves produced by explosions, velocity, Everett F. Cox—180(A)

Microwaves (see also **Electromagnetic theory; electronic tubes, spectra, microwave**)
Conductivity of metals, B. Serin—1261(L)
Frequency markers, Robert L. Carter and William V. Smith—1265(L)
Nuclear quadrupole spectra and the 'pseudo-quadrupole' effect in diatomic molecules, H. M. Foley—504
Nuclear and molecular information, C. H. Townes, A. N. Holden, and F. R. Merritt—740(A)
Methods and instruments
Absolute strength, M. L. Wiedenbeck—974(L)
Acceleration of electrons by a single resonant cavity, Frank L. Hereford, Jr.—159(A)
Accelerator for heavy particles, Rolf Wideröe—978(L)
Acoustic interferometer, R. J. Urick—746(A)
Alpha-particle counting by emulsion technique, Herman Yagoda and Nathan Kaplan—356(L)
Arcs between metallic contacts, G. F. Hull, Jr., W. Baer, and H. Saltzman—522(A)
Autoradiographic method, P. Demers and V. Fredette —538(A)
Basic optical formula, C. R. Fountain—166(A)
Bent crystal neutron spectrometer, R. B. Sawyer, E. O. Wollan, S. Bernstein, and K. C. Peterson—109
Beta-ray spectrometer, Franklin B. Shull and David M. Dennison—180(A), errata, 256(A); E. Quade and D. Halliday—181(A)
Boron absorption, resonance activation, H. V. Lichtenberger, R. G. Nobles, G. D. Monk, H. Kubitschek, and S. M. Dancoff—164(A)
Calibration of Eastman proton plates, R. A. Peck, Jr.— 1121(L)
Calorimeter controlling power supplied, Harold J. Hoge —182(A)
Calorimeter for gaseous heat capacities, Paul F. Wacker, Ruth K. Cheney, and Russell B. Scott—182(A)
Capacity of electrical double layer, D. C. Grahame— 522(A)
Captive balloons to carry photographic emulsions, Niels Arley—1253(L)
Cavity accelerator for electrons, H. L. Schultz, R. Beringer, C. L. Clarke, J. A. Lockwood, R. L. McCarthy, C. G. Montgomery, P. J. Rice, and W. W. Watson—346(L)
Coding radiosonde, Norman Gibbs, Leigh Gibbs, and E. W. Pike—160(A)
Coincidence circuit, diodes, J. D. Shipman, Jr., B. Howland, and C. A. Schroeder—181(A)
Coincidence corrections of counting instruments, Truman P. Kohman—181(A)
Continuous corona discharge, voltage stabilization, I. H. Blifford and H. Friedman—185(A)
Cosmic-ray measurement in rockets, L. W. Fraser, R. P. Petersen, H. E. Tatel, and J. A. Van Allen—173(A)
Counter detection of Čerenkov radiation, Paul B. Weisz and B. L. Anderson—431(L)
Counters, low voltage self-quenching, S. H. Liebson— 181(A)
Decay time of short lived metastable states, Leon Madansky and M. L. Wiedenbeck—185(A)
Degenerative high voltage stabilizer, R. Pepinsky and P. Jarmotz—529(A)
Design and performance of ion-chambers, B. S. Smith, H. Carmichael, J. F. Steljes, C. O. Peabody, and D. S. Craig—527(A)
Detecting microwave spectra, Walter Gordy and Myer Kessler—644(L)
Detection of microwave spectra, Richard J. Watts and Dudley Williams—1122(L)
Diamond as a gamma-ray counter, L. F. Curtiss and B. W. Brown—643(L)
Differential measurements of gamma-rays, Clyde Wiegand—743(A)
Dimensional analysis and model experiments, J. C. Decius—178(A)
Direct current amplifier, Seville Chapman—745(A)
Discharge mechanism of self-quenching counters, S. H. Liebson—187(A)
Discharge spread in Geiger counters, J. D. Craggs and A. A. Jaffe—784
Disintegration by electrical discharges, A. M. Zarem, F. R. Marshall, and F. L. Poole—158(A)
Double focusing beta-ray spectrometer, Earl S. Rosenblum—731(L)
Electrical stimulator, C. B. Cosby—160(A)
Electronic computer for crystal structure analyses, R. Pepinsky—175(A)
Electrophotography, R. M. Schaffert and C. D. Oughton —535(A)
Electrostatic analyzer for 1.5-Mev protons, T. Lauritsen, W. A. Fowler, and C. C. Lauritsen—746(A)
Expansion ratio of high pressure cloud chambers, Thomas H. Johnson—86(L)
Fast coincidence circuit with pulse height selection, P. R. Bell, S. De Benedetti and J. E. Francis, Jr.— 160(A)
Fluctuations of proportional counters, Hartland S. Snyder—181(A)
Fluxmeter in the fluxbridge circuit, H. E. Wolf, H. E. Clearman, and W. C. Wineland—528(A)
Gamma-ray spectrometer, Boyce D. McDaniel, Guy von Dardel, and Robert L. Walker—985(L)
G.M. counters, low potentials, J. A. Simpson, Jr.— 181(A)
Graphite ionization chamber, Melvin Lax—61
Helium liquefier, R. B. Scott and J. W. Cook—161(A)
High frequency response of thermionic diodes, Edward H. Gamble—160(A)
Impulsive velocities, measurement of, George E. Hudson —178(A)
Index of refraction of liquids, 200 mμ to 1000 mμ, James L. Lauer, and P. H. Miller, Jr.—166(A)
Infra-red spectroscopy beyond 15μ, E. K. Plyler—165(A)
Injector for betatrons and synchrotrons, David C. dePackh and Andrew V. Haeff—247(L)
"Inside" counter for soft beta-emitters, L. W. Labaw— 187(A)
Latent image of nuclear tracks in photographic emulsion, J. La Palme and P. Demers—536(A)

Liquid helium cryostat, J. G. Daunt and H. L. Johnston —161(A)
Loading of resonant cavities, Wayne G. Abraham—741(A)
Long persistence phosphor, R. E. Johnson and A. E. Hardy—165(A)
Magnetic amplifiers in computing circuits, Robert T. Beyer—522(A)
Masses of cosmic-ray mesotrons, W. H. Furry—171(A)
Maxwell bridge at low frequencies, V. A. Brown and B. P. Ramsay—528(A)
Measurement of rainfall by radar, J. S. Marshall, R. C. Langille, W. M. Palmer, and D. W. Perrie—538(A)
Measurement of short time intervals, Luis W. Alvarez—741(A)
Micro-densitometer tracings, energy values, J. C. M. Brentano—166(A)
Microwave secondary electron multiplier, M. H. Greenblatt and P. H. Miller, Jr.—160(A)
Migration of nuclei in photographic emulsion, Pierre Demers—536(A)
Modulation spectrograph for microwaves, Stark-effect, Richard J. Watts and Dudley Williams—980(L)
Molecular weight determination, J. W. Beams—433(L)
Neutron detector, 10 kev to 3 Mev, A. O. Hanson and J. L. McKibben—673
Neutron velocity spectrometer, Wm. B. Jones, Jr.—362
Noise in electrometer tubes, A. Theodore Forrester—747(A)
Nuclear radiofrequency resonance absorption, Arthur Roberts—182(A)
Observation of Kerr effect, Wilbur Kaye and Richard Devaney—165(A)
Observing beat frequencies, A. Theodore Forrester, William E. Parkins, and Edward Gerjuoy—728(L)
Operation of 184-inch cyclotron, D. C. Sewell, L. Heinrich, and J. Vale—739(A)
Palletron, a new electron resonator, A. M. Skellett—180(A)
Peak pressure and duration of shock wave, R. R. Halverson—179(A)
Photographing angular distribution, Sylvan Rubin—1176
Photometric units, E. C. Crittenden—166(A)
Photo-multiplier radiation detector, Fitz-Hugh Marshall and J. W. Coltman—528(A); J. W. Coltman and Fitz-Hugh Marshall—528(A)
Probability for harmonic oscillator, A. J. F. Siegert—537(A)
Proton beam from $C^{12}(p, pn)C^{11}$, Warren W. Chupp and Edwin M. McMillan—873(L)
Proton-gamma coincidence counting, Bruce B. Benson—162(A)
Pulses in silver chloride crystal counters, Robert Hofstadter—747(A)
Radiofrequency detection by superconductivity, Donald H. Andrews and Chester W. Clark—161(A)
Radiofrequency spectrometer for resonance absorption, R. V. Pound—527(A)
Recording gamma-ray scattering apparatus, D. E. Alburger and E. C. Pollard—169(A)
Recording infra-red spectra, W. R. Wilson—156(A)
Resonant cavity absorption cell, Zeeman effect, C. K. Jen—986(L)
Rise of wire-potential in counters, S. A. Korff—477
Rotors driven by light pressure, J. W. Beams—987(L)
Self-quenching counters, R. D. Present—243; S. H. Liebson—602
Separation of isotopes of He^3 and He^4, J. G. Daunt, R. E. Probst, H. L. Johnston, L. T. Aldrich, and Alfred O. Nier—502
Shielding at the 184-inch cyclotron, B. J. Moyer, R. Hildebrand, N. Knable, T. J. Parmley, and H. York—744(A)
Shift of $1^2S_{\frac{1}{2}}$ level of H and He^+, detection, Ta-You Wu —976(L)
Silver chloride crystal counters, R. Hofstadter, J. C. D. Milton and S. L. Ridgway—977(L); Louis F. Wouters and Richard S. Christian—1127(L)
Speed gauge for *HV*-ion beams, William Altar, M. Garbuny, and J. W. Coltman—528(A)
Sulfide television white screen, Austin E. Hardy—166(A)
Surface tension of glass, H. B. Law—184(A)
Synthetic dielectrics in vacuum, Benjamin G. Hogg—522(A)
Thallium halide crystal counter, Robert Hofstadter—1120(L)
Theory of synchro-cyclotron, capture efficiency, D. Bohm and L. L. Foldy—649
Thermal neutron velocity selector, E. Fermi, J. Marshall, and L. Marshall—193
Thermal voltage of quartz crystal, Richard K. Cook, Martin Greenspan, and Pearl G. Weissler—175(A)
Thickness of shock front, measurement of, Donald F. Hornig—179(A)
Tourmaline gauges for piezoelectric measurement, A. B. Arons, R. H. Cole, W. D. Kennedy, and E. B. Wilson, Jr.—176(A)
Tracer micrography, L. Marton and P. H. Abelson—161(A)
Tracer of impurities, J. M. Cork, R. G. Shreffler, and C. M. Fowler—1209
Ultra-fast counters, S. H. Neddermeyer—741(A)
Ultra-short duration flash radiographs, J. C. Clark—741(A)
Underwater photography, Paul M. Frye—170(A)
Vacuum x-ray spectrometer, S. T. Stephenson and F. D. Mason—744(A)
Variational principle for scattering problems, Julian Schwinger—742(A)
X-ray diffraction curves, connections, Jesse W. M. DuMond—83(L)
X-ray photography of metallic single crystals, A. H. Geisler, J. K. Hill, and J. B. Newkirk—983(L)
X-ray wave-length standards, Elizabeth Armstrong Wood—436(L)

Molecular structure and constants (see also **Spectra, molecular,** etc.)

Of $C^{13}O^{16}$ and $C^{14}O^{16}$, Robert T. Lagemann, Alvin H. Nielsen, and Fred P. Dickey—284

Molecular structure and constants (continued)
Law of force and self-diffusion coefficients, I. Amdur—642(L)
Of CH_3Cl and CH_3Br, Walter Gordy, James W. Simmons, and A. G. Smith—344(L)

Neutrino (see also **Radioactivity; Scattering of electrons, neutrons and ions**)
Cloud-chamber search for low mass neutral particle, P. Gerald Kruger and Lyle W. Smith—360
Mass, Emil J. Konopinski—518(L)

Neutrons
Absorption of high-energy neutrons, R. Hildebrand and B. J. Moyer—1258(L)
Angular distribution, A. C. Helmholz, Edwin M. McMillan, and Duane C. Sewell—790(A), 1003
Angular distribution from a plane, G. Placzek—556
In atmosphere, H. M. Agnew, W. C. Bright, and Darol Froman—203
Cross-section measurements, R. B. Sawyer, E. O. Wollan, S. Bernstein, and K. C. Peterson—109
Cross sections of C and H, William Sleator, Jr.—207
Delayed neutrons from Pu^{239}, F. de Hoffman and B. T. Feld—567
Delayed neutrons from Pu and U, W. C. Redman and D. Saxon—570
Density near a plane, C. Mark—558
$(d-n)$ reactions, R. B. Roberts and P. H. Abelson—76(L)
Diffraction by crystalline powders, C. G. Shull and E. O. Wollan—168(A)
Diffraction by hydrogen and deuterium, W. L. Davidson, G. A. Morton, C. G. Shull, and E. O. Wollan—168(A)
Diffusion of monoenergetic neutrons, P. R. Wallace—525(A)
Effective temperature of neutrons, E. Fermi, J. Marshall, and L. Marshall—193
Fluctuations of intensity in pile, E. D. Courant and P. R. Wallace—526(A), 1038
From fission of U, Arthur H. Snell, V. A. Nedzel, H. W. Ibser, J. S. Levinger, R. G. Wilkinson, and M. B. Sampson—541
Interaction with electrons, E. Fermi and L. Marshall—1139; J. M. Jauch and K. Watson—1254(L)
Low mass neutral particle, search for, P. Gerald Kruger and Lyle W. Smith—360
Milne's problem, variational method, J. LeCaine—564
Neutron cross section with rotating shutter, T. Brill and H. V. Lichtenberger—585
Production by stripping, R. Serber—740(A), 748(A), 1007
Polarization of neutron, D. J. Hughes, J. R. Wallace, and R. H. Holtzman—168(A); J. R. Wallace, D. J. Hughes, and R. H. Holtzman—168(A); K. M. Watson—526(A)
Total cross sections of nuclei, Leslie J. Cook, Edwin M. McMillan, Jack M. Peterson, and Duane C. Sewell—1264(L)
Transport theory, G. Placzek and W. Seidel—550

Nuclear moments and spin (see also **Hyperfine structure**)
Of bromine, R. V. Pound—1273(L)
Of bromine isotopes, S. B. Brody, W. A. Nierenberg, and N. F. Ramsey—258(L)
Of the carbon isotopes, F. A. Jenkins—169(A)
Of Cb^{93}, Wilkison W. Meeks and Russell A. Fisher—451
Of columbium from hyperfine structure, Wilkison Meeks and Russell A. Fisher—169(A)
Deuteron-proton magnetic moment ratio, F. Bitter, N. L. Alpert, D. E. Nagle, and H. L. Poss—1271(L)
Of H^1 and H^2, F. Bloch, E. C. Levinthal and M. E. Packard—1125(L)
Magnetic exchange moment for H^3 and He^3, Felix Villars—256(L)
Magnetic moment of deuteron, R. G. Sachs—91; H. Primakoff—118; Arthur Roberts—979(L)
Magnetic moment of deuteron, relativistic correction, Gregory Breit and I. Bloch—135
Magnetic moment of Tl^{205}, H. L. Poss—637(L)
Nuclear quadrupole spectra, H. M. Foley—504
Quadrupole moment of N, Richard J. Watts and Dudley Williams—263
Of the triton, R. G. Sachs—312

Nuclear structure (see also **Disintegration of nucleus and Radioactivity**)
Binding energy of quadrielectron, Aadne Ore—521(A)
Energy levels in Mn^{56}, A. B. Martin—378
Energy levels of O^{17}, Ernest Pollard and Perry W. Davison—736(L)
"f-interaction", symmetry of Hamiltonian, Paul R. Zilsel, John S. Blair, and John L. Powell—155(A), 225
Integral and rational numbers in nuclear domain, Enos E. Witmer—154(A), 536(A)
Isomerism in Dy165, M. G. Inghram, A. E. Shaw, D. C. Hess, Jr., and R. J. Hayden—515(L)
Liquid drop model of fission, S. Frankel and N. Metropolis—914
Long-range forces, magnetic moment of deuteron, H. Primakoff—118
Of Mg^{24}, M. L. Wiedenbeck—429
Meson theory of nuclear forces, Leslie L. Foldy—125
Nuclear mass defect, Gertrude Schwarzmann—536(A)
Nucleus as crystalline solid, J. G. Winans—435(L)
Range of nuclear forces, H. C. Corben and Muaikal Corben—526(A)
Of Na, Mg, Al, Si, P, S, gamma-rays, Ernest Pollard and D. E. Alburger—1196
Tensor force in deuteron, William G. Guindon, S. J.—526(A)
Velocity dependence of nuclear forces, H. Snyder and R. E. Marshak—1253(L)

Optical constants and properties
Aberrations of eye, M. J. Koomen and R. Tousey—534(A)
Index of refraction of water vapor in infra-red, F. W. Brown and M. A. Greenfield—534(A)
Of Hg vapor, Jay M. Hansen and Harold W. Webb—332
Refractive index of films, W. H. Brattain and H. B. Briggs—174(A)

Photoconductivity
Of Ge contacts, S. Benzer—1267(L)
Of "incomplete phosphors", Rudolf Frerichs—594
Photodisintegration
Energy of photo-neutrons, D. J. Hughes and C. Eggler—892
Photoelectric effect and properties; cells
Properties of Cs–Sb films, J. A. Burton—531(A)
Photography
Electrophotography, R. M. Schaffert and C. D. Oughton—535(A)
Latent image of nuclear tracks, J. La Palme and P. Demers—536(A)
Migration of nuclei in photographic emulsion, Pierre Demers—536(A)
AgBr grain of emulsions, W. Knowles—535(A)
Photoionization
Of air by ultraviolet light, G. R. Wait—158(A)
Number of ions, fluctuations, U. Fano—26
Photometry
New basis for photometric units, E. C. Crittenden—166(A)
Piezoelectric effect
Of barium titanate, W. L. Cherry, Jr. and Robert Adler—981(L)
Of rochelle salt, Roland M. Lichtenstein—492
Polarization of radiation
Quenching and depolarization of Hg resonance radiation, Leonard O. Olsen and George P. Kerr, Jr.—115
Positrons
Binding energy of quadrielectron, Aadne Ore—521(A)
In field of electron, K. M. Watson—1060
Proceedings of the American Physical Society
Marietta, Ohio Meeting May 3, 1947—150
Washington, D. C. Meeting May 1–3, 1947—151
Amherst, Massachusetts Meeting May 31, 1947—521
Montreal, Quebec Meeting June 19–21, 1947—523
Stanford University, California Meeting July 11–12, 1947—738

Radiation
Heitler theory of radiation damping, John M. Blatt—466
Measuring radiation pressure, J. W. Beams—987(L)
Radiation patterns of dielectric rods, R. B. Watson and C. W. Horton—159(A)
Radio (see also **Ionosphere**)
Fadeouts coincident with solar flares, G. R. Wait—158(A)
Radioactivity (see also **Disintegration of nucleus**)
Alpha-particle counting by emulsion technique, Herman Yagoda and Nathan Kaplan—356(L)
Angular correlation of gamma-ray quanta, Edward L. Brady and Martin Deutsch—870(L)
Of Sb, multiple isomerism, E. Der Mateosian, M. Goldhaber, C. O. Muelhause, and M. McKeown—1271(L)
Of Sb and Sn; *K*-capture, K. D. Coleman and M. L. Pool—1070
Of Sb, Ta, W, and Ir, Swami Jnanananda—1124(L)
Of Be^{10}, Edwin M. McMillan—591
β-radiation of S^{35} and C^{14}, A. K. Solomon, R. G. Gould, and C. B. Anfinsen—1097
β-ray spectrometer, Franklin B. Shull and David M. Dennison—180(A)
β-ray spectrum of C^{14}, Paul W. Levy—248(L); W. E. Stephens and Margaret N. Lewis—526(A)
C^{14} in biological materials, E. C. Anderson, W. F. Libby, S. Weinhouse, A. F. Reid, A. D. Kirshenbaum, and A. V. Grosse—931
Of Cs^{134}, L. G. Elliott and R. E. Bell—979(L)
Of Co^{61}, Thomas J. Parmley and Burton J. Moyer—82(L), 746(A)
Coincidence measurements, beta-spectra, M. L. Wiedenbeck and K. Y. Chu—1164
Coincidence measurements, internal conversion, M. L. Weidenbeck and K. Y. Chu—1171
Coincidence study of Ga^{72}, C. E. Mandeville and Morris Scherb—520(L)
Of Cu^{60}, C. E. Leith, Alec Bratenahl, and B. J. Moyer—732(L), 745(A)
Of Cu^{64}, Martin Deutsch—729(L)
Coulomb functions for heavy nuclei, Arthur A. Broyles and John L. Powell—155(A)
Decay scheme of Sb^{124}, Walter E. Meyerhof and Gertrude Scharff-Goldhaber—164(A), 273
Decay of Sc^{48}, Arthur E. Miller and Martin Deutsch—527(A)
Decay of Ag^{110}, Martin Deutsch—527(A)
Differential measurements of gamma-rays, Clyde Wiegand—743(A)
Double focusing beta-ray spectrometer, Earl S. Rosenblom—731(L)
Of element 43, E. E. Motta, G. E. Boyd, and Q. V. Larson—1270(L)
Of element 61, G. W. Parker, P. M. Lantz, M. G. Inghram, D. C. Hess, Jr., and R. J. Hayden—85(L)
Of 8.5 day Ca, Roy Overstreet and Louis Jacobson—349(L)
Energy levels in Mn^{56}, A. B. Martin—378
40-kev transition of ThC″, B. B. Kinsey—526(A)
$(4n+1)$ radioactive series, A. C. English, T. E. Cranshaw, P. Demers, J. A. Harvey, E. P. Hincks, J. V. Jelley, and A. N. May—253(L)
Gamma-radiation of Na^{24}, M. L. Wiedenbeck—429
Gamma-ray of N^{13}, erratum, L. M. Langer, C. S. Cook, and M. B. Sampson—355(L)
Of granite, unknown source of gamma-rays, Victor Francis Hess—609
Half-life of tritium, Aaron Novick—972(L); M. Goldblatt, E. S. Robinson, and R. W. Spence—973(L)
Of In, D. J. Tendam and H. L. Bradt—527(A), 1118(L)
Internally converted gamma-rays, J. M. Cork, R. G. Schreffler, and A. Weaver—186(A)
Internally converted radiation, J. M. Cork, R. G. Shreffler, and C. M. Fowler—1209
Of Ir^{192} and Pa^{233}, Paul W. Levy—352(L)
Isomerism in Dy, M. G. Inghram, A. E. Shaw, D. C. Hess, Jr., and R. J. Hayden—515(L)
Of isotopes of Bi and Pb, D. H. Templeton, J. J. Howland, and I. Perlman—766

Radioactivity (continued)
Of isotopes of Po, D. H. Templeton, J. J. Howland, and I. Perlman—758
Of isotopes produced by neutron capture, Leo Seren, Herbert N. Friedlander, and Solomon H. Turkel—888
Of Li, D. J. Hughes, D. Hall, C. Eggler, and E. Goldfarb —646(L)
Measurements of absolute strength, M. L. Wiedenbeck —974(L)
Of Mo and Tc, J. E. Edwards and M. L. Pool—384
Positively charged particles and beta-rays of P^{32}, T. H. Pi and C. Y. Chao—639(L)
Positron-electron branching in Br^{80}, W. C. Barber—1156
Of K^{38}, Margaret M. Ramsey, J. Lawrence Meem, Jr., and Allan C. G. Mitchell—639(L)
Of K^{40}, Francis Birch—1128(L)
Of K^{40}, gamma-rays, E. Gleditsch and T. Gráf—640(L)
Radiations from Be^{131} and Cs^{131}, Bernard Finkle— 1260(L)
Radioactivity of K in geophysics, E. Gleditsch and T. Gráf—641(L)
Of Re^{186} and Re^{188}, David C. Hess, Jr., Richard J. Hayden, and Mark G. Inghram—730(L)
Of $_{45}Rh^{106}$, W. C. Peacock—1049
Of Sc^{46}, disintegration scheme, Charles Peacock and Roger G. Wilkinson—251(L)
Of Se^{75}, H. N. Friedlander, L. Seren, and S. H. Turkel— 23
Short lived metastable states, Leon Madansky and M. L. Wiedenbeck—185(A)
Of Ta produced by slow neutrons, Leo Seren, Herbert N. Friedlander, and Solomon Turkel—163(A)
Of Ta, Ir, and Au, energy levels, J. M. Cork—581
Theory in the momentum space, L. Infeld—154(A)
H^3 and mass of neutrino, Emil J. Konopinski—518(L)
of U^{233}, F. Hagemann, L. I. Katzin, M. H. Studier, A. Ghirso, and G. T. Seaborg—252(L)
X-rays from radioactive Ce, Pd, and Ca, David E. Matthews, and M. L. Pool—163(A)
X-rays from radioactive Sn, Sb, and W, K. D. Coleman, R. Nudenberg, and M. L. Pool—164(A)

Relativity
Clock problem, E. L. Hill—236
Continuous particles, M. Hessaby—536(A)
Electromagnetic field in quantized space-time, Hartland S. Snyder—68
General relativity theory, H. C. Corben—156(A)
Kinematics of uniformly accelerated systems, E. L. Hill —143
Lorentz transformation of charge and current densities, Boris Podolsky—624
Motion of particle in electromagnetic and gravitational field, H. C. Corben and Mulaika Corben—434(L)
Non-linear invariants, problem of motion, Christopher Gregory—72
Projective relativity and meson field, Banesh Hoffmann —154(A), 458
Quantized space-time, C. N. Yang—874(L)
Quantum theory of radiation, relativistic invariance, S. T. Ma—1090
Solutions of Einstein's field equations, Sudhansu Datta Majumdar—390
Statistical theory of space-time, Nathan Rosen—156(A)

Resonance radiation
Imprisonment in gases, T. Holstein—1212

Scattering of electrons, neutrons, and ions (see also **Electrons, scattering of; Electron diffraction cross section**)
Absorption of high-energy neutrons, R. Hildebrand and B. J. Moyer—1258(L)
Angular distribution of neutrons, A. C. Helmholz, Edwin M. McMillan, and Duane Sewell—740(A), 1003
Cross sections for fast neutrons, experimental results, H. H. Barschall, M. E. Battat, W. C. Bright, E. R. Graves, T. Jorgensen, and J. H. Manley—881
Cross sections for fast neutrons, method, H. H. Barschall, J. H. Manley, and V. F. Weisskopf—875
Elastic scattering of electrons, W. W. Buechner, R. J. Van de Graaff, A. Sperduto, E. A. Burrill, Jr., and H. Fesbach—678
Of fast neutrons by C and H, William Sleator, Jr.—207
Of fast neutrons by He, T. A. Hall and P. G. Koontz— 196
High energy neutron-proton scattering, J. Leite Lopes— 355(L)
High energy neutrons by stripping, R. Serber—740(A), 748(A), 1007
Inelastic scattering of neutrons in crystals, Otto Halpern —260(L)
Interaction of neutrons with electrons in Pb, W. W. Havens, Jr., I. I. Rabi, and L. J. Rainwater—634
Interaction with electrons, E. Fermi and L. Marshall— 1139; J. M. Jauch and K. Watson—1254(L)
Milne problem for large plane slab with constant source, R. E. Marshak—47
Multiple scattering of electrons, Lyle W. Smith and P. Gerald Kruger—357
Neutron absorption resonances in iodine, Wm. B. Jones, Jr.—362
Of neutrons by O_2, Otto Halpern—746(A)
Neutron scattering at Cd resonance, W. W. Beeman— 986(L)
Of neutrons in polycrystals, R. J. Finkelstein—907
Proton-proton scattering, I. H. Dearnley, C. L. Oxley, and J. E. Perry, Jr.—169(A)
Proton-proton scattering at 10 Mev, R. E. Peierls and M. A. Preston—250; Leslie L. Foldy—731(L)
Proton-proton scattering at 14.5 Mev, J. Leite Lopes and J. Tiomno—731(L); Robert R. Wilson, Edward J. Lofgren, J. Reginald Richardson, Byron T. Wright, and Robert S. Shankland—1131
Of protons by deuterons, R. Sherr, J. M. Blair, H. R. Kratz, C. L. Bailey, and R. F. Taschek—662
Proton scattering from Be^9, Sylvan Rubin—739(A)
Reactions at high energies, R. Serber—1114(L)
Relative cross sections of reactions, high energy neutrons, William J. Knox—1254(L)
Resonance scattering of neutrons, A. S. Langsdorf, Jr. and W. Arnold—167(A)

Resonance scattering of neutrons by Co, S. P. Harris, A. S. Langsdorf, Jr., and F. G. P. Seidl—866
Resonance scattering of neutrons by Mn^{55}, F. G. P. Seidl, S. P. Harris, and A. S. Langsdorf—168(A)
Scattering of electrons at relativistic energies, W. McKinley and H. Feshbach—155(A)
Scattering of neutrinos by hydrogen, E. O. Wollan—445
Slow neutrons by Be, Al, and Bi, spin dependence, E. Fermi and L. Marshall—408
Of slow neutrons by bound protons, P. R. Zilsel, B. T. Darling, and Gregory Breit—576
Slow neutrons by ortho- and parahydrogen, R. B. Sutton, T. Hall, E. E. Anderson, H. S. Bridge, J. W. DeWire, L. S. Lavatelli, E. A. Long, T. Snyder, and R. W. Williams—1147
Variational principle for scattering problems, Julian Schwinger—742(A)

Scattering of radiation
Compton scattering, low frequency photons, Res Jost—815
Processes of higher order, Otto Halpern and Norman M. Kroll—82(L)

Shock waves (see also **Explosion phenomena**)
Attenuation of a shock wave, Walker Bleakney and Richard G. Stoner—170(A)
Cylindrical charge underwater, Harry Polachek—177(A)
Interactions with ocean surface, Paul C. Cross and J. S. Coles—179(A)
From infinite cylinders of explosive, Stuart R. Brinkley, Jr. and John G. Kirkwood—1109
Non-steady shock waves, theory of, B. Cassen and J. Stanton—180(A)
On partly submerged plate, E. H. Kennard—178(A)
Peak pressure and duration of shock wave, R. R. Halverson—179(A)
Refraction of plane waves, A. H. Taub—51
Theoretical gas flow, M. M. Munk—176(A)
Theory of propagation, John G. Kirkwood and Stuart R. Brinkley, Jr.—171(A)
Underwater explosions, R. H. Cole—177(A)
Underwater measurement, J. S. Coles, P. C. Cross, and R. H. Cole—177(A)

Spark discharge (see also **Discharge of electricity**, etc.)
Luminous spark in $CuSO_4$ solutions, Hugh F. Henry—184(A)

Specific heat
Calorimeter for gaseous heat capacities, Paul F. Wacker, Ruth K. Cheney, and Russell B. Scott—182(A)
At high temperatures, R. J. Corruccini and D. C. Ginnings—183(A)
Of hydrocarbons, D. C. Ginnings and N. S. Osborne—182(A)

Spectra, absorption
In alkali halide crystals, C. C. Klick and R. J. Maurer—165(A)
Of carbonyl sulfide microwave, R. E. Hillger, M. W. P. Strandberg, T. Wentink, and R. L. Kyhl—157(A)
Exchange interaction in paramagnetic absorption, C. J. Gorter and J. H. Van Vleck—1128(L)
Of InCl, Harold M. Froslie and J. G. Winans—481
Inter-molecular vibration spectrum of water, Robert C. Johnson, Roy C. Weidler, and Dudley Williams—158(A)
Saturation in microwave spectrum of NH_3, William V. Smith and R. L. Carter—638(L)
Stark effect in the microwave spectrum, B. P. Dailey—84(L)

Spectra, atomic
Of A, Kr, Xe between 1.15 and 2.25 microns, W. R. Sittner and W. S. Huxford—535(A)
Of A, Kr, and Xe in near infra-red, Donald H. Hale—156(A)
D-terms of Li^7, K. W. Meissner and L. G. Mundie—535(A)
Electromagnetic shift of energy levels, H. A. Bethe—339(L); Willis E. Lamb, Jr. and Robert C. Retherford—241; Ta-You Wu—976(L)
Hyperfine structure of ground state of H and D atoms, Otto Halpern—245(L)
Hyperfine structure of H and D, Darragh E. Nagle, Renne S. Julian, and Jerrold R. Zacharias—971(L)
Interval formula for multiplets, Gentaro Araki—1255(L)
^5S State of C, A. G. Shenstone—411
Structure in He II, J. E. Mack and N. Austern—972(L)

Spectra, general
Dissociation energy of CO, H. D. Hagstrum—158(A)
Of electroplated electrodes, W. M. Cady, B. Cassen, and L. Blitzer—159(A)
Hyperfine structure, microwave spectrum of NH_3, Richard J. Watts and Dudley Williams—157(A)
Infra-red solar lines, Robert R. McMath, Arthur Adel, Leo Goldberg, and Orren C. Mohler—644(L)
Infra-red spectra of planets, Arthur Adel—538(A)
Normalization of differentials in continuous spectra, Aurel Wintner—516(L)
Observing beat frequencies, A. T. Forrester, William E. Parkins, and Edward Gerjuoy—728(L)
Stark effect in high frequency fields, C. H. Townes and F. R. Merritt—1266(L)

Spectra, microwave
Of NH_3, Dudley Williams—1122(L)
Detecting microwave spectra, Walter Gordy and Myer Kessler—644(L)
Fine structure in NH_3, Harald H. Nielsen and David M. Dennison—86(L), 1101
Frequency markers, Robert L. Carter and William V. Smith—1265(L)
Hyperfine structure in microwave spectrum of CH_3I, Walter Gordy, A. G. Smith, and James W. Simmons—249(L)
Of iodine monochloride, Richard T. Weidner—1268(L)
Of linear molecules, C. H. Townes, A. N. Holden, and F. R. Merritt—513(L)
Of CH_3Cl and CH_3Br, Walter Gordy, James W. Simmons, and A. G. Smith—344(L)
Of methyl cyanide and methyl isocyanide, Harold Ring, Howard Edwards, Myer Kessler, and Walter Gordy—1262(L)
Microwave spectra and Zeeman effect, C. K. Jen—986(L)

Spectra, microwave (continued)
Of N_2O, D. K. Coles, E. S. Elyash, and J. G. Gorman—973(L)
Nuclear and molecular information, C. H. Townes, A. N. Holden, and F. R. Merritt—740(A)
Of polyatomic molecules, B. P. Dailey and E. B. Wilson, Jr.—522(A)
Saturation effect in microwave spectrum of ammonia, T. Alexander Pond and Walter F. Cannon—1121(L)
Spectra, molecular (see also **Molecular structure and constants**)
Ammonia inversion spectrum, hyperfine structure and Stark effect, J. M. Jauch—712
b' and c states of N_2, R. B. Setlow and Roland Meyerott—186(A)
Of diacetylene, dimethylacetylene, and dimethyldiacetylene, Arnold G. Meister and Forrest F. Cleveland—157(A)
Of CsF, moment of inertia and electric dipole moment, Harold Kenneth Hughes—614
Infra-red spectrum of $C^{13}O^{16}$ and $C^{13}O^{16}$, Robert T. Lagemann, Alvin H. Nielsen, and Fred P. Dickey—284
Inversion spectrum of NH_3, Richard J. Watts and Dudley Williams—263
Microwave spectrum of SO_2, B. P. Dailey, S. Golden and E. Bright Wilson, Jr.—871(L)
Nuclear electric quadrupole interaction, Bernard T. Feld—1116(L)
'Pseudo-quadrupole' effect in diatomic molecules, H. M. Foley—504
Radiofrequency spectra of sodium halides, W. A. Nierenberg and N. F. Ramsey—1075
The $^2\pi_u \rightarrow {}^2\pi_g$ bands of CO_2+, S. Mrozowski—682, 691
Spectroscopy, technique
Detection of microwave spectra, Richard J. Watts and Dudley Williams—1122(L)
Infra-red spectroscopy beyond 15μ, E. K. Plyler—165(A)
Microdensitometer tracings, energy values, J. C. M. Brentano—166(A)
Modulation of Cs resonance lines, J. M. Frank, W. S. Huxford, and W. R. Wilson—156(A)
Precision frequency measurements, fine structure, W. E. Good and D. K. Coles—157(A)
Recording infra-red spectra, W. R. Wilson—156(A)
Stark effect
In high frequency fields, C. H. Townes and F. R. Merritt—1266(L)
In microwave spectroscopy, D. K. Coles and W. E. Good—156(A)
Microwave spectrum of methyl alcohol, B. P. Dailey—84(L)
Modulation spectrograph for microwaves, Richard J. Watts and Dudley Williams—980(L)
Surface tension
Expansion ratio of high pressure cloud chambers, pressure coefficients, Thomas H. Johnson—86(L)
Of glass, H. B. Law—184(A)

Thermal conductivity
Wiedemann-Franz-Lorenz ratio for Cu alloys, R. Ruedy—533(A)

Thermal diffusion
Of He^3, B. B. McInteer, L. T. Aldrich, and Alfred O. Nier—510(L)
Temperature variation in hydrogen, deuterium and helium, Byron F. Murphey—834
Thermionic emission; Emitting surfaces
Constants of Richardson's equation, life of oxide coated cathodes, Harold Jacobs and George Hees—174(A)
Of an oxide cathode interface, A. Eisenstein—531(A)
Thermodynamics
Calculation of first derivatives from Jacobians, F. H. Crawford—521(A)
Classification of phase transitions, L. Tisza—532(A)
Derivation of thermodynamical relations, H. Kaufman and A. Norman Shaw—537(A)
Solubility gaps in binary systems, A. W. Lawson—533(A)
Thermodynamic functions of gaseous CO_2, Fermi resonance, Harold W. Woolley—183(A)

X-rays, absorption
Absolute sensitivity of a graphite ionization chamber, Melvin Lax—61
Absorption coefficient, John A. Victoreen—869(L)
X-rays, diffraction, scattering, reflection, refraction, and polarization
Coincidence counting, quantum nature of x-rays, M. P. Givens—186(A)
Diffraction by randomly oriented line gratings, R. Clark Jones—175(A)
Diffraction lines from colloidal MgO, Chester Riddon Berry—942
Random absorption from coarse powders, Zigmond W. Wilchinsky—511(L)
Scattering at small angles, W. W. Beeman and Paul Kaesberg—512(L)
X-ray diffraction curves, small particle sizes, Jesse W. M. DuMond—83(L)
X-ray photography of metallic single crystals, A. H. Geisler, J. K. Hill and J. B. Newkirk—983(L)
X-rays, emission (see also **X-rays, spectra and spectroscopy,** etc.)
Associated with U^{234}, R. L. Macklin and G. B. Knight—435(L)
Structure near limit of continuous spectrum, Jesse W. M. DuMond—276
X-rays, spectra and spectroscopy, wave-length measurements (see also **X-rays, emission**)
X-ray wave-length standards, Elizabeth Armstrong Wood—436(L)
X-rays, tubes, apparatus
Ultra-short duration flash radiographs, J. C. Clark—741(A)
Vacuum spectrometer, S. T. Stephenson and F. D. Mason—744(A)

Zeeman effect
Microwave spectra, resonant cavity absorption cell, C. K. Jen—986(L)
In microwave spectroscopy, D. K. Coles and W. E. Good—156(A)

DEC 22 1947

THE PHYSICAL REVIEW

VOLUME Second Series NUMBER 12

DECEMBER 15, 1947

Published for the

AMERICAN PHYSICAL SOCIETY

by the

AMERICAN INSTITUTE OF PHYSICS

Lancaster, Pa., and New York, N. Y.

THE PHYSICAL REVIEW

A Journal of Experimental and Theoretical Physics established by E. L. Nichols in 1893

BOARD OF EDITORS

Editor

John T. Tate

Assistant Editors

J. W. Buchta and E. L. Hill

Associate Editors

J. B. Fisk — R. J. Kennedy — H. A. Barton
W. Pauli — E. H. Nicholas — L. A. Ringstorff
L. T. Smith — R. C. Pollard — W. H. Zachariasen

Manuscripts for publication should be submitted to John T. Tate, University of Minnesota, Minneapolis, Minnesota.

Proof and all correspondence concerning papers in the process of publication should be addressed to the Publication Manager, American Institute of Physics, 57 East 55 Street, New York 22, New York.

Subscription Price

United States and Canada $15.00
Elsewhere $16.50

Back Numbers

Complete sets: Series 1[1] Vol. 1, 1913–Vol. 70, 1946—$612.00
Yearly rate: $60.00
Single copies: $2.00 each, prior to July, 1929;
$1.50 each, July, 1929–December, 1941;
$3.00 each, January, 1942–December, 1946.
Current issue: $3.00 each.

Subscriptions and orders for back numbers should be addressed to Prince and Lemon Streets, Lancaster, Pennsylvania, or to the American Institute of Physics, 57 East 55 Street, New York 22, New York.

Changes of address in the case of members of the American Physical Society should be addressed to the Treasurer; in the case of other subscribers to the Business Manager, American Institute of Physics.

[1] For Series 1 begun at Physical Laboratory, Cornell University, Ithaca, New York.

The Physical Review is published semi-monthly at Prince and Lemon Streets, Lancaster, Pennsylvania.
Entered as second-class matter March 6, 1917, at the Post Office at Lancaster, Pennsylvania, under the Act of March 3, 1879.
Authorized for mailing at special rate of postage provided for in paragraph 4, section 538, P. L. & R., authorized January 27, 1925.

THE AMERICAN INSTITUTE OF PHYSICS

INCORPORATED

57 East 55 Street New York 22, N.Y.

MEMBER SOCIETIES:

American Physical Society
KARL K. DARROW, *Secretary*, Columbia University, New York 27, New York.

Optical Society of America
ARTHUR C. HARDY, *Secretary*, Massachusetts Institute of Technology, Cambridge 39, Massachusetts.

Acoustical Society of America
WALLACE WATERFALL, *Secretary*, 350 Fifth Avenue, 64th floor, New York 1, New York.

Society of Rheology
EARL C. FISCHER, *Secretary*, Institute of Textile Technology, Charlottesville, Virginia.

American Association of Physics Teachers
C. J. OVERBECK, *Secretary*, Northwestern University, Evanston, Illinois.

AFFILIATED SOCIETIES:

American Society for X-Ray and Electron Diffraction

Electron Microscope Society of America

Physical Society of Pittsburgh

Physics Club of Chicago

Physics Club of Philadelphia

Cleveland Physics Society

ASSOCIATES:

Over seventy-five leading industrial enterprises and other institutions which contribute to the support of the Institute.

JOURNALS:

The Physical Review

Reviews of Modern Physics
JOHN T. TATE, *Editor*—J. W. BUCHTA, E. L. HILL, *Assistant Editors*

Journal of the Optical Society of America
GEORGE R. HARRISON, *Editor*

The Journal of the Acoustical Society of America
FLOYD A. FIRESTONE, *Editor*

American Journal of Physics
DUANE ROLLER, *Editor*—JOSEPH D. ELDER, *Assistant Editor*

The Review of Scientific Instruments
GAYLORD P. HARNWELL, *Editor*

The Journal of Chemical Physics
JOSEPH E. MAYER, *Editor*

Journal of Applied Physics
ELMER HUTCHISSON, *Editor*

OFFICERS

GEORGE R. HARRISON, *Chairman*
Massachusetts Institute of Technology

WALLACE WATERFALL, *Secretary*
The Celotex Corporation

GEORGE B. PEGRAM, *Treasurer*
Columbia University

JOHN T. TATE,
Adviser on Publications
University of Minnesota

GOVERNING BOARD

E. U. CONDON
A. J. DEMPSTER
W. F. FAIR, JR.
FLOYD A. FIRESTONE
HARVEY FLETCHER
R. C. GIBBS
K. S. GIBSON
GEORGE R. HARRISON
PAUL E. KLOPSTEG
GEORGE B. PEGRAM
A. H. PFUND
JOHN T. TATE
WALLACE WATERFALL
M. W. WHITE
A. G. WORTHING

ADMINISTRATIVE STAFF

HENRY A. BARTON, *Director*
CLEVELAND NORCROSS,
Assistant Director
RUTH F. BRYANS,
Publication Manager
THEODORE VORBURGER,
Business Manager

THE American Institute of Physics was founded in 1931 as a federation of leading societies in the field of Physics. It combines into one operating agency those functions on behalf of physics which can best be done by the Societies Jointly. Its purpose is the advancement and diffusion of physics and its applications to human welfare. To this end it publishes for itself or the Societies the eight journals listed on this page; promotes unity and effectiveness of effort among all who are interested in physics; renders numerous direct services to physicists and to the public; and cooperates with government agencies, national associations, educational institutions, technical industries, and others in such manner as to realize the opportunities and fulfill the responsibilities of physics as an important and constructive human activity.